

A 'Toolkit' of Small Molecules for Polymer Assembly and Post-Synthetic Modification  
Using 'Click' and Photoactive Chemistries

Jeffrey R. Lancaster

Submitted in partial fulfillment of the  
requirements for the degree of  
Doctor of Philosophy  
in the Graduate School of Arts and Sciences

COLUMBIA UNIVERSITY  
2011

© 2011  
Jeffrey R. Lancaster  
All rights reserved

## Abstract

A 'Toolkit' of Small Molecules for Polymer Assembly and Post-Synthetic Modification Using 'Click' and Photoactive Chemistries

Jeffrey R. Lancaster

Small molecules have been synthesized toward the goals of constructing and modifying polymeric materials according to simple, generalizable, and universal processes. The prepared compounds rely upon a combination of photochemistry and the 'click' philosophy to alter the architecture, bulk properties, or surface chemistry of polymers. In Chapter 1, a review is presented that details the many implementations of the 'click' philosophy to polymer chemistry. The influence of 'click' and photochemistry upon macromolecules is discussed using a topological approach to polymer architecture. Chapter 2 details the synthesis of several second-generation homobifunctional exogenous photocrosslinkers that extend upon previous work from our group. Additionally, a first-generation crosslinker is used to core-crosslink micellar aggregates of block copolymers. Chapter 3 describes the design, synthesis, and implementation of a photoactive 'click' activator for polymer surfaces. This chapter extends the notion of a material-specific anchor from hard substrates to a range of soft polymer substrates. Chapter 4 is an inquiry into the nature of the photoreaction of a standard photoactive moiety – benzophenone – with model compounds that represent polymers in which the crosslinkers of Chapter 2 are embedded. Comparison of competitive rates of abstraction gives insight into the reactive preferences of the crosslinkers and anchors of the previous chapters. In Chapter 5 small molecules and macromonomers are described that build upon the compounds described in previous chapters which collectively form the basis of a 'toolkit' approach to polymer

assembly and modification. Variations and extensions upon the 'toolkit' are detailed in order to give a sense of the future possibilities of this approach.

# Table of Contents

List of Figures .....	iii
List of Tables.....	vii
Acknowledgements .....	ix
<b>1. Introduction .....</b>	<b>1</b>
<b>1.1. Introduction.....</b>	<b>1</b>
<b>1.2. Click Chemistries.....</b>	<b>3</b>
1.2.1. Azide-Alkyne Cycloaddition .....	4
1.2.2. Other Cycloaddition Reactions Including Diels-Alder Chemistry .....	9
1.2.3. Thiol-ene, Thiol-yne, Michael Addition .....	13
1.2.4. Other Click Chemistries .....	16
<b>1.2.5. Applications of ‘Click’ Chemistry .....</b>	<b>19</b>
<b>1.3. Polymers.....</b>	<b>20</b>
1.3.1. Polymer Architecture.....	22
1.3.2. Functionalization of polymers .....	25
1.3.3. Heterobifunctional Monomers and Polymers .....	34
1.3.4. Macroscopic Polymer Modification – Bulk and Surfaces .....	37
<b>1.4. Photochemistry for Polymers .....</b>	<b>39</b>
1.4.1. Polymer Crosslinking by Photochemistry .....	40
1.4.2. Photodegradable Linkages in Polymers .....	42
1.4.3. Patterning .....	45
<b>1.5. Summary.....</b>	<b>46</b>
<b>1.6. References.....</b>	<b>47</b>
<b>2. Homobifunctional Crosslinkers.....</b>	<b>54</b>
<b>2.1. Introduction, Motivation .....</b>	<b>55</b>
<b>2.2. Candidates for New ‘Universal’ Crosslinkers.....</b>	<b>59</b>
<b>2.3. Preparation of Homobifunctional Crosslinkers .....</b>	<b>64</b>
<b>2.4. Core-Crosslinked Micelles and Crosslinked Thin Films.....</b>	<b>66</b>
2.4.1. Introduction to Core-Crosslinked Micelles .....	66
2.4.2. Preparation of PS-b-PEG Micelles .....	68
2.4.3. Analysis.....	69
2.4.3.1. Surface Tension .....	69
2.4.3.2. Pyrene Fluorescence .....	71
2.4.4. Core-Crosslinking of PS-b-PEO Micelles .....	72
2.4.5. Application of Micelles in Drug Delivery .....	74
<b>2.5. Summary.....</b>	<b>75</b>
<b>2.6. References .....</b>	<b>77</b>
<b>3. ‘Click’ Functional Polymer Surfaces .....</b>	<b>85</b>
<b>3.1. Introduction, Motivation .....</b>	<b>85</b>
3.1.1. Click Functionalization of ‘Hard’ Substrates.....	87
3.1.2. Click Functionalization of ‘Soft’ Substrates.....	92
3.1.3. Patterning of Surface Click Functionality .....	97

<b>3.2.</b>	<b>Design of Universal ‘Photoclickers’</b> .....	<b>99</b>
<b>3.3.</b>	<b>Preparation of Surface Functionalizing Compounds</b> .....	<b>102</b>
<b>3.4.</b>	<b>Surface Preparation</b> .....	<b>104</b>
<b>3.5.</b>	<b>Surface Analysis</b> .....	<b>105</b>
3.5.1.	Water Contact Angle Analysis.....	106
3.5.2.	Infrared Spectroscopy.....	109
3.5.3.	Fluorogenic Coumarin Azide.....	113
3.5.4.	Surface Functionalization with Nanoparticles .....	114
<b>3.6.</b>	<b>Outlook</b> .....	<b>115</b>
<b>3.7.</b>	<b>Summary</b> .....	<b>117</b>
<b>3.8.</b>	<b>References</b> .....	<b>118</b>
<b>4.</b>	<b><sup>1</sup>H NMR Study of Hydrogen Abstraction in Polymers</b> .....	<b>126</b>
<b>4.1.</b>	<b>Introduction, Motivation</b> .....	<b>126</b>
<b>4.2.</b>	<b>Analysis</b> .....	<b>130</b>
<b>4.3.</b>	<b>Discussion</b> .....	<b>133</b>
<b>4.4.</b>	<b>Hydrogen Abstraction from Proteins, Polymers</b> .....	<b>141</b>
<b>4.5.</b>	<b>Experimental</b> .....	<b>144</b>
<b>4.6.</b>	<b>Summary</b> .....	<b>145</b>
<b>4.7.</b>	<b>References</b> .....	<b>146</b>
<b>5.</b>	<b>Complex Architectures Using ‘Click’ Chemistry</b> .....	<b>148</b>
<b>5.1.</b>	<b>Introduction, Motivation</b> .....	<b>148</b>
5.1.1.	Dendrimer Synthesis .....	152
5.1.2.	Dendrimers by Click: CuAAC and Thiol-Ene.....	153
5.1.3.	Dendron Brushes.....	155
<b>5.2.</b>	<b>Preparation and Analysis of Toolkit Compounds</b> .....	<b>157</b>
5.2.1.	Small Molecules (NMR, FTIR).....	159
5.2.2.	$\alpha$ -(TMS-alkyne), $\omega$ -azide Heterobifunctional Polymers .....	162
<b>5.3.</b>	<b>Construction of Dendrimacromers</b> .....	<b>163</b>
<b>5.4.</b>	<b>Outlook and Other Possible Architectures</b> .....	<b>167</b>
5.4.1.	Sequence-Specific Brush and Bottle-Brush Polymers .....	168
5.4.2.	AB-CD <sub>2</sub> and AB-CD Dendrimers .....	170
5.4.3.	Fluorinated Dendrimers.....	175
<b>5.5.</b>	<b>Summary</b> .....	<b>177</b>
<b>5.6.</b>	<b>References</b> .....	<b>178</b>
<b>6.</b>	<b>Appendix</b> .....	<b>184</b>

## List of Figures

Figure 1.1. Formation of an azide from a bromide by reaction (activation) with sodium azide. ....	6
Figure 1.2. Selection of alkynes used in azide-alkyne click chemistries. ....	7
Figure 1.3. Selection of protecting groups for alkynes. ....	9
Figure 1.4. A ‘photoclick’ reaction between a substituted tetrazole and an alkene to form a 1,3,5-substituted pyrazole. ....	11
Figure 1.5. A protection/deprotection scheme for Diels-Alder adducts that undergo reversible cycloaddition. ....	13
Figure 1.6. A protection/deprotection scheme for thiol: oxidation to the disulfide and reduction to the thiol. ....	16
Figure 1.7. Generic mechanism for the controlled polymerizations ATRP and RAFT. <i>Note: throughout the text parentheses are indicative of a polymer though the degree of polymerization has often been omitted for simplicity unless it is instructive.</i> ....	22
Figure 1.8. Cartoons of several polymer architectures constructed from different monomers that are represented by different colored chains. ....	24
Figure 1.9. Generic topology of a linear polymer chain composed of chain ends (a), a backbone (b) and pendant groups (c) attached to the backbone. ....	25
Figure 1.10. (a) Condensation of propargyl alcohol with bromoisobutryl bromide and subsequent polymerization by ATRP. (b) (from left to right) An azido-functional ATRP initiator, an alkynyl functional ATRP initiator, and an $\alpha$ -alkynyl, $\omega$ -bromo-PtBA-b-PMMA block copolymer by ATRP. ....	27
Figure 1.11. Conversion of an ATRP-polymerized polystyrene bromide end group into terminal azide by reaction with sodium azide. ....	27
Figure 1.12. Functionalization of bis-OH-terminal polyethylene glycol with alkynes and azides by condensation with symmetrical anhydrides. ....	28
Figure 1.13. (a) Chain end functionalization of an oligopeptide by butynyl chloroformate. (b) Chain end functionalization of an acetoxy-protected disaccharide by coupling with azidoethanol followed by deprotection. (c) Chain end functionalization of a amine-terminated polynucleotide by NHS-ester-activated azide. ....	28
Figure 1.14. Azide-alkyne coupling of an azido-terminal polystyrene (Figure 1.11) with an alkyne-functional oligopeptide (Figure 1.13a) to generate a synthetic-biopolymer hybrid. ....	29
Figure 1.15. (a) Synthesis of an azide-functional methacrylic monomer followed by two sequential ATRP steps and CuAAC to generate a diblock copolymer with pendant R groups attached via triazole linkages. (b) ATRP of a TMS-protected alkyne-functional methacrylic monomer followed by deprotection to yield a polymer with pendant alkyne functionality. ....	30
Figure 1.16. Natural amino acids and unnatural amino acid derivatives for the biosynthesis of CuAAC functional peptides. ....	31
Figure 1.17. Post-polymerization modification for azide- and alkyne-functionalized poly(acrylic acid) and poly(N-isopropylacrylamide-co-acrylic acid). ....	32
Figure 1.18. Functionalization of a polyvalerolactone with pendant alkynes by azide-alkyne reaction with an azide-terminal RGD oligopeptide for cell adhesion. ....	33

Figure 1.19. Condensation polymerization schemes: (a) AB. (b) A <sub>2</sub> + B <sub>2</sub> . (c) AB*. (d) AB + CD. The circle represents the adduct of A and B while the squares represent the adducts of B and C or A and D. ....	34
Figure 1.20. Synthesis of a generic $\alpha$ ,azide- $\omega$ ,TMS-alkyne heterobifunctional polymer by ATRP. ....	36
Figure 1.21. Reversible polymer photocrosslinking by the [2+2] cycloaddition of (a) pendant coumarins and (b) pendant cinnamoyl groups. ....	41
Figure 1.22. Mechanism of the photocleavage of an ortho-nitrobenzyl ester to form a nitrosoaldehyde and a carboxylic acid. ....	42
Figure 1.23. Photocleavage of ortho-nitrobenzyl groups: (a) in the center of a polymer backbone; (b) at the chain end of a polymer; (c) to induce degradation of a polymer ....	44
Figure 2.1. Crosslinking schemes: (a) during polymerization; (b) by symmetrical pendant functionalities; (c) reaction of a bifunctional molecule with particular pendant functionalities; (d) degradation and reformation of polymer backbone to entangle; and (e) indiscriminate reaction of a bifunctional molecule. ....	58
Figure 2.2. Mechanisms of the photoreaction of (a) benzophenone hydrogen abstraction, (b) phthalimide hydrogen abstraction, and (c) phenyl azide nitrene insertion and ring expansion. ....	63
Figure 2.3. Synthesis of bis-benzophenone, 1. ....	65
Figure 2.4. Synthesis of mixed 3- and 4-benzoylbenzoate crosslinkers, 2. ....	65
Figure 2.5. Synthesis of bis-xanthone, 3. ....	65
Figure 2.6. Synthesis of bis-phenyl azide, 4. ....	65
Figure 2.7. Synthesis of bis-phthalimide, 5. ....	65
Figure 2.8. Structures of compounds used in the micelle study in addition to 1: (a) polystyrene- <i>block</i> -poly(ethylene oxide); and (b) pyrene. ....	69
Figure 2.9. Surface tension (a) and pyrene fluorescence (b) measurements of aqueous solutions of PS- <i>b</i> -PEO. Extrapolation of the lines tangent to the steepest slope give the cmc of the native PS- <i>b</i> -PEO used as approximately 0.02 mg/mL. ....	70
Figure 2.10. Surface tension measurements of aqueous solutions of PS- <i>b</i> -PEO as compared to pure water. The data represents the ratio of the difference between the measured value of the surface tension of water and diluted PS- <i>b</i> -PEO solution (below the cmc, approx. 0.01 mg/mL) to the difference between the measured value of the surface tension of water and concentrated PS- <i>b</i> -PEO (above the cmc, approx. 0.1 mg/mL). A lower value of the ratio is indicative of the PS- <i>b</i> -PEO micelles disassembling in water upon dilution. The error on each value is less than 25%. ...	73
Figure 3.1. Cartoon representing the click-functional photoactive small molecule design showing the anchoring group (red), click functionality (blue), and tether (gray). ....	86
Figure 3.2. Representative hard, flat surface functionalization with alkynes and azides: (a) self-assembly of a thiol-alkyne on gold; (b) self-assembly of a PEGylated thiol-alkyne on gold; (c) self-assembly of a mixed monolayer of thiol-azide and alkanethiol on gold;.....	90
Figure 3.3. CuAAC surface functionalization strategies for various hard nanoparticulate surfaces: (a) azide on gold; (b) alkyne on cadmium selenide (CdSe); (c) azide on cadmium selenide (CdSe); (d) alkyne on silica (SiO <sub>2</sub> ); (e) azide on silica (SiO <sub>2</sub> ); (f) azide on iron oxide (hematite, Fe <sub>2</sub> O <sub>3</sub> ); (g) alkyne on iron oxide (ferrite, Fe <sub>3</sub> O <sub>4</sub> ); (h)	



azide on zinc oxide (ZnO); (i) alkyne on titanium dioxide (TiO <sub>2</sub> ); and (j) alkyne on carbon nanotube.....	91
Figure 3.4. Post-functionalization strategies on click-functionalized surfaces: (a) CuAAC for biotinylated, glycosylated, and protein-functionalized surfaces; (b) CuAAC for a DNA-functionalized PMMA-b-PS copolymer surface; and (c) Diels-Alder functionalization for an alkyne surface.....	92
Figure 3.5. Polymer substrate functionalization: (a) layer-by-layer CuAAC assembly of alkynyl- and azido-functional polymers; (b) functionalization with a diblock copolymer; and (c) radio frequency glow discharge (RFGD) plasma polymerization of brominated polypropylene and azidification.....	95
Figure 3.6. Functional dendritic polymer nanoparticles: (a) alkyne-functional; and (b) azide-functional.....	96
Figure 3.7. CuAAC functionalization of cowpea mosaic virus capsid.....	96
Figure 3.8. Liposome surface functionalization (left) using alkynylated DOPE (right).....	96
Figure 3.9. Photoactive anchors: (a) phthalimide; (b) benzophenone; (c) xanthone; (d) phenyl azide; (e) sulfonyl azide; and (f) trifluoromethyl phenyl diazirine.....	100
Figure 3.10. Scheme of hydrogen abstraction from R-H (blue) by phthalimide.....	100
Figure 3.11. Click reactions of an alkyne: CuAAC and thiol-yne.....	101
Figure 3.12. Synthesis of phthalimide-alkyne, 8 (R = H) and trimethylsilyl-protected phthalimide-alkyne, 9 (R = TMS) from 6-bromohexanoyl chloride and propargyl alcohols.....	102
Figure 3.13. Synthesis of prop-2-yn-1-yl 6-bromohexanoate, 6 (top) and 3-(trimethylsilyl)prop-2-yn-1-yl 6-bromohexanoate, 7 (bottom).....	103
Figure 3.14. Synthesis of prop-2-yn-1-yl 6-phthalimidohexanoate, 8 (top) and 3-(trimethylsilyl)prop-2-yn-1-yl 6-phthalimidohexanoate, 9 (bottom).....	103
Figure 3.15. Synthesis of 10-azidodec-1-ene, 10.....	103
Figure 3.16. ATR-FTIR spectra of prop-2-yn-1-yl 6-phthalimidohexanoate, 8 (top) and 3-(trimethylsilyl)prop-2-yn-1-yl 6-phthalimidohexanoate, 9 (bottom).....	104
Figure 3.17. Water contact angle analysis tracking the unoptimized preparation of alkyne-functionalized surfaces on polystyrene (black, 8, and gray, 9) and poly(acrylic acid) (blue, 8, and navy, 9).....	107
Figure 3.18. Water contact angle analysis following the optimized preparation of polystyrene (gray) and poly(acrylic acid) (blue) surfaces functionalized with 8.....	108
Figure 3.19. Optical micrographs of polymer surfaces coated with 8 and irradiated at 300 nm for 30 min: (a) PS; and (b) PAA.....	109
Figure 3.20. FTIR Spectra of bare glass slide (blue, bottom), PS film (green), 8 mixed into PS film (red), and 8 deposited onto PS film (purple, top). All spectra were recorded prior to UV irradiation.....	110
Figure 3.21. IR absorption spectra for 8 on PS at various irradiation times referenced to a clean glass slide. From bottom: 0, 5, 10, 20, 30, 40, 50, 60 min.....	112
Figure 3.22. IR absorption spectra for 8 on PS at various irradiation times referenced to PS on a glass slide. From bottom: 0, 5, 10, 20, 30, 40, 50, 60 min.....	112
Figure 3.23. A non-fluorescent coumarin azide reacts with an alkyne to generate a fluorescent adduct.....	113
Figure 3.24. DRIFTS spectrum of azide functionalized silica nanoparticles.....	114
Figure 3.25. Images of electrospun PS fibers.....	116

Figure 3.26. Possible phthalimide-ATRP initiator synthesis.....	117
Figure 4.1. Excitation of benzophenone and subsequent hydrogen abstraction from a hydrogen donor (blue).....	127
Figure 4.2. Structures of the compounds used in this study: caprolactam, 11; methylcaprolactam, 12; caprolactone, 13; <i>sec</i> -butylbenzene, 14; ethylbenzene, 15; methyl trimethylacetate, 16; 2,2-dimethylbutane, 17; trans-3-hexene, 18; and butyl isovalerate, 19.....	129
Figure 4.3. Comparison of C-C bond dissociation energies in ethylbenzene, 15, and styrene.....	130
Figure 4.4. 300 MHz <sup>1</sup> H NMR spectra of a 96.9 mM solution of 11 (CD <sub>3</sub> CN) and benzophenone after 0 min (bottom), 30 min (middle), and 120 min (top) irradiation at 350nm.....	131
Figure 4.5. Difference between 300 MHz <sup>1</sup> H NMR spectra of 11 (CD <sub>3</sub> CN) and benzophenone before and after 120 min irradiation at 350nm.....	132
Figure 4.6. Plot of <sup>1</sup> H NMR integrals for protons a-d of compound 11 scaled by initial integral and number of protons with increasing irradiation time. Each set of data points is fit with Equation 4.1.....	133
Figure 4.7. Energy state diagram for hydrogen abstraction by benzophenone (BP) from a substrate, S, followed by recombination.....	135
Figure 4.8. Resonance structure (bottom) showing possible polar effects during the transition state (top) of hydrogen abstraction from X-H by triplet benzophenone..	141
Figure 5.1. (a) Tinker toys and (b) K'Nex form complex architectures from simple components.....	149
Figure 5.2. Several $\alpha$ -azide- $\omega$ -alkyne heterobifunctional monomers.....	151
Figure 5.3. Generic convergent dendron synthesis by CuAAC using the bis-alkyne chlorides (a-c).....	154
Figure 5.4. Cartoons of brush growth (a) linearly and (b) including branching.....	156
Figure 5.5. Synthetic scheme of the CuAAC 'click' functional branch point, 21.....	159
Figure 5.6. Synthesis of 6-azidohexanol, 22.....	160
Figure 5.7. Synthesis of 6-azidohexyl 3-benzoylbenzoate, 23.....	160
Figure 5.8. Synthesis of 6-azidohexyl pyrene-1-carboxylate, 24.....	161
Figure 5.9. Photoactive moieties: (a) phthalimide; (b) benzophenone; (c) xanthone; (d) phenyl azide; (e) sulfonyl azide; and (f) trifluoromethyl phenyl diazirine.....	161
Figure 5.10. Other carboxylic acid precursors to 'reporter' molecules: (a) anthracene-9-carboxylic acid; (b) TEMPO-carboxylic acid; and (c) biotin-carboxylic acid.....	161
Figure 5.11. Synthesis of $\alpha$ -(TMS-alkyne)- $\omega$ -azido heterobifunctional photodegradable CuAAC monomer, 25.....	162
Figure 5.12. Synthesis of 3-(trimethylsilyl)prop-2-yn-1-yl 2-bromo-2-methylpropanoate, 26.....	163
Figure 5.13. Atom transfer radical polymerization (ATRP) of styrene and subsequent reaction with sodium azide to yield $\alpha,\omega$ -heterobifunctional polystyrene, 27.....	163
Figure 5.14. Possibilities for dendrimer synthesis from toolkit.....	165
Figure 5.15. C <sub>4</sub> BM <sub>1</sub> BM <sub>2</sub> BM <sub>3</sub> dendrimacromer constructed from multiple macromonomers and a branch unit.....	167

Figure 5.16. Monomer-by-monomer growth from a homobifunctional bisalkyne core via sequential addition of $\alpha,\omega$ -heterobifunctional TMS-alkyne-azide monomer followed by deprotection of the TMS group to regenerate a terminal alkyne. ....	169
Figure 5.17. Monomer-by-monomer growth from a polymer with pendant alkynes via sequential addition of $\alpha,\omega$ -heterobifunctional TMS-alkyne-azide monomer followed by deprotection of the TMS group to regenerate a terminal alkyne. ....	169
Figure 5.18. Monomer-by-monomer growth from an alkyne-functional surface via sequential addition of $\alpha,\omega$ -heterobifunctional TMS-alkyne-azide monomer followed by deprotection of the TMS group to regenerate a terminal alkyne. ....	170
Figure 5.19. The AB <sub>2</sub> -CD <sub>2</sub> synthesis of a dendrimer (4 <sup>th</sup> generation is shown) using complementary heterotrifunctional branched small molecules. ....	171
Figure 5.20. Potential building blocks for an AB-CD <sub>2</sub> dendrimer using complementary heterobifunctional and heterotrifunctional molecules. ....	172
Figure 5.21. Building blocks for an AB-CD <sub>2</sub> dendrimer using the complementary heterobifunctional and heterotrifunctional molecules in Figure 5.20a. ....	172
Figure 5.22. Two sets of building blocks for an AB-CD dendrimer using complementary heterobifunctional molecules. ....	173
Figure 5.23. Synthesis of an AB-CD dendrimer using complementary heterobifunctional molecules. ....	174
Figure 5.24. Proposed fluorinated components for the synthesis of dendrimacromers by AB-CD <sub>2</sub> approach and their characterization using <sup>19</sup> F NMR: (a) macromonomer; (b) branch; (c) core; and (d) chain terminator. ....	176
Figure 5.25. Simulated <sup>19</sup> F NMR spectra of dendrimers grown using fluorinated branch and macromonomer, normalized to macromonomer intensity. ....	176
Figure 5.26. Simulated <sup>19</sup> F NMR spectra of dendrimers grown using fluorinated branch, macromonomer, core, and terminator. ....	177

## List of Tables

Table 1.1. Examples of click chemistry using azide-alkyne cycloadditions to form substituted 1,2,3-triazoles. ....	4
Table 1.2. Peptidomimicry of the amide (peptide) bond by the 1,4-triazole. ....	6
Table 1.3. Various cycloaddition click reactions. ....	12
Table 1.4. Various thiol-ene and thiol-yne click chemistries. ....	15
Table 1.5. Additional click chemistries and ‘spring loaded’ reactions. ....	18
Table 2.1. Candidates for improved photoactive bis-functional crosslinkers. ....	62
Table 3.1. Moieties for the surface functionalization of ‘hard’ substrates. ....	89
Table 4.1. Structural comparison of some typical polymers and model compounds used. ....	129
Table 4.2. Values of $k$ using Equation 4.1 to fit the data in Figure 4.6 for 11. ....	133
Table 4.3. Compounds with representative bond dissociation energies for the protons of 1, the relation of each representative bond to 11, and the value of $k$ determined for that proton. ....	136

Table 4.4. Compounds with representative bond dissociation energies for the protons of 18, the relation of each representative bond to 18, and the value of $k$ determined for that proton.....	137
Table 4.5. Compounds with representative bond dissociation energies for the protons of 16, the relation of each representative bond to 16, and the value of $k$ determined for that proton.....	140
Table 4.6. Compounds with representative bond dissociation energies for the protons of 17, the relation of each representative bond to 17, and the value of $k$ determined for that proton.....	140
Table 5.1. First, second, third and fourth ‘generation’ dendrimers from a bifunctional ( $C_2$ ) core with branches (B) and macromonomers (M).....	166

## Acknowledgements

I would like to first and foremost acknowledge and thank my research advisors, Professors Nicholas Turro and Jeffrey Koberstein. Their guidance and inspiration have made it possible for me to explore my creativity within an exciting and diverse research program. I also want to thank the various members of my doctoral committee, including Professors Kenneth Eisenthal, Luis Campos, Nima Akhavan, and Sanat Kumar.

Second I must thank the various collaborators with whom I undertook these several research projects, and the colleagues with whom fruitful conversation directed the course of the research. The work presented in Chapter 2 was the result of collaboration with Nicholas Carbone and Madalina Ene who used the second generation crosslinkers in polymer thin films, and also a collaboration with Kavita Vemishetti who performed much of the core-crosslinked micelle work. Gregory Carroll generously provided inspiration and mentoring for the work in Chapter 2. Chapter 3 is the result of collaboration with Professor John Rabolt whose expertise in infrared spectroscopy was invaluable. Bryan Lim contributed to the synthesis of compounds in Chapter 3, and Ellane Park and Tina Wagenaar contributed to the characterization of the polymer surfaces. Stanislav Presolski generously donated the azidocoumarin with which visualization studies were attempted. Chapter 4 is largely the work of Rachael Smilowitz, and I thank Professor Massimo Bietti for a number of useful discussions about hydrogen abstraction. Jeremiah Johnson, Dan Margulies and Liang Cao generously contributed to the planning and synthesis of the compounds presented in Chapter 5, and Benjamin Dach and Yanir Maidenberg are continuing to employ the molecular ‘toolkit’ to synthesize novel architectures.

Lastly I want to thank my family and friends for their support during the course of my doctoral work, and for graciously letting me attempt to explain my research to them using metaphor and analogy. Thank you especially to my Mom and Dad who have always taken an interest in my work, who have enthusiastically supported and encouraged me, and who I love very much.

The work presented is my own, and I am responsible for any errors herein.

For my Mom and Dad.

“Macromolecules are all about us and we ought therefore to try to understand them. Substances so intimate to us, and in us for that matter, should surely engage the interests of the scientist.”

– Paul J. Flory in Ridgway, D. W. *J. Chem. Ed.* **1977**, *54*, 341.

Mr. McGuire: I just want to say one word to you. Just one word.

Benjamin: Yes, sir.

Mr. McGuire: Are you listening?

Benjamin: Yes, I am.

Mr. McGuire: Plastics.

Benjamin: Exactly how do you mean?

– Walter Brooke and Dustin Hoffman in *The Graduate*, 1967.

*E pluribus unum.*

Out of many, one.

# 1. Introduction

## 1.1. Introduction

The field of synthetic polymer chemistry is relatively new when compared to other chemical subdisciplines such as natural products or analytical chemistry. The ‘original’ reaction in the field of polymer chemistry took place in the late 1830’s when Charles Goodyear added sulfur to natural rubber to produce a durable elastic rubber in a process that came to be known as vulcanization. At the time, the chemical structure of natural polymers was largely unknown, but still chemists were able to modify the properties of these natural substances. Completely synthetic polymers have historically been useful substitutes for natural or rare substances with desirable material properties, such as nylon substituting for the more arduously produced silk, or polyurethane coatings substituting for lacquer made from insect resin. The recent progress of polymer chemistry over the last 50 years, however, indicates that the field is still rife with potential for impact in numerous practical and commercial areas from materials to biology and medicine.

Polymers as a class of molecules are some of the most prevalent in our biology. DNA, proteins and carbohydrates are polymeric materials composed of nucleotides, amino acids, and saccharides, respectively. Nature has developed complex systems relying on coded sequences that determine the chemical and material properties of biopolymers. Just as Nature has developed methods to synthesize polymers from biological components, developments in the construction of synthetic polymers have led to an increasing number of polymerization methods, especially in the last 20 years. The drive for new methods has been aimed at generating materials with higher and higher



degrees of control over the particular arrangement, order, and functionality of monomers within a polymer. This increased control has led to a wide range of potential material architectures, which in turn has led to a vast array of properties for an ever-growing number of new applications.

It should come as no surprise then that Biology and Nature have in served as inspiration for current trends in synthetic polymer chemistry toward increasing degrees of control, order, and functionality. Nature has developed machinery to produce polymers with virtually the same length, sequence, and stereochemistry, and currently the best that chemists can do relies largely upon manipulating statistical processes and rates, and sometimes luck. As a result, chemists must look for ways to reliably manipulate the properties of polymers that go beyond the tools that Nature has been able to develop. By approaching the synthesis and manipulation of polymeric materials from a different point of view, we can take the best of what Nature has to offer while simultaneously going beyond its limitations. Many of the forthcoming practical challenges in polymer science will necessarily be material in scope, and solutions will rely upon developing new ways to modify, tune, and alter the properties of materials in addition to developing new methods to synthesize those materials.<sup>1</sup>

Here I will describe our recent progress in efforts to develop methods for the modification of already-synthesized polymers, as well as our effort to combine the approaches of modification and synthesis toward the construction of materials that are expected to have unusual properties that would otherwise be unattainable using more conventional synthetic methods.

## 1.2. Click Chemistries

Parallel to advances in polymer chemistry over the last decade has been the emergence of a chemical philosophy called ‘click chemistry’. Since 2001, click chemistry has had a profound impact upon materials chemistry and engineering, polymer chemistry and engineering, and biomedical engineering. Although click chemistry has made many of the recent advances in polymer design possible, Sharpless and coworkers initially espoused it as an approach to the design of pharmaceutical drug libraries.<sup>2</sup>

Click chemistry is not one particular reaction, but is instead a set of reactions that share common characteristics. Foremost, click type reactions are intended to be high yielding, modular, widely applicable and should not generate offensive or dangerous byproducts. Additionally, click reactions should be carried out under relatively simple conditions using available or easily prepared reagents in no or easily removed solvent, and the products must be easily isolable. Finally, click reactions are intended to be chemoselective between reactive groups on the constituent reagents. That is, there should be no undesirable side reactions with functional groups other than where the reaction is intended.

This set of characteristics is ideal for the rapid generation of libraries of compounds for subsequent pharmacological examination, and is clearly inspired by Nature’s approach to the construction of biomolecules. Nature also constructs complex molecules from simple components using a common set of reactions and cannot afford deleterious side reactions or byproducts. The set of linkages used by Nature is relatively limited in scope: phosphate linkages for DNA, amides for peptides, esters for carbohydrates. Click chemistry mirrors Nature’s approach, but has the added advantage

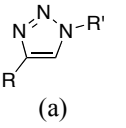
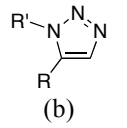
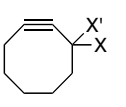
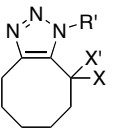
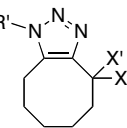
of not being limited to one set of linkages or another per material. Click chemistry uses orthogonal functionalities, i.e. separate functionalities that will not react with each other, but only with their appropriate counterpart.

Because it is a philosophy of linking components together, click chemistry is ideal for the synthesis, modification, and functionalization of natural, synthetic, and especially hybrid polymers and polymeric materials.<sup>3-5</sup> To date, however, the term ‘click chemistry’ has been expanded to a number of reactions and its precise definition continues to be a source of debate for polymer chemists.<sup>6,7</sup>

### 1.2.1. Azide-Alkyne Cycloaddition

The premier click reaction is the Huisgen 1,3-dipolar cycloaddition reaction between an azide and an alkyne. Since its re-introduction as an effective coupling reaction by Sharpless, variations on the thermal Huisgen reaction have been introduced using catalysts and ring-strain to promote the cycloaddition. Taken together, azide-alkyne click chemistry has been implemented in numerous areas of chemistry, from synthesis and drug discovery to surface functionalization and conductive materials.

**Table 1.1.** Examples of click chemistry using azide-alkyne cycloadditions to form substituted 1,2,3-triazoles.

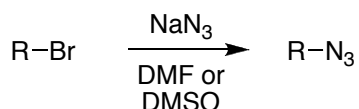
Components		Adduct		Variations	References
$R-C\equiv C$	$\overset{-}{N}=\overset{+}{N}=\overset{-}{N}-R'$	 (a)	 (b)	1. Cu(I) catalyzed (a only) 2. Ru(II) catalyzed (b only) 3. Thermal activation (a and b)	[8] - [15] [20] [25]
Alkyne	Azide	1,4-Triazole	1,5-Triazole		
$\overset{-}{N}=\overset{+}{N}=\overset{-}{N}-R'$		 (a)	 (b)	No catalyst, Room temperature	[26] - [32]
Azide	Cyclooctyne	Triazole			

Of the variations on azide-alkyne cycloaddition chemistry (Table 1.1), the most widely adopted synthetic strategy is to use a catalytic amount of copper(I) to preferentially generate the *E*-regioisomer of a 1,2,3-triazole from an azide and a terminal alkyne.<sup>8</sup> This reaction, known as copper catalyzed azide-alkyne cycloaddition (CuAAC), has been used widely in large part because it places the substituents of the triazole in the least sterically hindered orientation at the 1 and 4 positions. Although the mechanism is still being debated<sup>9</sup>, CuAAC generally proceeds with minimal Cu<sup>+</sup> that can be provided directly in aqueous or organic solution by the reduction of a soluble Cu<sup>2+</sup> salt, a ligated Cu<sup>+</sup> complex<sup>10-12</sup>, or even by a small amount of salt in conjunction with the equilibrium amount of dissolved Cu<sup>+</sup> from a solid copper wire<sup>13</sup>. In synthetic chemistry, general CuAAC techniques have been developed to form triazoles in a one pot reaction from the product of a substrate with trimethylsilylacetylene followed by deprotection and CuAAC with a second azido-functional substrate.<sup>14,15</sup> Since the azide and alkyne do not readily react with most biological functionalities, CuAAC has also been widely used to synthesize nucleotide and nucleoside derivatives.<sup>16</sup>

Variations of CuAAC have been developed where it is desirable to have an iodo- or sulfonyl-functionalized triazole.<sup>17-19</sup> Additionally, if ruthenium(II) is used in place of copper(I), the *Z*-regioisomer of the 1,2,3-triazole is preferentially formed with the substituents in more sterically hindered 1 and 5 positions of the triazole (Table 1.1).<sup>20</sup> The reaction between the azide and the alkyne can also be induced thermally around 70°C to generate a mixture of the *E* and *Z* regioisomers of the triazole.

Azide-alkyne click chemistry is advantageous in chemical synthesis for a number of reasons. First, the azide and alkyne functionalities are relatively easy to introduce to

molecules containing a wide variety of other functionalities – including sugars<sup>21</sup> and nucleotides<sup>22</sup> – and they are relatively inert to most other functionalities. The azide can be easily introduced by the S<sub>N</sub>2 reaction of a primary or secondary bromide with excess sodium azide (Figure 1.1), or even via diazotization of an aniline derivative followed by azidification. The alkyne can easily be introduced via several routes, including esterification or amidation of carboxylic acids with propargyl alcohol or propargyl amine. Second, the reaction between the azide and alkyne can be carried out in water, which is incredibly useful for the functionalization of biomolecules that may be harmed by dissolution in conventional organic solvents. Third, the triazole adduct is peptidomimetic; functional groups are placed nearly the same distance apart as its biological analogue, the amide bond (Table 1.2).<sup>23,24</sup> Lastly, in cases where it is undesirable to have transition metals present as catalysts, the 1,3-dipolar cycloaddition may be induced under relatively inert thermal or microwave conditions.<sup>25</sup>

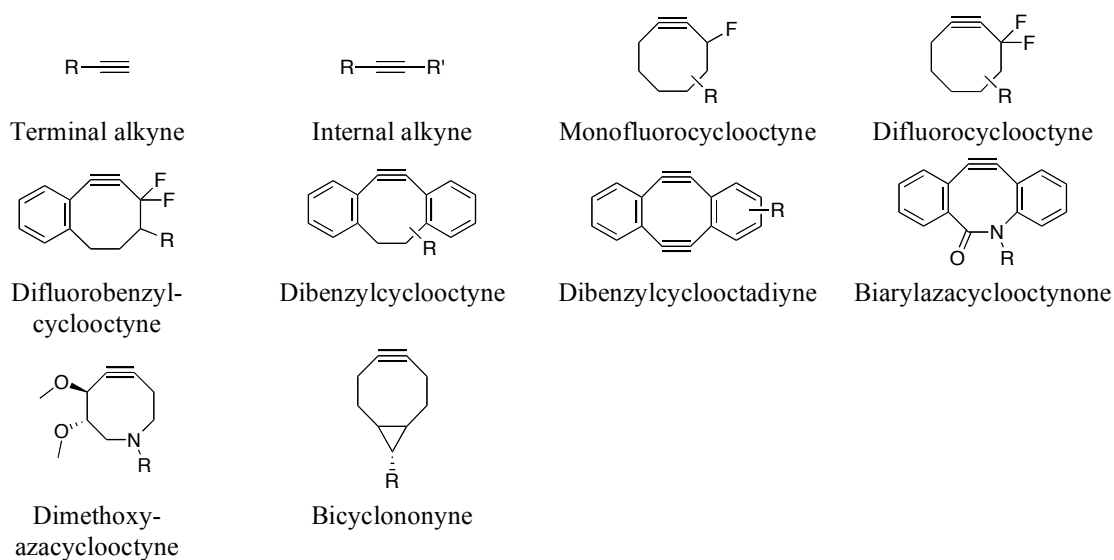


**Figure 1.1.** Formation of an azide from a bromide by reaction (activation) with sodium azide.

**Table 1.2.** Peptidomimicry of the amide (peptide) bond by the 1,4-triazole.

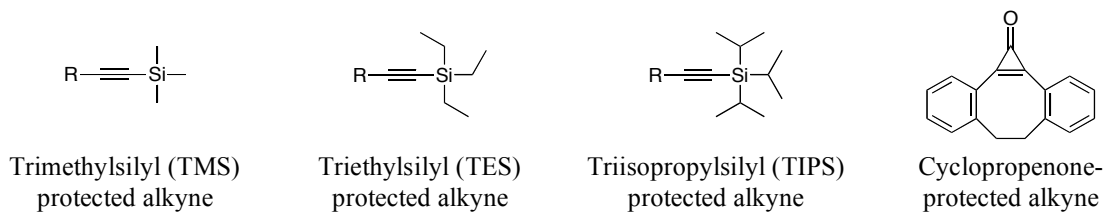
Components		Adduct
Biology	$\begin{array}{c} \text{H}_2\text{N} \\   \\ \text{R}-\text{C}-\text{COOH} \end{array}$	$\begin{array}{c} \text{O} \\    \\ \text{H}_2\text{N}-\text{C}-\text{N}-\text{C}-\text{COOH} \\   \quad   \\ \text{R} \quad \text{R}' \end{array}$
	Amino acid	Amide (Peptide)
Click	$\text{R}-\text{C}\equiv\text{C}$	$\begin{array}{c} \text{N}=\text{N} \\   \quad   \\ \text{R}-\text{C}=\text{N}-\text{R}' \end{array}$
	Alkyne	1,4-Triazole

The major practical drawback to the Cu(I) and Ru(II) catalyzed azide-alkyne cycloadditions is that the transition metals used to catalyze the reaction can be toxic to living cells.<sup>26</sup> For biological applications, strained alkynes (e.g. cyclooctyne, Table 1.1) have been found to react with azides without the need for metal catalysts; these are typically called Cu-free or strain-promoted click reactions.<sup>26-32</sup> Variations of the strained cyclooctyne have been developed – principally by the Bertozzi group – with substituted cyclooctyne rings to modify the hydrophilicity of the whole molecule and the ring-strain or electrophilicity of the alkyne.<sup>26-32</sup> Developed derivatives include azadimethoxy-, monofluoro-, difluoro-, difluorobenzyl- and dibenzylcyclooctyne derivatives (Figure 1.2). Novel variations include dibenzylcyclooctadiyne<sup>30</sup> with two alkynes in the cyclooctyne ring, biarylazacyclooctynone<sup>31</sup> where the cyclooctyne ring contains an amide bond, and bicyclononyne<sup>32</sup> where a functionalized cyclopropyl group acts as a handle to the cyclooctyne ring.



**Figure 1.2.** Selection of alkynes used in azide-alkyne click chemistries.

When working with click chemistries, it is worthwhile to protect or inactivate the azide or the alkyne while another process is taking place, and then to make the latent functionality available by activation or deprotection at a later time. Such latent groups are very useful in materials applications, especially in polymer chemistry and polymer synthesis. The most straight-forward approach to ‘protect’ an azide is to delay activating the bromide to the azide until such time as it is required (Figure 1.1). Activation as a strategy is ideal to introduce the azide because the reaction to form the azide is high yielding and optionally requires only simple aqueous separation of residual sodium azide. In contrast, it is generally more advantageous to introduce an alkyne in a protected form over the course of a synthesis instead of trying to introduce it immediately before reacting. Terminal alkynes are best protected using alkylsilyl derivatives, several of which are shown in Figure 1.3.<sup>33-35</sup> The groups shown are semi-orthogonal to each other since judicious selection of deprotection conditions has been shown to selectively deprotect one alkyne while leaving the others intact.<sup>36</sup> Sequential deprotection and reaction by CuAAC was shown to generate polytriazoles with multiple different substituents clicked to alkynes on the same substrate. Although protection by alkylsilyl moieties is not feasible for an internal alkyne, cyclopropenones effectively mask a strained alkyne.<sup>37</sup> Deprotection of the cyclopropenone is effected photochemically to liberate carbon monoxide and the strained alkyne, and has been used to label azido-modified cells *in vivo*.



**Figure 1.3.** Selection of protecting groups for alkynes

Although azide-alkyne cycloaddition chemistry has become the gold-standard of click chemistries, the development, expansion, and application of the click chemistry philosophy to other chemical reactions has opened wide new synthetic and material possibilities.

### 1.2.2. Other Cycloaddition Reactions Including Diels-Alder Chemistry

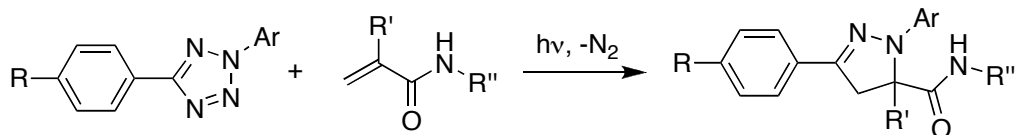
In addition to the copper(I), ruthenium(II), thermal, and strain promoted variations of azide-alkyne cycloaddition chemistry, there are numerous other examples of cycloaddition and strain-promoted chemistries (Table 1.3). While some are comparable to CuAAC, many of these are preferable to CuAAC because they do not require toxic transition metal catalysis.<sup>38</sup>

The most closely related variations of azide-alkyne cycloaddition chemistry are azide-nitrile cycloaddition to form a tetrazole, and the reaction of an alkyne with a nitrile-N-oxide or a nitron to form a substituted isoxazole. In the first case, the reaction of an azide and nitrile is nearly identical to the reaction of an azide with an alkyne except the nitrile has a terminal nitrogen in place of the terminal C-H of the alkyne. The same issue of regioisomeric (*E* and *Z*) products holds for the 1,2,3,4-tetrazole. If the azide is replaced with another 1,3-dipolar compound like a nitrile-N-oxide or a nitron, then similar 1,3-dipolar cycloaddition reactions occur as with an alkyne.<sup>39,40</sup> In the case of an



internal alkyne, reaction with a nitrile-N-oxide generates a 3,4,5-trisubstituted isoxazole, while reaction with a nitron can yield a more highly substituted isoxazole.<sup>41</sup> If the nitron used is not highly substituted and reacts with a terminal alkyne, then the five-membered isoxazole ring can rearrange and contract to a  $\beta$ -lactam. Another closely related reaction is that of an azide with an *ortho*-(trimethylsilyl)phenyl triflate.<sup>42</sup> In the presence of fluoride and crown ether, loss of the trimethylsilyl and triflate groups generates a reactive aryne that reacts with the azide. Although the yields are not high enough (<85%) to truly be considered a click reaction, it bears the same motif as the azide-alkyne cycloaddition.

One of the most interesting extensions of the click methodology beyond the azide-alkyne cycloaddition is the photoinduced reaction between an alkene and an aryl-substituted tetrazole.<sup>43-45</sup> This 'photoclick' reaction proceeds via excitation of the conjugated chromophore containing the tetrazole (254 - 365 nm), loss of molecular nitrogen from the 3 and 4 positions of the tetrazole, and reaction with an alkene to generate either a 1,3,5-substituted pyrazole or a 1,3,4,5-substituted pyrazole depending on the extent of substitution of the alkene (Figure 1.4). This photoclick approach is highly compatible for reactions in biological environments because light is a clean reagent and the amount of nitrogen given off is relatively inert. A derivative of the amino acid phenylalanine bearing a *para*-tetrazole has been shown to incorporate into a protein via a biosynthetic pathway and then react *in vivo* with an alkene-functionalized dye.<sup>45</sup>


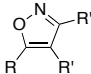
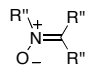
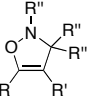
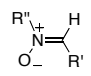
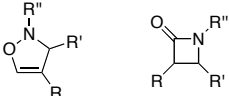
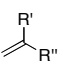
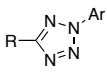
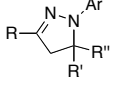
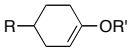
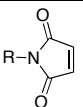
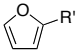
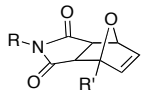
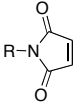
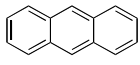
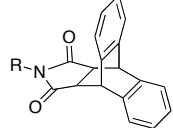
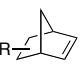
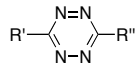
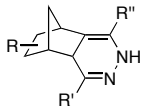
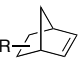
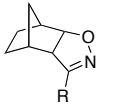
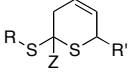


**Figure 1.4.** A ‘photoclick’ reaction between a substituted tetrazole and an alkene to form a 1,3,5-substituted pyrazole.

The most commonly thought-of class of cycloaddition reactions is between a diene and a dienophile: Diels-Alder cycloadditions. These reactions are either thermally- or catalytically-induced<sup>46</sup> and tend to be valued for their combined properties of stability and lability under varied stresses. The exemplar Diels-Alder cycloaddition between maleimide and furan is thermally-induced around 70°C and the retro-Diels-Alder reaction occurs around 110°C depending on solvent conditions. Once the Diels-Alder adduct is formed, however, it is quite stable to mechanical stress.

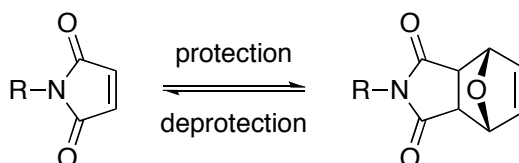
Two additional Diels-Alder chemistries in particular have been considered that attempt to satisfy the click philosophy: first, the reaction of norbornene with tetrazine diene or nitrile N-oxide, and second the reaction between a dithioester and a diene.<sup>47 48 49</sup> As with the ‘photoclick’ reaction of an alkene with a tetrazole, the reaction of norbornene – a strained alkene – with the tetrazine diene is accompanied by loss of molecular nitrogen resulting in a stable, non-reversible Diels-Alder adduct. Similarly, the reaction of norbornene with nitrile N-oxide is comparable to the reaction of a strained alkyne with nitrile N-oxide resulting in a polycyclic isoxazole. In the second case, the dithioester group is commonly found at the chain ends of a polymer synthesized by reversible addition-fragmentation chain transfer polymerization (RAFT) and has been shown to undergo a Diels-Alder reaction with dienes. This useful reaction for chain-end functionalization of RAFT polymers was optimized to an ‘ultrafast’ click reaction by introducing an electron-withdrawing group (Z in Table 1.3) in the  $\alpha$ -position of the

**Table 1.3.** Various cycloaddition click reactions.

Components		Adduct	References
$R-C\equiv N$	$\overset{-}{N}=\overset{+}{N}=N-R'$		[4], [8]
Nitrile	Azide	Tetrazole	
$R-C\equiv R'$	$\overset{-}{O}-\overset{+}{N}\equiv R''$		[39], [40]
Alkyne	Nitrile N-oxide	Isoxazole	
$R-C\equiv R'$			[41]
Internal alkyne	Nitronium	Isoxazole	
$R-C\equiv$			[41]
Terminal alkyne	Nitronium	Isoxazole or $\beta$ -Lactam	
			[43] - [45]
Alkene	Tetrazole	Pyrazole	
$R-CH=CH_2$	$CH_2=CH-OR'$		[2]
Dienophile	Diene	Diels-Alder adduct	
			[46]
Maleimide	Furan	Diels-Alder adduct	
			[46]
Maleimide	Anthracene	Diels-Alder adduct	
			[47]
Norbornene	Tetrazine diene	Diels-Alder adduct	
	$\overset{-}{O}-\overset{+}{N}\equiv R'$		[48]
Norbornene	Nitrile N-oxide	Diels-Alder adduct	
$R-S-C(=S)-Z$	$CH_2=CH-CH=CH-R'$		[49]
Dithioester	Diene	2-Thioester-3H,6H-thiopyran	

dithioester and reacting with a ring-strained diene (e.g. cyclopentadiene).<sup>49</sup> Standard reaction conditions of 50°C for 2 - 24 h for a normal dithioester-diene reaction were reduced to 10 min at room temperature for the ‘ultrafast’ protocol.

Just as with the azide-alkyne cycloaddition chemistry, it is advantageous to protect and readily deprotect the components of a Diels-Alder cycloaddition. The most straight-forward protection scheme is to protect one moiety (e.g. the alkene or maleimide, Figure 1.5) using a sacrificial dummy of the complementary moiety (e.g. furan). Deprotection simply involves removing the dummy group by retro-cycloaddition and then reacting with the same moiety in its functionalized incarnation. A number of novel materials take advantage of this ease of reversibility of the Diels-Alder adduct, including gels with adjustable crosslink density, self-healing materials, and thermoplastic elastomers.



**Figure 1.5.** A protection/deprotection scheme for Diels-Alder adducts that undergo reversible cycloaddition.

### 1.2.3. Thiol-ene, Thiol-yne, Michael Addition

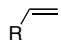
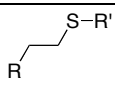
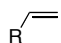
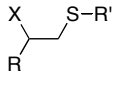
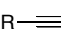
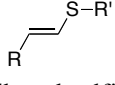
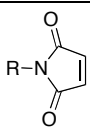
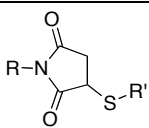
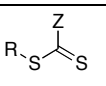
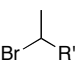
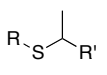
Two of the most recent reactions to be identified with the click chemistry philosophy are the reaction of thiols with alkenes (thiol-ene) and alkynes (thiol-yne) (Table 1.4).<sup>50-52</sup> Reaction of a thiol with a terminal alkene generates an anti-Markovnikov thioester where the sulfur is bound to the less substituted carbon of the alkene. Reaction with a terminal alkyne first generates the monoaddition product of an

alkenyl sulfide, but in the presence of excess thiol, a second addition across the alkene generates a dithioacetal. These thioetherification reactions are most often induced photochemically in the presence of a radical initiator, although they can also be effected thermally.<sup>53</sup> A special case of the thiol-ene reaction is the Michael addition of a thiol to maleimide in the presence of catalytic amounts of base or acid.<sup>54</sup> This rapid room temperature reaction has a high yield under mild conditions.

Thiol-ene and thiol-yne chemistries have been widely used in the bioconjugation community because of the biological availability of thiols in proteins as sites for attaching probes, surface anchors or other analytes. The thiol of the amino acid cysteine is often oxidized and bound to the thiol of another cysteine residue to form a disulfide bridge. Disulfide bridges are some of the only covalent crosslinks between sections of a polypeptide that give stability to the secondary structure of the protein.

In polymer chemistry, thiol-ene and thiol-yne chemistries have become very heavily adopted in recent years because of their chemical compatibility to bridge functional groups present in both material and biological applications.<sup>50,55</sup> Thiol-yne chemistry is also ideal for applications where structural branching is desirable (discussed in Section 1.3.1 below) because of the two-fold addition across the alkyne to form a dithioacetal. As a result, thiol-yne chemistry has been used to generate branched and dendrimeric polymers<sup>56</sup> and networks via photopolymerization<sup>57,58</sup>.

**Table 1.4.** Various thiol-ene and thiol-yne click chemistries.

Components		Adduct	References
	H-SR'		[50] - [53]
Alkene	Thiol	Thioether	
	X-SR'		[50]
Alkene	Sulfenyl halide	$\beta$ -Halothioether	
	H-SR'		[50]
Alkyne	Thiol	Alkenyl sulfide or Dithioacetal	
	H-SR'		[54]
Maleimide	Thiol	Michael addition product	
			[59]
Dithioester	$\alpha$ -Bromide	Thioether	

Just as with azide-alkyne and Diels-Alder cycloadditions, it is advantageous to either protect or activate thiols, alkenes, and alkynes for reaction. Protection of alkynes was discussed in Section 1.2.1, and protection of the maleimide functionality was discussed in Section 1.2.2. A similar approach to that taken with Diels-Alder chemistry (Figure 1.5) is useful when approaching the protection of thiols (Figure 1.6). Oxidation and capping a thiol with itself or with a second inconsequential thiol generates a disulfide that will not undergo thiol-ene or thiol-yne chemistry. Reduction of the disulfide – and release of the sacrificial thiol when applicable – regenerates the original functionality for reaction. Capping with an inconsequential thiol is an ideal way to protect surface bound functionalities because the released thiol is dissolved into solution and can be easily

washed away. Masking the alkene is also possible, but as will be discussed below, the ‘protected’ form of the alkene may be a more highly reactive species than the alkene itself.



**Figure 1.6.** A protection/deprotection scheme for thiol: oxidation to the disulfide and reduction to the thiol.

#### 1.2.4. Other Click Chemistries

In addition to the chemistries described above, the click philosophy has been ascribed to a number of other chemistries, both synthetic and biological. These additional click chemistries are summarized in Table 1.5 and represent an ever-expanding notion of what comprises the toolkit for reliable construction of complex molecular architectures. Although most of these chemistries have not been utilized in this work, understanding their benefits and uses leads to a more full ability to take advantage of the click philosophy. This work relied upon only a limited set of click chemistries, but thinking topologically about click, orthogonality, and chemoselectivity leads to a wellspring of extensions and applications of the concepts presented herein. The chemistries of Table 1.5 can be split into several categories: activated alkene chemistry, activated carboxylic acid chemistry, isocyanate chemistry, and selective non-covalent biological interactions.

The reaction of either an epoxide or an aziridine with a nucleophile is a standard organic chemistry reaction. Each proceeds with or without catalytic acid depending on the strength of the nucleophile, and the product is generally the  $\beta$ -substituted alcohol or

amine. By viewing each as a spring-loaded alkene, however, we can imagine scenarios where the epoxide or aziridine is kept dormant as an alkene and then is activated via epoxidation or aziridination for subsequent reaction with a nucleophile that would not have otherwise reacted with the original alkene. Under somewhat harsh conditions, the alkene may also be activated by oxidation to a ketone or aldehyde and reacted with an O-hydroxylamine or a hydrazide to generate an oxime ether or hydrazone, respectively.

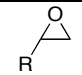
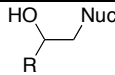
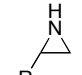
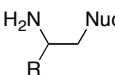
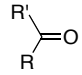
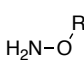
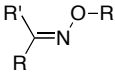
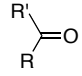
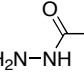
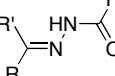
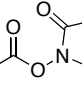
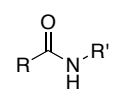
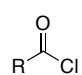
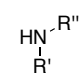
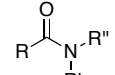
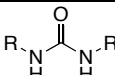
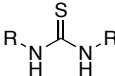
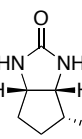
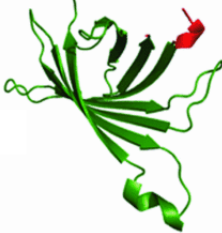

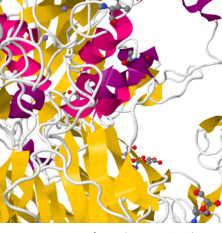
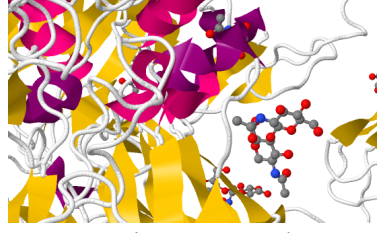
Also well known to organic chemists is the reaction of an activated ester or an acid chloride with an amine. These reactions proceed with very little activation to generate amides, and the reaction does not occur as long as the carboxylic acid is not yet derivatized. Although the aforementioned alkene might be oxidized to a carboxylic acid under harsh conditions, carboxylic acids are prevalent in many natural and some synthetic polymers.

Less prevalent in natural materials are isocyanates and isothiocyanates. These two functional groups readily react with amines or alcohols to generate carbamides (ureas) or thiocarbamides (thioureas) and carbamates (urethanes) or thiocarbamates (thiourethanes), respectively. These reactions are often found in a number of common material applications including paints, coatings, adhesives, and plastics.

The final two entries in Table 1.5 are representative of the very selective non-covalent interactions of some biomolecules, either with a particular moiety like biotin, or with a particular sequence of amino acids such as the arginine-glycine-aspartic acid sequence known by its abbreviated form, RGD. Biotin selectively interacts very strongly with the protein streptavidin, a tetrameric protein consisting of four identical  $\beta$ -barrel subunits (only one subunit is shown in Table 1.5). The RGD sequence, on the other



**Table 1.5.** Additional click chemistries and ‘spring loaded’ reactions.

Components		Adduct	References
 Epoxide	Nuc Nucleophile	 Alcohol	[2], [60]
 Aziridine	Nuc Nucleophile	 Amine	[2], [60]
 Ketone / Aldehyde	 O-hydroxylamine	 Oxime Ether	[2], [60]
 Ketone / Aldehyde	 Hydrazide	 Hydrazone	[2], [60]
 NHS-Ester	H <sub>2</sub> N-R' Amine	 Amide	[2], [60]
 Acyl Halide	 Amine	 Amide	[2], [60]
R-N=C=O Isocyanate	H <sub>2</sub> N-R' Amine	 Urea	[2], [60]
R-N=C=S Isothiocyanate	H <sub>2</sub> N-R' Amine	 Thiourea	[2], [60]
 Biotin	 Streptavidin	 Streptavidin-Biotin complex	[60], [66]
R-Arg-Gly-Asp-R' RGD	 Integrin (αVβ3)	 Integrin-RGD complex	[24], [25], [48], [66], [78], [94]

hand, is a more universal peptide sequence found in a number of adhesive proteins including fibronectin that selectively bind to a site on another protein such as an integrin. The RGD-mediated recognition of fibronectin by integrin at the periphery of the cell facilitates communication between the cell and the extracellular matrix environment by transmitting force two. Although RGD is not the only such binding peptide sequence to have been recognized and integrins are not the only class of proteins known to bind RGD, the RGD-integrin interaction is an exemplar of this type of selective biological non-covalent click chemistry.

### **1.2.5. Applications of ‘Click’ Chemistry**

Specific applications of these many click chemistries will be discussed at length throughout this and subsequent chapters, but the paradigms of how chemists and materials scientists have taken to using click chemistry to date merit discussion.<sup>60</sup> Click chemistry is principally a set of techniques for linking components in a selective, predictable, and high-yielding manner. Click chemistries can be used to link two very incompatible entities that would not normally have been linked in close proximity. Chief among these hybrids are synthetic-biological conjugate materials where one biologically-derived section is linked via a click chemistry to another component that is synthetically-derived.<sup>61</sup> Additionally, pre-functionalization of complex molecules can be followed by click chemistry to attach a precious, expensive, or short-lived moiety that might have gone to waste in low-yielding synthetic steps. For example, CuAAC has been used to join labels such as radiochemical  $^{18}\text{F}$  to biomolecules for use in positron emission tomography (PET) in order to enhance imaging and recognition<sup>62</sup>, and to efficiently

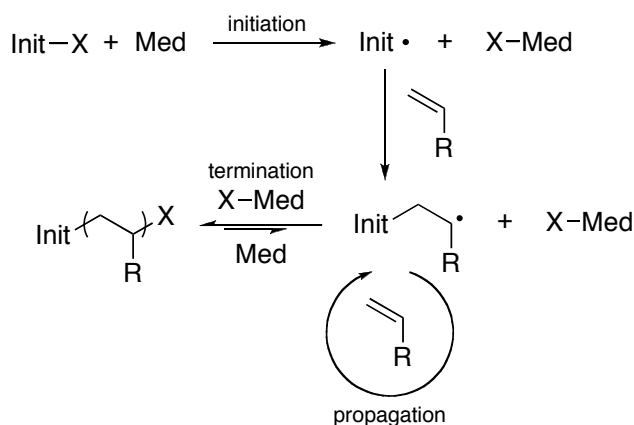
functionalize the surfaces of a large variety of different materials, biomolecules, and nanoparticles with other materials, biomolecules and nanoparticles (Chapter 3).<sup>63,64</sup> Click chemistries have also been used to make, modify, and functionalize a tremendous number of soft materials, including synthetic polymers, biopolymers, and polymer micelles (Chapter 5).<sup>65-68</sup> Click is especially adept at making new materials where it is important to have well-defined linkages to optimize mechanical, electrical or optical properties. To that end, CuAAC has been used to construct complex molecular architectures such as (interlocking) macrocycles that might not have been able to be formed using other synthetic strategies.<sup>69</sup>

### 1.3. Polymers

One of the foremost applications of the click philosophy has been to synthetic polymer chemistry, which is inherently a chemistry of linking together subunits into larger, more complex architectures.<sup>3-5</sup> In order to understand how click chemistry has been applied to the field of polymer chemistry, it is useful to examine the topology of polymer architectures as well as some of the chemistries used to assemble them. Our approach to polymer functionalization relies heavily upon the nature of the connections between units and reliably making those connections in a high yielding, chemically orthogonal manner in keeping with the philosophy of click chemistry.

Two of the most commonly used polymerization techniques for well-defined linear polymer chains with low dispersion are atom-transfer radical polymerization (ATRP) and reversible addition-fragmentation chain transfer polymerization (RAFT).<sup>70-72</sup> Both ATRP and RAFT are living polymerizations since the molecular weight of the

polymer depends linearly on the amount of reaction time. In both cases, the polymer grows from an initiator comprised of a substrate with a leaving group bound by a labile covalent bond (Figure 1.7). When that bond breaks homolytically, the resulting radical on the substrate can add an alkenyl monomer (e.g. an acrylate, styrene, etc.) to generate a new, generally secondary, radical at the growing end. The radical end can either add another monomer to continue to grow the chain, or the leaving group – now bound to a mediating functionality – can return to cap the propagating chain radical and regenerate the labile bond. Because the equilibrium between the chain-bound radical and the terminated chain lies predominantly to the side of the covalent bond, the addition of monomers to the growing chain is accomplished in a controlled manner with a very low probability of radical-radical recombination between two growing polymer chain ends.<sup>73</sup> The living character of the polymerizations is due to this low probability of unintended termination events. In ATRP there is generally a single growing chain employing bromide or chloride as the leaving group, while in RAFT a chain transfer agent – generally a dithioester – alternately acts as a leaving group for one chain while it caps another chain end grown from its opposite side. An understanding of these polymerization mechanisms is necessary to take account of the possibilities for chain end functionalization, monomer orthogonality during polymerization, and what architectures are possible during polymerization including crosslinking and branching.<sup>74-76</sup>



**Figure 1.7.** Generic mechanism for the controlled polymerizations ATRP and RAFT. *Note: throughout the text parentheses are indicative of a polymer though the degree of polymerization has often been omitted for simplicity unless it is instructive.*

### 1.3.1. Polymer Architecture

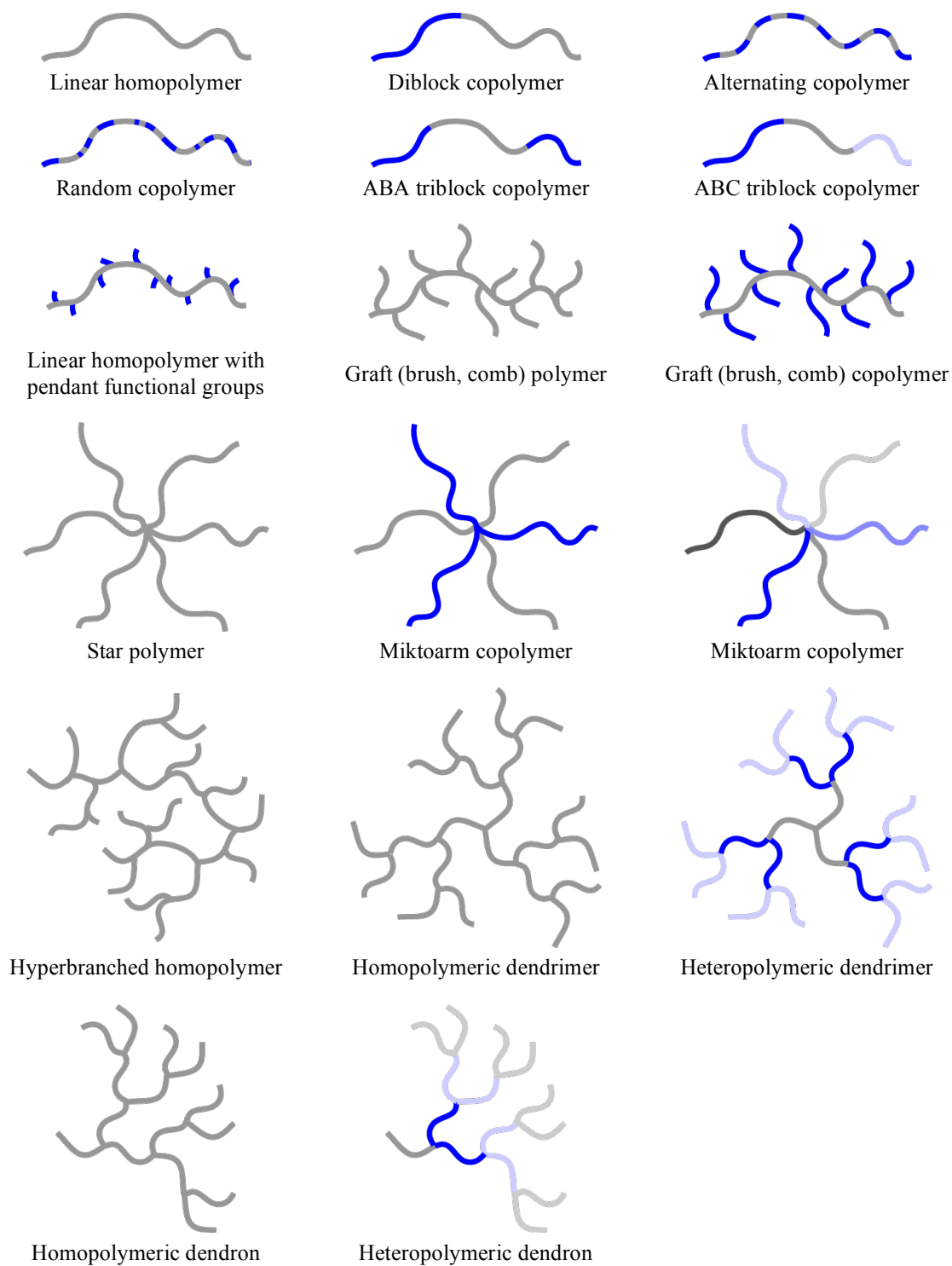
The living character of polymerizations like ATRP and RAFT makes it very easy to imagine complex polymer architectures that result from materials with blocks, regions, or alternating series of monomers joined together in a polymer.<sup>77</sup> From the simplest architecture of a linear homopolymer we can imagine that a sequence of monomers can be varied to include the architectures shown in the first two rows of Figure 1.8. Diblock copolymers are typically polymerized in sequence to generate a single chain with two regions, each made from a monomer that can have similar or very different properties from the monomer comprising the other block. Single chain polymers that alternate between monomers or that vary randomly along the chain have also been developed, in addition to triblock copolymers where the ends may contain the same (ABA) or different polymers (ABC).

Branching out from the linear backbone chains of many polymers are pendant functional groups that imbue a polymer with particular properties, from pH sensitivity to thermal reactivity, and from crosslinkable or degradable functionality to hydrophobic or

hydrophilic functionality. Pendant groups can either be relatively small functional moieties, or else can be polymers themselves grown from – “grafted from” – or attached to – “grafted to” – the backbone (Figure 1.8, third row from top). These two strategies produce polymers that have been given a number of different names including graft polymers, comb polymers, or brush polymers, and the grafts can either be the same polymer as the backbone or a different polymer altogether. A third grafting strategy – “grafting through” – has also been introduced whereby the functional ends of the polymer grafts are polymerized together to form special high-density graft polymers called bottle-brush polymers.

Polymers attached together at some central multifunctional core are called star polymers, and the arms grown from (or attached to) the core can either be the same polymer or different polymers (Figure 1.8, fourth row from top). When the arms are different, the stars are called miktoarm copolymers, and the arms can differ in molecular weight in addition to chemical identity. Polymers can also be assembled into poorly-defined network structures called hyperbranched polymers where there is not a uniform pattern of branching, chain ends, and structure (Figure 1.8, fifth row from top). Polymers with well-defined branching are called dendrimers, and can vary in chemical functionality as they are assembled.<sup>78</sup> If a dendrimeric structure is focused to a single point in a wedge-like structure, then it is called a dendron (Figure 1.8, sixth row from top).

The structures shown in Figure 1.8 are by no means all of the possible single-molecule polymer structures one can imagine, especially considering the possibility for block, alternating, and random linear configurations in each of the graft, star,



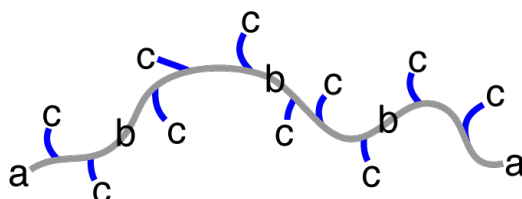
**Figure 1.8.** Cartoons of several polymer architectures constructed from different monomers that are represented by different colored chains.

hyperbranched and dendrimeric polymers. This versatility of construction has given the field of polymer science a wide canvas on which to manipulate the material and chemical properties of polymers. Additionally, when considering how polymers may aggregate, orient, and segregate, the supramolecular possibilities of polymer chemistry are truly profound, and will not be discussed here at any length.

### 1.3.2. Functionalization of polymers

With a basic understanding of the click philosophy and polymer architectures in hand, it is necessary to develop a topological view of polymer chains and how the click philosophy has been adapted to construct each of these structures.<sup>79-82</sup> In order to somewhat limit this perspective, this section will focus predominantly upon the application of azide-alkyne click chemistry to the functionalization of polymers, but it is by no means the only method that has been used to do so. In each example represented below, the azide and alkyne functionalities could – in principle – be replaced pairwise by any of the other functionalities described in Section 1.2 above.

A linear polymer chain is comprised of three distinct regions that are affected by functionalization with azides and alkynes: the chain ends, the backbone, and pendant

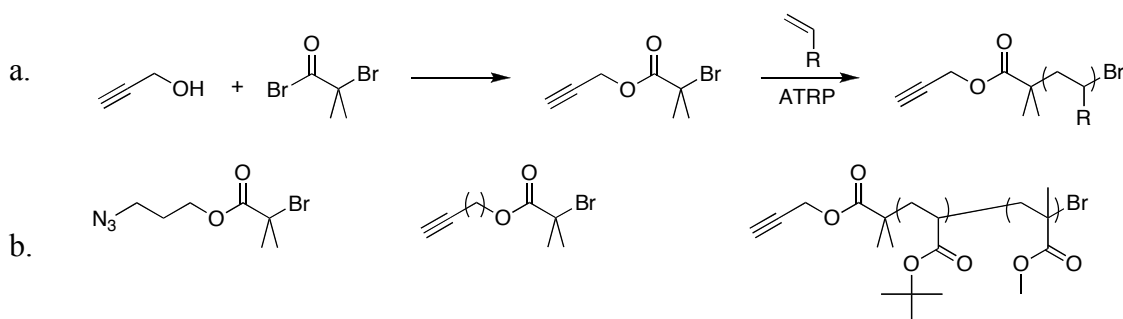


**Figure 1.9.** Generic topology of a linear polymer chain composed of chain ends (a), a backbone (b) and pendant groups (c) attached to the backbone.

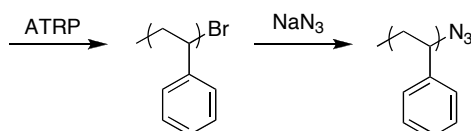


groups (Figure 1.9). Of these three, the CuAAC functionality in the backbone stands apart because it is the result of an azide-alkyne cycloaddition, bearing the triazole as the linkage between monomers. As was discussed above, this linkage is analogous to amide bond formation in peptides, and poly(triazoles) have been reported to result from the polymerization of either homobifunctional monomers ( $A_2 + B_2$ ) or heterobifunctional monomers (AB).<sup>83</sup>

There have been a vast number of schemes to modify polymer chain ends, and each depends greatly on the functional groups present as a result of the polymerization method. For the living polymerizations ATRP and RAFT, the initiator and leaving group determine the chain end functionality, whereas other polymerization techniques deposit other functionalities at the chain ends. ATRP is especially versatile because the ATRP initiator can be pre-functionalized with a compatible moiety that must only be orthogonal to the ATRP mechanism in order to be present on the polymer chain end.<sup>83,84</sup> A typical ATRP initiator is a bromoisobutyryl derivative formed from base-promoted condensation of bromoisobutyryl bromide with an alcohol or amine (Figure 1.10), and both azide and alkyne functional initiators have been shown to be orthogonal to ATRP.<sup>85,86</sup> A serendipitous benefit of ATRP is that the leaving group bromide is easily converted to an azide by reaction with sodium azide, but the bromide has also been converted into a nitroxide, biotin, pyrene, or difunctional branch, to name a few.<sup>87,88</sup>



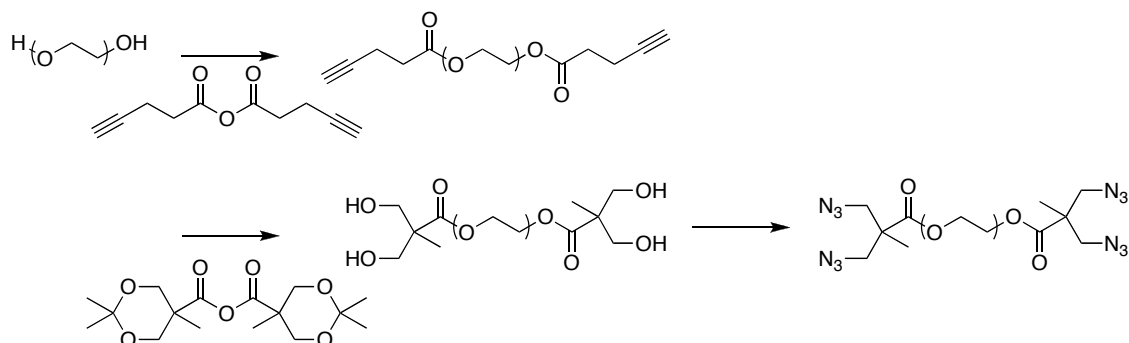
**Figure 1.10.** (a) Condensation of propargyl alcohol with bromoisobutyryl bromide and subsequent polymerization by ATRP. (b) (from left to right) An azido-functional ATRP initiator, an alkynyl functional ATRP initiator, and an  $\alpha$ -alkynyl, $\omega$ -bromo-PtBA-b-PMMA block copolymer by ATRP.



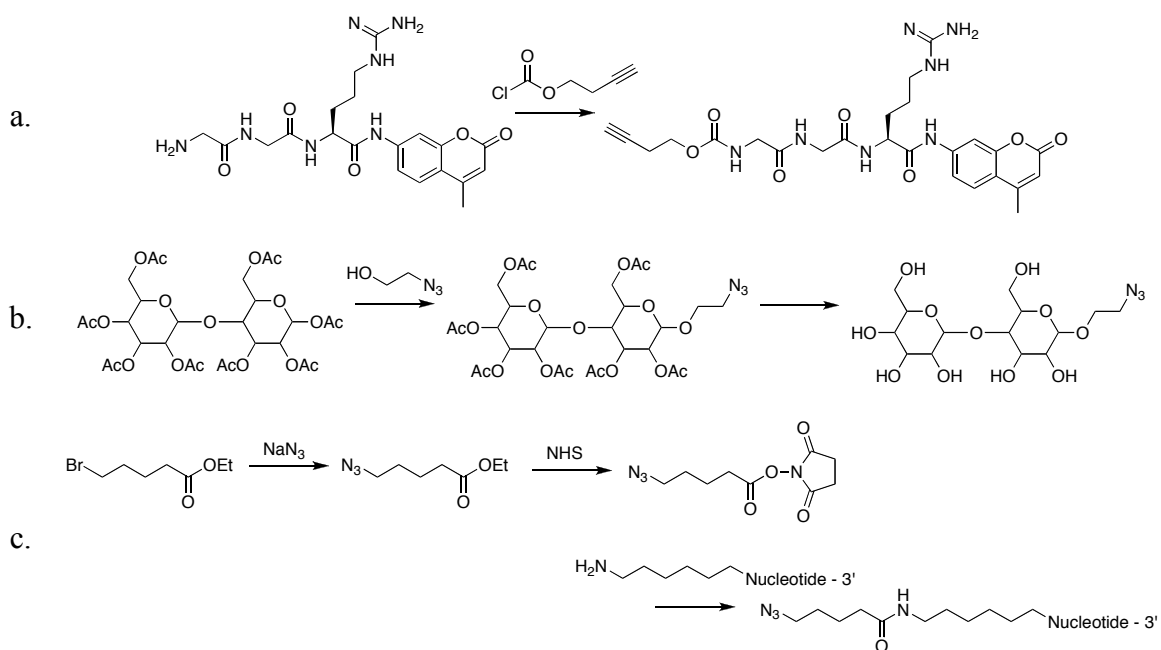
**Figure 1.11.** Conversion of an ATRP-polymerized polystyrene bromide end group into terminal azide by reaction with sodium azide.

Polyethylene glycol (PEG), a polymer that is not polymerized by ATRP, has also been end-functionalized with alkynes and azides. One technique to do so is to react telechelic hydroxy-terminal PEG with symmetrical anhydrides to directly link an alkyne to both ends, or to use an acetal anhydride to install twice as many azides at the ends as there were alcohols initially (Figure 1.12).<sup>89</sup> In addition to the anhydride coupling, traditional carbodiimide coupling (DCC, EDC) can be used with alkynyl- and azido-carboxylic acids to generate telechelic alkynyl- and azido-polymers from telechelic hydroxy-terminal polymers. Natural polymers can be derivatized similarly depending on their end groups: amines and carboxylic acids of polypeptides, alcohols and protected-alcohols of polysaccharides<sup>21</sup>, and phosphates and alcohols of polynucleotides. In these cases, functionalization has been accomplished using similar coupling strategies such as

alkynylchloroformate derivatives, traditional carbodiimide coupling, or activated ester coupling to an amine<sup>22</sup> (Figure 1.13).<sup>68</sup>

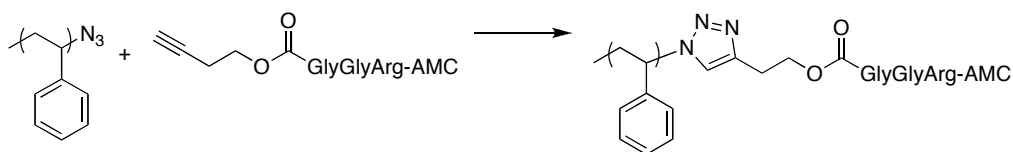


**Figure 1.12.** Functionalization of bis-OH-terminal polyethylene glycol with alkynes and azides by condensation with symmetrical anhydrides.



**Figure 1.13.** (a) Chain end functionalization of an oligopeptide by butynyl chloroformate. (b) Chain end functionalization of an acetoxy-protected disaccharide by coupling with azidoethanol followed by deprotection. (c) Chain end functionalization of an amine-terminated polynucleotide by NHS-ester-activated azide.

Once a polymer is end-functionalized with a particular click moiety, it is readily apparent that subsequent reaction with any number of complementarily functionalized molecules – including other polymers – may yield a desirable coupling product. An example is shown in Figure 1.14 where the coupling of an azide-terminal polystyrene (Figure 1.11) and an alkyne-terminal oligopeptide (Figure 1.13) forms a synthetic-biopolymer hybrid material.<sup>61</sup> It is readily apparent that the triazole adduct of the azide and alkyne is present in the polymer backbone of the newly formed hybrid material.

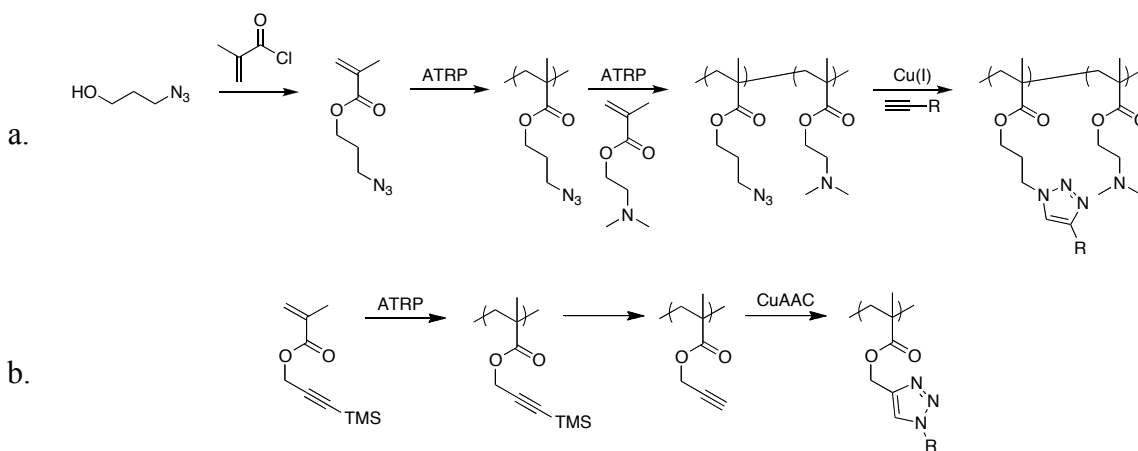


**Figure 1.14.** Azide-alkyne coupling of an azido-terminal polystyrene (Figure 1.11) with an alkyne-functional oligopeptide (Figure 1.13a) to generate a synthetic-biopolymer hybrid.

In addition to functionalization of linear polymers on the backbone and at the chain ends, many polymers have been click functionalized at pendant moieties covalently bound to the backbone.<sup>83</sup> Depending on the monomers used to form the polymer, click functionalities can either be present directly as a result of polymerization, or can be added using orthogonal chemistry post-polymerization.

Azide-functional monomers are ideal for incorporation during polymerization because the azide is orthogonal to ATRP in its reactivity.<sup>90</sup> Figure 1.15a shows the synthesis of an azide-functional monomer via condensation of an azido alcohol with an acid chloride to yield a methacrylate with a pendant azide.<sup>91</sup> Subsequent ATRP yields a block of poly(methyl methacrylate) (PMMA) with the pendant azide before a second ATRP step incorporated a block of dimethylamino-functional PMMA. Finally, post-

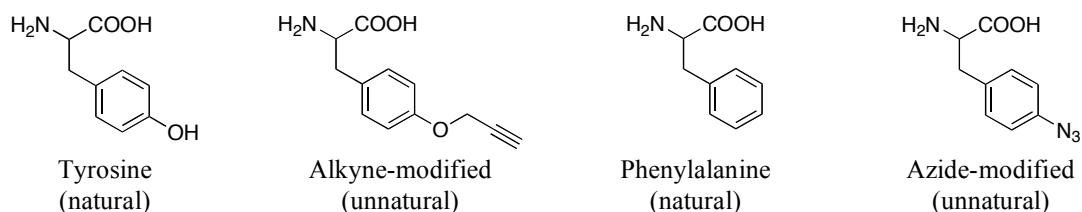
functionalization of the polymer by CuAAC with an alkyne functional group yields a polymer with functionalized pendant groups. More care must be taken, however, to retain an alkyne when polymerizing an alkyne-functional monomer; ATRP can add across a triple bond to yield a polyacetylene. To that end, Figure 1.15b shows that a TMS-protected alkyne-functional methacrylate was polymerized by ATRP where the TMS group protects the alkyne from polymerization.<sup>92</sup> Post-polymerization deprotection of the TMS groups along the polymer chain yields PMMA with pendant alkynes.



**Figure 1.15.** (a) Synthesis of an azide-functional methacrylic monomer followed by two sequential ATRP steps and CuAAC to generate a diblock copolymer with pendant R groups attached via triazole linkages. (b) ATRP of a TMS-protected alkyne-functional methacrylic monomer followed by deprotection to yield a polymer with pendant alkyne functionality.

CuAAC functional biopolymers have also been synthesized *in vivo* via natural biosynthetic pathways.<sup>93</sup> The unnatural amino acids in Figure 1.16 are a propargyl ether modified tyrosine (left) and an azide modified phenylalanine (right). The minor changes to the natural amino acid structures do not inhibit incorporation of these unnatural amino acids in the resulting peptide, though the unnatural amino acids may affect protein folding and secondary structure relative to the native protein. Once biosynthesized in

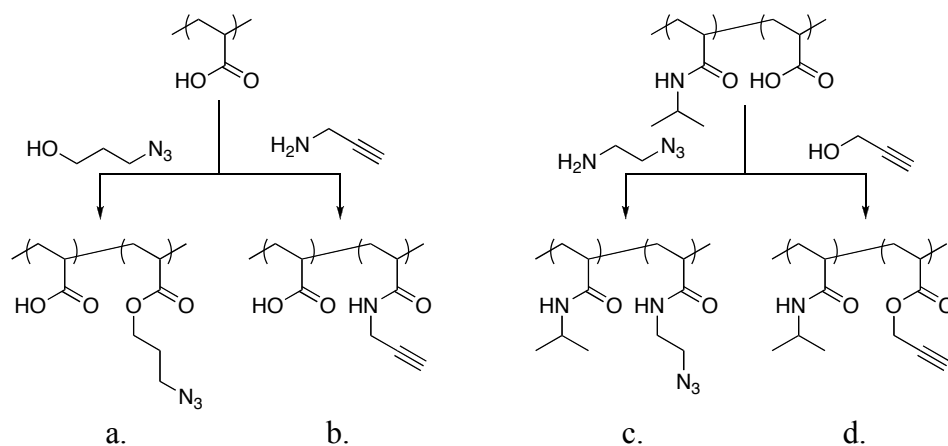
yeast, for example, alkyne- or azide-functional proteins have been tagged with any number of reporters, including dyes and fluorophores, biotin, or TEMPO to study processes occurring in cells.



**Figure 1.16.** Natural amino acids and unnatural amino acid derivatives for the biosynthesis of CuAAC functional peptides.

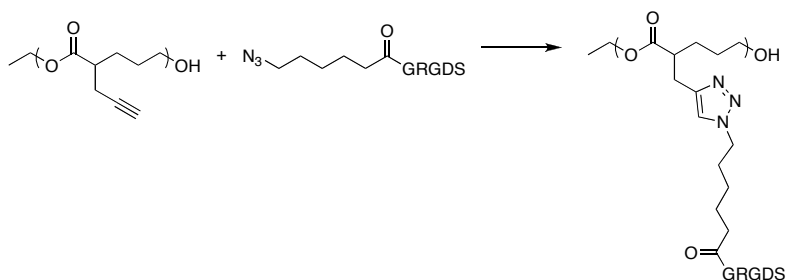
A polymer with functional sidechains can also be derivatized in a straightforward manner with azide- or alkyne-functional molecules depending on the functionality of the polymer and its orthogonality to the azide and alkyne. Polymerization of acrylic acid monomer yields a polymer with easily functionalizable carboxylic acids pendant to the backbone. Figure 1.17 shows the functionalized products of a poly(acrylic acid) (PAA) homopolymer (a, b) and copolymer (c, d) achieved through standard carbodiimide coupling with azido- and alkynyl- alcohols and amines. The degree of functionality of the PAA can be tuned by adding sub-stoichiometric amounts of the alcohol or amine to yield greater or fewer functional groups randomly along the polymer chain.

Once a polymer has been functionalized with a click moiety, the possibilities for subsequent functionalization are limited only by chemical orthogonality and the imagination. Conjugation to pendant moieties along a backbone can generate variable densities of functional groups depending on the original composition of the polymer. Figure 1.18 shows the functionalization of a polyvalerolactone bearing pendant alkynes at



**Figure 1.17.** Post-polymerization modification for azide- and alkyne-functionalized poly(acrylic acid) and poly(N-isopropylacrylamide-co-acrylic acid).

each repeat unit of the polymer by an azide-functional oligopeptide containing the RGD peptide sequence.<sup>94</sup> The high density of RGD groups in the resulting hybrid polymer were intended to facilitate the attachment of cells via the RGD-integrin coupling described in Section 1.2.4 above. Conductive polymers have also benefited from the functionalization of pendant azides and alkynes to afford materials with more desirable properties for various electronic applications. Polyhexylthiophenes with pendant azide and alkyne groups have been CuAAC functionalized with fluorinated sidechains for increased hydrophobicity<sup>95</sup>, fluorophores for visualization<sup>95</sup>, and naphthalimides for electrically conductive films with advantageous photophysical properties<sup>96</sup>. In each case, the target side chains are too fragile to have survived the initial polymerization conditions, so a post-polymerization strategy is ideally suited to generating these types of materials.



**Figure 1.18.** Functionalization of a polyvalerolactone with pendant alkynes by azide-alkyne reaction with an azide-terminal RGD oligopeptide for cell adhesion.

The preceding discussion focused on the use of azide-alkyne cycloaddition chemistries to synthesize, modify, and functionalize polymers, but it is important to recognize that the strategies presented have also been applied using other click systems. Cu-free click between a bis-nitrile N-oxide and bis-alkyne has been used to polymerize materials ( $A_2 + B_2$ ) where the isoxazole adduct is a constituent of the polymer backbone.<sup>40</sup> Bulk PMMA with pendant furans has been crosslinked by bis-maleimide small molecules for self-healing applications<sup>97</sup> while DNA with pendant norbornenes has been functionalized by tetrazine dienes<sup>47</sup> or nitrile N-oxides<sup>48</sup> for fluorescent tagging and affinity labeling. Pendant and end-functional alkenes resulting from several types of polymerizations – ATRP, RAFT, and ring-opening polymerization (ROP) – have also been functionalized post-polymerization using thermal and photochemical thiol-ene chemistry to generate a wide array of functional materials.<sup>53</sup> Though the predominant use of the click philosophy in polymer chemistry has been for post-polymerization functionalization of synthetic and natural polymers, there is a growing literature on the use of click as a polymerization technique in and of itself.<sup>83</sup>

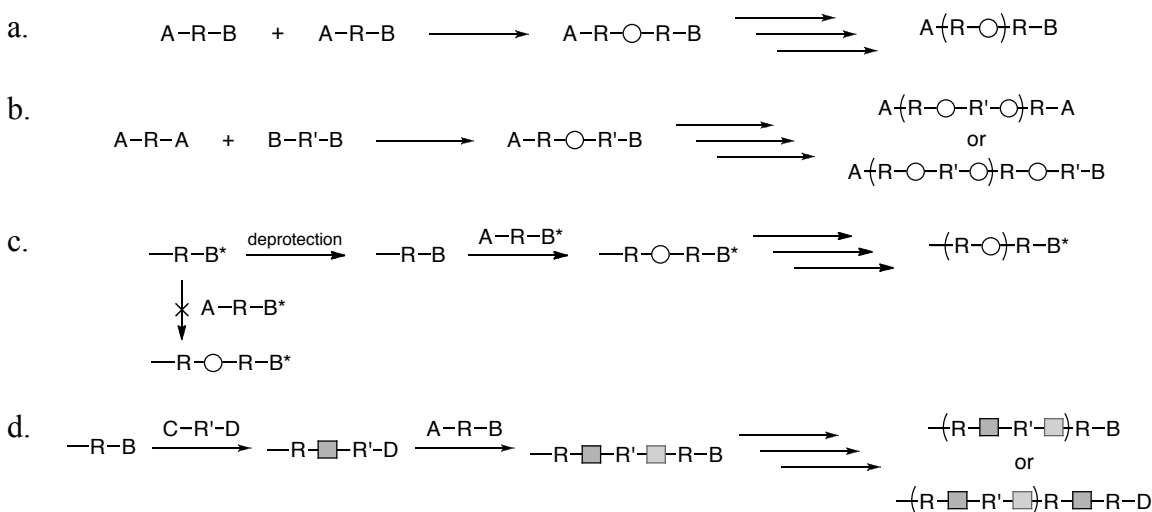
Furthermore, although the preceding discussion focused on the use of click chemistries for the modification of linear polymers, the same strategies apply to the



synthesis of non-linear structures, such as hyperbranched polymers, dendrons, and dendrimers.

### 1.3.3. Heterobifunctional Monomers and Polymers

One of the keys to the growing use of the click philosophy as a polymerization scheme is the synthesis of heterobifunctional monomers and polymers. The number of requirements for heterobifunctional molecules used in polymer synthesis is proportional to the level of desired control over the final polymer architecture.



**Figure 1.19.** Condensation polymerization schemes: (a) AB. (b) A<sub>2</sub> + B<sub>2</sub>. (c) AB\*. (d) AB + CD. The circle represents the adduct of A and B while the squares represent the adducts of B and C or A and D.

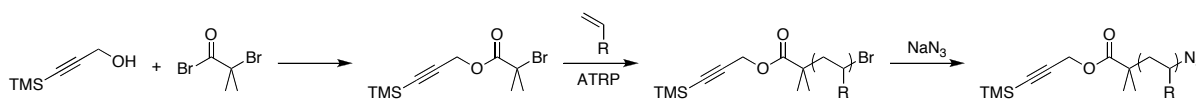
Foremost, heterobifunctional molecules must have two different reactive groups (A and B). If A and B are complementary, that is, if they will react with each other, then AB functional molecules can produce a polymer by the sequential addition of A's to B's, and B's to A's (Figure 1.19a). AB condensation polymerization contrasts with another variety of condensation polymerization, A<sub>2</sub> + B<sub>2</sub>, where difunctional molecules – each with one type of complementary reactive group or the other – react to form the polymer

(Figure 1.19b).<sup>98</sup> Additional variations of this type of condensation using molecules with higher functionalities have also produced  $A_3 + B_2$  branched and hyperbranched polymers.

In cases where a higher degree of control and/or precision over the polymer architecture is warranted, two main strategies have been developed to restrict the uncontrolled addition of AB units. The first strategy relies upon protected or latent functional groups that cannot undergo reaction until they have been deprotected or activated. In order to grow polymers using this controlled technique, each protected monomer ( $AB^*$ ) must be added to the reactive end group and deprotected before the next protected monomer in the sequence can be integrated (Figure 1.19c).<sup>99,100</sup> The literature on this strategy is extensive, especially for the synthesis of biopolymers such as oligopeptides, but the  $AB^*$  strategy has also been used to grow synthetic poly(caprolactone)s<sup>99</sup> and poly(fluorene)s<sup>100</sup>, each up to the 64-mer. The second strategy to control the addition of monomers has been to use two orthogonal chemistries in an AB + CD scheme (Figure 1.19d). By judiciously selecting functionalities that will only react with a complementary functionality – B only reacts with C, D only reacts with A – polymers are grown by alternating the addition of AB molecules and CD molecules without the need for protecting groups and deprotection steps.

Though this approach has most often been used with small molecule monomers, it can also be used with end-functional polymers to make heterobifunctional macromonomers. These asymmetrical telechelic polymers, also known as  $\alpha,\omega$ -heterobifunctional polymers, can act in the same way as the small molecule heterobifunctional monomers to generate block copolymers with highly complex sequences of blocks. Because it is possible to vary any number of parameters of the

polymer in a controlled manner (molecular weight, sequence, tacticity, or side chain functionality), the constructed multi-block copolymer can be more highly complex than would be possible using conventional polymerization schemes alone. Additionally, the adducts of such a scheme can reach increasingly high total molecular weights.



**Figure 1.20.** Synthesis of a generic  $\alpha$ ,azide- $\omega$ ,TMS-alkyne heterobifunctional polymer by ATRP.

ATRP is ideally suited to generating  $\alpha,\omega$ -heterobifunctional polymers for use with azide-alkyne chemistry in terms of the AB\* methodology presented above. Synthesis of a TMS-protected alkyne ATRP initiator is easily accomplished by the triethylamine-promoted condensation of 3-(trimethylsilyl)-prop-2-yn-1-ol with  $\alpha$ -bromoisobutyryl bromide (Figure 1.20). ATRP under standard conditions is followed by the conversion of the terminal bromide to azide by stirring with sodium azide in N,N-dimethylformamide. The resulting  $\alpha$ ,azide- $\omega$ -TMS-alkyne polymer is then topologically equivalent to an AB\* small molecule, where the heterobifunctional end groups are connected by a polymer.

To this point, the discussion has primarily focused on the functionalization of linear polymers, but each of the strategies above can apply to non-linear architectures as well: branched, hyperbranched, dendrimeric, and even macrocycles.<sup>101,102</sup> In those cases the distinctions between a chain end and a pendant group are less clear, however, the chemistries used to modify the polymers are the same. Chapter 5 will revolve around the

synthesis of molecules to generate these more complex architectures while retaining control over connections by using click chemistries.

#### **1.3.4. Macroscopic Polymer Modification – Bulk and Surfaces**

Stepping away from the molecular perspective of polymers to a macroscopic material perspective, a tremendous number of post-polymerization polymer modification techniques have been developed, and they can roughly be divided into two categories: bulk modifications and surface modifications. Bulk modifications – crosslinking, swelling, and UV curing<sup>103</sup>, for example – are affected throughout the entire polymeric material. Surface modifications, however, are those that are limited to the interface between the polymer and its environment. Examples of surface modifications include ozonolysis (and other self-limiting surface reactions), surface-initiated polymer brush growth, grafting to a polymer surface, adhesion, and self-healing. Bulk and surface modification reactions are crucial in order to tune the material properties of a polymer without requiring alterations to its synthesis. Some modifications, in fact, cannot be accomplished during a polymerization, and can only be accomplished afterwards.

One of the primary reactions undertaken on bulk polymeric materials is to crosslink polymer chains. Crosslinking can be accomplished during polymerization – using a bifunctional monomer – or after polymerization – as a result of some external stimulus. Crosslinking during polymerization is preferable when preparing a polymer for which the material properties will be known given a certain set of synthetic conditions. This approach is often used industrially to generate large quantities of polymer where the goals of uniformity and quality have dictated consistent synthetic recipes. Crosslinking

after polymerization, however, gives the laboratory engineer an opportunity to tune the properties of a polymer without resynthesizing the polymer.<sup>104</sup> In situations where it is desirable to alter material properties such as elastic modulus, swellability, or thermoplasticity, post-polymerization crosslinking may be a more appropriate route to optimizing a material for subsequent applications.

Surface modifications can, in principle, also be undertaken during polymerization or afterwards. Specific functionalities, sidechains, or endblocks that self-segregate to a surface can be included on each chain during polymerization, thereby inducing reorientation and effective surface functionalization. This approach, however, can leave residual functionalities in the bulk of the material, and so is not ideal in situations when it is desirable to retain a bulk polymer with particular properties and only change the surface. In instances where selective surface-functionalization is required, the polymer surface must often be pre-functionalized by oxidative degradation or else coated with a material containing some functionality that effectively binds to the surface. Oxidation of a polymer is often not feasible because it is not possible to control the degree to which the polymer structure is degraded. Coatings, in contrast, are often specific to the material they intend to cover. Coatings are also often held in place either by physical adsorption or by reacting with a particular functional group of the polymer. Because of the range of surface and bulk properties of polymers – hydrophilicity, hydrophobicity, elasticity, deformation, etc. – finding a coating to permanently attach to a specific polymer surface without chipping or flaking can be difficult; finding a coating to permanently attach to and functionalize *any* polymer surface is therefore quite a challenge.

It is the notion of ‘universality’ of polymer synthesis and modification that is the goal of Chapters 2 and 3. Chapter 2 demonstrates an approach to bulk polymer modification that is intended to crosslink any polymer chains irrespective of their chemistry, while Chapter 3 demonstrates an approach to polymer surface modification that is intended to functionalize any polymer surface irrespective of its chemistry. Both of these approaches rely upon photochemical methods to activate functionalization in a *universal* manner.

#### **1.4. Photochemistry for Polymers**

Photochemical methods are some of the most versatile techniques for both synthetic and natural polymer modification. Photochemistry has long been used in synthetic chemistry as a means of applying or removing protecting group functionalities<sup>105</sup>, and it has been used in biochemistry for affinity labeling of proteins<sup>106</sup> and for the cleavage of synthetic peptides from substrates<sup>107,108</sup>. The synthetic polymer community takes cues from the biochemistry community on ways to creatively adapt photochemistry to the modification and functionalization of polymers. Although photochemical methods have long been used as the initiation step in numerous types of polymerizations, photochemistry has moved past simply being a source of radicals. New implementation of photoactive groups allows polymeric materials to interact with their environment, to change properties as a result of stimulus by light, and to be activated and differentiated (e.g. patterned) using photons.

Just as click functionalities have been incorporated into the architecture of polymers – as end groups, along the backbone, pendant, etc. (Section 1.3.2) – photoactive

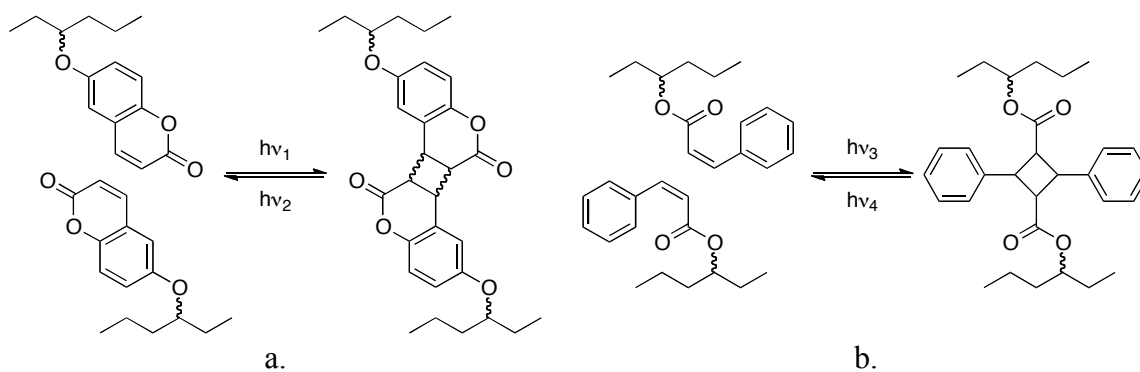
moieties have also been built into polymers at the same positions. Photoactive groups are just latent functionalities, protected by the absence of photons. Once irradiated, the photoactive groups act in a predictable way to functionalize, degrade, or activate the polymer. Light has already been seen to activate the ‘photoclick’ reaction between an alkene and a tetrazole (Section 1.2.2) and to induce thioetherification in thiol-ene and thiol-yne chemistries (Section 1.2.3), but below are several additional examples of how photochemistry has been used effectively to modify polymers.

#### **1.4.1. Polymer Crosslinking by Photochemistry**

Conventional crosslinking of polymers is achieved either during polymerization or in an indiscriminate matter following polymerization. Inclusion of a difunctional monomer (e.g. a diacrylate) during polymerization causes polymer chains to add through both ends of the same molecule, thereby forming a junction where the two chains are covalently linked together. The degree of crosslinking is determined by the relative ratio of the difunctional monomer to the monofunctional monomer used in the polymer synthesis. This type of crosslinking is common when forming bulk crosslinked polymers, especially for applications where the polymer is intended to swell or requires mechanical toughness or elasticity. Post-polymerization crosslinking can also be achieved via ultraviolet (UV) curing of a polymer.<sup>103</sup> UV light is absorbed by the polymer, which causes some of the covalent bonds in the polymer to break. The resultant radicals recombine with other radicals to form crosslinks between different polymer chains, or even to form interlocking loops of the same polymer chain. It can be difficult to control the extent of crosslinking by UV curing, and the crosslinks are not necessarily uniform in

chemical composition. Unless some additional functionality is built into the polymer backbone or the difunctional monomer, the crosslinks in both cases are irreversible.

It is often desirable, however, to have a polymer that can crosslink on demand, and it is even more desirable if the separation of those crosslinks can be controlled on demand. Two exemplar systems of this type are shown in Figure 1.21. Each relies upon the photoinduced [2+2] cycloaddition of substituted alkenes to form a cyclobutane derivative. This highly strained cyclobutane can be stable, but irradiation still leads to a photoinduced retro-[2+2] cycloaddition to regenerate the initial moieties. Both coumarins and cinnamoyl moieties are known to undergo this reversible photoinduced reaction, and have been included in polymer backbones and also pendant to the backbone as shown. When the [2+2] adduct is included in a polymer backbone, the entire structure of the polymer can be quickly degraded under irradiation, and when the free functionalities are pendant, the polymer can be crosslinked and un-crosslinked by irradiating with different wavelengths of light.

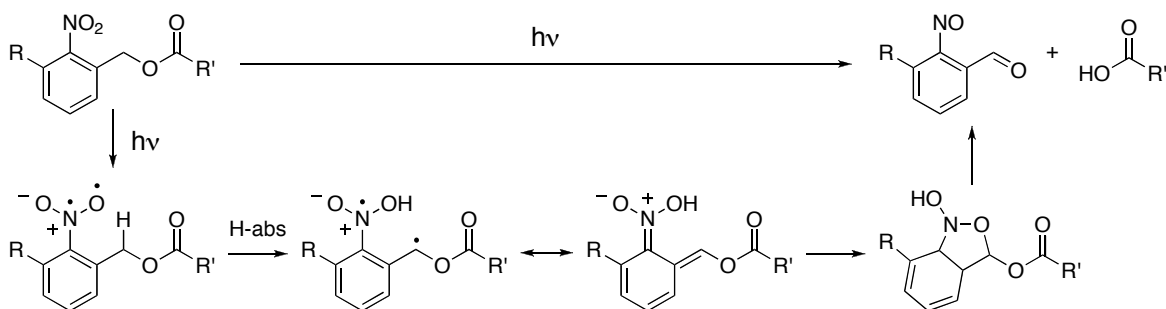


**Figure 1.21.** Reversible polymer photocrosslinking by the [2+2] cycloaddition of (a) pendant coumarins and (b) pendant cinnamoyl groups.



### 1.4.2. Photodegradable Linkages in Polymers

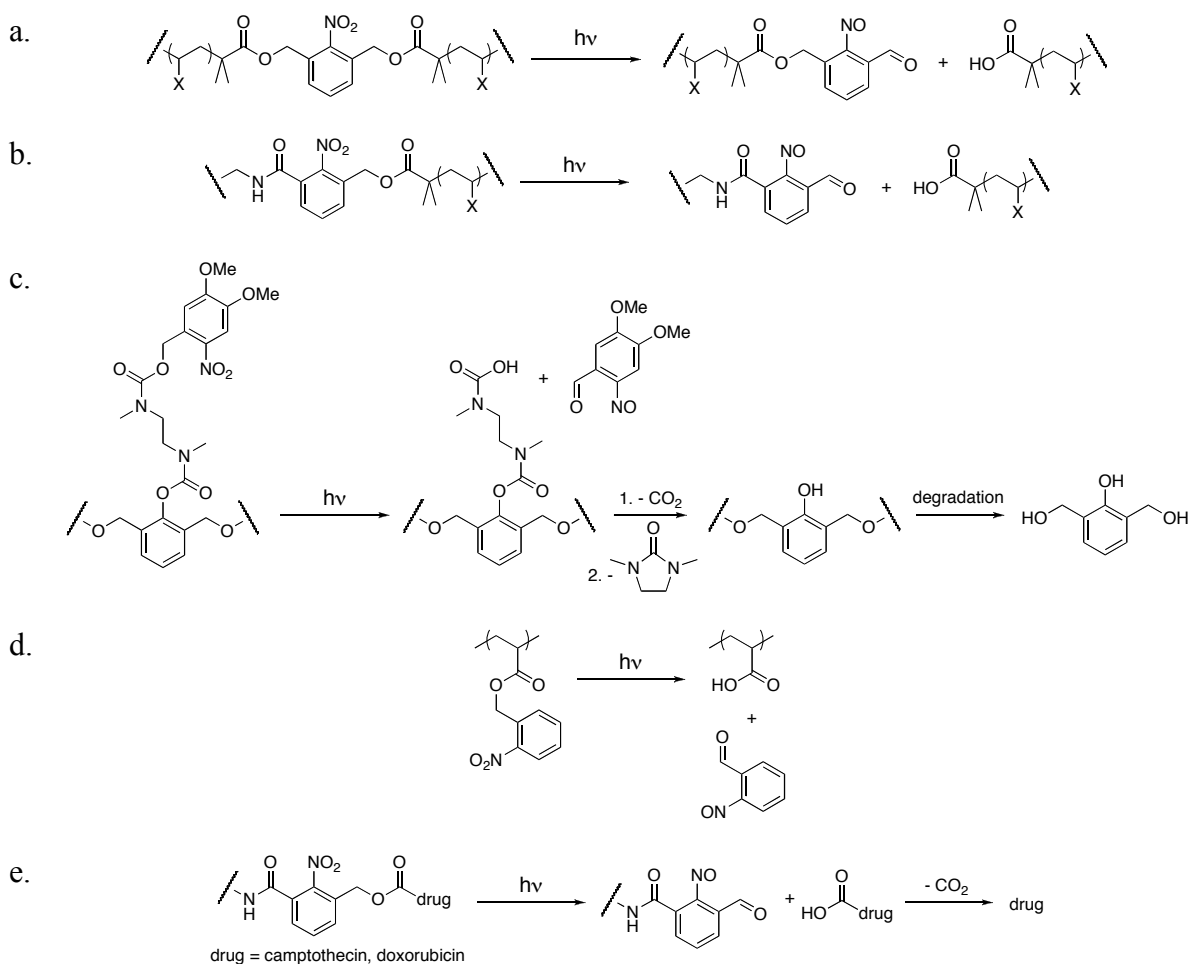
Not all photoactive moieties included in polymers lend reversible properties however. A number of photodegradable polymer systems have been developed that rely upon light to break apart a polymer structure or else to release a bound molecule from the polymer. The photocleavage of an ortho-nitrobenzyl (ONB) ester – also known as an ortho-nitrobenzyloxycarbonyl (NBOC) – serves as an exemplar for the role of photodegradable units in polymers (Figure 1.22).<sup>109</sup> When irradiated, a nitrobenzyl diradical is generated that abstracts a proton from the  $\alpha$  carbon in the ortho position relative to the nitro group. Following cyclization to a unstable five-membered ring and subsequent rearrangement, a nitrosoaldehyde and a carboxylic acid are released as the cleavage products of the ONB ester. The ONB moiety has been used extensively as a protecting group not only for carboxylic acids as shown, but also for alcohols, amines, and amides.<sup>105,110,111</sup> When the ONB group is installed via a carbonate or carbamate linkage, degradation is typically accompanied by loss of  $\text{CO}_2$  to form an alcohol or amine. Furthermore, substituents bound to the benzyl ring can shift the excitation wavelength and can be manipulated to tune the conditions under which deprotection or cleavage occurs.<sup>112,113</sup>



**Figure 1.22.** Mechanism of the photocleavage of an ortho-nitrobenzyl ester to form a nitrosoaldehyde and a carboxylic acid.

In polymers, ONB groups have been used at various positions in polymer architectures to selectively degrade polymer networks<sup>114</sup>, to cleave polymer brushes from surfaces where they were grown<sup>107,108</sup>, to modify the physical properties of polymers, and to release bound drugs<sup>115</sup>. Figure 1.23a shows how a polymer network constructed from symmetrical chains containing a central ONB group are degraded to yield polymer chain segments with half the molecular weight of the precursor polymer.<sup>114</sup> Depending on the functionality of the end junction used to construct the network (typically tri- or tetra-functional), the actual molecular weights of the fragments were integer (3 or 4) multiples of half of the precursor molecular weight. In order to release entire chains from a star polymer, or else to degrade a polymer into asymmetric units, the end-functional ONB polymer was also synthesized (Figure 1.23b). An ONB pendant to a polyester can induce full degradation of the polymer backbone in the self-immolative process shown in Figure 1.23c.<sup>116</sup> After cleavage of the ONB and formation of the nitrosoaldehyde, loss of carbon dioxide is followed by formation of a cyclic urea in a cascade-type reaction. Chain backbone cleavage is induced by the resulting phenolic moiety to fully degrade the polymer backbone.

ONB's pendant to a polymer backbone can also generate functionality when irradiated. Figure 1.23d shows a simple example of the deprotection of a pendant carboxylic acid by irradiation to remove the ONB. The resulting polymer – poly(acrylic acid) (PAA) – is a very hydrophilic polymer owing to the carboxylic acid, whereas the precursor polymer was significantly more hydrophobic. Changes in surface properties such as hydrophilicity/hydrophobicity are commonly manipulated using



**Figure 1.23.** Photocleavage of ortho-nitrobenzyl groups: (a) in the center of a polymer backbone; (b) at the chain end of a polymer; (c) to induce degradation of a polymer chain; (d) to deprotect a pendant carboxylic acid and form poly(acrylic acid); and (e) to release a covalently bound drug molecule.

photodeprotection strategies because of the desire to pattern regions of a surface using light; the benefits to patterning using light are discussed in Section 1.4.3 below.

Finally, ONB's have been used to release drugs by breaking covalent attachments to polymeric materials.<sup>115</sup> Pharmaceutical drugs are often delivered into the body as salts of the active compound because the salt is easier to isolate and work into solid form (e.g. pills). Figure 1.23e demonstrates how cleavage of an ONB carbonate or carbamate releases a drug (camptotecin or doxorubicin) in its native state, without the need to make it a salt. Irradiation of the pendant ONB releases the drug as a carbonic or carbamic acid,

followed by loss of carbon dioxide to generate the drug with its native alcohol or amine, respectively.

### 1.4.3. Patterning

Throughout the following chapters, additional examples of the use of photochemistry to modify polymer architectures will be discussed, however, one particular application – patterning – deserves mentioning because it is a technique that employs photochemistry to localize the effects of an external stimulus. Whereas changes in temperature, pH, and shape are generally applied to a bulk material as a whole, the application of light can easily be restricted to particular areas of a material via irradiation through a photomask. This ability to pattern a material with light allows the engineer a large range of control over the material properties of a polymer. Although the polymer chemist is typically concerned with establishing domains of chemical functionality within the polymer chain, macroscopic domains larger in size than the polymer itself can be delineated as a result of photopatterning. For example, photopatterning can selectively crosslink polymers with pendant coumarin groups (Figure 1.21) to generate regions of stiff, crosslinked polymer chains and regions of flexible, uncrosslinked polymer chains. Photopatterning can selectively deprotect pendant ONB's to generate hydrophilic PAA regions in contrast to hydrophobic regions of unprotected ONB for deposition and reaction of water-soluble analytes (Figure 1.23d). Photopatterning can also selectively induce 'photoclick' reactions between an alkene and a tetrazole (Table 1.3) or thiol-ene and thiol-yne reactions (Table 1.4) within a polymer scaffold to selectively attach molecules only to particular regions. Chapter 3 will take up the notion of patterning and

further develop it within the context of the application of the click philosophy to polymer surfaces.

## 1.5. Summary

- The ‘click’ philosophy is one of linking components together and manifests in many different combinations of chemical functionality.
- The ‘click’ philosophy is ideally suited to polymer synthesis, which is also a chemistry of linking together components regardless of whether the polymer is natural, synthetic, or a combination.
- Protection and activation schemes are crucial to controlling the extent of high-yielding ‘click’ reactions.
- Polymers can essentially bear functionalization at three distinct positions: chain ends, along the backbone, and pendant to the backbone. ‘Click’ chemistries have been used at each position.
- Bulk polymers and polymer surfaces have been photochemically modified in numerous ways via crosslinking, photodegradation, and patterning.

## 1.6. References

---

1. Ober, C. K.; Cheng, S. Z. D.; Hammond, P. T.; Muthukumar, M.; Reichmanis, E.; Wooley, K. L.; Lodge, T. P. Research in Macromolecular Science: Challenges and Opportunities for the Next Decade. *Macromolecules* **2009**, *42*, 465-471.
2. Kolb, H. C.; Finn, M. G.; Sharpless, K. B. Click Chemistry: Diverse Chemical Function from a Few Good Reactions. *Angewandte Chemie International Edition* **2001**, *40*, 2004-2021.
3. Qin, A.; Lam, J. W. Y.; Tang, B. Z. Click Polymerization: Progresses, Challenges, and Opportunities. *Macromolecules* **2010**, *43*, 8693-8702.
4. Golas, P. L.; Matyjaszewski, K. Marrying click chemistry with polymerization: expanding the scope of polymeric materials. *Chemical Society Reviews* **2010**, *39*, 1338-1354.
5. Nandivada, H.; Jiang, X.; Lahann, J. Click Chemistry: Versatility and Control in the Hands of Materials Scientists. *Advanced Materials* **2007**, *19*, 2197-2208.
6. Ball, P. The click concept. *Chemistry World* **2007**, *4*, 46-51.
7. Barner-Kowollik, C.; Du Prez, F. E.; Espeel, P.; Hawker, C. J.; Junkers, T.; Schlaad, H.; Van Camp, W. "Clicking" Polymers or Just Efficient Linking: What Is the Difference? *Angewandte Chemie International Edition* **2011**, *50*, 60-62.
8. Meldal, M.; Tornøe, C. W. Cu-catalyzed azide-alkyne cycloaddition. *Chemical Reviews* **2008**, *108*, 2952-3015.
9. Buckley, B. R.; Dann, S. E.; Heaney, H. Experimental Evidence for the Involvement of Dinuclear Alkynylcopper(I) Complexes in Alkyne-Azide Chemistry. *Chemistry - A European Journal* **2010**, *16*, 6278-6284.
10. Rodionov, V. O.; Presolski, S. I.; Gardinier, S.; Lim, Y.-hee; Finn, M. G. Benzimidazole and related ligands for Cu-catalyzed azide-alkyne cycloaddition. *Journal of the American Chemical Society* **2007**, *129*, 12696-12704.
11. Rodionov, V. O.; Presolski, S. I.; Díaz, D. D.; Fokin, V. V.; Finn, M. G. Ligand-accelerated Cu-catalyzed azide-alkyne cycloaddition: a mechanistic report. *Journal of the American Chemical Society* **2007**, *129*, 12705-12712.
12. Presolski, S. I.; Hong, V.; Cho, S.-H.; Finn, M. G. Tailored ligand acceleration of the Cu-catalyzed azide-alkyne cycloaddition reaction: practical and mechanistic implications. *Journal of the American Chemical Society* **2010**, *132*, 14570-14576.
13. Wang, Q.; Chan, T. R.; Hilgraf, R.; Fokin, V. V.; Sharpless, K. B.; Finn, M. G. Bioconjugation by copper(I)-catalyzed azide-alkyne [3 + 2] cycloaddition. *Journal of the American Chemical Society* **2003**, *125*, 3192-3193.
14. Ackermann, L.; Potukuchi, H. K.; Landsberg, D.; Vicente, R. Copper-catalyzed "click" reaction/direct arylation sequence: modular syntheses of 1,2,3-triazoles. *Organic Letters* **2008**, *10*, 3081-3084.
15. Friscourt, F.; Boons, G.-J. One-pot three-step synthesis of 1,2,3-triazoles by copper-catalyzed cycloaddition of azides with alkynes formed by a Sonogashira cross-coupling and desilylation. *Organic Letters* **2010**, *12*, 4936-4939.
16. Amblard, F.; Cho, J. H.; Schinazi, R. F. Cu(I)-catalyzed Huisgen azide-alkyne 1,3-dipolar cycloaddition reaction in nucleoside, nucleotide, and oligonucleotide chemistry. *Chemical Reviews* **2009**, *109*, 4207-4220.
17. Hein, J. E.; Tripp, J. C.; Krasnova, L. B.; Sharpless, K. B.; Fokin, V. V. Copper(I)-catalyzed cycloaddition of organic azides and 1-iodoalkynes. *Angewandte Chemie International Edition* **2009**, *48*, 8018-8021.

18. Spiteri, C.; Moses, J. E. Copper-catalyzed azide-alkyne cycloaddition: regioselective synthesis of 1,4,5-trisubstituted 1,2,3-triazoles. *Angewandte Chemie International Edition* **2010**, *49*, 31-33.
19. Raushel, J.; Fokin, V. V. Efficient synthesis of 1-sulfonyl-1,2,3-triazoles. *Organic Letters* **2010**, *12*, 4952-4955.
20. Zhang, L.; Chen, X.; Xue, P.; Sun, H. H. Y.; Williams, I. D.; Sharpless, K. B.; Fokin, V. V.; Jia, G. Ruthenium-catalyzed cycloaddition of alkynes and organic azides. *Journal of the American Chemical Society* **2005**, *127*, 15998-15999.
21. Sun, X.-L.; Grande, D.; Baskaran, S.; Hanson, S. R.; Chaikof, E. L. Glycosaminoglycan mimetic biomaterials. 4. Synthesis of sulfated lactose-based glycopolymers that exhibit anticoagulant activity. *Biomacromolecules* **2002**, *3*, 1065-1070.
22. Seo, T. S.; Li, Z.; Ruparel, H.; Ju, J. Click chemistry to construct fluorescent oligonucleotides for DNA sequencing. *Journal of Organic Chemistry* **2003**, *68*, 609-612.
23. Narendra, N.; Vishwanatha, T. M.; Sureshbabu, V. V. Peptidomimetics Through Click Chemistry: Synthesis of Novel  $\beta$ -Keto Triazole Acids from N-Protected Amino Acids. *International Journal of Peptide Research and Therapeutics* **2010**, *16*, 283-290.
24. Holub, J. M.; Kirshenbaum, K. Tricks with clicks: modification of peptidomimetic oligomers via copper-catalyzed azide-alkyne [3 + 2] cycloaddition. *Chemical Society Reviews* **2010**, *39*, 1325-1337.
25. Kappe, C. O.; Van der Eycken, E. Click chemistry under non-classical reaction conditions. *Chemical Society Reviews* **2010**, *39*, 1280-1290.
26. Jewett, J. C.; Bertozzi, C. R. Cu-free click cycloaddition reactions in chemical biology. *Chemical Society Reviews* **2010**, *39*, 1272-1279.
27. Baskin, J. M.; Prescher, J. A.; Laughlin, S. T.; Agard, N. J.; Chang, P. V.; Miller, I. A.; Lo, A.; Codelli, J. A.; Bertozzi, C. R. Copper-free click chemistry for dynamic in vivo imaging. *Proceedings of the National Academy of Sciences of the United States of America* **2007**, *104*, 16793-16797.
28. Sletten, E. M.; Bertozzi, C. R. A hydrophilic azacyclooctyne for Cu-free click chemistry. *Organic Letters* **2008**, *10*, 3097-3099.
29. Sletten, E. M.; Nakamura, H.; Jewett, J. C.; Bertozzi, C. R. Difluorobenzocyclooctyne: synthesis, reactivity, and stabilization by beta-cyclodextrin. *Journal of the American Chemical Society* **2010**, *132*, 11799-11805.
30. Kii, I.; Shiraishi, A.; Hiramatsu, T.; Matsushita, T.; Uekusa, H.; Yoshida, S.; Yamamoto, M.; Kudo, A.; Hagiwara, M.; Hosoya, T. Strain-promoted double-click reaction for chemical modification of azido-biomolecules. *Organic & Biomolecular Chemistry* **2010**, 4051-4055.
31. Jewett, J. C.; Sletten, E. M.; Bertozzi, C. R. Rapid Cu-free click chemistry with readily synthesized biarylazacyclooctynones. *Journal of the American Chemical Society* **2010**, *132*, 3688-3690.
32. Dommerholt, J.; Schmidt, S.; Temming, R.; Hendriks, L. J. A.; Rutjes, F. P. J. T.; Hest, J. C. M. van; Lefeber, D. J.; Friedl, P.; Delft, F. L. van Readily Accessible Bicyclononynes for Bioorthogonal Labeling and Three-Dimensional Imaging of Living Cells. *Angewandte Chemie International Edition* **2010**, 9422-9425.
33. Wuts, P. G. M.; Greene, T. W. *Greene's Protective Groups in Organic Synthesis*; John Wiley and Sons, 2007; p. 1082.
34. Scott, L. T.; Cooney, M. J.; Johnels, D. Cyclynes. 7. Homoconjugated cyclic poly(diacetylene)s. *Journal of the American Chemical Society* **1990**, *112*, 4054-4055.
35. Nielsen, M. B.; Diederich, F. Modules for Acetylenic Scaffolding. *Synlett* **2002**, 2002, 544-552.

- 
36. Valverde, I. E.; Delmas, A. F.; Aucagne, V. Click à la carte: robust semi-orthogonal alkyne protecting groups for multiple successive azide/alkyne cycloadditions. *Tetrahedron* **2009**, *65*, 7597-7602.
37. Poloukhtine, A. A.; Mbuja, N. E.; Wolfert, M. A.; Boons, G.-J.; Popik, V. V. Selective labeling of living cells by a photo-triggered click reaction. *Journal of the American Chemical Society* **2009**, *131*, 15769-15776.
38. Becer, C. R.; Hoogenboom, R.; Schubert, U. S. Click chemistry beyond metal-catalyzed cycloaddition. *Angewandte Chemie International Edition* **2009**, *48*, 4900-4908.
39. Singh, I.; Zarafshani, Z.; Lutz, J.-F.; Heaney, F. Metal-Free "Click" Chemistry: Efficient Polymer Modification via 1,3-Dipolar Cycloaddition of Nitrile Oxides and Alkynes. *Macromolecules* **2009**, *42*, 5411-5413.
40. Lee, Y.-Gi; Koyama, Y.; Yonekawa, M.; Takata, T. New Click Chemistry: Polymerization Based on 1,3-Dipolar Cycloaddition of a Homo Ditopic Nitrile N -Oxide and Transformation of the Resulting Polymers into Reactive Polymers. *Macromolecules* **2009**, *42*, 7709-7717.
41. Ning, X.; Temming, R. P.; Dommerholt, J.; Guo, J.; Ania, D. B.; Debets, M. F.; Wolfert, M. A.; Boons, G.-J.; van Delft, F. L. Protein modification by strain-promoted alkyne-nitrone cycloaddition. *Angewandte Chemie International Edition* **2010**, *49*, 3065-3068.
42. Campbell-Verduyn, L.; Elsinga, P. H.; Mirfeizi, L.; Dierckx, R. A.; Feringa, B. L. Copper-free "click": 1,3-dipolar cycloaddition of azides and alkynes. *Organic & Biomolecular Chemistry* **2008**, *6*, 3461-3463.
43. Wang, Y.; Hu, W. J.; Song, W.; Lim, R. K. V.; Lin, Q. Discovery of long-wavelength photoactivatable diaryltetrazoles for bioorthogonal 1,3-dipolar cycloaddition reactions. *Organic Letters* **2008**, *10*, 3725-3728.
44. Song, W.; Wang, Y.; Qu, J.; Lin, Q. Selective functionalization of a genetically encoded alkene-containing protein via "photoclick chemistry" in bacterial cells. *Journal of the American Chemical Society* **2008**, *130*, 9654-9655.
45. Wang, J.; Zhang, W.; Song, W.; Wang, Y.; Yu, Z.; Li, J.; Wu, M.; Wang, L.; Zang, J.; Lin, Q. A biosynthetic route to photoclick chemistry on proteins. *Journal of the American Chemical Society* **2010**, *132*, 14812-14818.
46. Reymond, S.; Cossy, J. Copper-catalyzed Diels-Alder reactions. *Chemical Reviews* **2008**, *108*, 5359-5406.
47. Schoch, J.; Wiessler, M.; Jäschke, A. Post-synthetic modification of DNA by inverse-electron-demand Diels-Alder reaction. *Journal of the American Chemical Society* **2010**, *132*, 8846-8847.
48. Gutmiedl, K.; Wirges, C. T.; Ehmke, V.; Carell, T. Copper-free "click" modification of DNA via nitrile oxide-norbornene 1,3-dipolar cycloaddition. *Organic Letters* **2009**, *11*, 2405-2408.
49. Inglis, A. J.; Sinnwell, S.; Stenzel, M. H.; Barner-Kowollik, C. Ultrafast click conjugation of macromolecular building blocks at ambient temperature. *Angewandte Chemie International Edition* **2009**, *48*, 2411-2414.
50. Hoyle, C. E.; Lowe, A. B.; Bowman, C. N. Thiol-click chemistry: a multifaceted toolbox for small molecule and polymer synthesis. *Chemical Society Reviews* **2010**, *39*, 1355-1387.
51. Hoyle, C. E.; Bowman, C. N. Thiol-ene click chemistry. *Angewandte Chemie International Edition* **2010**, *49*, 1540-1573.
52. Hoyle, C. E.; Lee, T. Y.; Roper, T. Thiol-enes: Chemistry of the past with promise for the future. *Journal of Polymer Science Part A: Polymer Chemistry* **2004**, *42*, 5301-5338.
53. Campos, L. M.; Killops, K. L.; Sakai, R.; Paulusse, J. M. J.; Damiron, D.; Drockenmuller, E.; Messmore, B. W.; Hawker, C. J. Development of Thermal and Photochemical Strategies for Thiol-Ene Click Polymer Functionalization. *Macromolecules* **2008**, *41*, 7063-7070.



- 
54. Mather, B. D.; Viswanathan, K.; Miller, K. M.; Long, T. E. Michael addition reactions in macromolecular design for emerging technologies. *Progress in Polymer Science* **2006**, *31*, 487-531.
55. Dondoni, A. The emergence of thiol-ene coupling as a click process for materials and bioorganic chemistry. *Angewandte Chemie International Edition* **2008**, *47*, 8995-8997.
56. Hoogenboom, R. Thiol-yne chemistry: a powerful tool for creating highly functional materials. *Angewandte Chemie International Edition* **2010**, *49*, 3415-3147.
57. Chan, J. W.; Shin, J.; Hoyle, C. E.; Bowman, C. N.; Lowe, A. B. Synthesis, Thiol-Yne "Click" Photopolymerization, and Physical Properties of Networks Derived from Novel Multifunctional Alkynes. *Macromolecules* **2010**, *43*, 4937-4942.
58. Chan, J. W.; Zhou, H.; Hoyle, C. E.; Lowe, A. B. Photopolymerization of Thiol-Alkynes: Polysulfide Networks. *Chemistry of Materials* **2009**, *21*, 1579-1585.
59. Xu, J.; Tao, L.; Boyer, C.; Lowe, A. B.; Davis, T. P. Combining Thio-Bromo "Click" Chemistry and RAFT Polymerization: A Powerful Tool for Preparing Functionalized Multiblock and Hyperbranched Polymers. *Macromolecules* **2010**, *43*, 20-24.
60. Moses, J. E.; Moorhouse, A. D. The growing applications of click chemistry. *Chemical Society Reviews* **2007**, *36*, 1249-1262.
61. Dirks, A. J. T.; van Berkel, S. S.; Hatzakis, N. S.; Opsteen, J. A.; van Delft, F. L.; Cornelissen, J. J. L. M.; Rowan, A. E.; van Hest, J. C. M.; Rutjes, F. P. J. T.; Nolte, R. J. M. Preparation of biohybrid amphiphiles via the copper catalysed Huisgen [3 + 2] dipolar cycloaddition reaction. *Chemical Communications* **2005**, 4172-4174.
62. Glaser, M.; Robins, E. G. "Click labelling" in PET radiochemistry. *Journal of Labelled Compounds and Radiopharmaceuticals* **2009**, *52*, 407-414.
63. Nebhani, L.; Barner-Kowollik, C. Orthogonal Transformations on Solid Substrates: Efficient Avenues to Surface Modification. *Advanced Materials* **2009**, *21*, 3442-3468.
64. van Dijk, M.; Rijkers, D. T. S.; Liskamp, R. M. J.; van Nostrum, C. F.; Hennink, W. E. Synthesis and applications of biomedical and pharmaceutical polymers via click chemistry methodologies. *Bioconjugate Chemistry* **2009**, *20*, 2001-2016.
65. Guo, J.; Chen, G.; Ning, X.; Wolfert, M. A.; Li, X.; Xu, B.; Boons, G.-J. Surface Modification of Polymeric Micelles by Strain-Promoted Alkyne-Azide Cycloadditions. *Chemistry - A European Journal* **2010**, *16*, 13360-13366.
66. Iha, R. K.; Wooley, K. L.; Nyström, A. M.; Burke, D. J.; Kade, M. J.; Hawker, C. J. Applications of orthogonal "click" chemistries in the synthesis of functional soft materials. *Chemical Reviews* **2009**, *109*, 5620-5686.
67. Baskin, J.; Bertozzi, C. Bioorthogonal Click Chemistry: Covalent Labeling in Living Systems. *QSAR & Combinatorial Science* **2007**, *26*, 1211-1219.
68. Pieters, R.; Rijkers, D. S.; Liskamp, R. J. Application of the 1,3-Dipolar Cycloaddition Reaction in Chemical Biology: Approaches Toward Multivalent Carbohydrates and Peptides and Peptide-Based Polymers. *QSAR & Combinatorial Science* **2007**, *26*, 1181-1190.
69. Megiatto, J. D.; Schuster, D. I. General method for synthesis of functionalized macrocycles and catenanes utilizing "click" chemistry. *Journal of the American Chemical Society* **2008**, *130*, 12872-12873.
70. Odian, G. G. *Principles of Polymerization*; John Wiley and Sons, 2004; p. 812.
71. Wang, J.-S.; Matyjaszewski, K. Controlled/"living" radical polymerization. Atom transfer radical polymerization in the presence of transition-metal complexes. *Journal of the American Chemical Society* **1995**, *117*, 5614-5615.

- 
72. Matyjaszewski, K. In *Controlled/Living Radical Polymerization: Progress in ATRP*; Matyjaszewski, K., Ed.; American Chemical Society: Washington, DC, 2009; pp. 4-13.
73. Russell, G. T. In *Controlled/Living Radical Polymerization: Progress in ATRP*; Matyjaszewski, K., Ed.; American Chemical Society: Washington, DC, 2009; pp. 15-31.
74. Durmaz, Y. Y.; Aydogan, B.; Cianga, I.; Yagci, Y. In *Controlled/Living Radical Polymerization: Progress in ATRP*; Matyjaszewski, K., Ed.; American Chemical Society: Washington, DC, 2009; pp. 171-187.
75. Gao, H.; Li, W.; Min, K.; Matyjaszewski, K. In *Controlled/Living Radical Polymerization: Progress in ATRP*; Matyjaszewski, K., Ed.; American Chemical Society: Washington, DC, 2009; pp. 203-213.
76. Jakubowski, W.; Tsarevsky, N. V.; McCarthy, P. In *Controlled/Living Radical Polymerization: Progress in ATRP*; Matyjaszewski, K., Ed.; American Chemical Society: Washington, DC, 2009; pp. 343-355.
77. Matyjaszewski, K.; Tsarevsky, N. V. Nanostructured functional materials prepared by atom transfer radical polymerization. *Nature Chemistry* **2009**, *1*, 276-288.
78. Astruc, D.; Boisselier, E.; Ornelas, C. Dendrimers designed for functions: from physical, photophysical, and supramolecular properties to applications in sensing, catalysis, molecular electronics, photonics, and nanomedicine. *Chemical reviews* **2010**, *110*, 1857-1959.
79. Fu, R.; Fu, G.-D. Polymeric nanomaterials from combined click chemistry and controlled radical polymerization. *Polymer Chemistry* **2011**, *2*, 465.
80. Cameron, G. G. In *Macromolecular Chemistry*; Jenkins, A. D.; Kennedy, J. F., Eds.; Royal Society of Chemistry: Cambridge, 1980; Vol. 1, pp. 350-369.
81. Cameron, G. G. In *Macromolecular Chemistry*; Jenkins, A. D.; Kennedy, J. F., Eds.; Royal Society of Chemistry: Cambridge, 1982; Vol. 2, pp. 271-295.
82. Sherrington, D. C. In *Macromolecular Chemistry*; Jenkins, A. D.; Kennedy, J. F., Eds.; Royal Society of Chemistry: Cambridge, 1984; Vol. 3, pp. 303-330.
83. Mansfeld, U.; Pietsch, C.; Hoogenboom, R.; Becer, C. R.; Schubert, U. S. Clickable initiators, monomers and polymers in controlled radical polymerizations – a prospective combination in polymer science. *Polymer Chemistry* **2010**.
84. Matyjaszewski, K.; Tsarevsky, N. V. Nanostructured functional materials prepared by atom transfer radical polymerization. *Nature Chemistry* **2009**, *1*, 276-288.
85. Matyjaszewski, K.; Xia, J. In *Handbook of Radical Polymerization*; Matyjaszewski, K.; Davis, T. P., Eds.; John Wiley & Sons, Inc. Hoboken, NJ, USA, 2002; pp. 523-628.
86. Topham, P. D.; Sandon, N.; Read, E. S.; Madsen, J.; Ryan, A. J.; Armes, S. P. Facile Synthesis of Well-Defined Hydrophilic Methacrylic Macromonomers Using ATRP and Click Chemistry. *Macromolecules* **2008**, *41*, 9542-9547.
87. Lutz, J.-F.; Börner, H. G.; Weichenhan, K. Combining ATRP and “Click” Chemistry: a Promising Platform toward Functional Biocompatible Polymers and Polymer Bioconjugates. *Macromolecules* **2006**, *39*, 6376-6383.
88. Jia, Z.; Bell, C. A.; Monteiro, M. J. Rapid and Highly Efficient Functionalization of Polymer Bromide End-Groups by SET-NRC. *Macromolecules* **2011**, *44*, 1747-1751.
89. Malkoch, M.; Vestberg, R.; Gupta, N.; Mespouille, L.; Dubois, P.; Mason, A. F.; Hedrick, J. L.; Liao, Q.; Frank, C. W.; Kingsbury, K.; Hawker, C. J. Synthesis of well-defined hydrogel networks using Click chemistry. *Chemical Communications* **2006**, 2774-2776.
90. Ladmiral, V.; Legge, T. M.; Zhao, Y.; Perrier, S. “Click” Chemistry and Radical Polymerization: Potential Loss of Orthogonality. *Macromolecules* **2008**, *41*, 6728-6732.

- 
91. Sumerlin, B. S.; Tsarevsky, N. V.; Louche, G.; Lee, R. Y.; Matyjaszewski, K. Highly Efficient “Click” Functionalization of Poly(3-azidopropyl methacrylate) Prepared by ATRP. *Macromolecules* **2005**, *38*, 7540-7545.
  92. Ladmiral, V.; Mantovani, G.; Clarkson, G. J.; Cauet, S.; Irwin, J. L.; Haddleton, D. M. Synthesis of neoglycopolymers by a combination of “click chemistry” and living radical polymerization. *Journal of the American Chemical Society* **2006**, *128*, 4823-4830.
  93. Deiters, A.; Cropp, T. A.; Mukherji, M.; Chin, J. W.; Anderson, J. C.; Schultz, P. G. Adding amino acids with novel reactivity to the genetic code of *Saccharomyces cerevisiae*. *Journal of the American Chemical Society* **2003**, *125*, 11782-11783.
  94. Parrish, B.; Breitenkamp, R. B.; Emrick, T. PEG- and peptide-grafted aliphatic polyesters by click chemistry. *Journal of the American Chemical Society* **2005**, *127*, 7404-7410.
  95. Daugaard, A. E.; Hvilsted, S.; Hansen, T. S.; Larsen, N. B. Conductive Polymer Functionalization by Click Chemistry. *Macromolecules* **2008**, *41*, 4321-4327.
  96. Benanti, T. L.; Kalaydjian, A.; Venkataraman, D. Protocols for Efficient Postpolymerization Functionalization of Regioregular Polythiophenes. *Macromolecules* **2008**, *41*, 8312-8315.
  97. Kavitha, A. A.; Singha, N. K. “Click chemistry” in tailor-made polymethacrylates bearing reactive furfuryl functionality: a new class of self-healing polymeric material. *Applied Materials & Interfaces* **2009**, *1*, 1427-1436.
  98. Hartmann, L.; Krause, E.; Antonietti, M.; Börner, H. G. Solid-phase supported polymer synthesis of sequence-defined, multifunctional poly(amidoamines). *Biomacromolecules* **2006**, *7*, 1239-1244.
  99. Takizawa, K.; Tang, C.; Hawker, C. J. Molecularly defined caprolactone oligomers and polymers: synthesis and characterization. *Journal of the American Chemical Society* **2008**, *130*, 1718-1726.
  100. Wang, Q.; Qu, Y.; Tian, H.; Geng, Y.; Wang, F. Iterative Binomial Synthesis of Monodisperse Polyfluorenes up to 64-mers and Their Chain-Length-Dependent Properties. *Macromolecules* **2011**, *44*, 1256-1260.
  101. Urbani, C. N.; Lonsdale, D. E.; Bell, C. A.; Whittaker, M. R.; Monteiro, M. J. Divergent synthesis and self-assembly of amphiphilic polymeric dendrons with selective degradable linkages. *Journal of Polymer Science Part A: Polymer Chemistry* **2008**, *46*, 1533-1547.
  102. Urbani, C. N.; Bell, C. A.; Lonsdale, D.; Whittaker, M. R.; Monteiro, M. J. Self-Assembly of Amphiphilic Polymeric Dendrimers Synthesized with Selective Degradable Linkages. *Macromolecules* **2008**, *41*, 76-86.
  103. Khudyakov, I. V. Post-Polymerization. *Radtech Report* **2010**, 47-52.
  104. Randall, J. P.; Meador, M. A. B.; Jana, S. C. Tailoring mechanical properties of aerogels for aerospace applications. *ACS Applied Materials & Interfaces* **2011**, *3*, 613-626.
  105. Isidro-Llobet, A.; Alvarez, M.; Albericio, F. Amino acid-protecting groups. *Chemical Reviews* **2009**, *109*, 2455-2504.
  106. Chen, Y.; Wu, Y.; Henklein, P.; Li, X.; Hofmann, K. P.; Nakanishi, K.; Ernst, O. P. A photo-cross-linking strategy to map sites of protein-protein interactions. *Chemistry - A European Journal* **2010**, *16*, 7389-7394.
  107. Ramos, R.; Manning, B.; Aviñó, A.; Gargallo, R.; Eritja, R. Photocleavage of Peptides and Oligodeoxynucleotides Carrying 2-Nitrobenzyl Groups. *Helvetica Chimica Acta* **2009**, *92*, 613-622.
  108. James, I. Linkers for solid phase organic synthesis. *Tetrahedron* **1999**, *55*, 4855-4946.
  109. Bley, F.; Schaper, K.; Görner, H. Photoprocesses of molecules with 2-nitrobenzyl protecting groups and caged organic acids. *Photochemistry and Photobiology* **2008**, *84*, 162-171.

- 
110. Albini, A.; Fagnoni, M. *Handbook of Synthetic Photochemistry*; Wiley-VCH, 2010; p. 463.
111. Daragics, K.; Fügedi, P. (2-Nitrophenyl)acetyl: a new, selectively removable hydroxyl protecting group. *Organic Letters* **2010**, *12*, 2076-2079.
112. Aujard, I.; Benbrahim, C.; Gouget, M.; Ruel, O.; Baudin, J.-B.; Neveu, P.; Jullien, L. O-Nitrobenzyl Photolabile Protecting Groups With Red-Shifted Absorption: Syntheses and Uncaging Cross-Sections for One- and Two-Photon Excitation. *Chemistry - A European Journal* **2006**, *12*, 6865-6879.
113. Schäfer, F.; Joshi, K. B.; Fichte, M. A. H.; Mack, T.; Wachtveitl, J.; Heckel, A. Wavelength-Selective Uncaging of dA and dC Residues. *Organic Letters* **2011**, *13*, 1450-1453.
114. Johnson, J. A.; Finn, M. G.; Koberstein, J. T.; Turro, N. J. Synthesis of Photocleavable Linear Macromonomers by ATRP and Star Macromonomers by a Tandem ATRP-Click Reaction: Precursors to Photodegradable Model Networks. *Macromolecules* **2007**, *40*, 3589-3598.
115. Johnson, J. A.; Lu, Y. Y.; Burts, A. O.; Xia, Y.; Durrell, A. C.; Tirrell, D. A.; Grubbs, R. H. Drug-Loaded, Bivalent-Bottle-Brush Polymers by Graft-through ROMP. *Macromolecules* **2010**, *43*, 10326-10335.
116. Fomina, N.; McFearin, C.; Sermsakdi, M.; Edigin, O.; Almutairi, A. UV and near-IR triggered release from polymeric nanoparticles. *Journal of the American Chemical Society* **2010**, *132*, 9540-9542.

## 2. Homobifunctional Crosslinkers

The goal of Chapter 2 is to develop compounds that are capable of crosslinking *any* polymeric material in a localized manner without degrading the polymer structure. By retaining the chemical properties of the bulk material and only changing the amount of exogenous crosslinker added to the polymer, we hope to tune the crosslink density of a polymer in order to alter its mechanical properties (moduli), durability, swellability, and architecture. This strategy obviates the need to synthesize a new polymer for each different set of desired properties, and would therefore be advantageous when seeking to tune a material for a given application. Additionally, when a polymer is comprised of highly complex monomers or blocks, crosslinking by a degradative process such as ultraviolet irradiation can eliminate functionality installed during a potentially expensive synthesis.

Modulation of crosslink density provides a method to alter the mechanical properties of a polymer network without altering its chemical properties. A crosslinked network is a single covalently bound molecule with a highly complex, branched architecture. By viewing the network as linear polymers connected at junction points to other linear polymers, however, it is possible to see how crosslink density can play a role in the network's mechanical strength, as well as its swellability and a propensity to intercalate other molecules. A higher number of crosslinks will bind polymer chains together more tightly, increasing the polymer modulus. The distance between junction points is also related to the size of the voids between polymer chains, so a higher number of junction points in a given volume will cause the voids between polymer chains to be smaller. When the polymer is swollen, the voids fill with solvent, increasing the overall

volume of the network. If the network is tight with a high crosslink density, less solvent will be able to fill the voids, while a looser network can contain more solvent. In addition to solvent, the voids may host intercalated, non-covalently bound molecules such as drugs, which, depending on the crosslinking density and degree of swelling, then navigate through the crosslinked network to be released to the environment.<sup>1,2</sup>

Crosslinked polymer networks and gels are an important class of biomedical materials.<sup>3-7</sup> By controlling crosslinking in the bulk and in films, polymer properties are optimized for use within the body where slight changes in pore size or modulus can be the difference between biocompatibility and rejection.<sup>8</sup> Whether as substrates on which cells are grown or as a locally injectible drug delivery system, hydrogels are used widely because they mimic the structural characteristics of the extracellular matrix and can readily be swollen with fluids that provide nutrients to growing cells.<sup>9-12</sup> Inclusion of photodegradable and biodegradable linkages in hydrogels has enabled the triggered and sustained release of drugs from polymer hydrogels *in vivo*.<sup>13</sup>

## 2.1. Introduction, Motivation

Crosslinking of a polymer has been accomplished in a number of ways and can be broadly classified as occurring either during polymerization or post-polymerization.<sup>14</sup> In order to occur during polymerization (Figure 2.1a), a difunctional monomer (e.g. a diacrylate, dark gray) must be copolymerized with a monofunctional monomer (e.g. an acrylate, light gray) such that reaction at both ends of the difunctional species yields covalent connections between otherwise linear polymers. By changing the relative ratio of monofunctional to difunctional monomers, the crosslink density can be adjusted.

Because not all difunctional monomers necessarily react at both ends in order to form a crosslink, the crosslink density cannot be known for certain *a priori*. Additional functionality such as degradability can be built into an architecture that is crosslinked during polymerization by including more complex monofunctional and difunctional monomers. Crosslinking by polymerization has also been used to tie together polymer brushes and to lock in place preorganized, supramolecular structures such as micelles. For example, pendant vinyl groups have been polymerized to vary the stiffness of a polymer film<sup>15</sup> while diacetylene units have been polymerized to crosslink organic shells around gold nanoparticles.<sup>16</sup>

Several post-polymerization crosslinking schemes depend upon the installation of pendant functionalities during polymerization or as a pre-crosslinking step after polymerization. Once installed, the pendant functionalities are crosslinked by reaction with each other (Figure 2.1b, dark gray) as in the case of pendant coumarins<sup>17-24</sup>, cinnamoyl groups<sup>25,26</sup>, thiols, and trithiocarbonates, or else the pendant functionalities can be reacted with a bifunctional exogenous crosslinker (Figure 2.1c, blue). Examples of the latter type include CuAAC to crosslink pendant alkynes using a diazido-PEG oligomer<sup>27-29</sup>, crosslinking pendant hydroxyl groups with a bisisocyanate<sup>30</sup>, crosslinking pendant isocyanates with a bisamine<sup>31</sup>, and crosslinking pendant furans with a bismaleimide<sup>32-34</sup>. Depending on the intended application, degradable or reversible crosslinks such as the [2+2] adduct of coumarin or the Diels-Alder adduct of maleimide and furan may be preferable to permanent covalent crosslinks such as the triazole from CuAAC. In both cases, not all of the pendant groups are likely to react to form crosslinks between different chains; some will remain unreacted while others may react with a pendant

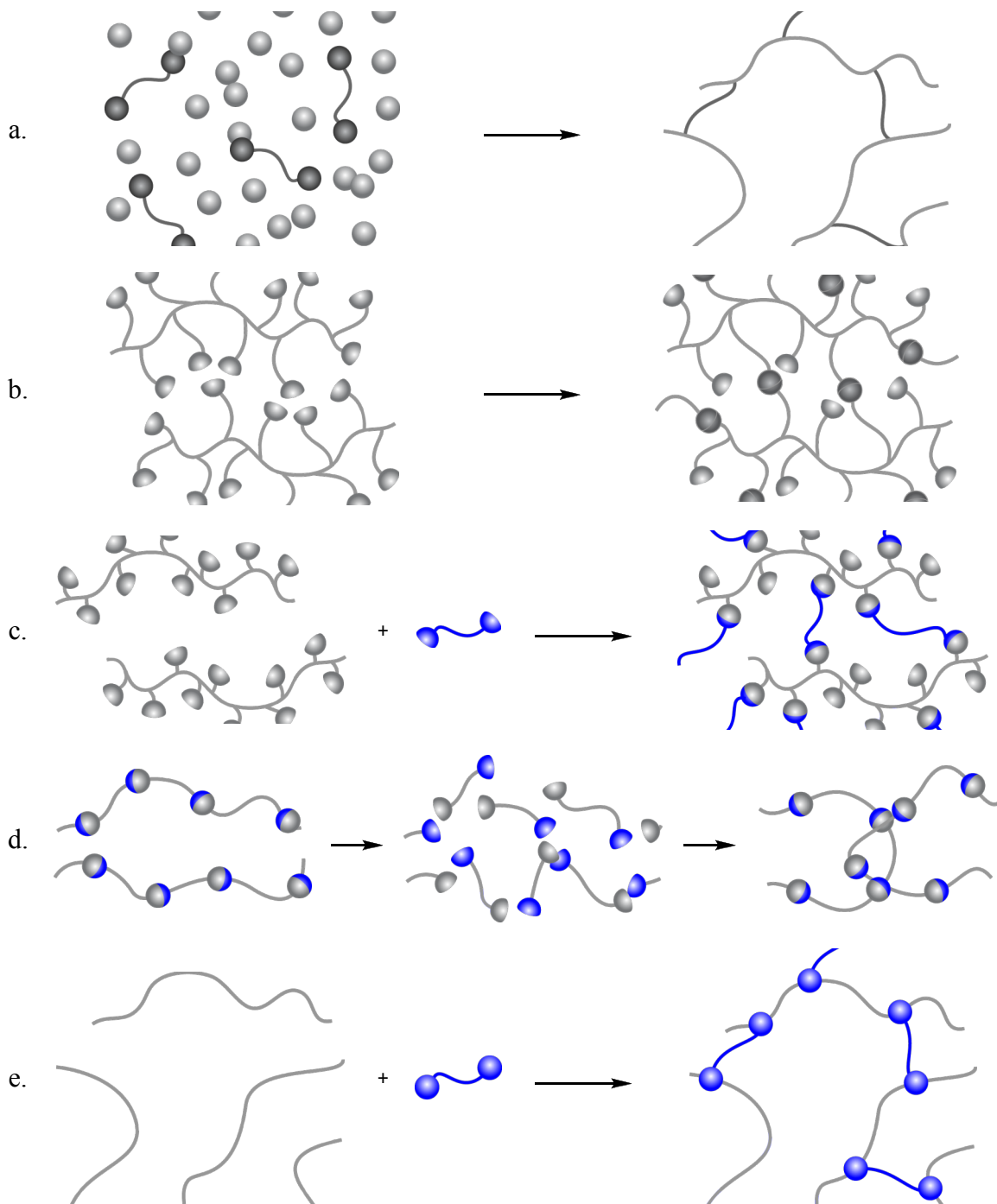
functional group on the same chain. Other schemes have been developed whereby a pendant functional group on one chain reacts directly and indiscriminately with another chain – e.g. polymer crosslinking via photochemical activation of pendant azides<sup>35</sup>, phenyl azides<sup>36</sup>, or benzophenones<sup>37,38</sup> – but such schemes still rely upon installation of functionality during polymerization or else a post-polymerization functionalization step with some particular moiety on the polymer.

A functional polymer backbone can also take part in crosslinking, albeit primarily in terms of physical entanglement as opposed to covalent binding. A backbone containing reversibly degradable linkages (e.g. maleimide-furan adducts or [2+2] coumarin or cinnamoyl adducts) can be degraded, and upon reformation polymer chains can entangle (Figure 2.1d).<sup>39</sup> If complementary functionalities are installed pendant to the chain, then a network is likely to be formed containing covalent crosslinks between polymer chains.

An ideal polymer crosslinking strategy would not require polymer pre-functionalization during polymerization or during a post-polymerization step, and would universally crosslink any polymer independent of the pre-existing functional groups on that polymer. Irradiation with ultraviolet light can induce polymer crosslinking, but the mechanism relies on breaking bonds to form radicals that then recombine indiscriminately to form crosslinks. Although this method is effective on large scales and for curing polymers to ‘completion’, it degrades the structure of the polymer and is not practical for well-defined crosslinking.

An alternate approach involves an exogenous molecule dissolved into the polymer and subsequently activated to bind to two different polymer chains (Figure 2.1e).<sup>40</sup> To a





**Figure 2.1.** Crosslinking schemes: (a) during polymerization; (b) by symmetrical pendant functionalities; (c) reaction of a bifunctional molecule with particular pendant functionalities; (d) degradation and reformation of polymer backbone to entangle; and (e) indiscriminate reaction of a bifunctional molecule.

first approximation, only 25% of the molecules introduced should form covalent crosslinks, but continued activation of the crosslinking molecules may increase that percentage well above the statistical value. This approach has been used to crosslink polystyrene films in order to inhibit dewetting, and forms the starting point for the improvements that are sought in this chapter.

## 2.2. Candidates for New 'Universal' Crosslinkers

Previous work has shown that dissolution of a bis-benzophenone small molecule, **1**, into a polystyrene thin film will inhibit the dewetting of the film after photochemical activation. The mechanism of its action upon the polymer is thought to involve hydrogen atom abstraction from a C-H bond by an excited benzophenone moiety, and subsequent radical-radical recombination to form a covalent bond to the atom from which the hydrogen was abstracted (Figure 2.2a). Because two benzophenones are tethered together in **1**, independent reaction at both ends yields a crosslink. That compound, however, was found to crystallize in thin films of other polymers, thereby limiting its ability to properly disperse throughout the film. As a result, we set about to synthesize analogous compounds that would still act to crosslink the polymer, but ones that would not crystallize upon dissolution in the polymer.<sup>41</sup>

Several characteristics of **1** are highly advantageous for a universal crosslinker: the molecule is activated using light at reasonable wavelengths; the hydrogen abstraction reaction by benzophenone is well-studied and proceeds with a high quantum yield; benzophenone reacts with C-H bonds which are present in nearly every conceivable polymer; and **1** is synthesized in a straight-forward, high-yielding DCC coupling. The ideal next generation universal crosslinker should share similar characteristics, but would

not phase separate when dissolved in a polymer. Taking inspiration from photoaffinity labeling in proteins<sup>42</sup> and cells<sup>43</sup>, several functional groups were found to satisfy some or all of these criteria (Table 2.1).

The extensive aromatic  $\pi$  system of benzophenone is likely responsible for the high crystallinity of **1** in bulk and in polymers, especially in polymers without aromatic rings that disrupt the  $\pi$  complexation of **1** with itself. Structurally similar compounds such as xanthone and thioxanthone would most likely still have unfavorable crystallinity, however their different photophysical properties<sup>44</sup> and their availability make them interesting candidates to include here regardless.

A photoactive moiety that contains fewer aryl groups per moiety compared to benzophenone is phthalimide. The photochemistry of the phthalimide is also well-studied, and its carbonyl undergoes photoinduced hydrogen abstraction like that of benzophenone (Figure 2.2b).<sup>45-47</sup> The phthalimide moiety is easily installed by  $S_N2$  reaction of a terminal bromide with potassium phthalimide salt, and unlike benzophenone, a phthalimide is comprised of two carbonyls, each of which is a potential site for hydrogen abstraction. A drawback to the use of phthalimide is that it is capable of numerous side reactions<sup>48-51</sup>, photorearrangements<sup>52</sup> and ring-enlargements<sup>53,54</sup> that may decrease its overall efficiency as a crosslinker.

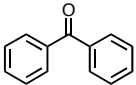
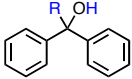
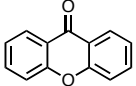
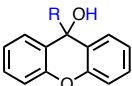
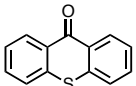
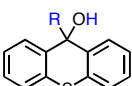
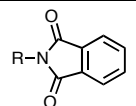
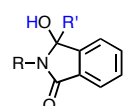
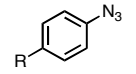

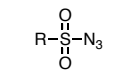
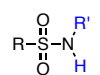
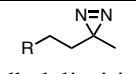
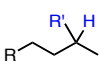
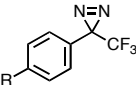
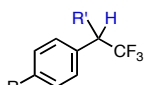
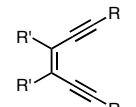
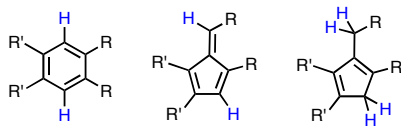
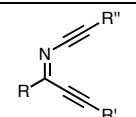
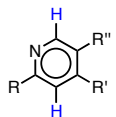
Nitrenes and carbenes, like hydrogen abstractors, are reactive with a wide range of functional groups present in polymers, including C-H, N-H, and C-C bonds, and can be generated photochemically.<sup>55,56</sup> Several functional groups are known to produce nitrenes or carbenes, including aryl azides, alkyl azides, diazo compounds and diazirines.<sup>42</sup>

Aryl azides have been used to label proteins<sup>57,58</sup> and membranes<sup>59,60</sup>, crosslink polymers<sup>36</sup>, and graft polymers to functionalized surfaces<sup>61,62</sup>. Photochemical excitation of the aryl azide liberates molecular nitrogen to generate a highly reactive nitrene, which can subsequently insert into a C-H or C-C bond, for example (Figure 2.2c).<sup>63</sup> The aryl ring and its substituents (e.g. fluorine atoms<sup>64</sup>) stabilize the aryl azide relative to an alkyl azide to increase its practical utility.<sup>65</sup> A drawback to the use of azides for labeling, however, is that side reactions occur to deactivate the nitrene: ring expansion of the aryl nitrene yields a cyclic ketenimine that can only then react with a nucleophile (Figure 2.2c).

Whereas azide photochemistry generates a nitrene, diazo compounds and diazirines decompose upon irradiation to release molecular nitrogen and generate a carbene.<sup>43,66</sup> Like the nitrenes, diazo compounds and diazirines have also been used to label proteins<sup>67-70</sup> and membranes<sup>71</sup>, and to graft analytes to functionalized surfaces<sup>72</sup>. Fluoroaryl and fluoroalkyl groups are often included in the  $\alpha$ -positions relative to the site of the carbene to increase the stability of the diazirine and the lifetime of the resultant carbene. The synthesis of diazirines requires a number of steps and is a major drawback to their use as universal crosslinkers.<sup>72,73</sup>

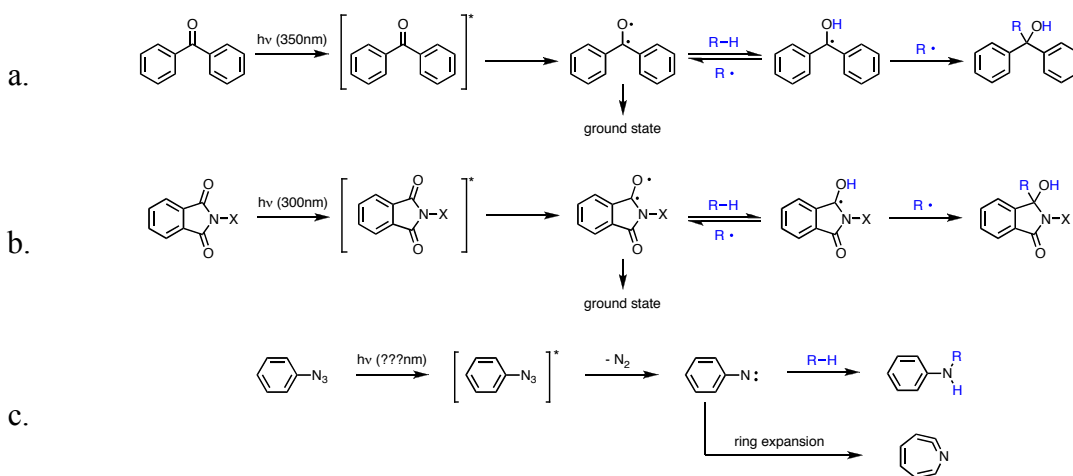
The final set of compounds considered as substitutes for benzophenone in a second generation universal photocrosslinker consists of enediynes<sup>74</sup> and dialkynyl imines<sup>75</sup>. Enediynes and dialkynyl imines cyclize thermally and photochemically to form 1,4-benzene and 2,5-pyridine diradicals via a Bergman cyclization.<sup>74,76,77</sup> Since the diradicals are in para positions on the aromatic rings, they do not readily recombine with each other; instead each can abstract a hydrogen atom from a nearby substrate.<sup>78,79</sup>

**Table 2.1.** Candidates for improved photoactive bis-functional crosslinkers.

Functional Group	Mechanism of Action	Adduct(s)	References
 Benzophenone	Hydrogen abstraction		[40]
 Xanthone	Hydrogen abstraction		[44]
 Thioxanthone	Hydrogen abstraction		[44]
 Phthalimide	Hydrogen abstraction		[45] - [54]
 Aryl azide	Nitrene bond insertion		[36], [42], [55], [57] - [65]
 Sulfonyl azide	Nitrene bond insertion		[80]
 Alkyl diazirine	Carbene bond insertion		[43], [56], [66] - [73]
 Fluoroalkyl diazirine	Carbene bond insertion		[43], [56], [66] - [73]
 Eneidyne	Double or quadruple hydrogen abstraction		[74], [76] - [79]
 Dialkynyl imine	Double hydrogen abstraction		[75]

Although this hydrogen atom transfer does not directly produce a covalent bond to the source of the hydrogen atom as in the case of benzophenone, the radicals on the substrate can recombine to form crosslinks. In the presence of an electron donor, the benzyl product of the Bergman cyclization can absorb another photon, rearrange, and effect two additional hydrogen atom transfers from a substrate, yielding two additional radicals for recombination. A drawback of using enediynes and dialkynyl imines, however, is that latent radicals on the crosslinker may persist in the material without a mechanism for deactivation.

Given the potential benefits, drawbacks, and availability of each of the functional groups in Table 2.1, several second generation homobifunctional universal crosslinkers were designed and synthesized. In addition to the symmetrical bis-xanthone, bis-phthalimide-, and bis-phenyl azide derivatives, an asymmetrical benzophenone derivative was designed and synthesized in an attempt to disrupt the crystallinity of compound **1** while retaining the photophysical properties of the benzophenone moieties.



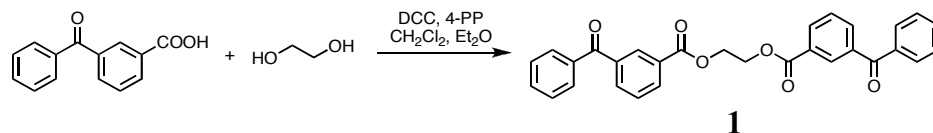
**Figure 2.2.** Mechanisms of the photoreaction of (a) benzophenone hydrogen abstraction, (b) phthalimide hydrogen abstraction, and (c) phenyl azide nitrene insertion and ring expansion.

### 2.3. Preparation of Homobifunctional Crosslinkers

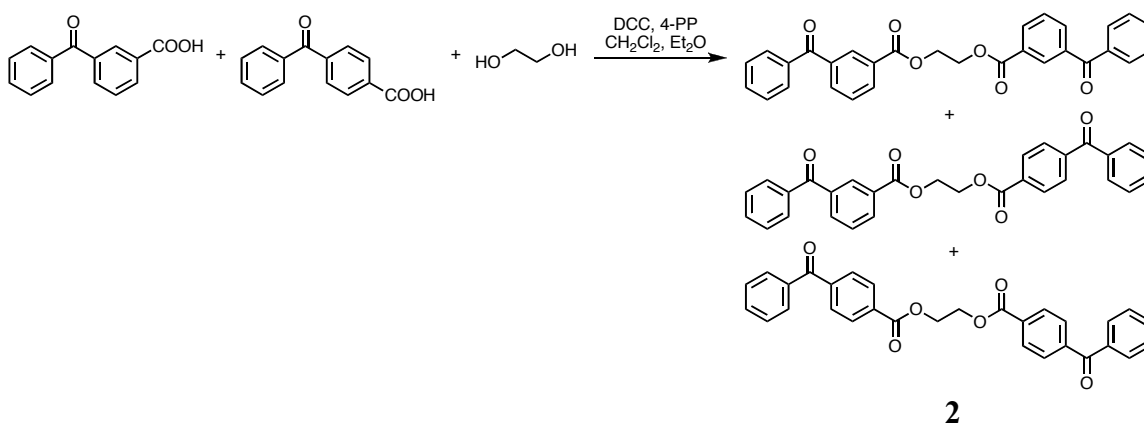
The procedure for the synthesis of the bis-benzophenone, **1**, was previously reported by Carroll, et al., and involves the esterification of a 3-benzoylbenzoic acid with ethylene glycol promoted by dicyclohexylcarbodiimide (DCC) and 4-pyrrolidinopyridine (4-PP).<sup>40</sup> Purification by filtration then washing with water, 5% acetic acid, water, and saturated sodium chloride solution was followed by column chromatography to yield the symmetrical crosslinker, **1** (Figure 2.3).<sup>81</sup> That procedure was modified to synthesize the second-generation crosslinkers **2** - **4** (Figure 2.4 - Figure 2.6).<sup>82-84</sup> Compound **2** was synthesized using a 1:1 mixture of 3- and 4-benzoylbenzoic acids, while **3** and **4** were prepared using 3-carboxyxanthone and 4-azidobenzoic acid, respectively. Compound **5** was prepared by the reaction of potassium phthalimide salt with 1,6-dibromohexane, and isolated by extraction with water and column chromatography (Figure 2.7).<sup>85</sup> The structures of compounds **1** - **5** were verified using <sup>1</sup>H NMR to ensure only difunctional molecules were used for subsequent crosslinking studies.

We hypothesized that the asymmetrical adduct of **2** would be less likely to crystallize *in situ*, so an attempt to remove symmetrical crosslinkers – 1,2-ethyl bis(3-benzoylbenzoate) and 1,2-ethyl bis(4-benzoylbenzoate) adducts – from the gummy, mixed product **2** by crystallization from hot ethanol yielded two fractions for evaluation: filtrand (A) and filtrate (B). Although it was not possible to determine the relative amounts of the 3 bis-functional products in each of the fractions A and B, the relative proportion of 3-benzoylbenzoate and 4-benzoylbenzoate moieties as determined by integration of characteristic peaks in the <sup>1</sup>H NMR spectrum was found to be 1:3 in A and

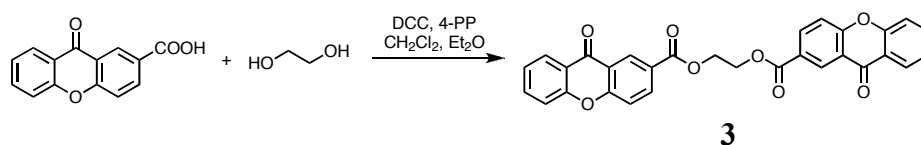
1:15 in B (Appendix). Crosslinkers **3 - 5** required no additional structural verification before use.



**Figure 2.3.** Synthesis of bis-benzophenone, **1**.



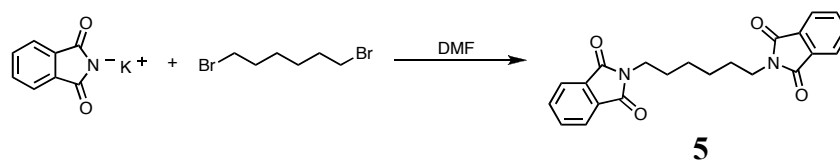
**Figure 2.4.** Synthesis of mixed 3- and 4-benzoylbenzoate crosslinkers, **2**.



**Figure 2.5.** Synthesis of bis-xanthone, **3**.



**Figure 2.6.** Synthesis of bis-phenyl azide, **4**.



**Figure 2.7.** Synthesis of bis-phthalimide, **5**.



## 2.4. Core-Crosslinked Micelles and Crosslinked Thin Films

(with Kavita Vemishetti and Nick Carbone)

To extend the use of the homobifunctional photocrosslinkers described above, we sought to apply the photocrosslinking methodology in systems such as homopolymer thin films and polymer micelles. The work on homopolymer thin films extends the original use of **1** in polymer thin films as a means to prevent film dewetting upon heating.<sup>40</sup> In order to investigate the behavior of the second-generation crosslinkers in polymer films, compounds **1** - **5** were codissolved with polymer in a suitable solvent, cast into films, irradiated, and analyzed using gel permeation chromatography. The results of these experiments are being reported in a forthcoming thesis, and so will not be repeated here.<sup>86</sup>

Similarly, experiments were undertaken to use **1** in an attempt to crosslink copolymer micelles in order to prevent dispersion upon dilution. The results of those experiments are detailed below.

### 2.4.1. Introduction to Core-Crosslinked Micelles

Block copolymers composed of dissimilar blocks aggregate in formations that maximize favorable polymer-polymer or polymer-solvent interactions while minimizing disfavorable interactions.<sup>87</sup> The morphology of the aggregate depends upon the constituent block lengths and identities, and can span a wide range of architectures: from micelles, spheres, and vesicles to loose clusters, lamellae, and cylinders.<sup>88-91</sup> Morphologies also vary depending on types and amounts of solvent, temperature, and the number and order of blocks composing the polymer.<sup>92</sup> In the case of a micelle, the total molecular weight of the aggregate varies depending on the copolymer molecular weight,

the relative amount of the soluble component of the copolymer, the number of blocks in the polymer (e.g. diblock vs. triblock), and changes in temperature that affect the mobility of the blocks in the aggregate.<sup>93</sup> In order to prevent external stimuli from altering an intended configuration of the block copolymer aggregate, *in situ* crosslinking can lock polymer chains in place. Crosslinking of micelles containing blocks bearing pendant cinnamoyl<sup>94</sup>, coumarin<sup>95</sup>, hydroxide<sup>96</sup>, pyridine<sup>97</sup>, and trimethoxysilane<sup>98</sup> functionalities has succeeded in holding together the micellar aggregate despite changes in concentration or temperature that might have otherwise degraded the micelle.<sup>99,100</sup> Crosslinked micellar structures such as these have potential application as drug delivery vehicles, colloidal additives to bulk polymeric materials, and as nanometer-sized three-dimensional patterns and templates.<sup>101-105</sup>

As mentioned above for other crosslinkable polymeric systems, a pendant crosslinking moiety has most often been included during synthesis of the block copolymer. This strategy is useful for crosslinking at particular locations in an aggregate (e.g. polymer end groups, midpoint, etc.), but it does not offer the possibility to universally crosslink any of these morphologies without resynthesizing the material itself. To overcome the synthetic necessity of including pendant crosslinkable moieties and to potentially facilitate the generation of libraries of micelles with varying crosslink density from the same preformed polymer, the homobifunctional crosslinker **1** was introduced to the core of a polystyrene-*block*-poly(ethylene oxide) (PS-*b*-PEO) micelle and irradiated. Examination by surface tensiometry and intercalated pyrene fluorescence showed retention of micellar properties after dilution below the critical micelle concentration (cmc), verifying that the core-crosslinked micelle was locked in place by molecular

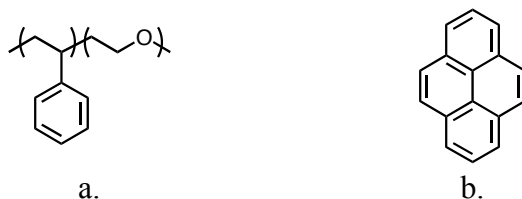
bridges formed by **1**. This ‘universal’ approach is advantageous because of the diversity of synthetic and natural polymers which have been shown to form micelles: block copolymers such as polystyrene-block-poly(acrylic acid)<sup>106</sup>, poly(n-butyl acrylate)-block-poly(acrylic acid)<sup>107,108</sup>, polybutadiene-block-poly(ethylene glycol)<sup>109</sup>; hyperbranched polymers<sup>110</sup>; DNA<sup>111</sup>; and phospholipids<sup>112</sup>.

#### **2.4.2. Preparation of PS-b-PEG Micelles**

PS-b-PEO (Figure 2.8a) is a well-behaved block copolymer that readily forms micelles in solution and is commercially available with PS and PEO blocks of many different molecular weights. Morphologies of PS-b-PEO are well studied at different concentrations, in different solvents, and at different temperatures.<sup>113-118</sup> Additionally, a number of analytical techniques have been used to monitor and characterize the formation of PS-b-PEO micelles, including static and dynamic light scattering<sup>119</sup>, small angle neutron scattering<sup>120</sup>, fluorescence of intercalated pyrene<sup>121</sup>, and computer simulations<sup>122</sup>.

The most important property to measure for any micelle-forming block copolymer is its critical micelle concentration (cmc), which is the concentration at which individual polymer chains in solution (unimers) begin to aggregate into micelles. At concentrations below the cmc, only unimers are present in solution with no micelles, and at concentrations above the cmc both unimers and micelles are present in solution. The cmc represents a balance of the driving forces for the copolymer blocks to form micelles and depends upon the absolute and relative molecular weights of the copolymer blocks, their chemical composition, the solvent and temperature. A low cmc indicates the polymer

readily forms micelles because of very unfavorable interactions of one block with the solvent while the other block interacts very favorably with it. Micelle formation is not likely to be observed if both blocks are soluble in the solvent. It is possible to directly measure the cmc because a number of properties change at the critical concentration: for example, surface tension, light scattering, and optical activity all change dramatically at the cmc.<sup>123</sup> For PS-*b*-PEO in water, a typical cmc is between 0.02 and 2 mg/mL, but is dependent upon the absolute and relative molecular weights of the PS and PEO blocks.



**Figure 2.8.** Structures of compounds used in the micelle study in addition to **1**: (a) polystyrene-*block*-poly(ethylene oxide); and (b) pyrene.

To form micelles, PS-*b*-PEO (Polymer Source, Inc.,  $M_n = \text{PS}(9500)\text{-}b\text{-PEO}(9500)$ ,  $\text{PS}_{91}\text{-}b\text{-PEO}_{216}$ ,  $M_w/M_n = 1.07$ ) was dissolved in Millipore filtered deionized water and stirred overnight. In order to determine the cmc of the PS-*b*-PEO, solutions were then subjected to either surface tensiometry or transferred to a vial containing a pyrene residue (Figure 2.8b) then stirred overnight once again for subsequent pyrene fluorescence measurements.

### 2.4.3. Analysis

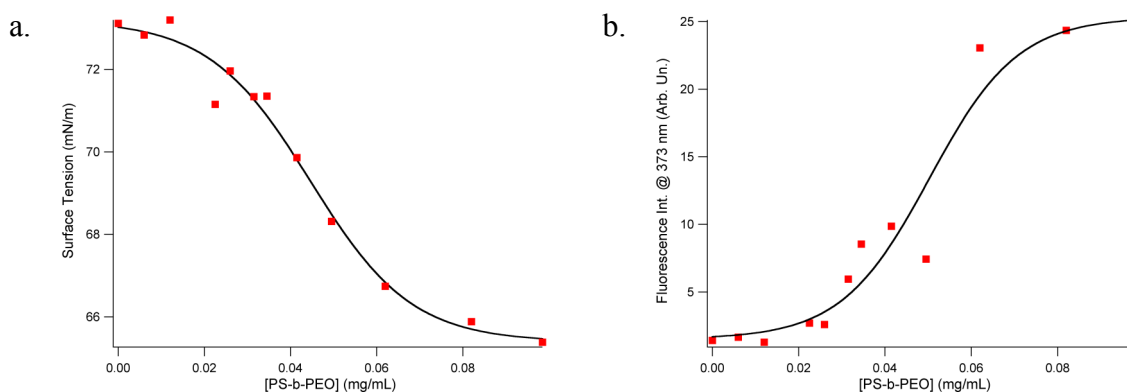
#### 2.4.3.1. Surface Tension

The surface tension of PS-*b*-PEO at various concentrations in water was determined using the Wilhelmy plate method on a Krüss K12 surface tensiometer. Since

block copolymer micelles do not rapidly adjust to changes in dilution, solutions in the range of 0 – 0.1 mg/mL of PS-b-PEO in water were prepared and equilibrated prior to measurement. A platinum plate of known width was dipped into each solution, and the force was measured as the plate was removed from the solution. The surface tension of the solution,  $\sigma$ , was calculated according to Equation 2.1 from the force exerted by the solution wetting the plate,  $F$ , the width of the plate,  $l$ , and the contact angle of the liquid,  $\theta$ . The surface tension of the PS-b-PEO in water is plotted in Figure 2.9a as a function of block copolymer concentration. The cmc of the block copolymer is the concentration at the intersection of a line tangent to the steepest part of the curve with a line tangent to the curve at pure water (where [PS-b-PEO] = 0). For the data plotted in Figure 2.9a, the cmc is approximately 0.02 mg/mL.

$$\sigma = \frac{F}{l \cos \theta} \quad \text{Equation 2.1}$$

**Equation 2.1.** Equation for surface tension,  $\sigma$ , by the Wilhelmy plate method calculated from the force exerted,  $F$ , the wetted length of the plate,  $l$ , and the contact angle of the liquid,  $\theta$ .



**Figure 2.9.** Surface tension (a) and pyrene fluorescence (b) measurements of aqueous solutions of PS-b-PEO. Extrapolation of the lines tangent to the steepest slope give the cmc of the native PS-b-PEO used as approximately 0.02 mg/mL.

### 2.4.3.2. Pyrene Fluorescence

To verify the cmc determined by surface tensiometry, the fluorescence of intercalated pyrene (Figure 2.8b) was also used to characterize the PS-b-PEO micelles. Prior to micelle formation, block copolymer unimers do not enhance the amount of insoluble pyrene in aqueous solution. Once aggregated, however, block copolymer micelles intercalate pyrene to their hydrophobic core. Since the solubility of pyrene is very low in pure water, fluorescence experiments can be used to monitor micelle formation according to the concentration of copolymer necessary to take up the fluorescent pyrene within the micelle core.<sup>106,114,121,124,125</sup> When pyrene intercalates into the polystyrene core of a copolymer micelle, the fluorescence spectrum undergoes three characteristic changes: the (0,0) band red shifts from 332 nm to 338 nm, the vibrational structure of the characteristic peaks changes, and the fluorescence lifetime increases from 200 ns to approximately 350 ns. As more pyrene is taken up into the micelle core, the broad excimer peak also increases in the range 425 – 550 nm. Its characteristic behavior in a broad range of environments makes pyrene an ideal probe to monitor the dynamics of free and aggregated polymers in solutions; pyrene fluorescence has been used to monitor the dynamics of polymer branch ends in solution<sup>126</sup> and to observe polymer end-to-end cyclization<sup>127</sup>.

Pyrene was deposited into a vial by evaporation from solution (2mM, CCl<sub>4</sub>) and aqueous solutions of PS-b-PEO were stirred over the pyrene residue. After stirring for several days, the fluorescence of the solutions was measured using a FluoroMax-2 UV-Vis spectrometer. After correcting spectral baselines, the ratio of the intensities of the first to third peak ( $I_1/I_3$ ) was plotted against the concentration of the PS-b-PEO copolymer in

solution (Figure 2.9b). Again, the cmc of PS-b-PEO was determined by extrapolation from the steepest part of the curve, and was found to be approximately 0.02 g/mL PS-b-PEO in water.

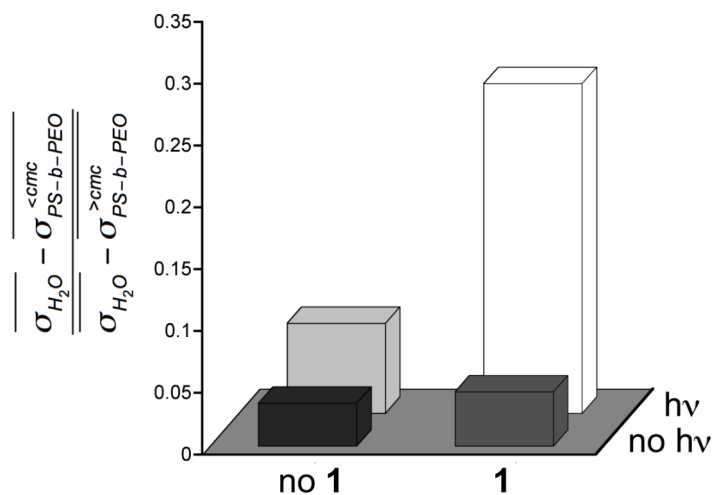
#### 2.4.4. Core-Crosslinking of PS-b-PEO Micelles

With a measurement of the cmc for the PS-b-PEO model system in hand ( $\sim 0.02$  mg/mL), experiments were undertaken to determine whether the glassy PS core of the copolymer micelles could be crosslinked using the homobifunctional crosslinker **1**. A solution of **1** was deposited by evaporation from  $\text{CHCl}_3$  into several vials and aqueous solutions of PS-b-PEO at concentrations well above the cmc (approx 0.1 mg/mL) were stirred over the residues in order to intercalate **1** into the micelles. In parallel, samples were prepared at the same PS-b-PEO concentration without **1**. Samples with and without **1** were then each split into two groups: half were irradiated at 350 nm for one hour (Rayonet reactor) and half were not. Following irradiation, aliquots of each sample were diluted tenfold so the resulting concentration of PS-b-PEO would fall below the cmc ( $\sim 0.01$  mg/mL). After stirring for several days, the surface tension of each solution was measured as before.

Figure 2.10 shows the results of the surface tension analysis of the PS-b-PEO micelles and the effects of **1** and irradiation upon the surface tension. Each bar is the average of two samples treated identically – with light and **1** (white), only light (light gray), only **1** (dark gray) and neither light nor **1** (black) – and represents the ratio of the difference between the surface tension of pure water and a solution below the cmc to the difference between the surface tension of pure water and a solution above the cmc. A

lower value of the ratio is indicative of the solution becoming more like pure water upon dissolution (e.g. disassembly of micelles), whereas a higher ratio is indicative of the solution retaining the qualities above the cmc (e.g. retention of micelles). Figure 2.10 shows that irradiation for one hour is sufficient to significantly alter the surface tension of a solution of PS-b-PEO with **1** relative to pure water, while solutions not having both the crosslinker and irradiation have surface tensions more like pure water.

We interpret Figure 2.10 to represent the retention of micelle-like properties of the crosslinked micelles – only those irradiated with **1** – relative to micelles that fall apart upon dilution. This indicates that **1** successfully intercalates into the copolymer micelle, and that the crosslinks formed prevent chains from untangling upon dilution. It is reasonable that the surface tension of diluted solutions would be less than that of solutions above the cmc because the weight percent of water is so much higher following dilution.



**Figure 2.10.** Surface tension measurements of aqueous solutions of PS-b-PEO as compared to pure water. The data represents the ratio of the difference between the measured value of the surface tension of water and diluted PS-b-PEO solution (below the cmc, approx. 0.01 mg/mL) to the difference between the measured value of the surface tension of water and concentrated PS-b-PEO (above the cmc, approx. 0.1 mg/mL). A lower value of the ratio is indicative of the PS-b-PEO micelles disassembling in water upon dilution. The error on each value is less than 25%.



However, despite the higher weight percent of water, the crosslinked micelles still retained approximately 30% of the character of a concentrated solution above the cmc.

In addition to surface tensiometry and pyrene fluorescence, a number of other methods could be used to further analyze the copolymer micelles: static and dynamic light scattering, small angle neutron scattering, viscosimetry, dilatometry, and sedimentation. From these techniques, the micelle core size, interaction radius, diffusivity, and molecular weight could be determined, however determination of those characteristics goes beyond the scope of the proof of this principle in diblock copolymer micelles.

The proof-of-principle method shown here for crosslinking a simple diblock copolymer micelle could readily extend to other morphologies of preformed block copolymers in solution and on surfaces as well. This technique is very powerful in that it does not require the unique synthesis of a block copolymer in order to achieve crosslinked copolymer nano- and microstructures, but instead it relies on specially tailored molecular bridges to intercalate into domains of the copolymer aggregate followed by photoactivation and crosslinking.

#### **2.4.5. Application of Micelles in Drug Delivery**

Micelles and block copolymer nanoparticles are important candidates for drug delivery vehicles and therapeutic/diagnostic (theranostic) applications because they offer a great deal of control over architecture and functionalization.<sup>101,104,128,129</sup> The core of a micelle can effectively encapsulate and shuttle a hydrophobic drug (e.g. doxorubicin<sup>130-</sup>

<sup>133</sup>) throughout the body while the shell of the micelle solubilizes the assembly and prevents non-specific release of the drug. Additionally, probe molecules can be intercalated into the core of the micelle as contrast agents for magnetic resonance imaging (MRI).<sup>134</sup> Furthermore, targeted drug delivery vehicles, for example, bear some peripheral moiety that binds to a specific site on a cell or protein so that release of a therapeutic agent causes a high local concentration of the drug at the delivery site while maintaining an overall low full-body concentration. Combining these possibilities into a single targeting, drug delivering, diagnostic material is highly desirable for patients, doctors, biomedical engineers, and pharmaceutical companies.

A drawback to the use of non-crosslinked micelles, however, is that delivery into the bloodstream lowers the micelle concentration below the cmc. Upon dispersion in the blood the micelle may quickly decompose, thereby releasing its cargo before it can find its targeted destination. Crosslinking micelles, therefore, is crucial to their successful application as drug delivery vehicles.

## **2.5. Summary**

- Homobifunctional compounds have been synthesized and characterized bearing photoactive moieties linked by aliphatic chains.
- The homobifunctional compounds are intended to incorporate into polymer thin films to crosslink polymer chains upon irradiation.
- The critical micelle concentration (cmc) of a block copolymer was measured using both surface tension and pyrene fluorescence measurements.

- A previously reported homobifunctional crosslinker was incorporated into the core of a block copolymer micelle, and irradiation decreased the disentanglement of the micelle upon dissolution below the cmc.
- Surface tension and pyrene fluorescence measurements verified that both light and the crosslinker are necessary to cause the copolymer aggregate to remain assembled.

## 2.6. References

1. Kim, S.-H.; Chu, C.-C. In vitro Release Behavior of Dextran-Methacrylate Hydrogels Using Doxorubicin and Other Model Compounds. *Journal of Biomaterials Applications* **2000**, *15*, 23-46.
2. Young, T.-H.; Chuang, W.-Y.; Wei, C.-W.; Tang, C.-Y. Investigation of the drug distribution and release characteristics from particulate membranes. *Journal of Membrane Science* **2001**, *191*, 199-205.
3. Liu, S.; Maheshwari, R.; Kiick, K. L. Polymer-Based Therapeutics. *Macromolecules* **2009**, *42*, 3-13.
4. Kulshrestha, A. S.; Mahapatro, A. In *Polymers for Biomedical Applications*; Mahapatro, A., Ed.; American Chemical Society: Washington, DC, 2008; pp. 1-7.
5. Tighe, B. J. In *Macromolecular Chemistry*; Jenkins, A. D.; Kennedy, J. F., Eds.; Royal Society of Chemistry: Cambridge, 1980; Vol. 1, pp. 416-428.
6. Tighe, B. J. In *Macromolecular Chemistry*; Jenkins, A. D.; Kennedy, J. F., Eds.; Royal Society of Chemistry: Cambridge, 1982; Vol. 2, pp. 347-360.
7. Tighe, B. J. In *Macromolecular Chemistry*; Jenkins, A. D.; Kennedy, J. F., Eds.; Royal Society of Chemistry: Cambridge, 1984; Vol. 3, pp. 375-386.
8. Choi, S.-W.; Zhang, Y.; Xia, Y. Three-dimensional scaffolds for tissue engineering: the importance of uniformity in pore size and structure. *Langmuir* **2010**, *26*, 19001-19006.
9. *The Nanoparticle Drug Delivery Market*; Market Research Report; Cientifica Ltd., August 2007; 300.
10. He, W.; Feng, Y.; Ma, Z.; Ramakrishna, S. In *Polymers for Biomedical Applications*; Mahapatro, A., Ed.; American Chemical Society: Washington, DC, 2008; pp. 310-335.
11. Shoichet, M. S. Polymer Scaffolds for Biomaterials Applications. *Macromolecules* **2010**, *43*, 581-591.
12. Shi, J.; Votruba, A. R.; Farokhzad, O. C.; Langer, R. Nanotechnology in Drug Delivery and Tissue Engineering: From Discovery to Applications. *Nano Letters* **2010**, *10*, 3223-3230.
13. Timko, B. P.; Dvir, T.; Kohane, D. S. Remotely triggerable drug delivery systems. *Advanced Materials* **2010**, *22*, 4925-4943.
14. Nicholson, J. W. In *Chemistry of Polymers*; Royal Society of Chemistry: Cambridge, 2006; pp. 54-65.
15. Vázquez, C. P.; Boudou, T.; Dulong, V.; Nicolas, C.; Picart, C.; Glinel, K. Variation of polyelectrolyte film stiffness by photo-cross-linking: a new way to control cell adhesion. *Langmuir* **2009**, *25*, 3556-3563.
16. Bartczak, D.; Kanaras, A. G. Diacetylene-Containing Ligand As a New Capping Agent for the Preparation of Water-Soluble Colloidal Nanoparticles of Remarkable Stability. *Langmuir* **2010**, *26*, 7072-7077.
17. He, J.; Tong, X.; Zhao, Y. Photoresponsive Nanogels Based on Photocontrollable Cross-Links. *Macromolecules* **2009**, *42*, 4845-4852.
18. Kehrloesser, D.; Baumann, R.-Peter; Kim, H.-Cheol; Hampp, N. Photochemistry of Coumarin-Functionalized SiO<sub>2</sub> Nanoparticles. *Langmuir* **2011**, *27*, 4149-4155.
19. Chujo, Y.; Sada, K.; Saegusa, T. Polyoxazoline having a coumarin moiety as a pendant group. Synthesis and photogelation. *Macromolecules* **1990**, *23*, 2693-2697.
20. Zhao, L.; Vaupel, M.; Loy, D. A.; Shea, K. J. Photoresponsive Hybrid Materials: Synthesis and Characterization of Coumarin-Dimer-Bridged Polysilsesquioxanes. *Chemistry of Materials* **2008**, *20*, 1870-1876.
21. Zhao, L.; Loy, D. A.; Shea, K. J. Photodeformable spherical hybrid nanoparticles. *Journal of the American Chemical Society* **2006**, *128*, 14250-14251.

- 
22. Iliopoulos, K.; Krupka, O.; Gindre, D.; Sallé, M. Reversible two-photon optical data storage in coumarin-based copolymers. *Journal of the American Chemical Society* **2010**, *132*, 14343-14345.
  23. He, J.; Tong, X.; Zhao, Y. Photoresponsive Nanogels Based on Photocontrollable Cross-Links. *Macromolecules* **2009**, *42*, 4845-4852.
  24. He, J.; Yan, B.; Tremblay, L.; Zhao, Y. Both core- and shell-cross-linked nanogels: photoinduced size change, intraparticle LCST, and interparticle UCST thermal behaviors. *Langmuir* **2011**, *27*, 436-444.
  25. Klinger, M.; Tolbod, L. P.; Gothelf, K. V.; Ogilby, P. R. Effect of polymer cross-links on oxygen diffusion in glassy PMMA films. *Applied Materials & Interfaces* **2009**, *1*, 661-667.
  26. Yang, H.; Jia, L.; Wang, Z.; Di-Cicco, A.; Lévy, D.; Keller, P. Novel Photolabile Diblock Copolymers Bearing Truxillic Acid Derivative Junctions. *Macromolecules* **2011**, *44*, 159-165.
  27. van der Ende, A. E.; Harrell, J.; Sathiyakumar, V.; Meschievitz, M.; Katz, J.; Adcock, K.; Harth, E. "Click" Reactions: Novel Chemistries for Forming Well-defined Polyester Nanoparticles. *Macromolecules* **2010**, *43*, 5665-5671.
  28. Garg, S. M.; Xiong, X.-Bing; Lu, C.; Lavasanifar, A. Application of Click Chemistry in the Preparation of Poly(ethylene oxide)-block-poly( $\epsilon$ -caprolactone) with Hydrolyzable Cross-Links in the Micellar Core. *Macromolecules* **2011**, *44*, 2058-2066.
  29. Ochs, C. J.; Such, G. K.; Yan, Y.; van Koeverden, M. P.; Caruso, F. Biodegradable click capsules with engineered drug-loaded multilayers. *ACS Nano* **2010**, *4*, 1653-1663.
  30. Mulik, S.; Sotiriou-Leventis, C.; Leventis, N. Macroporous Electrically Conducting Carbon Networks by Pyrolysis of Isocyanate-Cross-Linked Resorcinol-Formaldehyde Aerogels. *Chemistry of Materials* **2008**, *20*, 6985-6997.
  31. Beck, J. B.; Killops, K. L.; Kang, T.; Sivanandan, K.; Bayles, A.; Mackay, M. E.; Wooley, K. L.; Hawker, C. J. Facile Preparation of Nanoparticles by Intramolecular Cross-Linking of Isocyanate Functionalized Copolymers. *Macromolecules* **2009**, *42*, 5629-5635.
  32. Gheneim, R.; Perez-Berumen, C.; Gandini, A. Diels-Alder Reactions with Novel Polymeric Dienes and Dienophiles: Synthesis of Reversibly Cross-Linked Elastomers. *Macromolecules* **2002**, *35*, 7246-7253.
  33. Peterson, A. M.; Jensen, R. E.; Palmese, G. R. Reversibly cross-linked polymer gels as healing agents for epoxy-amine thermosets. *Applied Materials & Interfaces* **2009**, *1*, 992-995.
  34. Ishida, K.; Yoshie, N. Two-Way Conversion between Hard and Soft Properties of Semicrystalline Cross-Linked Polymer. *Macromolecules* **2008**, *41*, 4753-4757.
  35. Yoo, M.; Kim, S.; Lim, J.; Kramer, E. J.; Hawker, C. J.; Kim, B. J.; Bang, J. Facile Synthesis of Thermally Stable Core-Shell Gold Nanoparticles via Photo-Cross-Linkable Polymeric Ligands. *Macromolecules* **2010**, *43*, 3570-3575.
  36. Wu, G.; Shi, F.; Wang, Z.; Liu, Z.; Zhang, X. Poly(acrylic acid)-Bearing Photoreactive Azido Groups for Stabilizing Multilayer Films. *Langmuir* **2009**, *25*, 2949-2955.
  37. Zillessen, A.; Bartsch, E. Synthesis of photo-cross-linkable microgel colloids for cluster formation studies. *Langmuir* **2010**, *26*, 89-96.
  38. Bunte, C.; Prucker, O.; König, T.; Rühle, J. Enzyme containing redox polymer networks for biosensors or biofuel cells: a photochemical approach. *Langmuir* **2010**, *26*, 6019-6027.
  39. Shi, D.; Matsusaki, M.; Kaneko, T.; Akashi, M. Photo-Cross-Linking and Cleavage Induced Reversible Size Change of Bio-Based Nanoparticles. *Macromolecules* **2008**, *41*, 8167-8172.

- 
40. Carroll, G. T.; Sojka, M. E.; Lei, X.; Turro, N. J.; Koberstein, J. T. Photoactive additives for cross-linking polymer films: Inhibition of dewetting in thin polymer films. *Langmuir* **2006**, *22*, 7748-7754.
41. Kestur, U. S.; Lee, H.; Santiago, D.; Rinaldi, C.; Won, Y.-Y.; Taylor, L. S. Effects of the Molecular Weight and Concentration of Polymer Additives, and Temperature on the Melt Crystallization Kinetics of a Small Drug Molecule. *Crystal Growth & Design* **2010**, *10*, 3585-3595.
42. Sinz, A. Chemical cross-linking and mass spectrometry for mapping three-dimensional structures of proteins and protein complexes. *Journal of Mass Spectrometry: JMS* **2003**, *38*, 1225-1237.
43. Tanaka, Y.; Bond, M. R.; Kohler, J. J. Photocrosslinkers illuminate interactions in living cells. *Molecular bioSystems* **2008**, *4*, 473-480.
44. Angulo, G.; Grilj, J.; Vauthey, E.; Serrano-Andrés, L.; Rubio-Pons, O.; Jacques, P. Ultrafast decay of the excited singlet states of thioxanthone by internal conversion and intersystem crossing. *ChemPhysChem* **2010**, *11*, 480-488.
45. Kanaoka, Y. Photoreactions of cyclic imides. Examples of synthetic organic photochemistry. *Accounts of Chemical Research* **1978**, *11*, 407-413.
46. Oelgemöller, M.; Griesbeck, A. G. Photochemistry of Phthalimides: Decarboxylation, Addition, Macrocyclization and Deprotection. *Internet Photochemistry & Photobiology* **2000**.
47. Nájera, F.; García-Segura, R.; Pérez-Inestrosa, E.; Sánchez-Sánchez, C.; Suau, R. Photoinduced addition of phthalimide to unactivated alkynes. *Photochemistry and Photobiology* **2006**, *82*, 248-253.
48. Warzecha, K.-D.; Görner, H.; Griesbeck, A. G. Photoinduced decarboxylative benzylation of phthalimide triplets with phenyl acetates: a mechanistic study. *Journal of Physical Chemistry A* **2006**, *110*, 3356-3363.
49. Yoon, U. C.; Oh, S. W.; Lee, J. H.; Park, J. H.; Kang, K. T.; Mariano, P. S. Applications of Phthalimide Photochemistry to Macrocyclic Polyether, Polythioether, and Polyamide Synthesis. *Journal of Organic Chemistry* **2001**, *66*, 939-943.
50. Lee, Y. J.; Lee, C. P.; Jeon, Y. T.; Mariano, P. S.; Yoon, U. C.; Kim, D. U.; Kim, J. C.; Lee, J. G. The operation of H-atom and TMS-group transfer processes in the photochemistry of silylamidoalkyl- and silylalkyl-ketones and -phthalimides. *Tetrahedron Letters* **1993**, *34*, 5855-5858.
51. Fu, H.-Ping; Zhang, M.; Shi, H.-Guang; Xu, J.-Hua. Photoinduced [2 + 2] cycloaddition (the Paterno-Büchi reaction) of N-methyl-4,5,6,7-tetrachlorophthalimide with alkenes. *Research on Chemical Intermediates* **2004**, *30*, 383-395.
52. Coyle, J. D.; Harriman, A.; Newport, G. L. Reversible photorearrangement of N-substituted phthalimides: a flash photolysis study. *Journal of the Chemical Society, Perkin Transactions 2* **1979**, 799.
53. Maruyama, K.; Kubo, Y. Photochemistry of phthalimides with olefins. Solvent-incorporated addition vs. cycloaddition to imide C(=O)-N bond accompanying ring enlargement. *Journal of Organic Chemistry* **1985**, *50*, 1426-1435.
54. Kanaoka, Y.; Migita, Y.; Koyama, K.; Sato, Y.; Nakai, H.; Mizoguchi, T. Photochemistry of the phthalimide system. IV. Photocyclization of N-alkylphthalimides to benzazepinone lactams: Unusual two-fold norrish type II reactions. *Tetrahedron Letters* **1973**, *14*, 1193-1196.
55. Khlebnikov, A. F.; Novikov, M. S.; Kostikov, R. R. In *Advances in Heterocyclic Chemistry*; Academic Press, Inc., 1996; pp. 93-233.
56. Rosenberg, M. G.; Brinker, U. H. Constrained Carbenes. *European Journal of Organic Chemistry* **2006**, *2006*, 5423-5440.

- 
57. Fleet, G. W.; Knowles, J. R.; Porter, R. R. The antibody binding site. Labelling of a specific antibody against the photo-precursor of an aryl nitrene. *The Biochemical Journal* **1972**, *128*, 499-508.
58. Geiger, M. W.; Elliot, M. M.; Karacostas, V. D.; Moricone, T. J.; Salmon, J. B.; Sideli, V. L.; Onge, M. A. S. Aryl Azides As Protein Photolabels: Absorption Spectral Properties and Quantum Yields of Photodissociation. *Photochemistry and Photobiology* **1984**, *40*, 545-548.
59. Bayley, H.; Knowles, J. R. Photogenerated reagents for membrane labeling. 1. Phenylnitrene formed within the lipid bilayer. *Biochemistry* **1978**, *17*, 2414-2419.
60. Dockter, M. E.; Koseki, T. Covalent modification of hydrophilic and hydrophobic domains of yeast cytochrome c oxidase with fluorescent azides. *Biochemistry* **1983**, *22*, 3954-3961.
61. Gross, A. J.; Yu, S. S. C.; Downard, A. J. Two-component mixed and patterned films on carbon surfaces through the photografting of arylazides. *Langmuir* **2010**, *26*, 7285-7292.
62. Gann, J. P.; Yan, M. A versatile method for grafting polymers on nanoparticles. *Langmuir* **2008**, *24*, 5319-5323.
63. Gritsan, N.; Platz, M. In *Organic Azides: Syntheses and Applications*; John Wiley & Sons Ltd, 2010; pp. 311-372.
64. Liu, L.-H.; Yan, M. Perfluorophenyl azides: new applications in surface functionalization and nanomaterial synthesis. *Accounts of Chemical Research* **2010**, *43*, 1434-1443.
65. Samour, C. M.; Mason, J. P. Preparation and Reactions of Bis-diazoalkanes. *Journal of the American Chemical Society* **1954**, *76*, 441-445.
66. Tomioka, H. Reactions of Carbenes in Solidified Organic Molecules At Low Temperature. *Research on Chemical Intermediates* **1994**, *20*, 605-634.
67. Song, Z.; Zhang, Q. Fluorous aryldiazirine photoaffinity labeling reagents. *Organic Letters* **2009**, *11*, 4882-4885.
68. Hosoya, T.; Hiramatsu, T.; Ikemoto, T.; Aoyama, H.; Ohmae, T.; Endo, M.; Suzuki, M. Design of dantrolene-derived probes for radioisotope-free photoaffinity labeling of proteins involved in the physiological Ca<sup>2+</sup> release from sarcoplasmic reticulum of skeletal muscle. *Bioorganic & Medicinal Chemistry Letters* **2005**, *15*, 1289-1294.
69. Hatanaka, Y.; Nakamura, N.; Wakabayashi, M.; Fujioka, T.; Kikuchi, T. Synthesis and Characterization of Novel Photoreactive Naltrexone Analogs as Isomeric Carbene-Generating Probes for Opioid Receptors. *Heterocycles* **1996**, *43*, 519-522.
70. Blencowe, A.; Hayes, W. Development and application of diazirines in biological and synthetic macromolecular systems. *Soft Matter* **2005**, *1*, 178.
71. Brunner, J.; Semenza, G. Selective labeling of the hydrophobic core of membranes with 3-(trifluoromethyl)-3-(m-[<sup>125</sup>I]iodophenyl)diazirine, a carbene-generating reagent. *Biochemistry* **1981**, *20*, 7174-7182.
72. Ismaili, H.; Lee, S.; Workentin, M. S. Diazirine-modified gold nanoparticle: template for efficient photoinduced interfacial carbene insertion reactions. *Langmuir* **2010**, *26*, 14958-14964.
73. Herdon, H. J.; Jerman, J. C.; Chan, W. N. Novel Receptor **1996**, 27. Patent WO 96/18650.
74. Kauffman, J. F.; Turner, J. M.; Alabugin, I. V.; Breiner, B.; Kovalenko, S. V.; Badaeva, E. A.; Masunov, A.; Tretiak, S. Two-photon excitation of substituted enediynes. *Journal of Physical Chemistry A* **2006**, *110*, 241-251.
75. Hoffner, J.; Schottelius, M. J.; Feichtinger, D.; Chen, P. Chemistry of the 2,5-Didehydropyridine Biradical: Computational, Kinetic, and Trapping Studies toward Drug Design. *Journal of the American Chemical Society* **1998**, *120*, 376-385.

- 
76. David, W. M.; Kerwin, S. M. Synthesis and Thermal Rearrangement of C,N -Dialkynyl Imines: A Potential Aza-Bergman Route to 2,5-Didehydropyridine. *Journal of the American Chemical Society* **1997**, *119*, 1464-1465.
77. Pandithavidana, D. R.; Poloukhine, A.; Popik, V. V. Photochemical generation and reversible cycloaromatization of a nine-membered ring cyclic enediyne. *Journal of the American Chemical Society* **2009**, *131*, 351-356.
78. Bergman, R. G. Reactive 1,4-dehydroaromatics. *Accounts of Chemical Research* **1973**, *6*, 25-31.
79. Chen, P. Design of Diradical-based Hydrogen Abstraction Agents. *Angewandte Chemie International Edition* **1996**, *35*, 1478-1480.
80. Raghuraman, G. K.; Schuh, K.; Prucker, O.; Rühle, J. Attachment of polymer films to solid surfaces via thermal activation of self-assembled monolayers containing sulphonyl azide group. *Langmuir* **2010**, *26*, 769-74.
81. Synthesis of **1**: JRL1p63. <sup>1</sup>H NMR of **1**: JRL-081108exp1. <sup>1</sup>H NMR of monomer: JRL\_10\_0128\_3-COOH\_benzophenone, JRL\_10\_0130\_3-COOH\_benzophenone.
82. Synthesis of **2**: JRL1p57. <sup>1</sup>H NMR of **2** before crystallization: JRL-090108-mp-bis-BP. <sup>1</sup>H NMR of **2**, filtrand (A): JRL-092308-mp-bis-BPexp1(A). <sup>1</sup>H NMR of **2**, filtrate (B): JRL-092308-mp-bis-BPexp2(B).
83. Synthesis of **3**: JRL1p145, JRL2p19. <sup>1</sup>H NMR of **3**: JRL-083009-bisxanthone, JRL-121409-bisxanthone. <sup>1</sup>H NMR of monomer: JRL\_10\_0128\_xanthone.
84. Synthesis of **4**: JRL2p35. <sup>1</sup>H NMR of **4**: JRL041109-bisphenylazide, JRL\_10\_0128\_bis\_phenyl\_azide. <sup>1</sup>H NMR of monomer: JRL\_10\_0128\_phenyl\_azide, JRL\_10\_0130\_phenyl\_azide-COOH.
85. Synthesis of **5**: JRL1p37, JRL1p47, JRL1p49, JRL2p61. <sup>1</sup>H NMR of **5**: JRL\_10\_0421\_bisphthalimide-C6.
86. Carbone, N. Ph.D. Dissertation, Columbia University, New York, NY, 2011.
87. Andelman, D.; Rosensweig, R. E. Modulated Phases: Review and Recent Results. *Journal of Physical Chemistry B* **2009**, *113*, 3785-3798.
88. Giacomelli, C.; Schmidt, V.; Aissou, K.; Borsali, R. Block Copolymer Systems: From Single Chain to Self-Assembled Nanostructures. *Langmuir* **2010**, *26*, 15734-15744.
89. Tomas, S.; Milanesi, L. Hydrophobically self-assembled nanoparticles as molecular receptors in water. *Journal of the American Chemical Society* **2009**, *131*, 6618-6623.
90. Hosoi, A.; Kogan, D.; Devereaux, C.; Bernoff, A.; Baker, S. Two-Dimensional Self-Assembly in Diblock Copolymers. *Physical Review Letters* **2005**, *95*, 1-4.
91. Discher, D. E.; Eisenberg, A. Polymer vesicles. *Science* **2002**, *297*, 967-973.
92. Zhang, Y.; Lin, W.; Jing, R.; Huang, J. Effect of Block Sequence on the Self-Assembly of ABC Terpolymers in Selective Solvent. *Journal of Physical Chemistry B* **2008**, *112*, 16455-16460.
93. Chen, J.; Zeng, F.; Wu, S. Construction of energy transfer systems within nanosized polymer micelles and their fluorescence modulation properties. *ChemPhysChem* **2010**, *11*, 1036-1043.
94. Yusa, S.-Ichi; Sugahara, M.; Endo, T.; Morishima, Y. Preparation and characterization of a pH-responsive nanogel based on a photo-cross-linked micelle formed from block copolymers with controlled structure. *Langmuir* **2009**, *25*, 5258-5265.
95. Jiang, J.; Qi, B.; Lepage, M.; Zhao, Y. Polymer Micelles Stabilization on Demand through Reversible Photo-Cross-Linking. *Macromolecules* **2007**, *40*, 790-792.



- 
96. Siebert, M.; Henke, A.; Eckert, T.; Richtering, W.; Keul, H.; Möller, M. Polystyrene-block-polyglycidol micelles cross-linked with titanium tetraisopropoxide. laser light and small-angle X-ray scattering studies on their formation in solution. *Langmuir* **2010**, *26*, 16791-16800.
97. Hui, T.; Chen, D.; Jiang, M. A One-Step Approach to the Highly Efficient Preparation of Core-Stabilized Polymeric Micelles with a Mixed Shell Formed by Two Incompatible Polymers. *Macromolecules* **2005**, *38*, 5834-5837.
98. Wei, H.; Wu, D.-Q.; Li, Q.; Chang, C.; Zhou, J.-P.; Zhang, X.-Z.; Zhuo, R.-X. Preparation of Shell Cross-Linked Thermoresponsive Micelles as well as Hollow Spheres Based on P(NIPAAm-co-HMAAm-co-MPMA)-b-PCL. *Journal of Physical Chemistry C* **2008**, *112*, 15329-15334.
99. Zhao, Y.; Bertrand, J.; Tong, X.; Zhao, Y. Photo-cross-linkable polymer micelles in hydrogen-bonding-built layer-by-layer films. *Langmuir* **2009**, *25*, 13151-13157.
100. Murata, H.; Chang, B.; Prucker, O.; Dahm, M.; Rühe, J. Polymeric coatings for biomedical devices. *Surface Science* **2004**, *570*, 111-118.
101. Tyrrell, Z. L.; Shen, Y.; Radosz, M. Fabrication of Micellar Nanoparticles for Drug Delivery Through the Self-Assembly of Block Copolymers. *Progress in Polymer Science* **2010**, *35*, 1128-1143.
102. Akiba, I.; Terada, N.; Hashida, S.; Sakurai, K.; Sato, T.; Shiraishi, K.; Yokoyama, M.; Masunaga, H.; Ogawa, H.; Ito, K.; Yagi, N. Encapsulation of a Hydrophobic Drug into a Polymer-Micelle Core Explored with Synchrotron SAXS. *Langmuir* **2010**, *26*, 7544-7551.
103. Lee, J. I.; Cho, S. H.; Park, S.-M.; Kim, J. K.; Kim, J. K.; Yu, J.-W.; Kim, Y. C.; Russell, T. P. Highly aligned ultrahigh density arrays of conducting polymer nanorods using block copolymer templates. *Nano Letters* **2008**, *8*, 2315-2320.
104. Addison, T.; Cayre, O. J.; Biggs, S.; Armes, S. P.; York, D. Incorporation of block copolymer micelles into multilayer films for use as nanodelivery systems. *Langmuir* **2008**, *24*, 13328-13333.
105. Morikawa, Y.; Kondo, T.; Nagano, S.; Seki, T. Photoinduced 3D Ordering and Patterning of Microphase-Separated Nanostructure in Polystyrene-Based Block Copolymer. *Chemistry of Materials* **2007**, *19*, 1540-1542.
106. Si, Z. H.; Wang, G. C.; Li, H. X.; Yuan, J. L.; He, B. L. Studies on Micellization of a Polystyrene-b-poly(acrylic acid) Copolymer in Aqueous Media by Pyrene Fluorescence. *Chinese Chemical Letters* **2003**, *14*, 39-41.
107. Colombani, O.; Ruppel, M.; Schubert, F.; Zettl, H.; Pergushov, D. V.; Müller, A. H. E. Synthesis of Poly(*n*-butyl acrylate)-block-poly(acrylic acid) Diblock Copolymers by ATRP and Their Micellization in Water. *Macromolecules* **2007**, *40*, 4338-4350.
108. Cristobal, G.; Berret, J.-F.; Chevallier, C.; Talingting-Pabalan, R.; Joanicot, M.; Grillo, I. Phase Behavior of Polyelectrolyte Block Copolymers in Mixed Solvents. *Macromolecules* **2008**, *41*, 1872-1880.
109. Mueller, W.; Koynov, K.; Fischer, K.; Hartmann, S.; Pierrat, S.; Basché, T.; Maskos, M. Hydrophobic Shell Loading of PB-b-PEO Vesicles. *Macromolecules* **2009**, *42*, 357-361.
110. Liu, J.; Huang, W.; Pang, Y.; Zhu, X.; Zhou, Y.; Yan, D. Self-Assembled Micelles from an Amphiphilic Hyperbranched Copolymer with Polyphosphate Arms for Drug Delivery. *Langmuir* **2010**, *26*, 10585-10592.
111. Liu, H.; Zhu, Z.; Kang, H.; Wu, Y.; Sefan, K.; Tan, W. DNA-based micelles: synthesis, micellar properties and size-dependent cell permeability. *Chemistry - A European Journal* **2010**, *16*, 3791-3797.
112. Kumar, R.; Ohulchanskyy, T. Y.; Roy, I.; Gupta, S. K.; Borek, C.; Thompson, M. E.; Prasad, P. N. Near-infrared phosphorescent polymeric nanomicelles: efficient optical probes for tumor imaging and detection. *Applied Materials & Interfaces* **2009**, *1*, 1474-1481.

- 
113. Jada, A.; Hurtrez, G.; Siffert, B.; Riess, G. Structure of polystyrene-block-poly(ethylene oxide) diblock copolymer micelles in water. *Macromolecular Chemistry and Physics* **1996**, *197*, 3697-3710.
114. Bhargava, P.; Zheng, J. X.; Li, P.; Quirk, R. P.; Harris, F. W.; Cheng, S. Z. D. Self-Assembled Polystyrene-block-poly(ethylene oxide) Micelle Morphologies in Solution. *Macromolecules* **2006**, *39*, 4880-4888.
115. Bhargava, P. Self-Assembled Polystyrene-block-Poly(Ethylene Oxide) (PS-b-PEO) Micelle Morphologies in Solution, 2007, pp. 1-110.
116. Bronstein, L. M.; Chernyshov, D. M.; Timofeeva, G. I.; Dubrovina, L. V.; Valetsky, P. M.; Khokhlov, A. R. Polystyrene-block-Poly(ethylene oxide) Micelles in Aqueous Solution. *Langmuir* **1999**, *15*, 6195-6200.
117. Tuzar, Z.; Kadlec, P.; Stepánek, P.; Kríz, J.; Nallet, F.; Noirez, L. Micelles of a Diblock Copolymer of Styrene and Ethylene Oxide in Mixtures of 2,6-Lutidine and Water. *Langmuir* **2008**, *24*, 13863-13865.
118. Seo, Y. Effect of interfacial tension on micellization of a polystyrene-poly(ethylene oxide) diblock copolymer in a mixed solvent system. *Polymer* **2002**, *43*, 5629-5638.
119. Xu, R.; Winnik, M. A.; Hallett, F. R.; Riess, G.; Croucher, M. D. Light-scattering study of the association behavior of styrene-ethylene oxide block copolymers in aqueous solution. *Macromolecules* **1991**, *24*, 87-93.
120. Mortensen, K.; Brown, W.; Almdal, K.; Alami, E.; Jada, A. Structure of PS-PEO Diblock Copolymers in Solution and the Bulk State Probed Using Dynamic Light-Scattering and Small-Angle Neutron-Scattering and Dynamic Mechanical Measurements. *Langmuir* **1997**, *13*, 3635-3645.
121. Wilhelm, M.; Zhao, C. L.; Wang, Y.; Xu, R.; Winnik, M. A.; Mura, J. L.; Riess, G.; Croucher, M. D. Poly(styrene-ethylene oxide) block copolymer micelle formation in water: a fluorescence probe study. *Macromolecules* **1991**, *24*, 1033-1040.
122. Chen, T.; Hynninen, A.-Pekka; Prud'homme, R. K.; Kevrekidis, I. G.; Panagiotopoulos, A. Z. Coarse-Grained Simulations of Rapid Assembly Kinetics for Polystyrene-b-poly(ethylene oxide) Copolymers in Aqueous Solutions. *Journal of Physical Chemistry B* **2008**, *112*, 16357-16366.
123. Rusanov, A. I.; Nekrasov, A. G. One more extreme near the critical micelle concentration: optical activity. *Langmuir* **2010**, *26*, 13767-13769.
124. Zhao, C. L.; Winnik, M. A.; Riess, G.; Croucher, M. D. Fluorescence probe techniques used to study micelle formation in water-soluble block copolymers. *Langmuir* **1990**, *6*, 514-516.
125. Sun, J.; Chen, X.; Lu, T.; Liu, S.; Tian, H.; Guo, Z.; Jing, X. Formation of reversible shell cross-linked micelles from the biodegradable amphiphilic diblock copolymer poly(L-cysteine)-block-poly(L-lactide). *Langmuir* **2008**, *24*, 10099-10106.
126. Yip, J.; Duhamel, J.; Bahun, G. J.; Adronov, A. A study of the dynamics of the branch ends of a series of pyrene-labeled dendrimers based on pyrene excimer formation. *Journal of Physical Chemistry B* **2010**, *114*, 10254-10265.
127. Chen, S.; Duhamel, J.; Winnik, M. A. Probing End-to-End Cyclization beyond Willemski and Fixman. *The Journal of Physical Chemistry B* **2011**, *115*, 3289-3302.
128. Guo, R.; Zhang, L.; Qian, H.; Li, R.; Jiang, X.; Liu, B. Multifunctional nanocarriers for cell imaging, drug delivery, and near-IR photothermal therapy. *Langmuir* **2010**, *26*, 5428-5434.
129. Block copolymer micelles as drug carriers. *Interaction of membranes with nano-objects*. <http://www.drug-delivery.ucoz.com/news/2008-10-31-4>, published October 31, 2008.

- 
130. Kwon, G.; Naito, M.; Yokoyama, M.; Okano, T.; Sakurai, Y.; Kataoka, K. Block copolymer micelles for drug delivery: loading and release of doxorubicin. *Journal of Controlled Release* **1997**, *48*, 195-201.
  131. Nakanishi, T.; Fukushima, S.; Okamoto, K.; Suzuki, M.; Matsumura, Y.; Yokoyama, M.; Okano, T.; Sakurai, Y.; Kataoka, K. Development of the polymer micelle carrier system for doxorubicin. *Journal of Controlled Release* **2001**, *74*, 295-302.
  132. Kim, J. O.; Kabanov, A. V.; Bronich, T. K. Polymer micelles with cross-linked polyanion core for delivery of a cationic drug doxorubicin. *Journal of Controlled Release* **2009**, *138*, 197-204.
  133. Gou, M.; Zheng, X.; Men, K.; Zhang, J.; Zheng, L.; Wang, X.; Luo, F.; Zhao, Y.; Zhao, X.; Wei, Y.; Qian, Z. Poly( $\epsilon$ -caprolactone)/poly(ethylene glycol)/poly( $\epsilon$ -caprolactone) nanoparticles: preparation, characterization, and application in doxorubicin delivery. *Journal of Physical Chemistry B* **2009**, *113*, 12928-12933.
  134. Villaraza, A. J. L.; Bumb, A.; Brechbiel, M. W. Macromolecules, dendrimers, and nanomaterials in magnetic resonance imaging: the interplay between size, function, and pharmacokinetics. *Chemical Reviews* **2010**, *110*, 2921-2959.

### 3. 'Click' Functional Polymer Surfaces

(with John Rabolt, Ellane Park, Tina Wagenaar)

In Chapter 2, small molecules were developed to crosslink bulk polymeric materials. In this chapter, the strategy of universal functionalization is extended to the surfaces of polymeric materials. The goal of this chapter is to develop small molecules that will universally bind to a polymer surface and activate it for subsequent functionalization by CuAAC click chemistry.

#### 3.1. Introduction, Motivation

Surface-specific attachment of molecules to a polymer is highly desirable for numerous material, biomedical, electronic and energy storage applications.<sup>1,2</sup> Examples include biomolecule surfaces for biological assays, analyte surfaces for sensors, fluorophore surfaces for diagnostics, and anti-microbial surfaces for anti-fouling membranes.<sup>3</sup> By selectively functionalizing the surface of a polymer, bulk properties can be retained while segregating a potentially very different chemistry to the surface. This strategy is in contrast to the reaction of pendant groups that are either statistically present at or segregate to the surface of a polymer.<sup>4,5</sup> Functionalization of the surface consumes less of the surface functionality than if it were to be dispersed throughout the bulk, and surface-specific methods allow greater control over the surface density, orientation, and pattern of the functionality.

Soft surfaces (polymer, biomaterials, etc.) are notoriously difficult to functionalize because of the wide variety of their surface properties: e.g. hydrophobicity or hydrophilicity, topography, and elasticity.<sup>6</sup> In contrast, functionalization of hard

surfaces (glass, metals, metal oxides, etc.) is more formulaic; certain materials are known to react selectively with specific anchor groups to form stable bonding interactions (Section 3.1.1). Taking these selective anchors as a starting point, Section 3.1.2 describes some ways in which particular polymer surfaces have been functionalized. Subsequent sections then detail the design and implementation of a method to universally functionalize polymer surfaces that will apply to nearly any polymer substrate without the need for unique polymer synthesis or indiscriminate degradation.



**Figure 3.1.** Cartoon representing the click-functional photoactive small molecule design showing the anchoring group (red), click functionality (blue), and tether (gray).

Our strategy relies upon the pre-functionalization of a polymer surface using a click-functional photoactive small molecule. That molecule will be comprised of three distinct moieties: (1) a photoactive anchoring group to bind the molecule to the surface (Figure 3.1, red), (2) a click moiety for subsequent click reaction with a complementary functional group (Figure 3.1, blue), and (3) a tether to link the two together (Figure 3.1, dark gray). Though the focus of this chapter will largely be on the use of CuAAC moieties as the desired click component of the small molecule, the approach described also applies to the other click chemistries detailed in Chapter 1. Once a surface has been

pre-functionalized, click reaction with any number of complementary click-functional analytes could proceed independent of the chemistry of the polymer surface without having to develop a new strategy to attach each analyte to the surface.<sup>7,8</sup> Potential analytes include nanoparticles, DNA, fluorophores, growth factors, bacteriocides, polymer loops and brushes, networks, gels, lubricants, receptors, hydrophobes, antibodies, anti-fouling compounds, RGD and other click moieties, etc. This technique would expedite the rapid synthesis of libraries of different molecules attached to polymer surfaces, and would negate the need for anchor-specific synthesis of analytes to attach to different substrates.

### 3.1.1. Click Functionalization of ‘Hard’ Substrates

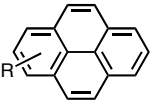
The pre-functionalization approach to polymer surfaces described above is inspired by similar strategies carried out on numerous hard surfaces, including gold, glass, silicon, and graphene.<sup>9-13</sup> Each process depends on the selection of an appropriate anchor moiety – or sticky foot – which adheres to substrate surface. The functional groups used for various hard substrates are summarized in Table 3.1. Most of the groups listed react with the surface to form a covalent bond between the substrate and the surface ligand, however non-covalent interactions such as  $\pi$ - $\pi$  stacking have also been used to anchor molecules (Table 3.1g).

Three classes of hard substrate photofunctionalization strategies merit mention: diradical chemistry (carbenes and nitrenes), photochemical degradation followed by defect functionalization, and photografting of alkenes and alkynes. The first approach, diradical chemistry, was discussed in Chapter 2 as an effective technique for covalent

bond formation with organic compounds containing C-H and C-C bonds, and has been used to functionalize materials composed completely of C-C bonds such as graphene. Phenyl azides anchor onto graphene as a result of photochemical nitrene production while other azides such as silyl derivatives have been shown to anchor via a thermally-induced nitrene mechanism.<sup>50,51</sup> The second approach, photochemical degradation followed by defect functionalization, indiscriminately produces carboxylic acids on the surface of a hard carbon substrate such as a carbon nanotube or graphene.<sup>14,15</sup> Once formed, the carboxylic acids are either converted to acid chlorides for subsequent reaction<sup>16,17</sup>, or carbodiimide coupling is used to react the carboxylic acid with an alcohol or amine.<sup>16</sup>

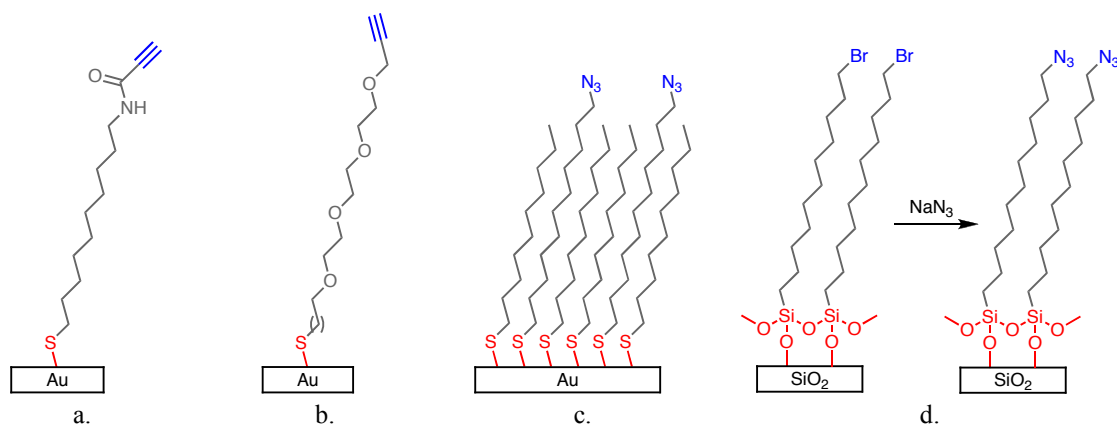
A third photochemical strategy to functionalize hard substrates is the ultraviolet photografting of alkenes and alkynes to a wide array of metals, metal oxides, and non-metals including silicon, titanium dioxide, and diamond.<sup>73,74,76</sup> CuAAC functional surfaces have been prepared by ultraviolet- and thermally-induced grafting of heterobifunctional alkenes such as  $\alpha$ -trimethylgermyl-protected alkyne- $\omega$ -alkene PEG oligomers<sup>64</sup>, and by homobifunctional alkynes such as 1,5-hexadiyne<sup>69</sup> and 1,8-nonadiyne<sup>71</sup>. Once the surface is alkyne-functionalized, azide-functional analytes such as biotin, carbohydrates<sup>65</sup>, and PEG<sup>66,69</sup> have been attached using CuAAC. Photografting alkenes has proven to be a robust and orthogonal method to add functionality to hard substrates. In addition to CuAAC functional groups, alkene-functional nanoparticles<sup>67</sup>, nitroxides<sup>71</sup>, activated esters<sup>70</sup>, and carboxylic acids<sup>75</sup> have been photografted to substrates such as silicon and carbon.

**Table 3.1.** Moieties for the surface functionalization of ‘hard’ substrates.

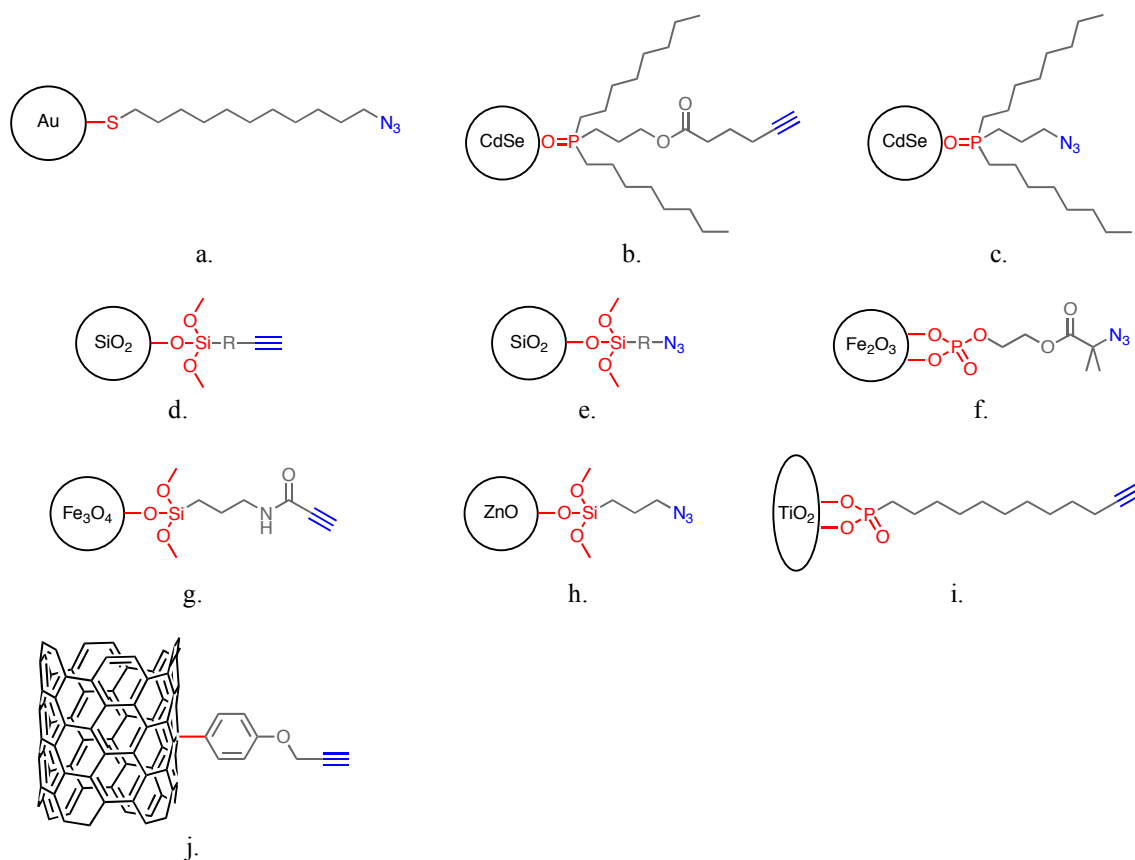
	Functional Group	Substrate(s)	References
a.	$\text{R-SH}$ Thiol $\text{R-S-S-R'}$ Dithiol	Au ZnO	[10], [18] - [23] [24]
b.	$\text{R-SiH}_3$ Silane	Glass Si SiO <sub>2</sub> ZnO Fe <sub>3</sub> O <sub>4</sub>	[25], [26] [26] [25], [27] [28] [29]
c.	$\begin{array}{c} \text{Cl} \\   \\ \text{R-Si-Cl} \\   \\ \text{Cl} \end{array}$ Trichlorosilane	SiO <sub>2</sub> Si	[25] [25]
d.	$\begin{array}{c} \text{O-R'} \\   \\ \text{R-Si-O-R''} \\   \\ \text{O-R'''} \end{array}$ Siloxane	ZnO Fe <sub>2</sub> O <sub>3</sub> Diamond	[30] [31] [32]
e.	$\text{R}-\text{C}_6\text{H}_4-\text{N}^+\equiv\text{N}^-$ (Aryl) Diazonium	SiO <sub>2</sub> Carbon Nanotube Ge Au Glassy C Stainless Steel Diamond	[33] [34] - [40] [41] [42], [43] [44], [45] [44] [32]
f.	$\text{R-NO}_2$ Nitration	Carbon Nanotube	[46], [47]
g.	 Pyrene	Carbon Nanotube	[48]
h.	$\text{R}-\text{C}_6\text{H}_4-\text{N}_3$ (Phenyl) Azide	Graphene Carbon Nanotube	[49] - [53] [54]
i.	$\begin{array}{c} \text{N}_2 \\   \\ \text{R}-\text{C}=\text{C}-\text{R}' \\    \\ \text{O} \end{array}$ Diazoester	Carbon Nanotube	[55]
j.	$\text{R}-\text{C}(\text{CF}_3)$ Carbene	Numerous	[54], [56]
k.	$\begin{array}{c} \text{R}' \\   \\ \text{C}=\text{N}^+-\text{R}'' \\   \\ \text{R} \\   \\ \text{O}^- \end{array}$ Nitrones	Carbon Nanotube	[57]
l.	$\begin{array}{c} \text{R} \\   \\ \text{R}'-\text{P}=\text{O} \\   \\ \text{R}'' \end{array}$ Phosphinoyl	CdSe	[58] - [60]
m.	$\begin{array}{c} \text{O-R'} \\   \\ \text{R}-\text{P}=\text{O} \\   \\ \text{O-R''} \end{array}$ Phosphonate $\begin{array}{c} \text{OH} \\   \\ \text{R}-\text{P}=\text{O} \\   \\ \text{OH} \end{array}$ Phosphonic Acid	Fe <sub>2</sub> O <sub>3</sub> TiO <sub>2</sub> ZnO	[61] [62] [24], [63]
n.	$\text{R}-\text{C}=\text{C}$ Alkene	Si Diamond C TiO <sub>2</sub>	[64] - [72] [73] [74], [75] [76]



With an understanding of the complementarity of particular moieties to certain surfaces, it is possible to understand how heterobifunctional small molecules have been used to modify a wide range of hard substrate surfaces. When one end of a small molecule anchors to the hard substrate, the other end generates a peripheral functional surface that is either the desired functionality or is available for subsequent reaction to make the desired functionality. The former approach relies upon the synthesis of heterobifunctional molecules with the desired functionality built in, whereas the latter approach dictates that the functional end of the ligand molecule is chosen so that it reacts in a second step to produce or bind the target surface functionality. Figure 3.2 shows examples of flat surfaces functionalized using heterobifunctional ligands to impart CuAAC functionality, and Figure 3.3 shows analogous examples of nanoparticle and nanotube surface functionalization.



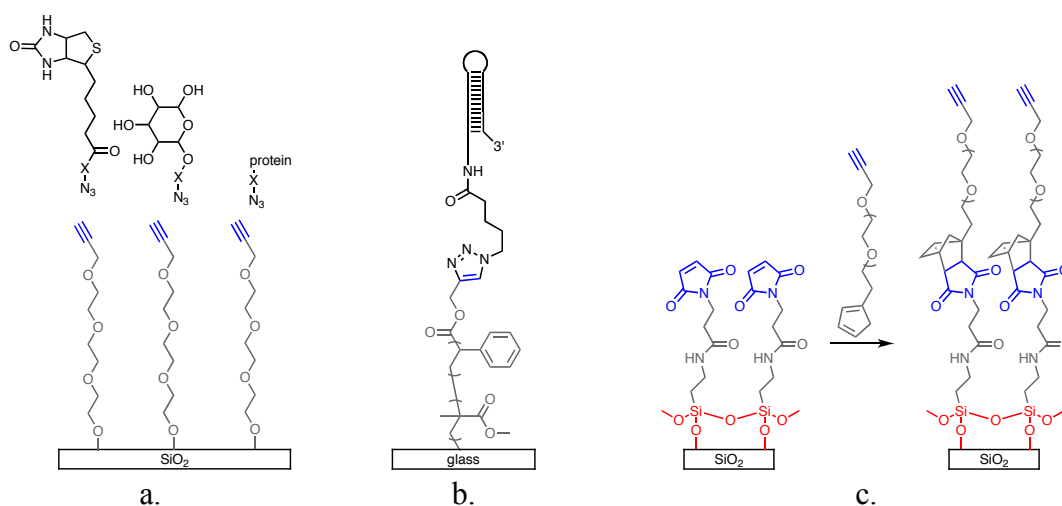
**Figure 3.2.** Representative hard, flat surface functionalization with alkynes and azides: (a) self-assembly of a thiol-alkyne on gold; (b) self-assembly of a PEGylated thiol-alkyne on gold; (c) self-assembly of a mixed monolayer of thiol-azide and alkanethiol on gold; (d) conversion of a bromosilane silica surface to azidosilane via reaction with sodium azide.



**Figure 3.3.** CuAAC surface functionalization strategies for various hard nanoparticulate surfaces: (a) azide on gold; (b) alkyne on cadmium selenide (CdSe); (c) azide on cadmium selenide (CdSe); (d) alkyne on silica (SiO<sub>2</sub>); (e) azide on silica (SiO<sub>2</sub>); (f) azide on iron oxide (hematite, Fe<sub>2</sub>O<sub>3</sub>); (g) alkyne on iron oxide (ferrite, Fe<sub>3</sub>O<sub>4</sub>); (h) azide on zinc oxide (ZnO); (i) alkyne on titanium dioxide (TiO<sub>2</sub>); and (j) alkyne on carbon nanotube.

The pre-functionalization approach has been used to generate a wide range of functionalized hard surfaces. Figure 3.4a and Figure 3.4b are representative of how hard substrates functionalized with alkynes – alkyne terminal PEG and PMMA-b-PS copolymer, respectively – are then modified using CuAAC to attach biotin, carbohydrates, proteins, and DNA.<sup>22</sup> Figure 3.4c is an example of how a parallel click chemistry, Diels-Alder cycloaddition, is used to generate an alkyne surface on silica similar to the one in Figure 3.4a.<sup>11</sup> The Diels-Alder adduct, however, imparts a thermally labile release mechanism to the surface following CuAAC functionalization.

Although each pre-functionalized surface in Figure 3.4 is an alkyne, an azide can also be attached to a surface for the attachment of alkyne-terminal analytes or polymers.<sup>10,21,77,78</sup> This strategy is especially common for polymer brushes grown by surface-initiated ATRP.<sup>79-81</sup> Immobilization of an initiator onto a hard substrate makes possible the polymerization of linear polymers anchored at one end to the substrate surface.<sup>82,83</sup> As shown in Chapter 1, the terminal bromide of polymers made by ATRP is easily converted to an azide for CuAAC with an alkyne-functional analyte. Polymer brushes could alternately be formed by the “grafting to” approach whereby linear polymers bind to a functionalized substrate; an azide-terminal polymer made by ATRP can be attached to surface-bound alkynes like those in Figure 3.4.<sup>84</sup>



**Figure 3.4.** Post-functionalization strategies on click-functionalized surfaces: (a) CuAAC for biotinylated, glycosylated, and protein-functionalized surfaces; (b) CuAAC for a DNA-functionalized PMMA-b-PS copolymer surface; and (c) Diels-Alder functionalization for an alkyne surface.

### 3.1.2. Click Functionalization of ‘Soft’ Substrates

Soft substrate functionalization has not yet reached the reliability of hard substrate functionalization in large part because of the wide array of surface properties of

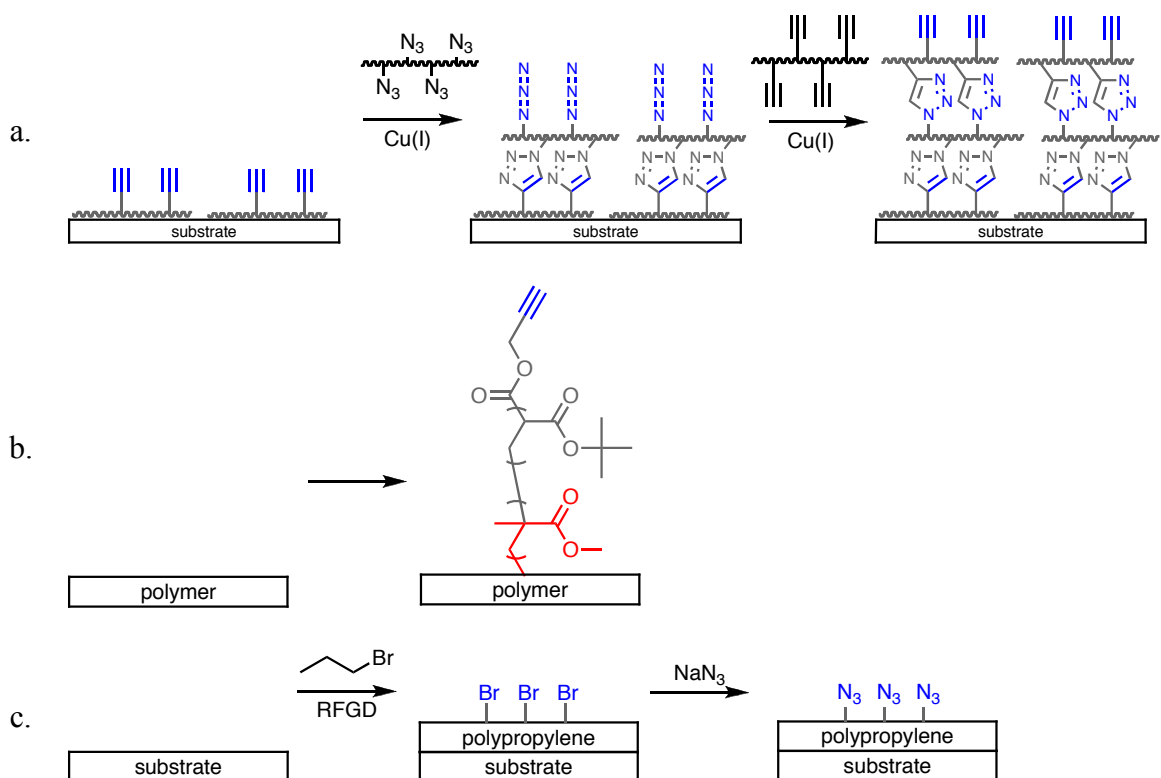
polymeric and soft materials. Chapter 1 discussed how the chemical properties of polymers have been adapted to include reactive functionality within a polymer, however the focus of this chapter is on extrinsic, post-polymerization methods to functionalize the surfaces of polymer substrates.

Harsh ozonolysis oxidizes the bonds of a polymer and generates a highly imprecise surface chemistry consisting of carboxylic acids, aldehydes, alcohols, peroxides, etc. Despite the high number and types of functionalities created on the surface, reorganization of the polymer to minimize its surface energy can bury the small functional groups away from the polymer-air interface. If executed quickly, analytes can react with the oxidized surface, however, the precise chemistry and functional density of the surface is not readily controlled. Furthermore, ozonolysis degrades the surface of the polymer to a self-limiting depth, potentially compromising the integrity of the bulk material.

Instead of degrading the polymer surface, layer-by-layer assembly of polymers can build up a functionalizing layer upon a substrate surface.<sup>85-89</sup> Typical layer-by-layer assemblies are constructed from alternating layers of cationic and anion polymers, but neutral polymers with alternating complementary functionality can also layer to functionalize a surface. By alternating the application of azide- and alkyne-functional polymers, a CuAAC functional surface membrane with exposed azides and/or alkynes can be grown upon a substrate (Figure 3.5a). This method still relies upon the synthesis of copolymers, and depending on the desired substrate, new azide- or alkyne-functional polymers must be synthesized.

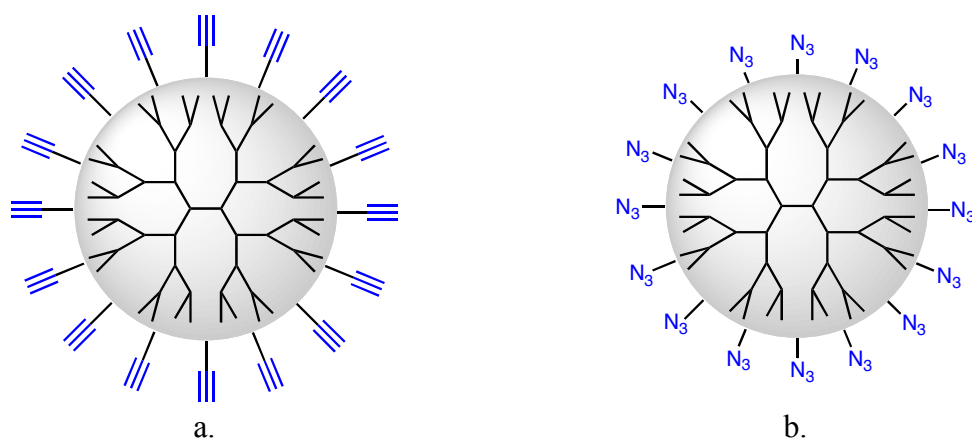
Another method that still requires the synthesis of block copolymers but is slightly more generalizeable is the construction of block copolymers to functionalize polymer substrates.<sup>90</sup> A copolymer in which one block is the same identity as the substrate while the other is poly(*tert*-butyl acrylate) (PtBA) can be applied via spin coating and annealed to form a polymer brush-like surface (Figure 3.5b). Deprotection of the PtBA groups using a photoacid generator has been shown to impart the surface with regions of poly(acrylic acid) (PAA); the pendant carboxylic acids of the PAA are then available for standard reactions such as metal deposition or DCC coupling to add CuAAC functionality. A diblock copolymer with alkyne-functional ends has also been used to functionalize a polymer surface.<sup>91</sup>

An effective combined degradative/additive approach is the plasma polymerization of monomers to create thin, highly crosslinked polymer surface layers (Figure 3.5c).<sup>68,92-94</sup> Plasma polymerization is an *in situ* polymerization method that simultaneously crosslinks a polymer film and binds it to the surface of a substrate. This method is advantageous because it can be applied to numerous hard and soft substrates, is easily scalable for industrial applications, and can incorporate many functionalities – including azides and alkynes – via diverse monomer selection. However, plasma polymerization requires an expensive vacuum apparatus, and the architecture of the film is not well defined or easily controlled due to the large number of ions and free radicals present in both the plasma and the growing polymer film. The ions or radicals may also cause the substrate polymer functionality to deleteriously degrade, so a technique with low local radical concentration is preferable.



**Figure 3.5.** Polymer substrate functionalization: (a) layer-by-layer CuAAC assembly of alkyne- and azido-functional polymers; (b) functionalization with a diblock copolymer; and (c) radio frequency glow discharge (RFGD) plasma polymerization of brominated polypropylene and azidification.

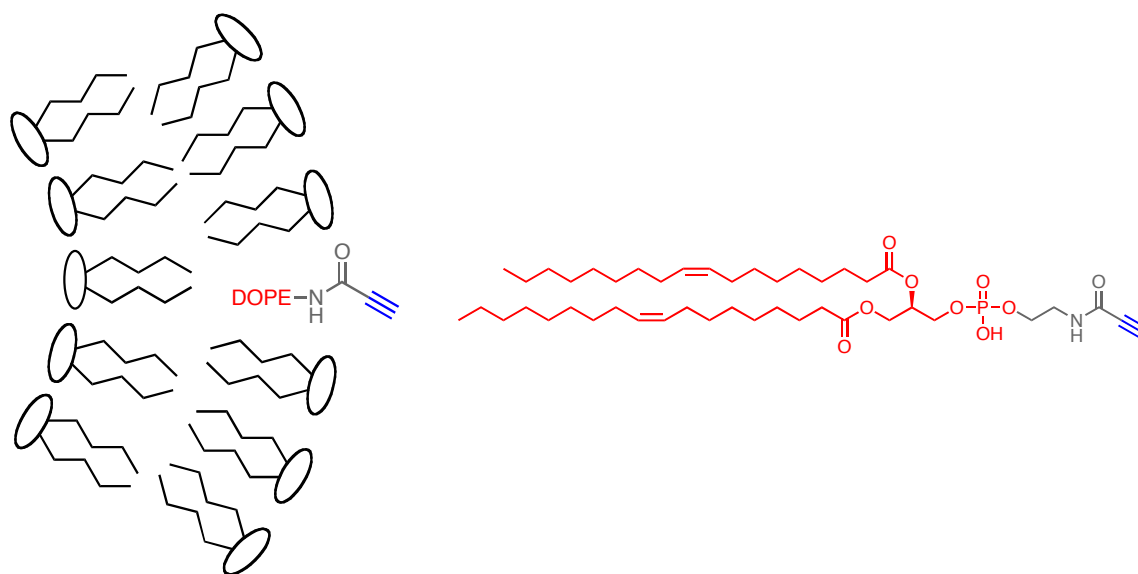
In addition to the soft flat substrates described above, several soft nanoscale particulate materials have been CuAAC functionalized as well. These materials are composed of synthetic or natural polymers and extend the notion of surface functionalization from two to three dimensions. Synthetic polymer dendrites have been end-functionalized with azides and alkynes for materials similar to the layer-by-layer polymers in Figure 3.5c.<sup>87</sup> Instead of attaching polymers to other polymers in flat films, the complementary functionalities on the particles in Figure 3.6 react to form a porous membrane composed of adjoining colloidal polymer nanoparticles. CuAAC functionality has been covalently added to the periphery of biopolymer nanoparticles such as the cowpea mosaic virus<sup>95,96</sup> and to synthetic polymer micelles<sup>97</sup> via coupling to surface



**Figure 3.6.** Functional dendritic polymer nanoparticles: (a) alkyne-functional; and (b) azide-functional.



**Figure 3.7.** CuAAC functionalization of cowpea mosaic virus capsid.



**Figure 3.8.** Liposome surface functionalization (left) using alkyne-functionalized DOPE (right).

amines and carboxylic acids, respectively (Figure 3.7). The periphery of liposomes can be CuAAC-functionalized by the incorporation of an alkyne-functional unimer; as the liposome self-assembles in solution, the alkyne-functional unimer intercalates with the native

unimer to present a CuAAC moiety at the surface for reaction with an azide-functional analyte.<sup>98</sup>

### 3.1.3. Patterning of Surface Click Functionality

An advantage of the prefunctionalization approach to surface modification is the ability to precisely pattern analytes that would otherwise be disrupted or destroyed during a patterning step. Patterning allows for spatial control and density manipulation of CuAAC functional groups on the surface prior to reaction with the complementary functionality on the analyte. Azides and alkynes have been patterned on both hard and soft substrates by several mechanical, electrochemical, and photochemical methods.

Microcontact printing provides a direct route to patterning CuAAC functional groups onto a surface.<sup>99</sup> Patterning begins with the development of a stamp – typically made of polydimethylsiloxane (PDMS) – and proceeds by the physisorption of molecules to the patterned PDMS stamp and transfer to the desired substrate. Advantages of this method include the robustness of the PDMS stamp and the possibility for replication and duplication, and for the azide-alkyne cycloaddition in particular, the cycloaddition can be effected without Cu(I). However, forming the initial pattern mold can be expensive and the sensitivity of the PDMS limits the threshold of patternable feature sizes.

Electrochemical methods to pattern using CuAAC have relied upon the spatial activation of the copper catalyst – reduction of Cu(II) to Cu(I) – using scanning electron microscopy (SEM)<sup>100</sup> or atomic force microscopy (AFM)<sup>101</sup>. As a voltage is applied between the microscope tip and the surface, free Cu(II) in solution is reduced, thereby locally activating CuAAC between a surface bound alkyne (or azide) and azide-functional (or alkyne-functional) analytes in solution. This method generates patterns



with very small feature sizes, but is not reasonably scalable to pattern large surfaces quickly or inexpensively since it requires an SEM or AFM instrument. A different electrochemical method relies upon the electro-oxidation of an alkane monolayer to form a pattern of carboxylic acids.<sup>102</sup> Deposition of a heterobifunctional bromosilane onto the oxidized regions of the surface followed is by conversion of the bromide to azide and subsequent CuAAC. Although this method claims to facilitate nanometer resolution of patterns, it still suffers from the disadvantages mentioned above: lack of scalability and need for expensive instrumentation. Similarly, depositing functionality on pre-patterned conducting polymer electrodes has been accomplished using electrochemically-activated CuAAC simply by controlling the voltage passed through the pre-patterned polymer.<sup>103</sup>

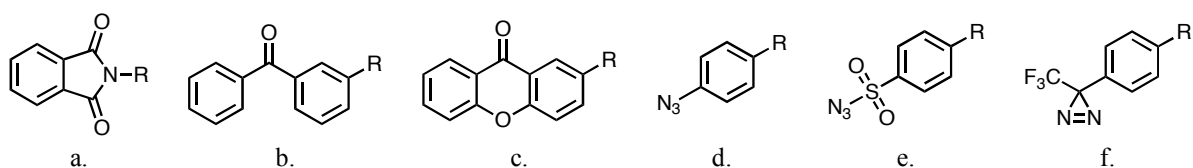
Photolithography via electron beam irradiation has also been used to pattern a CuAAC functional surface.<sup>104</sup> Conventional lithographic and etching techniques were used to pattern an electron beam sensitive resist in order to etch a polymer bearing pendant alkyne groups. After rinsing off the resist, polymer that had not been etched away was then available for subsequent functionalization with azide-functional nanoparticles or dyes using CuAAC. Taking cues from photoaffinity labeling, other photochemical methods have been used to pattern analytes, but in those cases the analyte is first functionalized with a photoactive anchor group such as a phenyl azide, and irradiation binds the anchor group to a polymer substrate.<sup>105</sup>

None of these existing techniques satisfied the desire for a method to functionalize a wide range of polymer substrates in a straightforward way. While some of the functionalization and patterning methods require expensive apparatus, others do not provide the potential for scalability. Still others demand a new chemical synthesis for

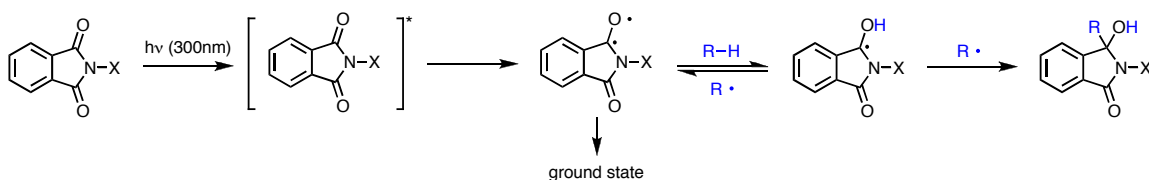
each different substrate that is to be functionalized. Our goal was therefore to develop a facile and reliable technique to install click moieties on a polymer surface via a pre-functionalization step toward a “universal” functionalization strategy for polymer surfaces. This “universal” chemistry should operate equally on a wide range of surfaces without the need for substrate-specific synthesis.

### 3.2. Design of Universal ‘Photoclickers’

The design of a single molecule to photofunctionalize a wide range of surfaces begins with the recognition that photo-excited molecules react with many different types of chemical bonds present in polymers. Some photoexcited chromophores hydrogen atom abstract from C-H, N-H, and O-H bonds, and carbenes and nitrenes insert into C-C and C-H bonds. Since most polymers contain C-H bonds and C-C bonds, potential candidates for a polymer anchoring moiety would react with C-H or C-C bonds in the polymer – bonds not normally thought of as reactive functional groups – to covalently bind to the polymer surface. Candidates are shown in Figure 3.9, and include photoactive hydrogen abstractors (phthalimide, benzophenone, and xanthone)<sup>106,109</sup>, nitrene precursors (phenyl azide, sulfonyl azide)<sup>23,27,110,114</sup> and a carbene precursor (trifluoromethyl phenyl diazirine)<sup>115</sup>. Phthalimide was chosen as the first-generation anchor because it embodies several promising characteristics: its hydrogen abstraction mechanism has been well-studied and is known to be effective with polymers (Figure 3.10); it has two carbonyls which gives it a higher probability per moiety of reacting with the surface; and the chemistry to install the phthalimide functionality is synthetically straightforward.

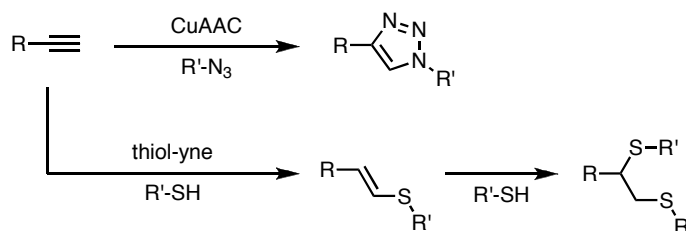


**Figure 3.9.** Photoactive anchors: (a) phthalimide; (b) benzophenone; (c) xanthone; (d) phenyl azide; (e) sulfonyl azide; and (f) trifluoromethyl phenyl diazirine.



**Figure 3.10.** Scheme of hydrogen abstraction from R-H (blue) by phthalimide.

Tethered to the phthalimide photoactive anchor would be one of the numerous click functionalities describes in Chapter 1. Of the many potential candidates, a terminal alkyne and a trimethylsilyl-protected alkyne provide the most promising characteristics for subsequent click reaction. Previous work had shown that alkynes and TMS-alkynes orient toward the air-polymer interface because of their low surface energies, and that the TMS-alkyne is readily deprotected to yield an alkyne-functional surface.<sup>116</sup> Additionally, alkynes are reactive with both azides and thiols via CuAAC and thiol-yne chemistry, respectively, thereby increasing the versatility of the pre-functionalization step (Figure 3.11). Although many surfaces have been functionalized with azides because of their significant IR absorbance, the photochemistry of the azide group made it unattractive for use here; photoreaction would prematurely activate the azide and render it unavailable for CuAAC during the intended functionalization step with an alkyne-functional analyte.



**Figure 3.11.** Click reactions of an alkyne: CuAAC and thiol-yne.

To connect the phthalimide to the alkyne, a simple alkyl linker was chosen. The length of the linker was based upon a desire to balance the necessity to have several carbons whose van der Waals forces would assist in orienting the molecule in the desired configuration with the need to prevent the intramolecular cyclization of the phthalimide with the alkyl chain.<sup>117,118</sup> Additionally, the linker must have enough flexibility to sample its orientational space in order for the terminal alkyne to react with azide-functional analytes.

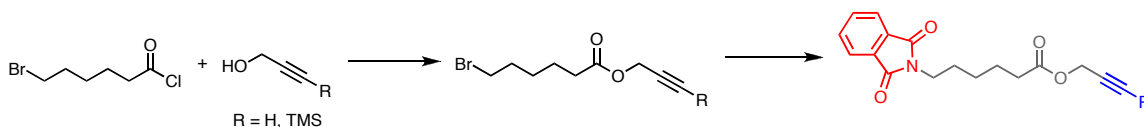
These three components – phthalimide, alkyl linker, and alkyne or TMS-alkyne – were combined in the synthesis of the heterobifunctional compounds **8** and **9** described below. Since the anchor moiety is photoactivated in order to bind to the polymer surface, compounds **8** and **9** can be patterned onto a polymer surface by irradiation through a photolithographic mask to produce a ‘negative’ tone pattern of alkynes; compounds **8** and **9** would bind to the surface only where light passes through the mask.<sup>6</sup> This simple approach enables the pre-functionalization of polymer surfaces using pre-existing photolithographic technology so that *any* analyte could bind to the surface of *any* polymer without needing to completely re-strategize for a new polymer. Subsequent click reactions will produce a range of patterned polymer substrates, such as biomolecule-functionalized surfaces for biological assays, analyte-functionalized surfaces for sensors,

fluorophore-functionalized surfaces, anti-microbial-functionalized surfaces, and secondarily functionalized surfaces to selectively bind other molecules.

Although the alkyne was selected as the click functionality in what follows, the strategy of pre-functionalizing a surface with similar photoactive heterobifunctional molecules could easily extend to other click methodologies.

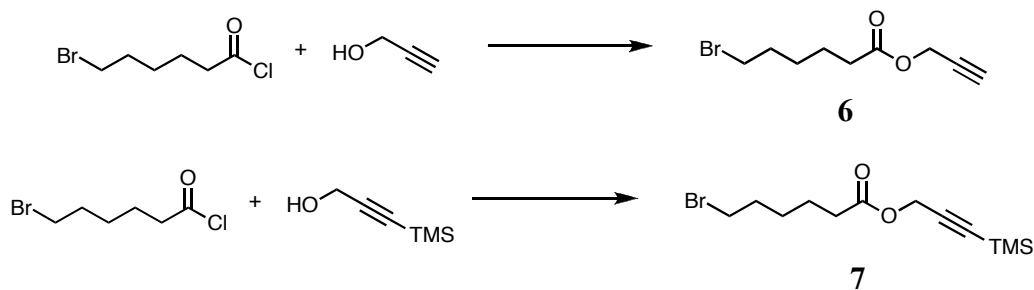
### 3.3. Preparation of Surface Functionalizing Compounds

The terminal alkyne derivative of the surface functionalizing compound, prop-2-yn-1-yl 6-phthalimidohexanoate, **8**, is the result of condensation between propargyl alcohol and 6-bromohexanoyl chloride followed by substitution of the bromide with phthalimide using potassium phthalimide (Figure 3.12). The trimethylsilyl-protected alkyne derivative, 3-(trimethylsilyl)-prop-2-yn-1-yl 6-bromohexanoate, **9**, is prepared in a similar fashion via condensation of 6-bromohexanoyl chloride with 3-(trimethylsilyl)-prop-2-yn-1-ol followed by substitution of the bromide with potassium phthalimide.

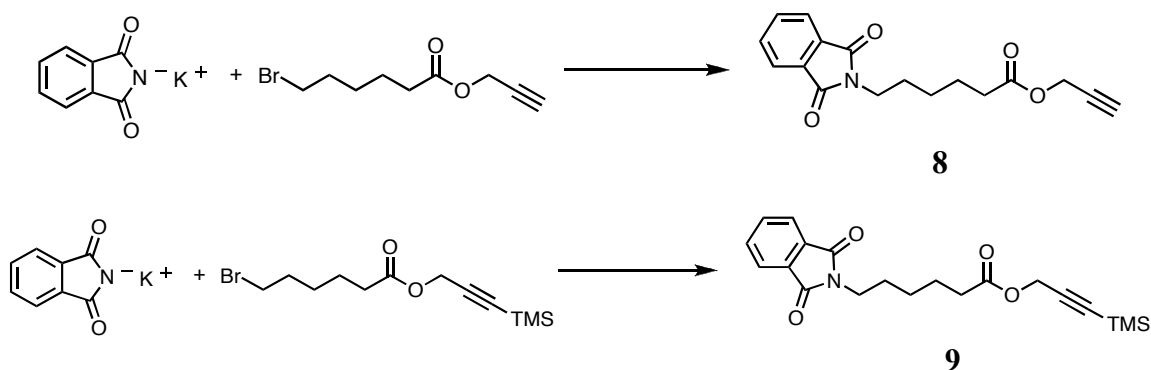


**Figure 3.12.** Synthesis of phthalimide-alkyne, **8** (R = H) and trimethylsilyl-protected phthalimide-alkyne, **9** (R = TMS) from 6-bromohexanoyl chloride and propargyl alcohols.

Condensation of 6-bromohexanoyl chloride with a propargyl alcohol (R = H or TMS) in pyridine and benzene was followed by purification to yield **6** and **7** (Figure 3.13).<sup>119,120</sup> Compounds **6** and **7** were then stirred overnight in DMF with potassium phthalimide salt and separated to yield **8** and **9** as brown oils (Figure 3.14).<sup>121,122</sup>

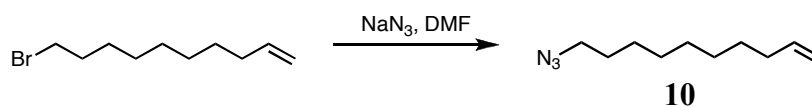


**Figure 3.13.** Synthesis of prop-2-yn-1-yl 6-bromohexanoate, **6** (top) and 3-(trimethylsilyl)prop-2-yn-1-yl 6-bromohexanoate, **7** (bottom).



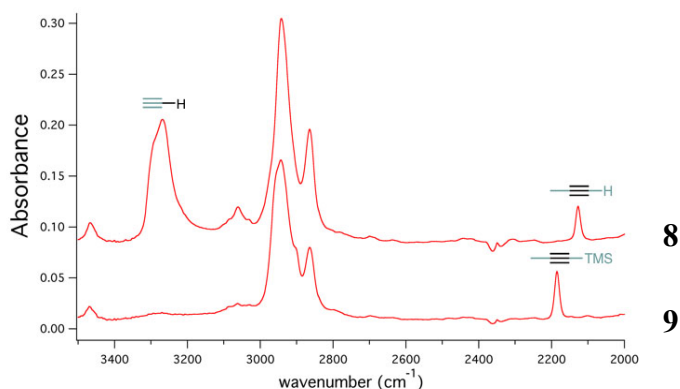
**Figure 3.14.** Synthesis of prop-2-yn-1-yl 6-phthalimido-hexanoate, **8** (top) and 3-(trimethylsilyl)prop-2-yn-1-yl 6-phthalimido-hexanoate, **9** (bottom).

In addition to the two surface functionalizing molecules **8** and **9**, the simple heterobifunctional ‘click transfer’ agent, **10**, was synthesized (Figure 3.15). Stirring 10-bromodec-1-ene with excess sodium azide in DMF was followed by aqueous workup to yield 10-azidodec-1-ene, **10**.<sup>123-125</sup> Compound **10** takes advantage of the orthogonality of CuAAC and thiol-ene chemistry, and is a proof-of-principle molecule to show how an alkyne-functional surface would easily be converted to a surface functionalized with another click functionality (e.g. alkene for thiol-ene).



**Figure 3.15.** Synthesis of 10-azidodec-1-ene, **10**.

Compounds **6-10** were characterized by  $^1\text{H}$  NMR using a Bruker 400 MHz spectrometer, and those spectra are included in the Appendix. The  $^1\text{H}$  NMR spectra are identical except for the terminal alkynyl proton of **8** (1H) which is shifted to  $\delta$ 2.4ppm whereas the trimethylsilyl protons of **9** (9H's) are shifted to  $\delta$ 0.15ppm. ATR-IR spectra were obtained using a Nicolet Nexus 870 FT-IR with an Avatar Smart Multi-bounce HATR accessory. The IR spectra of **8** and **9** are effectively identical in the region from 2000-3500  $\text{cm}^{-1}$  except for the stretches resulting from the different alkyne functionalities (Figure 3.16). The terminal alkyne of **8** exhibits both a C–H stretch at 3250  $\text{cm}^{-1}$  and a C $\equiv$ C stretch at 2120  $\text{cm}^{-1}$  while the TMS-protected alkyne of **9** exhibits a C $\equiv$ C stretch at the slightly higher frequency of 2190  $\text{cm}^{-1}$  and no terminal C–H stretch as expected. Additionally, mass spectra (FAB+) showed the expected M+1 molecular weight peaks at 300.45 for **8** and 372.2 for **9**.



**Figure 3.16.** ATR-FTIR spectra of prop-2-yn-1-yl 6-phthalimidohexanoate, **8** (top) and 3-(trimethylsilyl)prop-2-yn-1-yl 6-phthalimidohexanoate, **9** (bottom).

### 3.4. Surface Preparation

Polymer films on glass substrates were prepared for click surface functionalization by compounds **8** and **9**. Glass microscope slides were cut in half, rinsed

with water and ethanol, and dried in an oven. For an exemplar hydrophobic surface, a 1% w/w solution of polystyrene (Polymer Laboratories,  $M_p = 1,056,000$ ,  $M_w/M_n = 1.03$ ) in toluene was spin-coated (2500 rpm, 1 min) on the glass. For an exemplar hydrophilic surface, a 1% w/w solution of poly(acrylic acid) (Sigma Aldrich, 35 wt% solution in water, avg.  $M_w = 100,000$ ) in water was spin-coated (2500 rpm, 1 min) on the glass. In a typical experiment, substrates were then spin-coated (2500 rpm, 1 min) with a 1-2% w/w solution of **8** or **9** in ethanol. Films were irradiated under a 300 nm lamp in air, and if a pattern was desired a chromium contact photomask was placed over the surface prior to irradiation. Unbound small molecules were removed by thrice rinsing with ethanol and drying with nitrogen. Necessary control surfaces were also prepared to show that irradiation is necessary for **8** and **9** to bind to the surface, that unirradiated **8** and **9** are fully rinsed from the surfaces by washing with ethanol, and that irradiation of the pure polymer surface at reasonable durations without **8** and **9** does not induce any detectable change. Additionally, after application of **8** and **9** the polymer surfaces visibly change from a clear, translucent to a hazy cloudy appearance. Differences between regions of **8** or **9** and pure polymer on patterned surfaces are visible to the naked eye.

### **3.5. Surface Analysis**

Analysis of the functionalized surfaces was primarily conducted using two techniques. First, water contact angle goniometry was used to characterize the surfaces at each step throughout processing to verify that change had been effected upon the polymer surfaces. Second, infrared spectroscopy was used to verify the presence of the alkyne



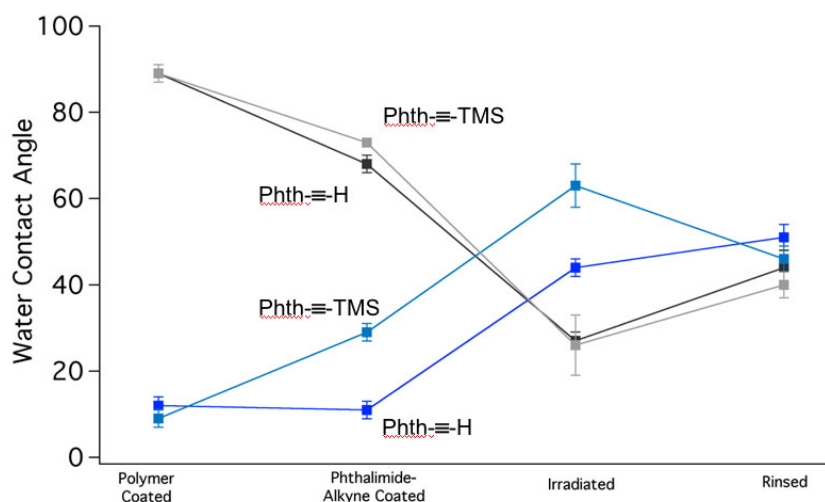
functionality on the surface, and then was used to identify the optimal conditions for surface preparation: exposure, concentration, washing, etc.

### 3.5.1. Water Contact Angle Analysis

Polymer surfaces with films of **8** and **9** were initially irradiated at 300 nm for an unoptimized two hours to ensure reaction of the phthalimide anchor onto the polymer surface. After washing, water contact angles were obtained using deionized water (>18.2 M $\Omega$  cm, Millipore, Milli-Q) measured at room temperature using a 100-00 contact angle goniometer (Rame-Hart, Inc.). Contact angles were measured for the pure polymer surfaces, after spin-coating **8** and **9** but prior to irradiation, following irradiation, and after washing (Figure 3.17).

The water contact angles seemed to show that surface functionalization by **8** and **9** led to the same range of surface energies represented by contact angles in the range of 35-50°. This implied that the water drop interacted with similar surfaces on both polymers despite vastly different underlying properties. The similarity was interpreted to mean that the surfaces had been coated in propargyl esters, and since the propargyl esters were essentially equivalent, the new properties of the surface were equivalent. For surfaces that began with contact angles having a difference of nearly 80°, to be rendered so similar was encouraging. The other changes in contact angle were also telling: the large changes during irradiation likely implied that surface molecules were reorganizing as a result of irradiation, and were possibly representative of the H-abstraction-induced anchoring of the phthalimide to the polymer surface. Similarly, the relatively small changes resulting from washing implied that unreacted **8** or **9** was removed, but did not heavily influence

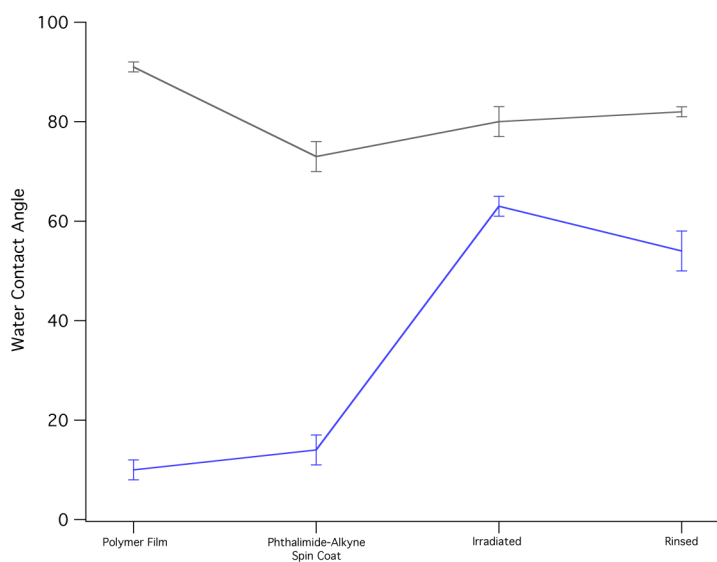
the measurement of the contact angle following irradiation. It was also recognized that the presence of the TMS group of **9** did not present a noticeably different surface energy relative to the terminal alkyne of **8**. Subsequent experiments therefore focused on surface functionalization by **8** since protection of the alkyne by TMS was deemed unnecessary.



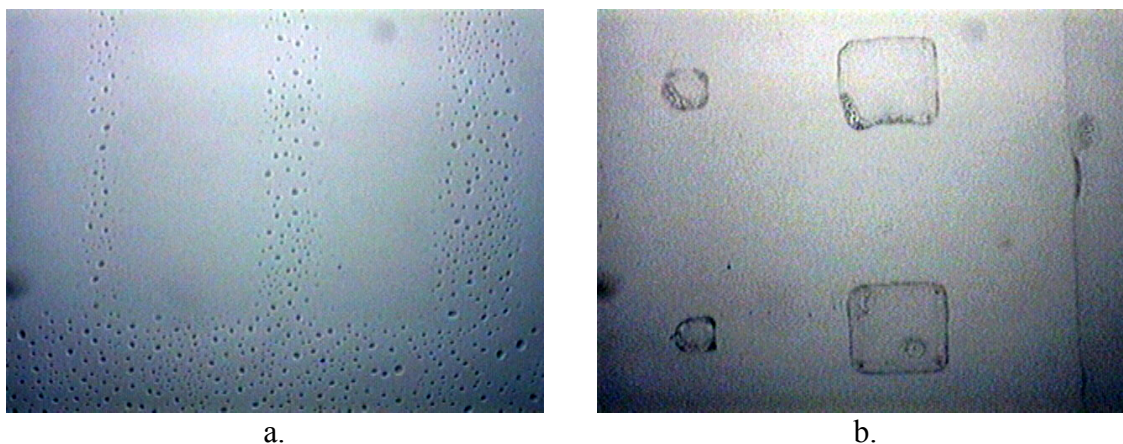
**Figure 3.17.** Water contact angle analysis tracking the unoptimized preparation of alkyne-functionalized surfaces on polystyrene (black, **8**, and gray, **9**) and poly(acrylic acid) (blue, **8**, and navy, **9**).

From FTIR experiments detailed below, two hours of irradiation was found to ablate a PS substrate, so care was taken to optimize the irradiation time. The water contact angle experiments were then repeated using the optimized irradiation time of 30 minutes, and the results are shown in Figure 3.18. As before, the water contact angles of both surfaces changed with application of **8**, but after irradiation for 30 minutes, the surfaces showed drastically different contact angles than in the case of irradiation for 2h. PAA acted in a similar fashion, but the contact angle of PS increased to about 80° instead of decreasing to 25-30° as before. The previous decrease was likely due to the very hydrophilic oxidation products that are known to result from long exposure to ultraviolet light. The unexpected increase of the water contact angle of PS after irradiation is likely

the result of surface droplets of **8** that result from the dewetting of **8** during irradiation. These droplets can clearly be seen in Figure 3.19a which is a PS substrate that has been irradiated through a contact mask pattern. Regions where **8** did not bind or dewet are visible as rectangular areas, and are surrounded by a sea of small dots of **8** that have dewetted. Changes in surface morphology from flat to rough on the order of micrometers and smaller are known to increase the water contact angle for a given material, so it would not be surprising if the increase in contact angle of **8** on PS was due to dewetting. The optical micrograph of **8** on PAA (Figure 3.19b), however, shows homogenous square regions of **8** surrounded by PAA, indicating that **8** wets PAA.



**Figure 3.18.** Water contact angle analysis following the optimized preparation of polystyrene (gray) and poly(acrylic acid) (blue) surfaces functionalized with **8**.



**Figure 3.19.** Optical micrographs of polymer surfaces coated with **8** and irradiated at 300 nm for 30 min: (a) PS; and (b) PAA.

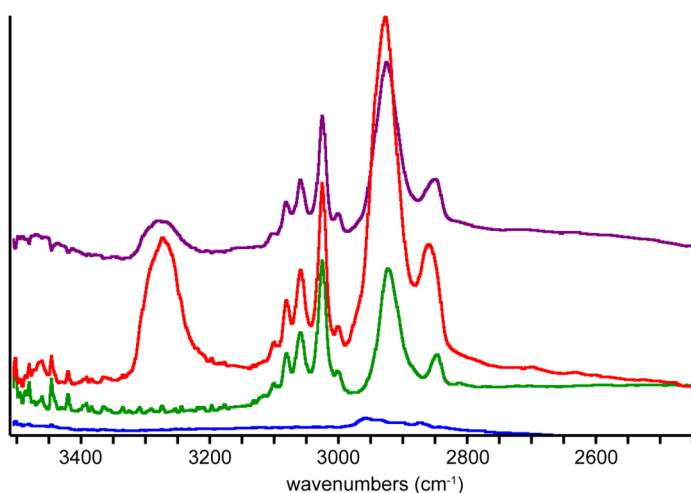
Analysis by water contact angles alone was not sufficient to verify the identity of the molecules bound to the surface, nor does it give any indication of the surface coverage, density, or orientation. For this verification, we turned to infrared spectroscopy.

### 3.5.2. Infrared Spectroscopy

Infrared spectroscopy has already been used to characterize the structures of compounds **8** and **9** (Figure 3.16) and it is a commonly used surface spectroscopy for both hard and soft surfaces. The goal of IR analysis was foremost to verify the presence of the alkyne functionalities on the surface, but the weak absorption intensity of the alkyne presented a notable challenge. CuAAC surfaces are more often functionalized with azides since the azide IR absorption at  $\sim 2100\text{ cm}^{-1}$  is well-separated from other absorption bands and is often of medium strength. As mentioned above, azide-functional molecules were not candidates for this surface functionalization approach because of the potential for photochemical reactions of the azides which would render them unavailable for subsequent CuAAC. Furthermore, structural characteristics of **8** make it amenable to

further characterization by IR. The orientation and overall reaction efficiency of surface-bound molecules could be determined using the strong signals from the three carbonyls: two in the phthalimide and one in the ester as internal standard ( $\sim 1650 - 1800 \text{ cm}^{-1}$ ).<sup>126</sup>

The first objective of IR characterization was to determine whether it is possible to observe **8** on PS, and to identify the signals we would expect to see during later IR experiments. The following samples were prepared and tested prior to irradiation: clean glass, pure PS, **8** mixed into PS, and **8** deposited onto PS. The spectra in Figure 3.20 are the result of 128 scans at  $2 \text{ cm}^{-1}$  resolution taken in transmission mode with approximately 15 minutes of nitrogen purging prior to measurement. Based on comparison of the IR spectrum of **8** (Figure 3.16) to the IR spectrum of pure PS (Figure 3.20, green), the large peak at  $3260 \text{ cm}^{-1}$  in the red and purple spectra is assigned to the terminal alkyne C-H stretch and will act as an indicator of the presence of **8** in future experiments. The feature from  $3000 - 3150 \text{ cm}^{-1}$  is primarily the characteristic multiplet



**Figure 3.20.** FTIR Spectra of bare glass slide (blue, bottom), PS film (green), **8** mixed into PS film (red), and **8** deposited onto PS film (purple, top). All spectra were recorded prior to UV irradiation.

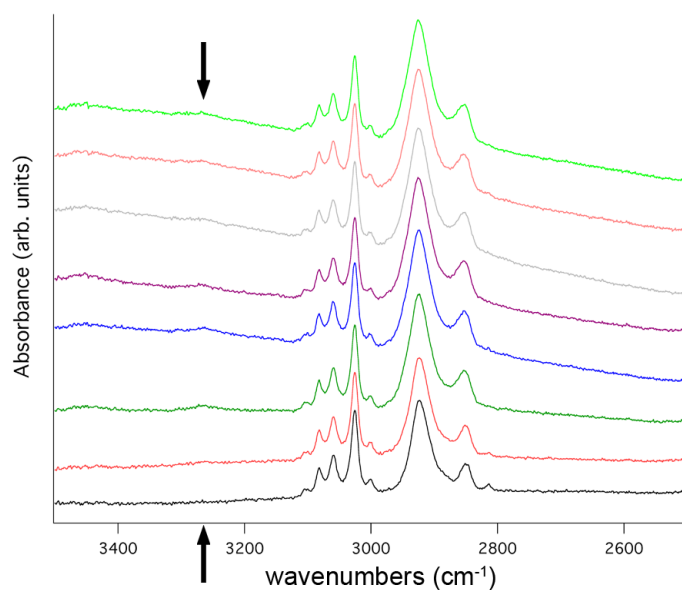
of PS from the aromatic ring C-H's, and the lopsided doublet from 2800 – 3000  $\text{cm}^{-1}$  is the result of overlapping alkane C-H signals from both **8** and PS.

The second objective of IR characterization was to determine the optimal irradiation conditions in order to maximize the attachment of **8** to the PS surface without ablating the polymer substrate. Films of **8** on PS were prepared and subjected to various irradiation times ranging from 0 min to 60 min; after washing with ethanol, spectra were recorded as before. Each spectrum was converted to an absorbance spectrum using the Beer-Lambert Law (Equation 3.1) where judicious selection of reference spectra,  $I_0$ , was intended to isolate the contribution of **8** to the overall spectrum.

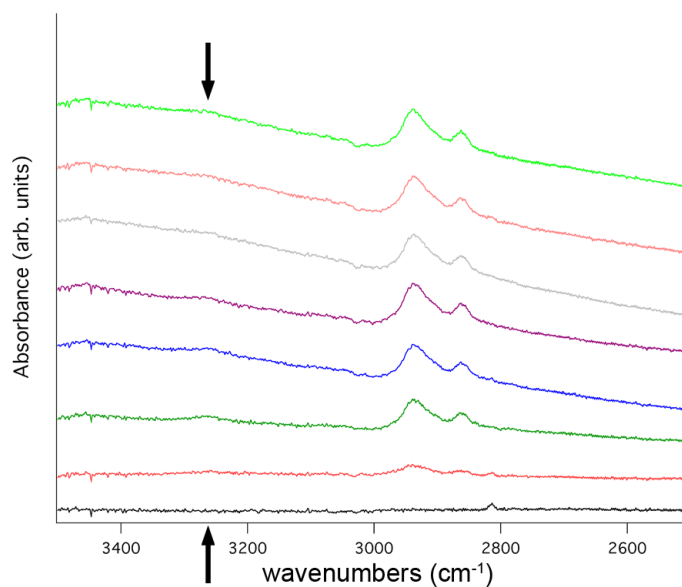
$$\text{Abs} = -\ln\left(\frac{I}{I_0}\right) \quad \text{Equation 3.1}$$

**Equation 3.1.** The Beer-Lambert Law.

Figure 3.21 shows absorption spectra of **8** on PS at various irradiation times referenced to a clean glass slide background. The characteristic set of PS peaks seen in Figure 3.20 is observed, however the alkyne C-H stretch at 3260  $\text{cm}^{-1}$  is visible but weak (shown by arrows). The low intensity of the alkyne C-H stretch relative to the unirradiated and unwashed film of **8** on PS in Figure 3.20 is due to a lower – but still detectable – surface concentration of alkynes after washing. In order to isolate the signals of **8** from the overwhelming PS signals, samples were prepared and irradiated in parallel but without application of **8**. Spectra resulting from the subtraction of a background consisting of both PS and glass are shown in Figure 3.22. Comparison of Figure 3.22 to the IR spectrum of **8** in Figure 3.16 shows that the two peaks from 2800 – 3000  $\text{cm}^{-1}$  and the weak peak at 3260  $\text{cm}^{-1}$  indicate the presence of **8** on the surface, and



**Figure 3.21.** IR absorption spectra for **8** on PS at various irradiation times referenced to a clean glass slide. From bottom: 0, 5, 10, 20, 30, 40, 50, 60 min.



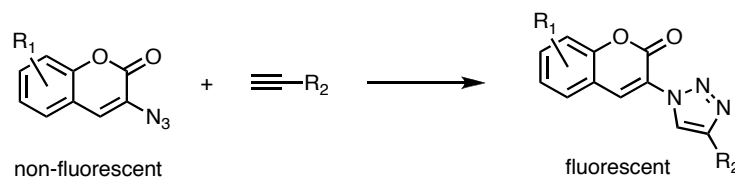
**Figure 3.22.** IR absorption spectra for **8** on PS at various irradiation times referenced to PS on a glass slide. From bottom: 0, 5, 10, 20, 30, 40, 50, 60 min.

that a very broad baseline feature grows in with longer irradiation times. Samples were measured in a random order, so the baseline drift is not purely instrumental. From Figure 3.22 the optimal irradiation time for samples was determined to be approximately 30

minutes since no significant growth of the characteristic peaks of **8** occurred with continued irradiation.

### 3.5.3. Fluorogenic Coumarin Azide

Although the IR data supports the presence of **8** on the irradiated polymer surface, the weak terminal C-H stretch intensity in the IR led to a desire for alternate methods to visualize the surface-bound **8**. The most promising visualization strategy was to use a non-fluorescent coumarin azide which, when clicked via CuAAC to an alkyne, would become fluorescent (Figure 3.23).<sup>127,128</sup> The advantage of this strategy was that non-specific adsorption of the coumarin dye would show no fluorescence, thereby eliminating the background signal that would be expected using a fluorescent dye. The ultimate drawback to this strategy, however, was that previous work using this fluorescent coumarin azide was done in solution. Although fluorescent analytes have been reacted with surfaces via CuAAC, the surface concentration of alkynes in those cases was high so visualization was readily accomplished.<sup>104</sup> Following Sivakumar, et al, the standard CuAAC reaction with the coumarin azide (Figure 3.23, R<sub>1</sub> = 7-OH) did not result in detection of surface fluorescence, presumably because of the low alkyne surface concentration.<sup>129</sup> The strategy is still believed to be promising, however, but proved too time-consuming to pursue.



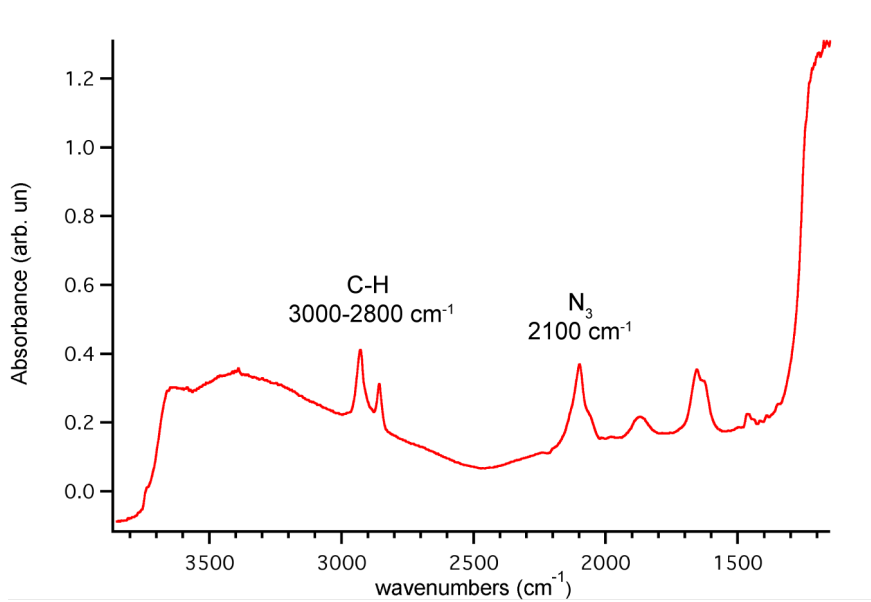
**Figure 3.23.** A non-fluorescent coumarin azide reacts with an alkyne to generate a fluorescent adduct.



### 3.5.4. Surface Functionalization with Nanoparticles

A second visualization strategy was undertaken to graft azide-functional silica nanoparticles to the alkyne-functionalized polymer surface. Functionalized silica nanoparticles have found potential uses as drug delivery vehicles, as surface lubricants, as platforms for biosensors, and in a number of other important applications, so they represent a reasonable test case for attaching analytes to the pre-functionalized polymer surface.<sup>130</sup> Azide-functional silica nanoparticles were prepared according to the literature, and their structure was verified using diffuse reflectance infrared fourier transform spectroscopy (DRIFTS) on a Nexus 870 FT-IR ESP (Figure 3.24).<sup>84</sup> The characteristic stretch at  $\sim 2100\text{ cm}^{-1}$  confirms the presence of the azide functionality. Furthermore, the absorption from  $2800 - 3000\text{ cm}^{-1}$  is due to alkane C-H's in the undecyl ligands and the absorption from  $1250 - 1100\text{ cm}^{-1}$  results from silica Si-O stretches.

A typical procedure for the CuAAC of the azide-functional silica nanoparticles onto a PS surface pre-functionalized by **8** involved dissolving the nanoparticles, a ligand



**Figure 3.24.** DRIFTS spectrum of azide functionalized silica nanoparticles.

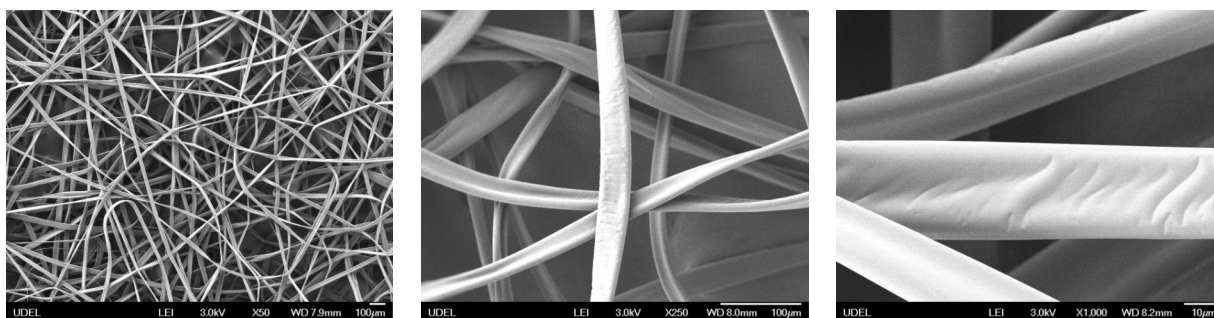
(1  $\mu\text{mol}$ , 0.5 eq.), and sodium ascorbate (100  $\mu\text{mol}$ , 50 eq.) in approximately 20 mL of a 1:4 mixture of water and THF. Copper(II) sulfate pentahydrate (2  $\mu\text{mol}$ , 1 eq.) was added and the solution was quickly poured over the glass slide on which the PS film had been deposited. After sitting in the reaction bath overnight, the slide was removed and rinsed with water, DMF, and ethanol, and finally dried in air.

The deposition of the silica nanoparticles onto the PS surface proved unsuccessful due to a number of limiting constraints. First, the silica nanoparticles quickly settled out of solution to the bottom of the reaction vessel and did not deposit onto polymer surface. Any nanoparticles that did deposit onto the surface seemed to adsorb non-specifically across a substrate patterned with **8**. Second, interactions between the glass and the silica nanoparticles resulted in a high degree of non-specific adsorption to the obverse, unfunctionalized side of the glass slides. Third, due to the high number of azides per nanoparticle, there was not a significant decrease in the azide IR absorption signal that would be expected to accompany the reaction of an azide to form a triazole.

### **3.6. Outlook**

The outlook for a polymer functionalization strategy such as the one presented here is promising with respect to a number of different applications in several diverse fields. Pre-functionalization with a click moiety extends the range of possible combinations of substrates and surface treatments, especially when taking into account patterning, whether for the attachment of analyte molecules such as drugs, fluorophores, or binding functionalities to a polymer surface, or for polymer surface passivation by a secondary material such as a different polymer, nanoparticles, or metal films.<sup>131-133</sup>

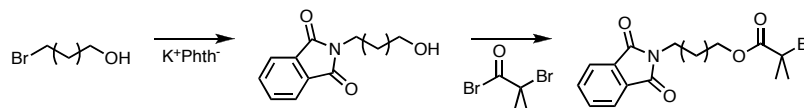
The technique can even be extended based on changes in the form and morphology of the polymer substrate. An ongoing collaboration that has not yet produced communicable results is aimed at the functionalization of PS nanofibers using this approach. The electrospun PS nanofibers have a vastly greater surface area to volume ratio than the films prepared on glass slides above. In principle, the increased surface area should lead to an increased surface loading of analytes, which in turn ought to be more easily detected. The higher surface loading will be important for applications in areas such as sensing, filtration, drug delivery, and cell growth scaffolds where a high quantity of surface-bound analyte is required while still allowing flow through the material.<sup>134,135</sup>



**Figure 3.25.** Images of electrospun PS fibers. (Wenqiong Tang and John Rabolt)

A number of outstanding questions still exist, however, and must be left for others: what is the density of alkynes on the surface? the coverage? What is the density of molecules grafted to the alkynes on the surface?<sup>136</sup> Will this technique work on non-polar surfaces, such as polyethylene? Additionally, extensions of the photoimmobilization strategy could easily be accomplished using the same phthalimide photoanchor with an end functionality other than a click moiety. For example, a phthalimide-ATRP initiator could be immobilized or patterned and then surface brushes could be polymerized (Figure 3.26), or a polymer could be synthesized with a

complementary end functionality and grafted to the polymer surface.<sup>137</sup> Both routes should easily be accomplished.



**Figure 3.26.** Possible phthalimide-ATRP initiator synthesis.

### 3.7. Summary

- Heterobifunctional small molecules have been synthesized that combine a photoactive anchor – phthalimide – with a CuAAC functional end group – a terminal alkyne or a trimethylsilyl-protected alkyne.
- These small molecules are intended to be applied to different polymer surfaces using common spin coating and irradiation techniques in order to pre-functionalize the surface with ‘click’ moieties.
- Polymer surfaces have been characterized using water contact angle goniometry and infrared spectroscopy to verify the photochemically-induced attachment of the small molecules to the polymer surface.
- The low surface concentration of attached molecules complicates the spectroscopic verification of surface functionalization.
- Other methods to verify the surface functionalization by CuAAC with azido-functional molecules were unsuccessful, and work continues to characterize the surfaces spectroscopically.

### 3.8. References

---

1. Walker, A. V. Building Robust and Reliable Molecular Constructs: Patterning, Metallic Contacts, and Layer-by-Layer Assembly. *Langmuir* **2010**, *26*, 13778-13785.
2. Nyholm, L.; Nyström, G.; Mihranyan, A.; Strømme, M. Toward Flexible Polymer and Paper-Based Energy Storage Devices. *Advanced Materials* **2011**, doi: 10.1002/adma.201004134.
3. Rana, D.; Matsuura, T. Surface modifications for antifouling membranes. *Chemical Reviews* **2010**, *110*, 2448-2471.
4. Fleischmann, S.; Hinrichs, K.; Oertel, U.; Reichelt, S.; Eichhorn, K.; Voit, B. Modification of Polymer Surfaces by Click Chemistry. *Macromolecular Rapid Communications* **2008**, *29*, 1177-1185.
5. Ostaci, R.-V.; Damiron, D.; Grohens, Y.; Léger, L.; Drockenmuller, E. Click chemistry grafting of poly(ethylene glycol) brushes to alkyne-functionalized pseudobrushes. *Langmuir* **2010**, *26*, 1304-1310.
6. Park, E. J.; Carroll, G. T.; Turro, N. J.; Koberstein, J. T. Shedding light on surfaces—using photons to transform and pattern material surfaces. *Soft Matter* **2009**, *5*, 36-50.
7. Meldal, M. Polymer “Clicking” by CuAAC Reactions. *Macromolecular Rapid Communications* **2008**, *29*, 1016-1051.
8. Lutz, J.-F. 1,3-Dipolar Cycloadditions of Azides and Alkynes: a Universal Ligation Tool in Polymer and Materials Science. *Angewandte Chemie International Edition* **2007**, *46*, 1018-1025.
9. Devaraj, N.; Collman, J. Copper Catalyzed Azide-Alkyne Cycloadditions on Solid Surfaces: Applications and Future Directions. *QSAR & Combinatorial Science* **2007**, *26*, 1253-1260.
10. Collman, J. P.; Devaraj, N. K.; Chidsey, C. E. D. “Clicking” functionality onto electrode surfaces. *Langmuir* **2004**, *20*, 1051-1053.
11. Sun, X.-L.; Stabler, C. L.; Cazalis, C. S.; Chaikof, E. L. Carbohydrate and protein immobilization onto solid surfaces by sequential Diels-Alder and azide-alkyne cycloadditions. *Bioconjugate Chemistry* **2006**, *17*, 52-57.
12. Lee, J. K.; Chi, Y. S.; Choi, I. S. Reactivity of acetylenyl-terminated self-assembled monolayers on gold: triazole formation. *Langmuir* **2004**, *20*, 3844-3847.
13. Devaraj, N. K.; Decreau, R. A.; Ebina, W.; Collman, J. P.; Chidsey, C. E. D. Rate of interfacial electron transfer through the 1,2,3-triazole linkage. *The Journal of Physical Chemistry B* **2006**, *110*, 15955-15962.
14. Boukhvalov, D. W.; Katsnelson, M. I. Chemical Functionalization of Graphene with Defects. *Nano Letters* **2008**, *8*, 4373-4379.
15. Steurer, P.; Wissert, R.; Thomann, R.; Mühlaupt, R. Functionalized Graphenes and Thermoplastic Nanocomposites Based upon Expanded Graphite Oxide. *Macromolecular Rapid Communications* **2009**, *30*, 316-327.
16. Sun, Y.-P.; Fu, K.; Lin, Y.; Huang, W. Functionalized Carbon Nanotubes: Properties and Applications. *Accounts of Chemical Research* **2002**, *35*, 1096-1104.
17. Kalinina, I.; Worsley, K.; Lugo, C.; Mandal, S.; Bekyarova, E.; Haddon, R. C. Synthesis, Dispersion, and Viscosity of Poly(ethylene glycol)-Functionalized Water-Soluble Single-Walled Carbon Nanotubes. *Chemistry of Materials* **2011**, *23*, 1246-1253.
18. Zirbs, R.; Kienberger, F.; Hinterdorfer, P.; Binder, W. H. Directed assembly of Au nanoparticles onto planar surfaces via multiple hydrogen bonds. *Langmuir* **2005**, *21*, 8414-8421.
19. Brennan, J. L.; Hatzakis, N. S.; Tshikhudo, T. R.; Dirvianskyte, N.; Razumas, V.; Patkar, S.; Vind, J.; Svendsen, A.; Nolte, R. J. M.; Rowan, A. E.; Brust, M. Bionanoconjugation via click chemistry:

- The creation of functional hybrids of lipases and gold nanoparticles. *Bioconjugate Chemistry* **2006**, *17*, 1373-1375.
20. Bertin, P. A.; Ahrens, M. J.; Bhavsar, K.; Georganopoulou, D.; Wunder, M.; Blackburn, G. F.; Meade, T. J. Ferrocene and maleimide-functionalized disulfide scaffolds for self-assembled monolayers on gold. *Organic Letters* **2010**, *12*, 3372-3375.
  21. Hudalla, G. A.; Murphy, W. L. Using "click" chemistry to prepare SAM substrates to study stem cell adhesion. *Langmuir* **2009**, *25*, 5737-5746.
  22. Chelmowski, R.; Köster, S. D.; Kerstan, A.; Prekelt, A.; Grunwald, C.; Winkler, T.; Metzler-Nolte, N.; Terfort, A.; Wöll, C. Peptide-based SAMs that resist the adsorption of proteins. *Journal of the American Chemical Society* **2008**, *130*, 14952-14953.
  23. Madwar, C.; Kwan, W. C.; Deng, L.; Ramström, O.; Schmidt, R.; Zou, S.; Cuccia, L. A. Perfluorophenyl azide immobilization chemistry for single molecule force spectroscopy of the concanavalin A/mannose interaction. *Langmuir* **2010**, *26*, 16677-16680.
  24. Perkins, C. L. Molecular Anchors for Self-Assembled Monolayers on ZnO: A Direct Comparison of the Thiol and Phosphonic Acid Moieties. *The Journal of Physical Chemistry C* **2009**, *113*, 18276-18286.
  25. Lummerstorfer, T.; Hoffmann, H. Click Chemistry on Surfaces: 1,3-Dipolar Cycloaddition Reactions of Azide-Terminated Monolayers on Silica. *The Journal of Physical Chemistry B* **2004**, *108*, 3963-3966.
  26. Ganesan, R.; Lee, H.-J.; Kim, J.-B. Photoactive diazoketo-functionalized self-assembled monolayer for biomolecular patterning. *Langmuir* **2009**, *25*, 8888-8893.
  27. Al-Bataineh, S. A.; Luginbuehl, R.; Textor, M.; Yan, M. Covalent immobilization of antibacterial furanones via photochemical activation of perfluorophenylazide. *Langmuir* **2009**, *25*, 7432-7437.
  28. Selegård, L.; Khranovsky, V.; Söderlind, F.; Vahlberg, C.; Åhrén, M.; Käll, P.-O.; Yakimova, R.; Uvdal, K. Biotinylation of ZnO Nanoparticles and Thin Films: A Two-Step Surface Functionalization Study. *Applied Materials & Interfaces* **2010**, *2*, 2128-2135.
  29. Zhou, Y.; Wang, S.; Xie, Y.; Guan, W.; Ding, B.; Yang, Z.; Jiang, X. 1,3-dipolar cycloaddition as a general route for functionalization of Fe<sub>3</sub>O<sub>4</sub> nanoparticles. *Nanotechnology* **2008**, *19*, 175601.
  30. Paoprasert, P.; Spalenka, J. W.; Peterson, D. L.; Ruther, R. E.; Hamers, R. J.; Evans, P. G.; Gopalan, P. Grafting of poly(3-hexylthiophene) brushes on oxides using click chemistry. *Journal of Materials Chemistry* **2010**, *20*, 2651-2658.
  31. Frickel, N.; Messing, R.; Gelbrich, T.; Schmidt, A. M. Functional silanes as surface modifying primers for the preparation of highly stable and well-defined magnetic polymer hybrids. *Langmuir* **2010**, *26*, 2839-2846.
  32. Liang, Y.; Ozawa, M.; Krueger, A. A general procedure to functionalize agglomerating nanoparticles demonstrated on nanodiamond. *ACS Nano* **2009**, *3*, 2288-2296.
  33. Flavel, B. S.; Gross, A. J.; Garrett, D. J.; Nock, V.; Downard, A. J. A Simple Approach to Patterned Protein Immobilization on Silicon via Electrografting from Diazonium Salt Solutions. *Applied Materials & Interfaces* **2010**, *2*, 1184-1190.
  34. Li, H.; Cheng, F.; Duft, A. M.; Adronov, A. Functionalization of single-walled carbon nanotubes with well-defined polystyrene by "click" coupling. *Journal of the American Chemical Society* **2005**, *127*, 14518-14524.
  35. Hirsch, A. Functionalization of Single-Walled Carbon Nanotubes. *Angewandte Chemie International Edition* **2002**, *41*, 1853-1859.

- 
36. Niyogi, S.; Hamon, M. A.; Hu, H.; Zhao, B.; Bhowmik, P.; Sen, R.; Itkis, M. E.; Haddon, R. C. Chemistry of Single-Walled Carbon Nanotubes. *Accounts of Chemical Research* **2002**, *35*, 1105-1113.
37. Liu, N.; Luo, F.; Wu, H.; Liu, Y.; Zhang, C.; Chen, J. One-Step Ionic-Liquid-Assisted Electrochemical Synthesis of Ionic-Liquid-Functionalized Graphene Sheets Directly from Graphite. *Advanced Functional Materials* **2008**, *18*, 1518-1525.
38. Sundaram, R. S.; Gómez-Navarro, C.; Balasubramanian, K.; Burghard, M.; Kern, K. Electrochemical Modification of Graphene. *Advanced Materials* **2008**, *20*, 3050-3053.
39. Bahr, J. L.; Yang, J.; Kosynkin, D. V.; Bronikowski, M. J.; Smalley, R. E.; Tour, J. M. Functionalization of Carbon Nanotubes by Electrochemical Reduction of Aryl Diazonium Salts: A Bucky Paper Electrode. *Journal of the American Chemical Society* **2001**, *123*, 6536-6542.
40. Bekyarova, E.; Itkis, M. E.; Ramesh, P.; Berger, C.; Sprinkle, M.; Heer, W. A. de; Haddon, R. C. Chemical modification of epitaxial graphene: spontaneous grafting of aryl groups. *Journal of the American Chemical Society* **2009**, *131*, 1336-1337.
41. Collins, G.; Fleming, P.; O'Dwyer, C.; Morris, M. A.; Holmes, J. D. Organic Functionalization of Germanium Nanowires using Arenediazonium Salts. *Chemistry of Materials* **2011**, *23*, 1883-1891.
42. Gam-Derouich, S.; Carbonnier, B.; Turmine, M.; Lang, P.; Jouini, M.; Ben Hassen-Chehimi, D.; Chehimi, M. M. Electrografted aryl diazonium initiators for surface-confined photopolymerization: a new approach to designing functional polymer coatings. *Langmuir* **2010**, *26*, 11830-11840.
43. Combellas, C.; Kanoufi, F.; Pinson, J.; Podvorica, F. I. Sterically hindered diazonium salts for the grafting of a monolayer on metals. *Journal of the American Chemical Society* **2008**, *130*, 8576-8577.
44. Iruthayaraj, J.; Chernyy, S.; Lillethorup, M.; Ceccato, M.; Røn, T.; Hinge, M.; Kingshott, P.; Besenbacher, F.; Pedersen, S. U.; Daasbjerg, K. On Surface-Initiated Atom Transfer Radical Polymerization Using Diazonium Chemistry To Introduce the Initiator Layer. *Langmuir* **2011**, *27*, 1070-1078.
45. Berisha, A.; Combellas, C.; Kanoufi, F.; Pinson, J.; Ustaze, S.; Podvorica, F. I. Indirect Grafting of Acetonitrile-Derived Films on Metallic Substrates. *Chemistry of Materials* **2010**, *22*, 2962-2969.
46. Dyke, C. A.; Tour, J. M. Solvent-free functionalization of carbon nanotubes. *Journal of the American Chemical Society* **2003**, *125*, 1156-1157.
47. Ménard-Moyon, C.; Fabbro, C.; Prato, M.; Bianco, A. One-Pot Triple Functionalization of Carbon Nanotubes. *Chemistry - A European Journal* **2011**, doi: 10.1002/chem.201003050.
48. Prencipe, G.; Tabakman, S. M.; Welscher, K.; Liu, Z.; Goodwin, A. P.; Zhang, L.; Henry, J.; Dai, H. PEG branched polymer for functionalization of nanomaterials with ultralong blood circulation. *Journal of the American Chemical Society* **2009**, *131*, 4783-4787.
49. Gao, C.; He, H.; Zhou, L.; Zheng, X.; Zhang, Y. Scalable Functional Group Engineering of Carbon Nanotubes by Improved One-Step Nitrene Chemistry. *Chemistry of Materials* **2009**, *21*, 360-370.
50. He, H.; Gao, C. General Approach to Individually Dispersed, Highly Soluble, and Conductive Graphene Nanosheets Functionalized by Nitrene Chemistry. *Chemistry of Materials* **2010**, *22*, 5054-5064.
51. Choi, J.; Kim, K.-Jeong; Kim, B.; Lee, H.; Kim, S. Covalent Functionalization of Epitaxial Graphene by Azidotrimethylsilane. *The Journal of Physical Chemistry C* **2009**, *113*, 9433-9435.
52. Liu, L.-Hong; Yan, M. Simple method for the covalent immobilization of graphene. *Nano Letters* **2009**, *9*, 3375-3378.

- 
53. Liu, L.-H.; Lerner, M. M.; Yan, M. Derivatization of Pristine Graphene with Well-Defined Chemical Functionalities. *Nano Letters* **2010**, *10*, 3754-3756.
54. Holzinger, M.; Vostrowsky, O.; Hirsch, A.; Hennrich, F.; Kappes, M.; Weiss, R.; Jellen, F. Sidewall Functionalization of Carbon Nanotubes. *Angewandte Chemie International Edition* **2001**, *40*, 4002-4005.
55. Schmidt, G.; Filoramo, A.; Derycke, V.; Bourgoin, J.-P.; Chenevier, P. Labile Diazo Chemistry for Efficient Silencing of Metallic Carbon Nanotubes. *Chemistry - A European Journal* **2011**, 1415-1418.
56. Ismaili, H.; Lagugné-Labarhet, F.; Workentin, M. S. Covalently Assembled Gold Nanoparticle-Carbon Nanotube Hybrids via a Photoinitiated Carbene Addition Reaction. *Chemistry of Materials* **2011**, *23*, 1519-1525.
57. Giambastiani, G.; Cicchi, S.; Giannasi, A.; Luconi, L.; Rossin, A.; Mercuri, F.; Bianchini, C.; Brandi, A.; Melucci, M.; Ghini, G.; Stagnaro, P.; Conzatti, L.; Passaglia, E.; Zoppi, M.; Montini, T.; Fornasiero, P. Functionalization of Multiwalled Carbon Nanotubes with Cyclic Nitrones for Materials and Composites: Addressing the Role of CNT Sidewall Defects. *Chemistry of Materials* **2011**, *23*, 1923-1938.
58. Binder, W. H.; Petraru, L.; Sachsenhofer, R.; Zirbs, R. Synthesis of Surface-Modified Nanoparticles via Cycloaddition-Reactions. *Monatshefte für Chemie - Chemical Monthly* **2006**, *137*, 835-841.
59. Binder, W. H.; Sachsenhofer, R.; Straif, C. J.; Zirbs, R. Surface-modified nanoparticles via thermal and Cu(I)-mediated “click” chemistry: Generation of luminescent CdSe nanoparticles with polar ligands guiding supramolecular recognition. *Journal of Materials Chemistry* **2007**, *17*, 2125-2132.
60. Binder, W. H.; Lomoschitz, M.; Sachsenhofer, R.; Friedbacher, G. Reversible and Irreversible Binding of Nanoparticles to Polymeric Surfaces. *Journal of Nanomaterials* **2009**, *2009*, 1-15.
61. White, M. A.; Johnson, J. A.; Koberstein, J. T.; Turro, N. J. Toward the syntheses of universal ligands for metal oxide surfaces: controlling surface functionality through click chemistry. *Journal of the American Chemical Society* **2006**, *128*, 11356-11357.
62. White, M. A.; Maliakal, A.; Turro, N. J.; Koberstein, J. T. “Click” Dielectrics: Use of 1,3-Dipolar Cycloadditions to Generate Diverse Core-Shell Nanoparticle Structures with Applications to Flexible Electronics. *Macromolecular Rapid Communications* **2008**, *29*, 1544-1548.
63. Voigt, M.; Klaumünzer, M.; Ebel, A.; Werner, F.; Yang, G.; Marczak, R.; Spiecker, E.; Guldi, D. M.; Hirsch, A.; Peukert, W. Surface Functionalization of ZnO Nanorods with C<sub>60</sub> Derivatives Carrying Phosphonic Acid Functionalities. *The Journal of Physical Chemistry C* **2011**, *115*, 5561-5565.
64. Li, Y.; Santos, C. M.; Kumar, A.; Zhao, M.; Lopez, A. I.; Qin, G.; McDermott, A. M.; Cai, C. “Click” immobilization on alkylated silicon substrates: model for the study of surface bound antimicrobial peptides. *Chemistry - A European Journal* **2011**, *17*, 2656-2665.
65. Qin, G.; Santos, C.; Zhang, W.; Li, Y.; Kumar, A.; Erasquin, U. J.; Liu, K.; Muradov, P.; Trautner, B. W.; Cai, C. Biofunctionalization on alkylated silicon substrate surfaces via “click” chemistry. *Journal of the American Chemical Society* **2010**, *132*, 16432-16441.
66. Li, Y.; Wang, J.; Cai, C. Rapid Grafting of Azido-Labeled Oligo(ethylene glycol)s onto an Alkynyl-Terminated Monolayer on Nonoxidized Silicon via Microwave-Assisted “Click” Reaction. *Langmuir* **2011**. doi: 10.1021/la104060j
67. Leem, G.; Zhang, S.; Jamison, A. C.; Galstyan, E.; Rusakova, I.; Lorenz, B.; Litvinov, D.; Lee, T. R. Light-induced covalent immobilization of monolayers of magnetic nanoparticles on hydrogen-terminated silicon. *Applied Materials & Interfaces* **2010**, *2*, 2789-2796.
68. Schofield, W. C. E.; Badyal, J. P. S. A substrate-independent approach for bactericidal surfaces. *Applied Materials & Interfaces* **2009**, *1*, 2763-2767.



- 
69. Britcher, L.; Barnes, T. J.; Griesser, H. J.; Prestidge, C. A. PEGylation of porous silicon using click chemistry. *Langmuir* **2008**, *24*, 7625-7627.
70. Yang, M.; Teeuwen, R. L. M.; Giesbers, M.; Baggerman, J.; Arafat, A.; de Wolf, F. A.; van Hest, J. C. M.; Zuilhof, H. One-step photochemical attachment of NHS-terminated monolayers onto silicon surfaces and subsequent functionalization. *Langmuir* **2008**, *24*, 7931-7938.
71. Ciampi, S.; Böcking, T.; Kilian, K. A.; James, M.; Harper, J. B.; Gooding, J. J. Functionalization of acetylene-terminated monolayers on Si(100) surfaces: a click chemistry approach. *Langmuir* **2007**, *23*, 9320-9329.
72. Busolo, F.; Franco, L.; Armelao, L.; Maggini, M. Dynamics of a nitroxide layer grafted onto porous silicon. *Langmuir* **2010**, *26*, 1889-1893.
73. Wang, X.; Landis, E. C.; Franking, R.; Hamers, R. J. Surface chemistry for stable and smart molecular and biomolecular interfaces via photochemical grafting of alkenes. *Accounts of Chemical Research* **2010**, *43*, 1205-1215.
74. Chehimi, M. M.; Hallais, G.; Matrab, T.; Pinson, J.; Podvorica, F. I. Electro- and Photografting of Carbon or Metal Surfaces by Alkyl Groups. *The Journal of Physical Chemistry C* **2008**, *112*, 18559-18565.
75. Lockett, M. R.; Carlisle, J. C.; Le, D. V.; Smith, L. M. Acyl chloride-modified amorphous carbon substrates for the attachment of alcohol-, thiol-, and amine-containing molecules. *Langmuir* **2009**, *25*, 5120-5126.
76. Li, B.; Franking, R.; Landis, E. C.; Kim, H.; Hamers, R. J. Photochemical grafting and patterning of biomolecular layers onto TiO<sub>2</sub> thin films. *Applied Materials & Interfaces* **2009**, *1*, 1013-1022.
77. Lee, B. S.; Lee, J. K.; Kim, W.-Joong; Jung, Y. H.; Sim, S. J.; Lee, J.; Choi, I. S. Surface-initiated, atom transfer radical polymerization of oligo(ethylene glycol) methyl ether methacrylate and subsequent click chemistry for bioconjugation. *Biomacromolecules* **2007**, *8*, 744-749.
78. Notestein, J. M.; Canlas, C.; Siegfried, J.; Moore, J. S. Covalent Grafting of m-Phenylene-Ethynylene Oligomers to Oxide Surfaces. *Chemistry of Materials* **2010**, *22*, 5319-5327.
79. Orski, S. V.; Fries, K. H.; Sheppard, G. R.; Locklin, J. High density scaffolding of functional polymer brushes: surface initiated atom transfer radical polymerization of active esters. *Langmuir* **2010**, *26*, 2136-2143.
80. Chang, B.; Prucker, O.; Groh, E.; Wallrath, A.; Dahm, M.; Rühle, J. Surface-attached polymer monolayers for the control of endothelial cell adhesion. *Colloids and Surfaces A: Physicochemical and Engineering Aspects* **2002**, *198-200*, 519-526.
81. Koberstein, J. T. J.; Duch, D. E. D.; Hu, W.; Lenk, T. J.; Bhatia, R.; Brown, H. R.; Lingelser, J.-P.; Gallot, Y. Creating Smart Polymer Surfaces with Selective Adhesion Properties. *The Journal of Adhesion* **1998**, *66*, 229-249.
82. Raghuraman, G. K.; Dhamodharan, R.; Prucker, O.; Rühle, J. A Robust Method for the Immobilization of Polymer Molecules on SiO<sub>2</sub> Surfaces. *Macromolecules* **2008**, *41*, 873-878.
83. Czaun, M.; Hevesi, L.; Takafuji, M.; Ihara, H. Novel Surface-Attachable Multifunctional Initiators: Synthesis, Grafting, and Polymerization in Aprotic and Protic Solvents. *Macromolecules* **2009**, *42*, 4539-4546.
84. Ranjan, R.; Brittain, W. J. Synthesis of High Density Polymer Brushes on Nanoparticles by Combined RAFT Polymerization and Click Chemistry. *Macromolecular Rapid Communications* **2008**, *29*, 1104-1110.
85. Such, G. K.; Quinn, J. F.; Quinn, A.; Tjijto, E.; Caruso, F. Assembly of ultrathin polymer multilayer films by click chemistry. *Journal of the American Chemical Society* **2006**, *128*, 9318-9319.

- 
86. Bergbreiter, D. E.; Simanek, E. E.; Owsik, I. New Synthetic Methods for the Formation of Basic, Polyvalent, Hyperbranched Grafts. *Journal of Polymer Science Part A: Polymer Chemistry* **2005**, *43*, 4654-4665.
87. Vestberg, R.; Malkoch, M.; Kade, M.; Wu, P.; Fokin, V. V.; Barry Sharpless, K.; Drockenmuller, E.; Hawker, C. J. Role of architecture and molecular weight in the formation of tailor-made ultrathin multilayers using dendritic macromolecules and click chemistry. *Journal of Polymer Science Part A: Polymer Chemistry* **2007**, *45*, 2835-2846.
88. Bergbreiter, D. E.; Chance, B. S. "Click"-Based Covalent Layer-by-Layer Assembly on Polyethylene Using Water-Soluble Polymeric Reagents. *Macromolecules* **2007**, *40*, 5337-5343.
89. El Haitami, A. E.; Thomann, J.-S.; Jierry, L.; Parat, A.; Voegel, J.-C.; Schaaf, P.; Senger, B.; Boulmedais, F.; Frisch, B. Covalent layer-by-layer assemblies of polyelectrolytes and homobifunctional spacers. *Langmuir* **2010**, *26*, 12351-12357.
90. Lancaster, J. R.; Jehani, J.; Carroll, G. T.; Chen, Y.; Turro, N. J.; Koberstein, J. T. Toward a Universal Method To Pattern Metals on a Polymer. *Chemistry of Materials* **2008**, *20*, 6583-6585.
91. Rengifo, H. R.; Chen, L.; Grigoras, C.; Ju, J.; Koberstein, J. T. "Click-functional" block copolymers provide precise surface functionality via spin coating. *Langmuir* **2008**, *24*, 7450-7456.
92. Dirani, A.; Roucoules, V.; Haidara, H.; Soppera, O. Plasma polymer tailoring of the topography and chemistry of surfaces at the nanoscale. *Langmuir* **2010**, *26*, 17532-17539.
93. Chen, R. T.; Muir, B. W.; Such, G. K.; Postma, A.; Evans, R. A.; Pereira, S. M.; McLean, K. M.; Caruso, F. Surface "click" chemistry on brominated plasma polymer thin films. *Langmuir* **2010**, *26*, 3388-3393.
94. Rosso, M.; Giesbers, M.; Schroën, K.; Zuilhof, H. Controlled oxidation, biofunctionalization, and patterning of alkyl monolayers on silicon and silicon nitride surfaces using plasma treatment. *Langmuir* **2010**, *26*, 866-872.
95. Wang, Q.; Chan, T. R.; Hilgraf, R.; Fokin, V. V.; Sharpless, K. B.; Finn, M. G. Bioconjugation by copper(I)-catalyzed azide-alkyne [3 + 2] cycloaddition. *Journal of the American Chemical Society* **2003**, *125*, 3192-3193.
96. Brunel, F. M.; Lewis, J. D.; Destito, G.; Steinmetz, N. F.; Manchester, M.; Stuhlmann, H.; Dawson, P. E. Hydrazone ligation strategy to assemble multifunctional viral nanoparticles for cell imaging and tumor targeting. *Nano Letters* **2010**, *10*, 1093-1097.
97. O'Reilly, R. K.; Joralemon, M. J.; Wooley, K. L.; Hawker, C. J. Functionalization of Micelles and Shell Cross-linked Nanoparticles Using Click Chemistry. *Chemistry of Materials* **2005**, *17*, 5976-5988.
98. Cavalli, S.; Tipton, A. R.; Overhand, M.; Kros, A. The chemical modification of liposome surfaces via a copper-mediated [3 + 2] azide-alkyne cycloaddition monitored by a colorimetric assay. *Chemical Communications* **2006**, 3193-3195.
99. Rozkiewicz, D. I.; Jańczewski, D.; Verboom, W.; Ravoo, B. J.; Reinhoudt, D. N. "Click" chemistry by microcontact printing. *Angewandte Chemie International Edition* **2006**, *45*, 5292-5296.
100. Ku, S.-Y.; Wong, K.-T.; Bard, A. J. Surface patterning with fluorescent molecules using click chemistry directed by scanning electrochemical microscopy. *Journal of the American Chemical Society* **2008**, *130*, 2392-2393.
101. Paxton, W. F.; Spruell, J. M.; Stoddart, J. F. Heterogeneous catalysis of a copper-coated atomic force microscopy tip for direct-write click chemistry. *Journal of the American Chemical Society* **2009**, *131*, 6692-6694.

- 
102. Haensch, C.; Hoepfner, S.; Schubert, U. S. "Clicking" on the nanoscale: 1,3-dipolar cycloaddition of terminal acetylenes on azide functionalized, nanometric surface templates with nanometer resolution. *Nanotechnology* **2009**, *20*, 135302.
103. Hansen, T. S.; Daugaard, A. E.; Hvilsted, S.; Larsen, N. B. Spatially Selective Functionalization of Conducting Polymers by "Electroclick" Chemistry. *Advanced Materials* **2009**, *21*, 4483-4486.
104. Im, S. G.; Kim, B.-Su; Lee, L. H.; Tenhaeff, W. E.; Hammond, P. T.; Gleason, K. K. A Directly Patternable, Click-Active Polymer Film via Initiated Chemical Vapor Deposition. *Macromolecular Rapid Communications* **2008**, *29*, 1648-1654.
105. Coll Ferrer, M. C.; Yang, S.; Eckmann, D. M.; Composto, R. J. Creating Biomimetic Polymeric Surfaces by Photochemical Attachment and Patterning of Dextran. *Langmuir* **2010**, *26*, 14126-14134.
106. Carroll, G. T.; Sojka, M. E.; Lei, X.; Turro, N. J.; Koberstein, J. T. Photoactive additives for cross-linking polymer films: Inhibition of dewetting in thin polymer films. *Langmuir* **2006**, *22*, 7748-7754.
107. Carroll, G. T.; Wang, D.; Turro, N. J.; Koberstein, J. T. Photochemical micropatterning of carbohydrates on a surface. *Langmuir* **2006**, *22*, 2899-2905.
108. Toh, C. R.; Fraterman, T. A.; Walker, D. A.; Bailey, R. C. Direct biophotolithographic method for generating substrates with multiple overlapping biomolecular patterns and gradients. *Langmuir* **2009**, *25*, 8894-8898.
109. Junk, M. J. N.; Berger, R.; Jonas, U. Atomic force spectroscopy of thermoresponsive photo-cross-linked hydrogel films. *Langmuir* **2010**, *26*, 7262-7269.
110. Geiger, M. W.; Elliot, M. M.; Karacostas, V. D.; Moricone, T. J.; Salmon, J. B.; Sideli, V. L.; Onge, M. A. S. Aryl Azides As Protein Photolabels: Absorption Spectral Properties and Quantum Yields of Photodissociation. *Photochemistry and Photobiology* **1984**, *40*, 545-548.
111. Sinz, A. Chemical cross-linking and mass spectrometry for mapping three-dimensional structures of proteins and protein complexes. *Journal of Mass Spectrometry: JMS* **2003**, *38*, 1225-1237.
112. Schuh, K.; Prucker, O.; Rhe, J. Surface Attached Polymer Networks through Thermally Induced Cross-Linking of Sulfonyl Azide Group Containing Polymers. *Macromolecules* **2008**, *41*, 9284-9289.
113. Li, B.; Chen, J.; Wang, J. H.-C. RGD peptide-conjugated poly(dimethylsiloxane) promotes adhesion, proliferation, and collagen secretion of human fibroblasts. *Journal of Biomedical Materials Research. Part A* **2006**, *79*, 989-998.
114. Raghuraman, G. K.; Schuh, K.; Prucker, O.; Rhe, J. Attachment of polymer films to solid surfaces via thermal activation of self-assembled monolayers containing sulphonyl azide group. *Langmuir* **2010**, *26*, 769-774.
115. Griffiths, J.-P.; Maliha, B.; Moloney, M. G.; Thompson, A. L.; Hussain, I. Surface Functional Polymers by Post-Polymerization Modification using Diarylcarbenes: Introduction, Release and Regeneration of Hydrogen Peroxide and Bactericidal Activity. *Langmuir* **2010**, *26*, 14142-14153.
116. Cai, C.; Vasella, A. Oligosaccharide Analogues of Polysaccharides. Part 3. A new protecting group for alkynes: Orthogonally protected dialkynes. *Helvetica Chimica Acta* **1995**, *78*, 732-757.
117. Kise, N.; Isemoto, S.; Sakurai, T. Electroreductive coupling of phthalimides with  $\alpha,\beta$ -unsaturated esters: unusual rearrangement of resulting silyl ketene acetals. *Organic Letters* **2009**, *11*, 4902-4905.
118. Basarić, N.; Horvat, M.; Mlinarić-Majerski, K.; Zimmermann, E.; Neudrfl, J.; Griesbeck, A. G. Novel 2,4-methanoadamantane-benzazepine by domino photochemistry of N-(1-adamanty)phthalimide. *Organic Letters* **2008**, *10*, 3965-3968.

- 
119. Synthesis of **6**: JRL1p97, JRL1p109, JRL2p83. <sup>1</sup>H NMR of **6**: JRL-042009-Br-alkyne-red, JRL-042209-Br-alkyne-yellow, JRL\_10\_0603\_bromohexanoyl-alkyne, JRL\_10\_0915\_bromo-alkyne
120. Synthesis of **7**: JRL1p103. <sup>1</sup>H NMR of **7**: JRL-042809-Br-alkyne-TMS.
121. Synthesis of **8**: JRL1p101, JRL2p85. <sup>1</sup>H NMR of **8**: JRL-042809-phth-alkyne-green, JRL\_10\_0609\_phthalimide-alkyne, JRL\_10\_0923\_phthalimide\_alkyne.
122. Synthesis of **9**: JRL1p105. <sup>1</sup>H NMR of **9**: JRL-050109-phth-alkyne-TMS.
123. Synthesis of **10**: JRL2p11. <sup>1</sup>H NMR of **10**: JRL-102409-azidodecene.
124. Yuan, H.; He, R.; Wan, B.; Wang, Y.; Pauli, G. F.; Franzblau, S. G.; Kozikowski, A. P. Modification of the side chain of micromolide, an anti-tuberculosis natural product. *Bioorganic & Medicinal Chemistry Letters* **2008**, *18*, 5311-5315.
125. Tsai, S.-C.; Fu, Y.-S.; Liao, J.-H.; Yu, S. Versatile and Efficient Synthesis of a New Class of Aza-Based Phosphinic Amide Ligands via Unusual P-C Cleavage. *Helvetica Chimica Acta* **2006**, *89*, 3007-3017.
126. Schlotter, N. E.; Rabolt, J. F. Measurements of the Optical Anisotropy of Trapped Molecules in Oriented Polymer Films by Waveguide Raman Spectroscopy (WRS). *Applied Spectroscopy* **1984**, *38*, 208-211.
127. Sivakumar, K.; Xie, F.; Cash, B. M.; Long, S.; Barnhill, H. N.; Wang, Q. A fluorogenic 1,3-dipolar cycloaddition reaction of 3-azidocoumarins and acetylenes. *Organic Letters* **2004**, *6*, 4603-4606.
128. Le Droumaguet, C.; Wang, C.; Wang, Q. Fluorogenic click reaction. *Chemical Society Reviews* **2010**, *39*, 1233-1239.
129. JRL2p117
130. Knopp, D.; Tang, D.; Niessner, R. Review: bioanalytical applications of biomolecule-functionalized nanometer-sized doped silica particles. *Analytica Chimica Acta* **2009**, *647*, 14-30.
131. Michel, O.; Ravoo, B. J. Carbohydrate microarrays by microcontact "click" chemistry. *Langmuir* **2008**, *24*, 12116-12118.
132. Goreham, R. V.; Short, R. D.; Vasilev, K. Method for the Generation of Surface-Bound Nanoparticle Density Gradients. *The Journal of Physical Chemistry C* **2011**, *115*, 3429-3433.
133. Wang, C.; Zhang, Y.; Seng, H. S.; Ngo, L. L. Nanoparticle-assisted micropatterning of active proteins on solid substrate. *Biosensors & Bioelectronics* **2006**, *21*, 1638-1643.
134. Wu, D.; Han, D.; Steckl, A. J. Immunoassay on free-standing electrospun membranes. *Applied Materials & Interfaces* **2010**, *2*, 252-258.
135. Reches, M.; Mirica, K. A.; Dasgupta, R.; Dickey, M. D.; Butte, M. J.; Whitesides, G. M. Thread as a Matrix for Biomedical Assays. *Applied Materials & Interfaces* **2010**, *2*, 1722-1728.
136. Jølck, R. I.; Sun, H.; Berg, R. H.; Andresen, T. L. Catalyst-free conjugation and in situ quantification of nanoparticle ligand surface density using fluorogenic Cu-free click chemistry. *Chemistry - A European Journal* **2011**, *17*, 3326-3331.
137. Paik, M. Y.; Xu, Y.; Rastogi, A.; Tanaka, M.; Yi, Y.; Ober, C. K. Patterning of Polymer Brushes. A Direct Approach to Complex, Sub-Surface Structures. *Nano Letters* **2010**, *10*, 3873-3879.

## 4. <sup>1</sup>H NMR Study of Hydrogen Abstraction in Polymers

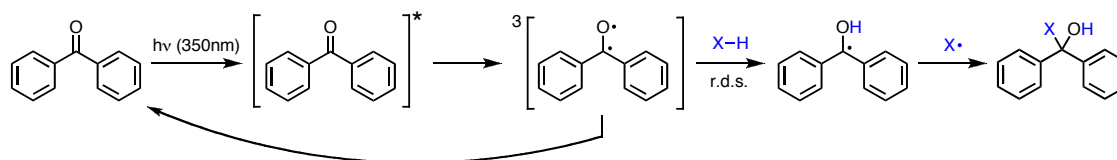
(with Rachael Smilowitz)

### 4.1. Introduction, Motivation

Light is a ‘clean’, simple, and selective reagent for the activation of photoactive moieties. In Chapter 2, homobifunctional crosslinkers bearing two photoactive groups were synthesized in order to covalently bind to – and bridge – polymer chains in the bulk. In Chapter 3, heterobifunctional molecules bearing a photoactive group and a click-functional group were synthesized in order to covalently bind to – and functionalize – polymer surfaces. As discussed in Section 1.4, photoactive moieties have also been used for photoaffinity labeling of biopolymers, to form polymer gels, and to initiate the degradation of polymer networks.<sup>1</sup> The versatility and potential for reactions of polymers with photoactive moieties such as benzophenone, phthalimide, xanthone, sulfonyl azide, phenyl azide, and ortho-nitrobenzyl alcohols has made it necessary to better understand how photoactive moieties interact with the polymers they modify.

Previous work from our group focused on the use of benzophenone as a hydrogen abstraction agent within a polymer film to induce crosslinking in order to inhibit dewetting.<sup>2</sup> Benzophenone is one of the most well-studied and well-behaved photoactive compounds, and has variously been used as a triplet sensitizer, a hydrogen abstractor, and a polymerization initiator.<sup>3,4</sup> Here, we examine the ability of triplet benzophenone to abstract hydrogen atoms from model compounds that are meant to represent commonly used polymers. Species other than triplet benzophenone have also been used to examine hydrogen atom abstraction processes including *tert*-butoxy, chlorine, and hydroxy radicals<sup>5-7</sup>, but the aim of this section is to develop a framework for understanding – and

possibly predicting and controlling – how the photochemical reaction of benzophenone will take place in a polymer.



**Figure 4.1.** Excitation of benzophenone and subsequent hydrogen abstraction from a hydrogen donor (blue).

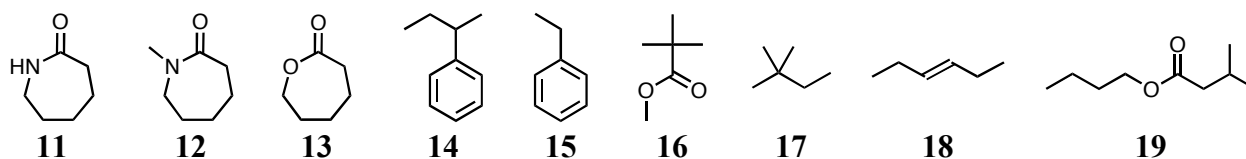
Hydrogen abstraction by benzophenone proceeds by the mechanism shown in Figure 4.1.<sup>8</sup> Irradiation of benzophenone excites the carbonyl to the  $n,\pi^*$  singlet state which quickly undergoes an intersystem crossing to the triplet state. The triplet diradical can recombine and relax to the ground state, or the oxy radical can abstract a hydrogen from a nearby donor. Because of differences in bond dissociation energies, the radical remaining on the hydrogen donor ( $X\cdot$ ) is unlikely to re-abtract the hydroxyl hydrogen from the diphenyl alcohol radical so it will form a new covalent bond by recombination with the carbon-centered radical on the diphenyl alcohol (or another nearby radical). To a first approximation, the rate and extent of the reaction of excited benzophenone with any hydrogen donor ought to depend primarily on the energy of the excited benzophenone and the bond strength of the  $X-H$  bond that is broken during the rate determining step (r.d.s. in Figure 4.1). Since the triplet energy of benzophenone is constant, we would expect hydrogens in similar chemical environments to have similar reactivities toward photoexcited benzophenone.<sup>9</sup>

$^1H$  NMR was used to monitor the extent of hydrogen abstraction reaction since protons are transferred between different chemical environments. At reasonable concentrations in solution, however, the  $^1H$  NMR signals from polymers or oligomers

would overwhelm any signal indicative of a change having occurred. In place of polymers or oligomers, we sought model compounds containing hydrogens in various chemical environments that map onto commonly used polymers (Table 4.1).<sup>10-14</sup> For instance, caprolactam (**11**) was used as a small molecule substitute for polycaprolactam, and  $\epsilon$ -caprolactone (**13**) was used for polycaprolactone. Selection of model compounds depended on both their similarity to target polymers and commercial availability.

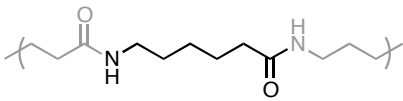
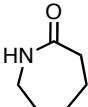
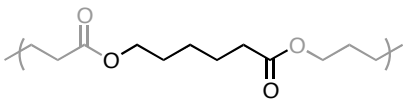
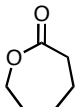
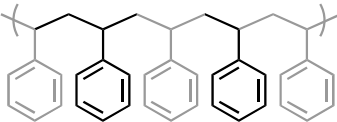

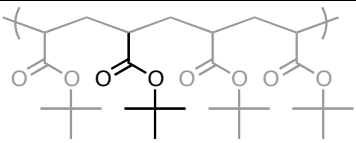
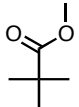
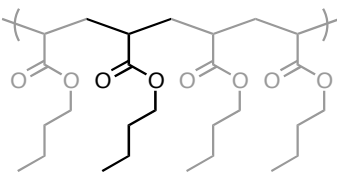
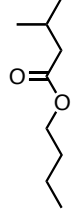
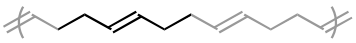
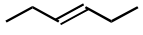
In some monomers, the energies of the bonds are significantly different than the energies of the bonds in the polymers they form. For instance, the energy of the bond  $\alpha$  to the aromatic ring of styrene is  $\sim 115$  kcal/mol, whereas the same bond in ethylbenzene – a compound with bonds more like those in polystyrene – is  $\sim 100$  kcal/mol (Figure 4.3). The hybridization and conjugation of the styrene vinyl group affects both the C-C and the C-H bond energies at the  $\alpha$  and  $\beta$  positions relative to the phenyl ring. Therefore, instead of using its monomer styrene, we chose *sec*-butylbenzene (**14**) and ethylbenzene (**15**) as the model compounds that best represent the bonds in polystyrene.

Other compounds were chosen that closely resembled portions of polymers, or were nearly analogous to the polymer structure. Methyl trimethylacetate (**16**) and butyl isovalerate (**19**) were chosen to represent poly(*tert*-butyl acrylate) and poly(*n*-butyl acrylate), respectively. Hydrocarbons 2,2-dimethylbutane (**17**) and trans-3-hexene (**18**) were chosen to mimic polymers such as branched polyethylene and polybutadiene.



**Figure 4.2.** Structures of the compounds used in this study: caprolactam, **11**; methylcaprolactam, **12**; caprolactone, **13**; *sec*-butylbenzene, **14**; ethylbenzene, **15**; methyl trimethylacetate, **16**; 2,2-dimethylbutane, **17**; *trans*-3-hexene, **18**; and butyl isovalerate, **19**.

**Table 4.1.** Structural comparison of some typical polymers and model compounds used.

Polymer	Model Compounds
 Polycaprolactam	 Caprolactam, <b>11</b>
 Polycaprolactone	 ε-Caprolactone, <b>13</b>
 Polystyrene	 <i>sec</i> -Butylbenzene, <b>14</b> Ethylbenzene, <b>15</b>
 Poly( <i>tert</i> -butyl acrylate)	 Methyl trimethylacetate, <b>16</b>
 Poly( <i>n</i> -butyl acrylate)	 Butyl isovalerate, <b>19</b>
 Polybutadiene	 <i>trans</i> -3-Hexene, <b>18</b>





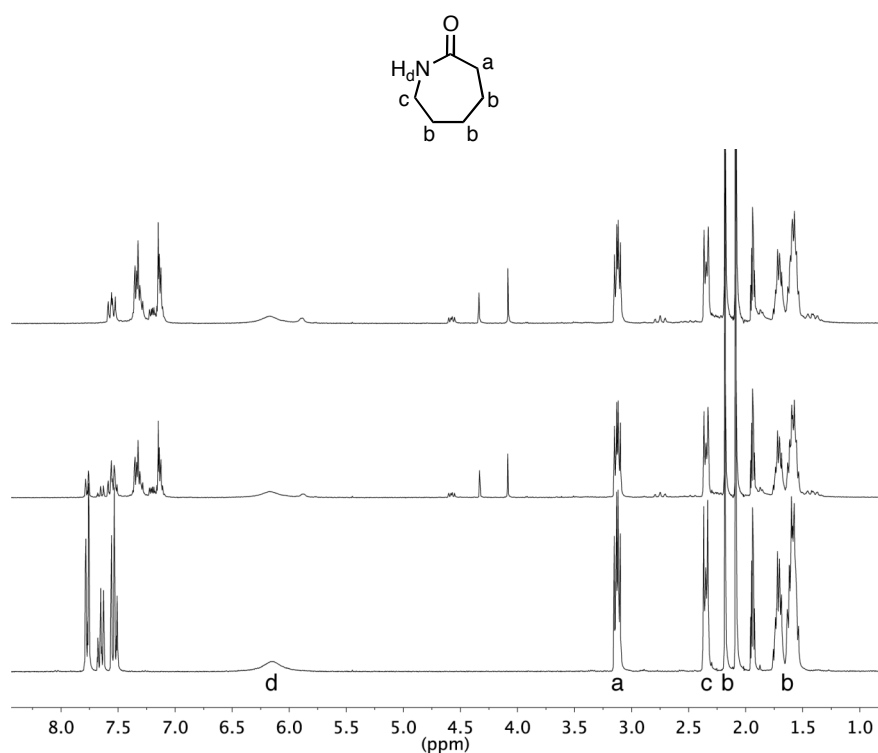
**Figure 4.3.** Comparison of C-C bond dissociation energies in ethylbenzene, **15**, and styrene.

## 4.2. Analysis

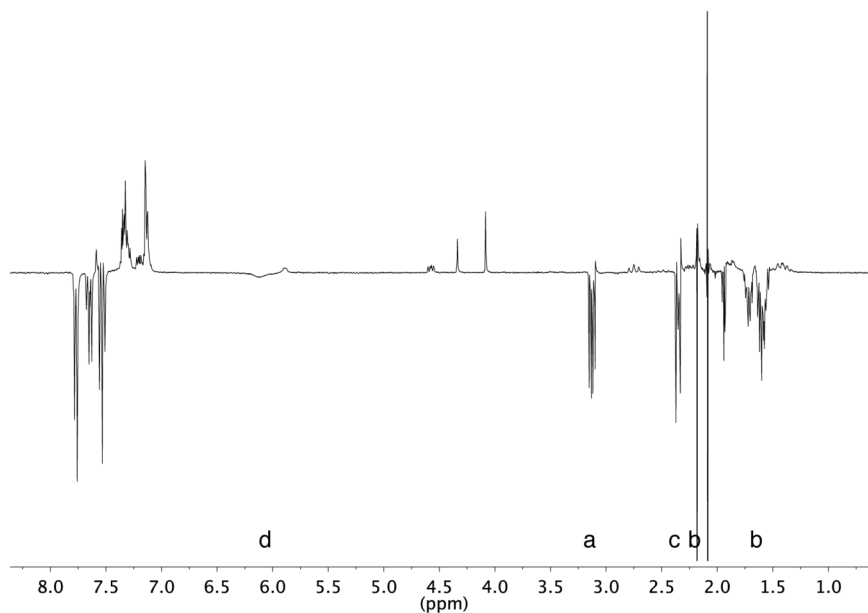
A set of  $^1\text{H}$  NMR spectra recorded for compound **11** is shown in Figure 4.4 and is representative of each model compound tested. The benzophenone C-H peaks ( $\delta$  7.0-8.0) are generally well separated from the proton signals of the model compounds, except in the case of compounds that contain aromatic protons (**14**, **15**). As the sample was irradiated at 350 nm, the peaks corresponding to benzophenone ( $\delta$  7.5-8.0) and the model compound decreased in intensity, while new peaks ( $\delta$  7.0-7.6, others) corresponding to the reaction products increased in intensity. This work was not concerned with assigning specific structures to the reaction products.

In order to quantitatively analyze the relative rates of decrease of each model compound X-H signal, the spectra were calibrated to a constant integral in the range  $\delta$  7.0-8.0. Control experiments indicated that benzophenone does not react with itself in  $\text{CD}_3\text{CN}$ , and therefore the number of aromatic protons from the benzophenone remains constant as an internal standard. Additionally, benzophenone did not react with the  $\text{CD}_3\text{CN}$  and the model compounds alone in  $\text{CD}_3\text{CN}$  did not react when irradiated. No decrease greater than 6% was found in the control experiments indicating that both benzophenone and the model compound must be present for the reaction to occur. In cases where the aromatic protons of a model compound overlap the benzophenone

region, the entire spectrum was calibrated under the assumption that the total number of protons in the solution remained constant. In cases where a water impurity peak overlaps with a model compound proton signal, the water peak was fit with a Lorentzian function in order to subtract its overlap. Once scaled appropriately, difference spectra were generated (Figure 4.5) to visualize the relative decreases of the initial model compound proton signals in comparison to the growth of new signals from the reaction products.



**Figure 4.4.** 300 MHz <sup>1</sup>H NMR spectra of a 96.9 mM solution of **11** (CD<sub>3</sub>CN) and benzophenone after 0 min (bottom), 30 min (middle), and 120 min (top) irradiation at 350nm.



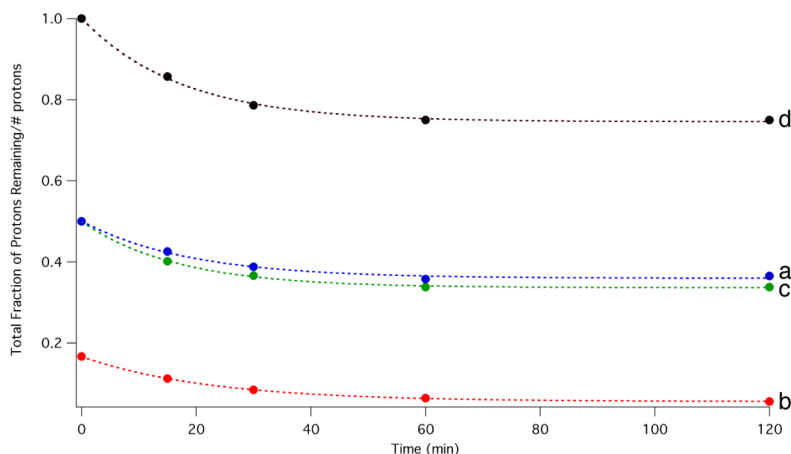
**Figure 4.5.** Difference between 300 MHz  $^1\text{H}$  NMR spectra of **11** ( $\text{CD}_3\text{CN}$ ) and benzophenone before and after 120 min irradiation at 350nm.

Samples were irradiated until either the initial benzophenone peaks had shifted completely to the characteristic product peaks (Figure 4.4,  $\delta$  7.0-7.6), or until the benzophenone peaks no longer decreased with increased irradiation time indicating the reaction was complete. Integrals of each region were normalized to the integral at  $t = 0$ . The resulting values are plotted in Figure 4.6 for model compound **11**. The integrals for each type of proton were fit according to Equation 4.1 (Figure 4.6, dotted lines) where  $t$  is the irradiation time in minutes:

$$y = Ae^{-kt} + C$$

Equation  
4.1

**Equation 4.1.**



**Figure 4.6.** Plot of  $^1\text{H}$  NMR integrals for protons a-d of compound **11** scaled by initial integral and number of protons with increasing irradiation time. Each set of data points is fit with Equation 4.1.

**Table 4.2.** Values of  $k$  using Equation 4.1 to fit the data in Figure 4.6 for **11**.

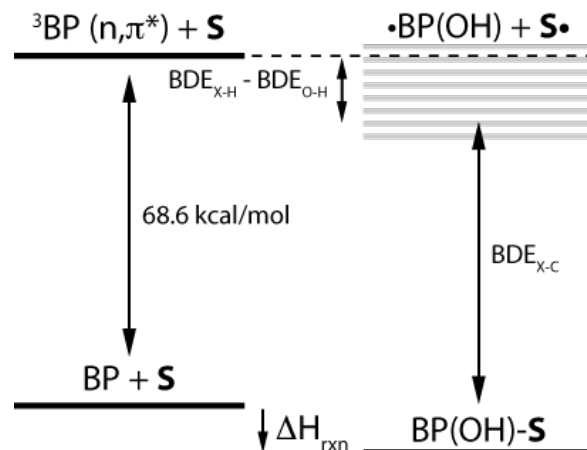
	$\text{H}_a$	$\text{H}_b$	$\text{H}_c$	$\text{H}_d$
$k$	$0.053 \pm 0.008$	$0.045 \pm 0.009$	$0.060 \pm 0.003$	$0.058 \pm 0.004$

### 4.3. Discussion

As discussed above and shown in Figure 4.1, photochemically induced hydrogen abstraction by benzophenone is initiated by photoexcitation of an electron pair from the singlet ground state to first singlet excited  $n,\pi^*$  state, which is quickly followed by an intersystem crossing to the triplet state. The triplet state, a diradical with one oxygen-centered radical and one carbon-centered radical, can either decay to the ground state or the oxygen-centered radical can abstract a hydrogen atom from a nearby molecule. The resulting pair of radicals can then either recombine to generate a covalent bond – a reaction we have employed to covalently crosslink polymeric materials (Chapter 2) – or can transfer the hydrogen back to its original location.

The relative energies of the starting materials (benzophenone, BP, and substrate, S) and the recombination product of photoinduced hydrogen abstraction are shown

schematically in Figure 4.7. The singlet  $n,\pi^*$  state of benzophenone is 75.5 kcal/mol higher in energy than the ground state and is not shown below because the singlet completely intersystem crosses to the triplet (68.6 kcal/mol) with a quantum yield of unity ( $\Phi_T = 1$ ).<sup>15</sup> Gray lines in Figure 4.7 represent a range of possible values of the energy of the hydrogen abstraction products – diphenyl alcohol radical and the substrate radical – that depends on the energy of the X-H bond that is broken since each O-H bond formed is identical. The last step in this process is recombination of the two radicals to generate a new X-C bond. Energies for the O-H, C-C, and N-C bonds formed can be estimated as 102, 75, and 65 kcal/mol respectively to give a range of the possible X-H bond energies that would be make the overall reaction exothermic ( $\Delta H_{\text{rxn}} < 0$ ).<sup>16-18</sup> Substituting the known or estimable energies into Equation 4.2 gives the upper limit of X-H bond energy that will undergo an exothermic hydrogen abstraction by benzophenone to be 108 kcal/mol. An additional limit is placed upon the reaction in order for the rate of hydrogen abstraction to be competitive with deactivation of the excited benzophenone. There must be little to no activation energy barrier to the formation of the hydrogen abstraction products during the rate determining step, so the hydrogen abstraction step must also be exothermic.<sup>8</sup> Taking this into account makes the upper limit of X-H bond energy approximately 102 kcal/mol.



**Figure 4.7.** Energy state diagram for hydrogen abstraction by benzophenone (BP) from a substrate, S, followed by recombination.

$$\begin{aligned} \Delta H_{rxn} &= [E(^3BP_{n,\pi^*}) + BDE_{X-H}] - [BDE_{O-H} + BDE_{X-C}] && \text{Equation} \\ &= [68.6 \frac{\text{kcal}}{\text{mol}} + BDE_{X-H}] - [102 \frac{\text{kcal}}{\text{mol}} + 75 \frac{\text{kcal}}{\text{mol}}] && 4.2 \end{aligned}$$

$$\Delta H_{rxn} < 0 \text{ when } BDE_{X-H} \leq 108 \frac{\text{kcal}}{\text{mol}}$$

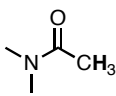
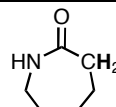
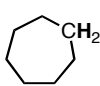
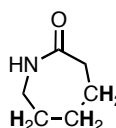
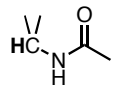
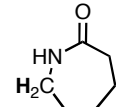
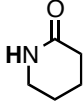
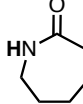
**Equation 4.2.**

The majority of the X-H bond dissociation energies of the model compounds **11-19** have not been measured or tabulated, so it is necessary to consult tables of representative compounds in order to infer relative bond dissociation energies.<sup>16-19</sup> Representative compounds for the X-H bonds of **11**, their bond dissociation energies, and their relationships to **11** are shown in Table 4.3 along with the value of *k* determined experimentally for each X-H bond. For compounds **11-19**, the X-H bond energies of most of the representative compounds are significantly lower in energy than 102 kcal/mol indicating that each ought to be abstractable by excited benzophenone. The only representative bond dissociation energies that fall outside the thermodynamically acceptable range of X-H bond energies are the N-H bond of **11** (109.5 kcal/mol) and the

alkenyl C-H of **18** (approx. 110 kcal/mol). Based upon thermodynamics alone, we would expect no abstraction of these two protons by excited benzophenone.

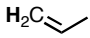
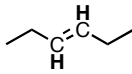
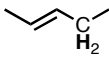
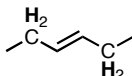
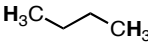
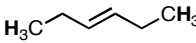
Directly and quantitatively comparing tabulated bond dissociation energies is problematic, however, because of the wide variety of methods used to determine bond dissociation energies: shock tube techniques, laser flash photolysis, correlation methods, etc.<sup>16-21</sup> A more holistic experimental method such as the one used here samples all X-H bonds simultaneously and provides a comprehensive picture of the competitive relationships between various X-H bonds within the same molecule without needing to directly measure bond dissociation energies.

**Table 4.3.** Compounds with representative bond dissociation energies for the protons of **11**, the relation of each representative bond to **11**, and the competitive rate value of  $k/k_a$  scaled for the number of protons.

Representative compound	X-H BDE (kcal/mol)	Relation to <b>11</b>	$k/k_a$
N,N-dimethylacetamide 	91.0 <sup>a</sup>	 H <sub>a</sub>	1
cycloheptane 	93.3 <sup>b</sup> 94.0 <sup>c</sup> 92.5±1 <sup>d</sup> 96.5 <sup>e</sup>	 H <sub>b</sub>	0.28
N-isopropylacetamide 	93.1 <sup>a</sup>	 H <sub>c</sub>	1.13
2-piperidone 	109.5 <sup>f</sup>	 H <sub>d</sub>	2.19

Methods for determination of bond dissociation energies: <sup>a</sup>Correlation. <sup>b</sup>Polanyi correlation. <sup>c</sup>Kinetics. <sup>d</sup>Photobromination. <sup>e</sup>Intersecting parabolas. <sup>f</sup>Acidity-oxidation potential measurement.

**Table 4.4.** Compounds with representative bond dissociation energies for the protons of **18**, the relation of each representative bond to **18**, and the competitive rate value of  $k/k_a$  scaled for the number of protons.

Representative compound	X-H BDE (kcal/mol)	Relation to <b>18</b>	$k/k_a$
propene 	109±2.4 <sup>h</sup> 111.1 <sup>h</sup>	 H <sub>a</sub>	1
( <i>E</i> )-2-pentene 	81.7±1.5 <sup>r</sup> 82.5 <sup>a</sup>	 H <sub>b</sub>	3.13
butane 	101±2 <sup>1</sup> 100.2 <sup>p</sup> 100.7 <sup>h</sup> 101.7±0.5 <sup>n</sup>	 H <sub>c</sub>	2.08

Methods for determination of bond dissociation energies: <sup>h</sup>Single-pulse shock tube technique. <sup>r</sup>Derived from  $\Delta H_f^\circ$ . <sup>a</sup>Correlation. <sup>1</sup>Electron impact. <sup>p</sup>Appearance energy measurements. <sup>n</sup>Photoionization mass spectrometry.

Differences in bond dissociation energy alone do not account for the preferential abstraction of particular hydrogens from compounds **11-19** by benzophenone. Table 4.3 shows that the alkyl C-H bonds (H<sub>a</sub>, H<sub>b</sub>, H<sub>c</sub>) of **11** have similar bond dissociation energies in the range of 91-96 kcal/mol but are not abstracted homogeneously. The N-H<sub>d</sub> bond is the most likely to be abstracted, however, despite being approximately 15 kcal/mol higher in energy than the C-H<sub>a</sub>, C-H<sub>b</sub> and C-H<sub>c</sub> bonds. The larger-than-expected rate for H<sub>d</sub> may result from the formation of a pre-reactive hydrogen-bonded complex between the N-H bond and a lone pair of electrons on the carbonyl oxygen of benzophenone. By bringing the reactive end of the benzophenone close to the amine hydrogen, the number of abstraction events from that position is increased relative to abstraction based on bond energies alone. Additionally, pre-reactive complexation weakens the N-H bond, making it more abstractable. Such an effect is not seen in **12** which lacks the ability to hydrogen bond. The hydrogens bonded to carbons next to the amide of **11** and of **12** are roughly



equally preferred sites for abstraction, while the alkyl C-H's are deactivated to abstraction relative to the other available hydrogens.

Comparison with another high bond energy C-H bond supports the notion of pre-reactive complexation by benzophenone and **11**. The alkenyl C-H of **18** has a high bond dissociation energy (approx. 110 kcal/mol) due to the  $sp^2$  hybridization of the carbon, but it cannot form a complex with the benzophenone. The rate of abstraction from the alkenyl C-H is less than the rate of abstraction from the alkyl C-H's ( $H_b$ ,  $H_c$ ) as would be expected (Table 4.4). It is worthwhile to recognize that the hydrogens on the carbon  $\alpha$  to the double bond are abstracted more readily than the terminal methyl protons, likely due to the resonance stabilization provided to the radical by the double bond.

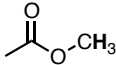
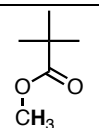
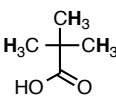
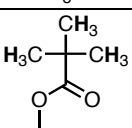
Radical stability plays a role in the hydrogen abstraction preferences in compounds such as **14**, **15**, and **17**. In each case, as expected, tertiary hydrogens are abstracted preferentially – relative to the number of protons available – then secondary and primary hydrogens. According to these data, secondary hydrogens are abstracted roughly three to four times as often as primary hydrogens (**15**, **17**), and roughly half as often as tertiary hydrogens (**14**). Some balance is achieved in the compounds studied since there are generally more primary hydrogens available than secondary, and more secondary available than tertiary.

Aside from bond dissociation energy and radical stability, steric effects and polar or charge transfer effects can influence the relative abstraction of hydrogen atoms by excited benzophenone. Steric effects play a clear role in the hydrogen abstraction preferences of **16**; the protons of compound **16** have comparable bond dissociation energies within 2.5 kcal/mol, however the *tert*-butyl hydrogens ( $H_b$ ) were abstracted

nearly twice as much as the methyl ester hydrogens ( $H_a$ ) (Table 4.5). This implies that peripheral protons that can freely sample the solvent volume around a molecule are more likely to be accessed by excited benzophenone. Hydrogens hidden in the interiors of molecules are less accessible, and therefore are abstracted less often despite having similar bond dissociation energies.

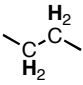
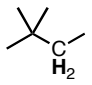
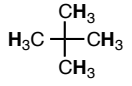
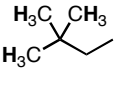
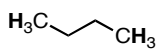
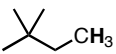
Contributions from polar or charge transfer effects on the linear transition state of the approaching radical must also be considered.<sup>7</sup> In cases where an alkyl C-H bond is to be broken, the polar diradical is neither stabilized nor destabilized during the transition state according to the resonance structure shown in Figure 4.8, and little polar effects would be expected. In other cases, a polar group – e.g. ester or amide – may direct the incoming radical toward particular positions on the structure; chlorine radicals are directed to the  $\beta$  position of propionic acid whereas non-polar alkyl and phenyl radicals are directed to the  $\alpha$  position. In compound **13**, the ester directs the incoming benzophenone radicals to the  $\omega$  position ( $H_c$ , 6 position for **13**) next to the ethereal oxygen of the ester. Reaction at that position is nearly five times greater than reaction at the  $\alpha$  position ( $H_a$ ) or the  $\beta$ - $\delta$  positions (collectively  $H_b$ ). Amides seem to instead direct equally to the  $\alpha$  and  $\omega$  positions, as shown for compounds **11** and **12**.

**Table 4.5.** Compounds with representative bond dissociation energies for the protons of **16**, the relation of each representative bond to **16**, and the competitive rate value of  $k/k_a$  scaled for the number of protons.

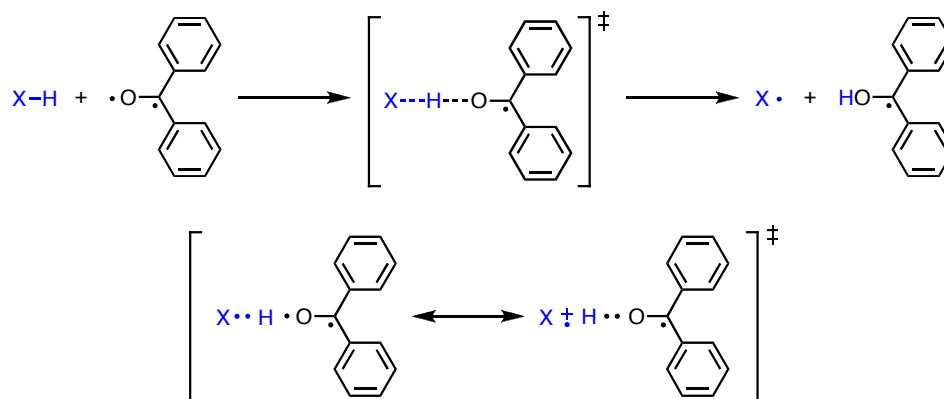
Representative compound	X-H BDE (kcal/mol)	Relation to <b>16</b>	$k/k_a$
acetic acid methyl ester 	96.7 <sup>a</sup>	 H <sub>a</sub>	1
2,2-dimethylpropanoic acid 	99.2 <sup>a</sup>	 H <sub>b</sub>	2.22

Methods for determination of bond dissociation energies: <sup>a</sup>Correlation.

**Table 4.6.** Compounds with representative bond dissociation energies for the protons of **17**, the relation of each representative bond to **17**, and the competitive rate value of  $k/k_a$  scaled for the number of protons.

Representative compound	X-H BDE (kcal/mol)	Relation to <b>17</b>	$k/k_a$
butane 	99.1±0.4 <sup>n</sup> 98.3±0.5 <sup>o</sup> 98.6±0.5 <sup>m</sup> 98.3±0.5 <sup>n</sup> 97.4±1.0 <sup>h</sup>	 H <sub>b</sub>	1
neopentane 	99.4±1 <sup>b</sup> 100.3±1 <sup>c</sup> 99.4±1 <sup>h</sup> 101.0±2 <sup>m</sup> 101.1 <sup>q</sup>	 H <sub>a</sub>	0.38
butane 	101±2 <sup>i</sup> 100.2 <sup>p</sup> 100.7 <sup>h</sup> 101.7±0.5 <sup>n</sup>	 H <sub>c</sub>	

Methods for determination of bond dissociation energies: <sup>n</sup>Photoionization mass spectrometry. <sup>o</sup>Resonance fluorescence detection. <sup>m</sup>Review. <sup>h</sup>Single-pulse shock tube technique. <sup>b</sup>Polanyi correlation. <sup>c</sup>Kinetics. <sup>q</sup>Laser flash photolysis. <sup>i</sup>Electron impact. <sup>p</sup>Appearance energy measurements



**Figure 4.8.** Resonance structure (bottom) showing possible polar effects during the transition state (top) of hydrogen abstraction from X-H by triplet benzophenone.

#### 4.4. Hydrogen Abstraction from Proteins, Polymers

A predictive framework for the differences in proton reactivity toward hydrogen abstraction by benzophenone identified by  $^1\text{H}$  NMR are cannot be based solely on differences in bond dissociation energies when the X-H bonds are below the threshold for abstraction. Since most of the X-H bond dissociation energies fall in a similar thermodynamic range, factors that influence the kinetics of the reaction likely dominate these hydrogen abstraction reactions. Sterics of sidechains and polymer backbones, solvent accessibility, backbone flexibility, radical stability, hydrogen bonding pre-reactive complexation, and polar effects will therefore likely place an increased role in determining abstraction preferences when these reactions occur in thin polymer films as opposed to in solution. Additionally, protons may be more or less accessible, mobile, and susceptible to attack by excited benzophenone depending on whether the polymer is in a melt or glassy state.

While this is the first study of these interactions using model compounds representative of synthetic polymers, other studies have found similar results when

examining model compounds representative of biopolymers. A series of amino acids with aliphatic and carboxylic- or ammonium-functional side chains was subjected to hydrogen abstraction by chlorine photolyzed in trifluoroacetic acid.<sup>22</sup> As expected, it was found that the rate of abstraction of tertiary hydrogens (CH) was greater than the rate of abstraction from methylene hydrogens (CH<sub>2</sub>), which in turn was greater than the reactivity of methyl hydrogens (CH<sub>3</sub>). Unexpectedly, however, the rate of abstraction was found to be greater for hydrogens farther away from the amino acid backbone. This effect was attributed to the repulsion of an incoming radical by the carboxyl and cationic amino functionalities in the small molecules, and was extrapolated to represent the effect of the amido linkage in the polyamide backbone upon hydrogen abstraction from proteins.<sup>7</sup>

A computational examination of hydrogen abstraction from amino acids stressed the various kinetic factors that contribute to radical preferences.<sup>23</sup> Pre-reactive complexation of a hydroxyl radical with amino and carbonyl groups, solvent accessibility, and the diminished role of bond dissociation energies are all considered to contribute to the preferences of a hydrogen abstracting radical. The authors also hypothesize that the increased reactivity of hydrogens farther from the amino acid backbone is due to the greater flexibility of those sidechains relative to the more rigid backbone.

The polymers considered in this study (Table 4.1) fall into two categories: those with aliphatic backbones, and those with amido- and ester-functional backbones. Based on the amino acid work described above, we would expect a number of differences between the model compounds studied and their polymeric counterparts. First, the model

compounds **11-13** retain the functionality that ultimately is present in the backbone of the polymer whereas the amino acids bear charged endgroups that do not accurately represent the protein amido linkages. Since the amido and ester groups of compounds **11-13** are isoelectronic with their representative polymers, we would expect no difference between the roles played by the amide and ester in **11-13** and their role in the parent polymers. For the remaining model compounds that represent polymers with aliphatic backbones, we would expect no difference from electronic effects since neither the model compound nor the polymer backbone is charged.

For the polymers represented by compounds **11-13**, where direction by amide and ester linkages may still occur, we might expect the hydrogens next to the linkages to be most readily abstracted if any effect at all is observed in the polymer. The absence of electronic diversity in the aliphatic backbones of the synthetic polymers represented by model compounds **14-19** should obviate the charge transfer effects and distance-dependent effects observed in proteins. We would not expect to observe an increased rate of hydrogen abstraction for sidechain hydrogens farther from the polymer backbone because of repulsive effects from aliphatic backbone.

We might, however, expect that effect to result from the difference in rigidity between the sidechains and the polymer backbone. The model compounds **11-19** lack distinct regions of rigidity that would be present in the polymers they represent. The sections of the model compounds that represent the backbone of the parent polymers are not restricted in any way, and therefore do not accurately account for how a polymer sidechain may sample space relative to the backbone. Although the bond energies of the model compounds may be analogous to those found in polymers, the motion,

accessibility, and shape of a polymer chain is not well represented by the model compounds.

#### 4.5. Experimental

Benzophenone (Acros Organics), caprolactam (Sigma Aldrich, **11**), methylcaprolactam (Sigma Aldrich, **12**),  $\epsilon$ -caprolactone (Sigma Aldrich, **13**), *sec*-butylbenzene (Alfa Aesar, **14**), ethylbenzene (Sigma Aldrich, **15**), methyl trimethylacetate (Sigma Aldrich, **16**), 2,2-dimethylbutane (Sigma Aldrich, **17**), trans-3-hexene (Sigma Aldrich, **18**), butyl isovelerate (SAFC, **19**) and CD<sub>3</sub>CN (Cambridge Isotopes & Acros Organics) were used as received. Solutions were irradiated in a Rayonet reactor (16 lamps, ~4.5 W each, The Southern New England Ultraviolet Company) at 350 nm. <sup>1</sup>H NMR spectra were recorded on a Bruker Spectrospin 300 MHz spectrometer.

Benzophenone (approx. 4 mg) was dissolved in 6 mL of an approximately 90 mM solution of model compound (**11-19**) in CD<sub>3</sub>CN. The solution was transferred to a quartz tube capable of being inserted into a standard NMR tube, and inert gas was bubbled through the solution for 5 minutes to remove oxygen. The quartz tube was sealed with a cap and Parafilm, placed into a standard NMR tube, and a <sup>1</sup>H NMR spectrum was recorded. The quartz tube was irradiated at 350 nm for up to 3 hours; periodically during irradiation the quartz tube was removed from the reactor, reinserted into the NMR tube and a <sup>1</sup>H NMR spectra was recorded. NMR spectra were processed using MestreNova.

## 4.6. Summary

- Model compounds were selected to represent common synthetic polymers.
- Model compounds were subjected to irradiation in the presence of benzophenone, a well-behaved hydrogen abstractor, as a model for hydrogen abstraction in polymers.
- $^1\text{H}$  NMR was used to monitor the hydrogen abstraction process, and competitive rate constants were calculated from exponential fits of the decreasing integrals of proton resonances.
- Differences in bond dissociation energy are not enough to explain the preference of benzophenone to abstract particular hydrogens since the bond dissociation energy of most X-H bonds falls within several kcal/mol.
- Pre-reactive complexation, sterics and charge transfer effects influence the abstraction of protons by benzophenone.



## 4.7. References

---

1. Johnson, J. A.; Baskin, J. M.; Bertozzi, C. R.; Koberstein, J. T.; Turro, N. J. Copper-free click chemistry for the in situ crosslinking of photodegradable star polymers. *Chemical Communications* **2008**, 3064-3066.
2. Carroll, G. T.; Sojka, M. E.; Lei, X.; Turro, N. J.; Koberstein, J. T. Photoactive additives for cross-linking polymer films: Inhibition of dewetting in thin polymer films. *Langmuir* **2006**, *22*, 7748-7754.
3. von Raumer, M.; Suppan, P.; Haselbach, E. Photoreduction of triplet benzophenone by amines: role of their structure. *Chemical Physics Letters* **1996**, *252*, 263-266.
4. von Raumer, M.; Suppan, P.; Haselbach, E. Photoreduction of Triplet Benzophenone by Tertiary Amines: Amine molecular structure and ketyl radical yield. *Helvetica Chimica Acta* **1997**, *80*, 719-724.
5. Finn, M.; Friedline, R.; Suleman, N. K.; Wohl, C. J.; Tanko, J. M. Chemistry of the t-butoxyl radical: evidence that most hydrogen abstractions from carbon are entropy-controlled. *Journal of the American Chemical Society* **2004**, *126*, 7578-7584.
6. Tanko, J. M.; Friedline, R.; Suleman, N. K.; Castagnoli, N. tert-Butoxyl as a model for radicals in biological systems: caveat emptor. *Journal of the American Chemical Society* **2001**, *123*, 5808-5809.
7. Russell, G. A. In *Free Radicals*; Kochi, J. K., Ed.; Wiley: New York, 1973; pp. 275-331.
8. Turro, N. J. *Modern Molecular Photochemistry*; University Science Books: Sausalito, California, 1991; p. 628.
9. Visanathan, K.; Hoyle, C. E.; Jönsson, E. S.; Nason, C.; Lindgren, K. Effect of Amine Structure on Photoreduction of Hydrogen Abstraction Initiators. *Macromolecules* **2002**, *35*, 7963-7967.
10. Aleman, C.; Domingo, V. M.; Fajari, L.; Julia, L.; Karpfen, A. Molecular and Electronic Structures of Heteroaromatic Oligomers : Model Compounds of Polymers with Quantum-Well Structures. *Journal of Organic Chemistry* **1998**, *63*, 1041-1048.
11. Ashton, P. R.; Huff, J.; Menzer, S.; Parsons, I. W.; Preece, J. A.; Stoddart, J. F.; Tolley, M. S.; White, A. J. P.; Williams, D. J. Bis[2]catenanes and a Bis[2]rotaxane-Model Compounds for Polymers with Mechanically Interlocked Components. *Chemistry - A European Journal* **1996**, *2*, 31-44.
12. Bortolus, P.; Dellonte, S.; Beggiato, G. Interaction between Singlet Oxygen ( $^1\Delta_g$ ) and Model Compounds for Polymers. A Flash Photolytic Study. *European Polymer Journal* **1977**, *13*, 185-188.
13. Allen, N. Photoinduced chemical crosslinking activity and photo-oxidative stability of amine acrylates: photochemical and spectroscopic study. *Polymer Degradation and Stability* **2001**, *73*, 119-139.
14. Mintsá, M. N.; Lecamp, L.; Loutelier-Bourhis, C.; Lange, C. M.; Baumgarten, S.; Bunel, C. Photocrosslinking of a novel  $\alpha,\omega$ -unsaturated copolyamide: mass spectrometric study on model compounds with benzophenone as photoinitiator. *Rapid Communications in Mass Spectrometry* **2009**, *23*, 3813-3823.
15. Montalti, M.; Prodi, L.; Credi, A.; Gandolfi, M. T. *Handbook of Photochemistry*; 3rd ed.; 2006; p. 629.
16. Luo, Y.-R. In *Handbook of bond dissociation energies in organic compounds*; CRC Press LLC, 2003; pp. 163-231.
17. Luo, Y.-R. In *Handbook of bond dissociation energies in organic compounds*; CRC Press LLC, 2003; Vol. 4, pp. 11-93.
18. Luo, Y.-R. In *Handbook of bond dissociation energies in organic compounds*; CRC Press LLC, 2003; pp. 232-270.
19. Tumanov, V. E.; Denisov, E. T. Evaluation of C-H Bond Dissociation Energies in Hydrocarbons and the Enthalpies of the Relevant Radicals from Kinetic Data. *Petroleum Chemistry* **2001**, *41*, 109-118.

- 
20. Kerr, J. A. Bond Dissociation Energies by Kinetic Methods. *Chemical Reviews* **1966**, *66*, 465-500.
  21. van Speybroeck, V.; Marin, G. B.; Waroquier, M. Hydrocarbon bond dissociation enthalpies: from substituted aromatics to large polyaromatics. *ChemPhysChem* **2006**, *7*, 2205-2214.
  22. Watts, Z. I.; Easton, C. J. Peculiar stability of amino acids and peptides from a radical perspective. *Journal of the American Chemical Society* **2009**, *131*, 11323-11325.
  23. Scheiner, S.; Kar, T. Analysis of the reactivities of protein C-H bonds to H atom abstraction by OH radical. *Journal of the American Chemical Society* **2010**, *132*, 16450-16459.

## 5. Complex Architectures Using ‘Click’ Chemistry

(with Dan Margulies, Liang Cao, Ben Dach, Yanir Maidenberg)

The interchangeability of the click systems discussed in Chapter 1 and then later used in Chapter 3 to modify polymer surfaces led us to consider an alternative approach to the synthesis of polymers. Instead of using sequential modification steps to generate a polymeric architecture, we sought access to a wide range of architectures using a set of complementary molecules that could be assembled into various configurations. The ‘toolkit’ of molecules would rely upon the click philosophy to produce well-defined polymeric architectures from a relatively simple set of components. This chapter will detail the ‘toolkit’ approach, and will consider the synthesis of several of the component molecules that comprise the ‘toolkit’. Finally several extensions and variations on the ‘toolkit’ approach are discussed.

### 5.1. Introduction, Motivation

Children’s toys provide a macroscopic analogy to the ‘toolkit’ approach we have developed for the synthesis of complex architectures from a set of simple components (Figure 5.1). Tinkertoys (1910’s) and K’nex (1990’s) both rely upon two classes of component in order to build complex structures: linear rods or linkers, and connectors or junctions. In each case, the linker and the junction are held together with a specific physical interaction; the Tinkertoy rods are cylindrical dowels that precisely fit into a complementary hole in the junction, and K’nex rods have shaped ends that snap into complementary sockets in the junctions. The complementarity of the rods and connectors makes a durable yet reformable junction when constructing a structure using these toys.



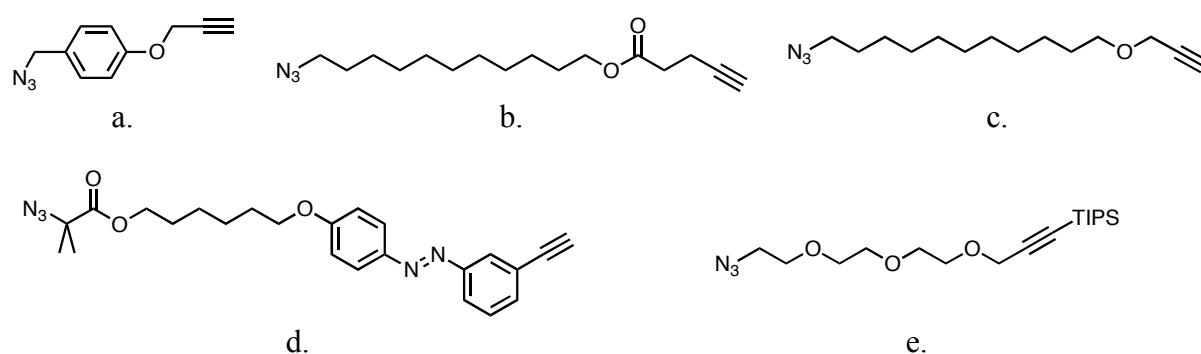
**Figure 5.1.** (a) Tinker toys and (b) K'Nex form complex architectures from simple components.

The same topological properties of the toy linkers and connectors can be applied to molecules for the construction of complex molecular architectures. The  $A_2 + B_3$  approach to hyperbranched polymer synthesis discussed in Chapter 1 involves the reaction of homobifunctional linkers ( $A_2$ ) and homotrifunctional connectors ( $B_3$ ) to generate a material with a network-like architecture.<sup>1,2</sup> The reaction of the A and B functionalities proceeds in an uncontrolled manner in the  $A_2 + B_3$  approach, and has led us to seek molecular components with which we can take a more controlled, sequential approach to addition.

We have developed our ‘toolkit’ methodology using heterofunctional molecules instead of the homofunctional molecules of the  $A_2 + B_3$  approach. Heterofunctionality lends a greater level of control over the assembly of a structure, and can also act as a built-in limitation to the extent of reaction for the molecules. By limiting the growth of a

structure at each step, it will be possible to introduce particular functionalities at predetermined positions in the overall architecture simply by controlling the order in which components are assembled. Libraries of similar molecules can then be constructed because small variations in structure will be based on variations to the order in which components are added. Since the properties of materials are determined by their structures, it will be possible to screen libraries of new materials for novel properties.

The set of heterofunctional molecules comprising the toolbox will be centered around the complementary azide and alkyne click moieties discussed in Section 1.2.1. The azide and alkyne react in the presence of Cu(I), Ru(II), and at elevated temperatures, are orthogonal to most other functionalities, and react in a very high yield.<sup>3,4</sup> Most importantly for the purposes of the toolkit components, both the azide and alkyne are synthetically straightforward to install and they are deprotected or activated through simple chemistry.<sup>5,6</sup> Figure 5.2a-d are several unprotected heterobifunctional azide-alkyne monomers that have been used for CuAAC polymerization.<sup>1,7,8</sup> These molecules are topologically similar to the linear rods in the toys described above. Each molecule is terminated on one end by an azide and one end by an alkyne, so linkages between these molecules will only occur at the predetermined locations as a result of the azide-alkyne cycloaddition. Protected variations of the heterobifunctional molecules provide more control over growth by capping one of the two end functionalities with a deactivating protecting group (Figure 5.2e).<sup>9,10</sup> Growth of an architecture stops after a single protected component adds to each available functional end. Greater control is retained over the final architecture because the capped ends must be deprotected or activated in order for growth to continue.



**Figure 5.2.** Several  $\alpha$ -azide- $\omega$ -alkyne heterobifunctional monomers.

The portion of the molecule connecting the azide and the alkyne can have a wide range of properties, compositions, lengths, and internal chemical functionalities. This versatility is shown in Figure 5.2 where molecules containing the same endgroups variously bear an internal aromatic ring, alkyl chain, ester, ether, azobenzene<sup>11</sup>, or polyether chain<sup>9</sup>. Since each component can be synthesized and characterized individually, it will be possible to develop a large set of similar molecules that can be combined in various ways to generate well-defined novel architectures. Though construction is based solely on the reaction of the azide and alkyne moieties, the properties of the final construct will likely be determined not by the linkages, but by the internal properties of the components themselves.<sup>12</sup>

Since the endgroups determine whether components can react with each other, this approach accommodates a wide array of building block functionalities, including small organic molecules, synthetic macromolecules, biological monomers – carbohydrates, amino acids, nucleotides – and natural biopolymers. Just as the sequence of natural polymers determines their function, the ability to reliably assemble combined synthetic and natural monomers and polymers in particular sequences may lead to control over secondary structure, function, and interactions with an environment. Furthermore,

control over points of branching and end group functionalities will lead to a remarkable degree of control over the complexity of the macromolecular structures that can be assembled using this strategy.

### 5.1.1. Dendrimer Synthesis

Dendrimers represent a complex polymer architecture for which the ‘toolkit’ approach is particularly useful, although branching is also necessary when constructing comb, brush, star, and hyperbranched polymer networks. Dendrimer synthesis necessitates a high level of molecular control in order to form a maximally branched architecture composed of a well-defined core and the most possible end groups.<sup>13</sup> In contrast, similar hyperbranched systems are less well-defined, having architectures that result from statistical control.<sup>14</sup> The ‘toolkit’ approach is advantageous because of the ease with which it introduces branching, forms hybrid materials, can control endgroup functionality, and is able to incorporate multiple different materials and functionalities into a single macromolecule. If branching can be introduced at positions within the architecture with a high degree of control, a wide range of forms will be generated that go beyond the current state of dendrimer synthesis.

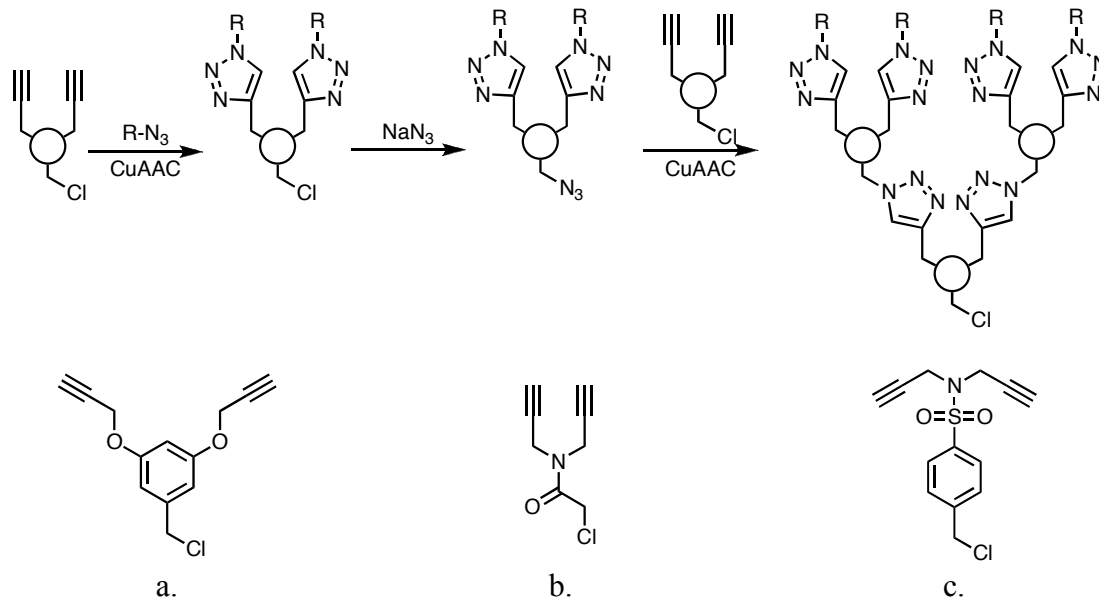
Since their discovery by Tomalia and Fréchet, dendrimers and dendrimeric materials have found application to fields as diverse as biomedicine, drug delivery, diagnostics, sensing, filtration, energy production, energy storage, catalysis, and coatings.<sup>15-19</sup> Organic dendrimers are either grown outward from the periphery of a small organic multi-functional core via a divergent synthetic approach, or their foci are joined together via a convergent synthetic approach.<sup>20</sup> Dendrons – dendrimeric wedge-shaped

molecules – can also be assembled independently or can be grown from flat or nanoparticle surfaces.<sup>21,22</sup> The number of generations to which each dendrimer can grow is limited by the steric interactions between parts of the growing molecule. Dendrimer growth cannot continue indefinitely because exponentially increasing numbers of end groups fold in on themselves, or dendrons become too bulky to couple together at their foci. These steric limitations also affect the range of potential molecular weights and sizes of dendrimeric materials.

### 5.1.2. Dendrimers by Click: CuAAC and Thiol-Ene

The click philosophy has been widely used in dendrimer synthesis because high chemical yields are crucial to well-defined growth.<sup>6,23-25</sup> CuAAC and thiol-ene chemistries in particular have been used to form the linkages between generations of a growing dendrimer, as well as to functionalize the periphery of a preformed dendrimer.<sup>26-33</sup> Figure 5.3 shows the convergent synthesis of a generic dendron using a reaction-activation strategy: CuAAC of a terminal alkyne with two azide-functional analytes is followed by activation of the chloride to an azide.<sup>27</sup> Subsequent cycles of reaction with a difunctional alkyne and activation of its chloride to azide yields a dendron having the initial azide-functionality at its periphery that always bears a chloride or azide at its focus. The chemical orthogonality of CuAAC and thiol-ene chemistry to each other and to other functional moieties has been leveraged to build dendrimers in conjunction with several other chemistries, including amine-carboxylic acid coupling<sup>34</sup>, halogen-carboxylic acid esterification<sup>35</sup>, alcohol-anhydride esterification<sup>36</sup>, acetal-protected diols<sup>37</sup>, and Diels-Alder cycloaddition between maleimide and furan<sup>38,39</sup>.





**Figure 5.3.** Generic convergent dendron synthesis by CuAAC using the bis-alkyne chlorides (a-c).

Architecturally, CuAAC has been used to add dendron arms to a functional core, to add terminating functionality to peripheral CuAAC moieties, and to install functionality within the internal cavity of the dendrimer. Cores with a wide range of chemical composition have been functionalized by CuAAC, including octa-azide-functional polyhedral oligomeric silsesquioxane (POSS)<sup>40</sup>, octa-alkyne-functional phthalocyanines<sup>41</sup>, and tri-alkyne-functional triazine<sup>42</sup>. Peripheral azides and alkynes at the termini of dendrimer arms, meanwhile, have been linked to a wide range of functionalities, including PEG<sup>43</sup>, ferrocene<sup>44</sup>, sugars<sup>45</sup>, and hydrocarbons such as adamantane, alkyl chains, anthracene, and many others.<sup>28</sup> Instead of reacting the peripheral CuAAC moieties with functional small molecules, dendritic polymer nanoparticles bearing peripheral azides or alkynes have been assembled with each other into membranes containing thinner film layers than comparable linear analogues.<sup>46</sup>

Internal functionalization of dendritic architectures has been accomplished by the incorporation of chemically orthogonal functionalities during dendrimer growth. Examples of incorporated functionalities include the Diels-Alder adduct between maleimide and furan<sup>38,39</sup>, an acid-degradable 1,3,5-triazaadamantane<sup>25</sup>, and the residual alcohol resulting from the opening of an epoxide<sup>33</sup>. In the case of the Diels-Alder adduct and the 1,3,5-triazaadamantane, degradation of the dendrimer proceeds by heating or treatment with acid, respectively, while the residual internal alcohol acts as a handle for post-polymerization functionalization by reaction with an acid chloride, for example.

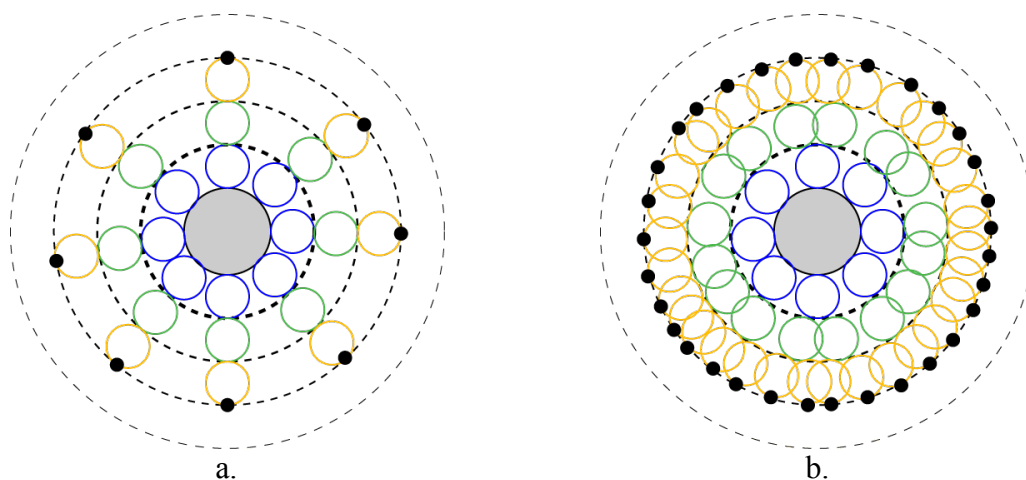
### 5.1.3. Dendron Brushes

In addition to the growth of dendrimers in solution, a parallel goal for the use of the ‘toolkit’ components described below is to grow dendron brushes from surfaces.<sup>47</sup> The controlled introduction of branching in a polymer brush will be crucial to controlling surface properties, whether the surface is macroscopically flat (e.g. a glass slide) or nanoscopically curved (e.g. a nanoparticle).

The number of brushes initially attached to a surface limits the number of linear brushes that can be grown from any surface. For flat surfaces this limitation is generally not detrimental to surface properties because the density of brushes can remain constant at distances normal to the surface. For curved surfaces, however, the radial density of linear brushes decreases by  $1/r^2$  at a given distance,  $r$ , from the center of the particle.<sup>48-51</sup> Figure 5.4 represents the benefit of branching for the growth of polymer brushes from a curved surface where each solid circle represents the sphere of space occupied by a polymer.<sup>52,53</sup> When grown linearly, the maximum number of chain ends,  $N$ , remains

constant throughout every generation,  $g$ . Introduction of a branch point that doubles the number of growing chain ends after each generation raises the total number of peripheral chain ends to  $N(2)^{g-1}$ , which will fill radial space more effectively.

A combination of the two extremes – all-linear or all-branched – will lead toward the ability to control the radial density of brushes grown from a nanoparticle by controlling the sequence in which components are bonded together.<sup>54</sup> For example, addition of several linear generations followed by several branching generations would create a structure with a low interior radial density and a high exterior radial density. A structure like this would be expected to be an effective drug delivery vehicle because it would possess a large interior payload for cargo and a dense exterior shell for *in vivo* stealth. Currently, we know of no other way to construct such a complex molecular architecture. Furthermore, each generation added to the brush can be a different small molecule or polymer; since the ‘toolkit’ employs the same end-functional connections regardless of the chemical properties linking the ends, a structure could be grown with a hydrophobic core (e.g. PS) and increasingly hydrophilic layers toward the periphery (e.g. PMMA-PAA-PEG).



**Figure 5.4.** Cartoons of brush growth (a) linearly and (b) including branching.

The high number of reactive end groups grown on a functionalized nanoparticle has already led to the creation of matrix-free nanoparticle composites.<sup>55</sup> Each nanoparticle may be functionalized with hundreds of reactive end groups and must make only three connections to other nanoparticles in order to reach its gel point (< 3%). In contrast, many small organic molecules may have only four peripheral functional groups, but gelation would still occur when three of the four (75%) had reacted. Materials with higher numbers of functional end groups, therefore, will gel at lower percent conversions than materials with fewer functional end groups. As shown in Figure 5.4, branching facilitates a rapid increase in the number of functional end groups, and therefore ought to further decrease the percentage of end groups that must react for gelation to occur. The lower percentage conversion necessary for gelation will also cause gelation to occur much more quickly than for an organic small molecule with fewer functional end groups. High numbers of reactive ends are not readily installed via radical polymerizations such as ATRP, however, because the likelihood of termination increases with the number of chain ends.

## 5.2. Preparation and Analysis of Toolkit Compounds

Care must be taken when designing molecules for use in the ‘toolkit’ beyond the simple chemical question of how to incorporate heterobifunctionality. Characterization of complex architectures is non-trivial, especially when that structure is attached to a substrate.<sup>56,57</sup> In designing the branching unit, **21**, below, a structure with aromatic protons was chosen such that <sup>1</sup>H NMR downfield resonances from the aromatic protons would be well separated from the upfield alkyl resonances. Since many of the polymers

we planned to use in the ‘toolkit’ do not have aromatic protons (PtBA, PAA, PMMA, PEG, etc.), we could be sure that branches are incorporating by changes in the aromatic region, and we could also determine the incorporation efficiency by comparing the  $^1\text{H}$  NMR spectrum to mass spectra. For polymers with aromatic protons (e.g. PS), we designed a fluorinated variation of the toolkit that is described below as a possible future extension to this approach (Section 5.4.3).

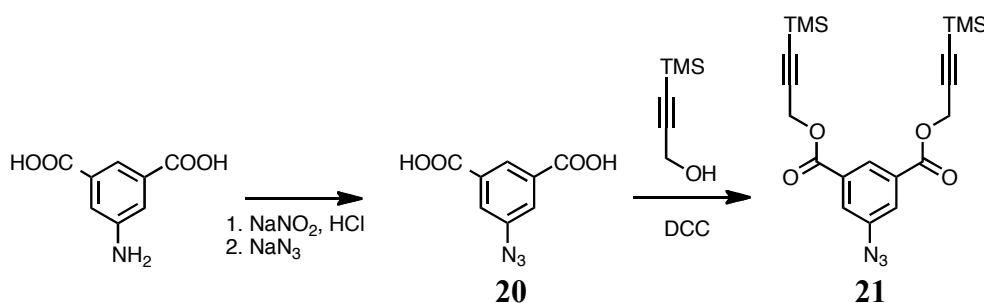
Construction of poly(triazole) architectures can also be monitored by changes in the alkynyl/triazolic proton resonance in the  $^1\text{H}$  NMR spectrum. The periphery of a growing architecture in this scheme is composed of alkynyl protons ( $\delta \sim 2.5$  ppm) which, upon azide-alkyne cycloaddition, shift far downfield ( $\delta \sim 7.75$  ppm) as a result of the aromaticity of the triazole. Comparison of the integrals at those resonances will determine the efficacy of the coupling reaction.

In addition to the branching unit, **21**, several other molecules were designed as both functional components and to aid in the characterization of the complex architectures. Compound **23** is included as an exemplar photofunctionalizing terminator molecule; addition of **23** to the periphery of a small or large molecule will imbue it with photografting capabilities as discussed in Chapters 2, 3, and 4. Compound **24** was synthesized as an exemplar reporter molecule. As discussed in Chapter 2, fluorescence measurements have been to monitor the dynamics of a pyrene guest in a number of different environments; the pyrenyl terminator **24** could be added to the periphery of a complex architecture in order to study the movement, complexation, and density of functional end groups. Compound **25** was designed to be a photodegradable ‘toolkit’ component where inclusion at pre-determined positions followed by irradiation would

enable the release of dendrons from a dendrimer core, the release of drugs from a network, or the severing of nanoparticles from a surface.<sup>58</sup> The utility of each ‘toolkit’ component is derived from the chemical functionality in between the terminal azide and TMS-protected alkyne(s).

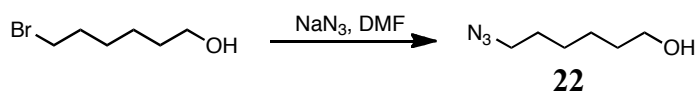
### 5.2.1. Small Molecules Synthesis

The preparation of the heterotrifunctional branching unit, **21**, began with the diazotization of 5-aminoisophthalic acid in hydrochloric acid by sodium nitrite (Figure 5.5). Addition of sodium azide yielded 5-azidoisophthalic acid, **20**, as a white powder.<sup>59,60</sup> DCC coupling of **20** with two equivalents of 3-(trimethylsilyl)-2-propyn-1-ol followed by column chromatography yielded **21** as a brown oil.<sup>61</sup> Care was taken to avoid longterm light exposure to **20** and **21** since the phenyl azide may dissociate via the nitrene mechanism discussed in Section 2.2.<sup>62</sup> In addition to their intended use here as a CuAAC branching unit, **20** and **21** could also be used as photoaffinity labels to imbue a biomolecule with two carboxylic acids or two protected alkyne handles for subsequent reaction.<sup>63-65</sup> Deactivating protection of the alkynes is necessary because AB<sub>2</sub> molecules with an internal alkyne and terminal azides have been shown to form hyperbranched polymers near room temperature.<sup>66</sup>

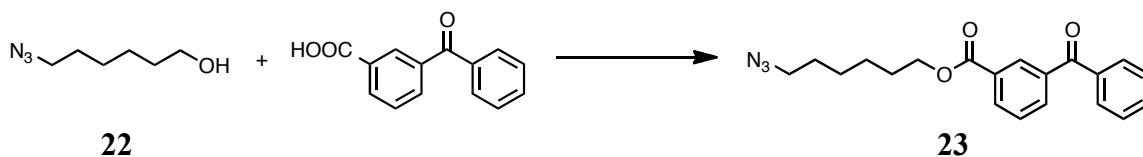


**Figure 5.5.** Synthetic scheme of the CuAAC ‘click’ functional branch point, **21**.

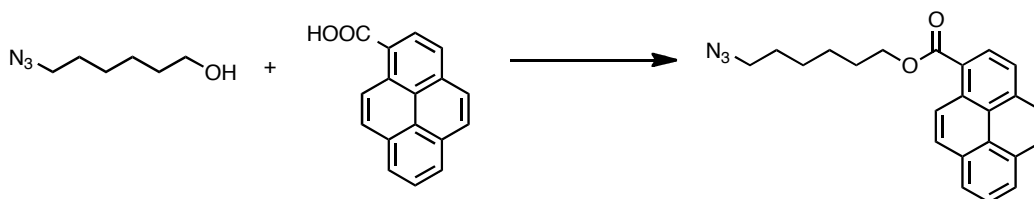
6-Azidohexanol, **22**, was prepared by stirring 6-bromohexanol with excess sodium azide in N,N-dimethylformamide overnight under nitrogen (Figure 5.6).<sup>67</sup> Aqueous workup removed remaining sodium azide to yield **22**, which was then used as an azide-functional handle for reaction with several carboxylic acid-functional moieties. DCC coupling of **22** with 3-benzoylbenzoic acid or pyrene-1-carboxylic acid yielded azide-functional benzophenone, **23**, and azide-functional pyrene, **24**, terminators, respectively (Figure 5.7, Figure 5.8).<sup>68,69</sup> Other carboxylic acid functional photoactive moieties such as those in Figure 5.9 and other carboxylic acid functional reporter molecules such as those in Figure 5.10 could be similarly azide functionalized via DCC coupling with **22**. The CuAAC reaction of a homobifunctional  $\alpha,\omega$ -bisalkyne polymer with any of these azide-functional molecules would yield a  $\alpha,\omega$ -homobifunctional polymer bearing endgroups terminated by the small molecule. Following this ‘toolkit’ approach, libraries of the same polymer with different functional end groups would be readily prepared.



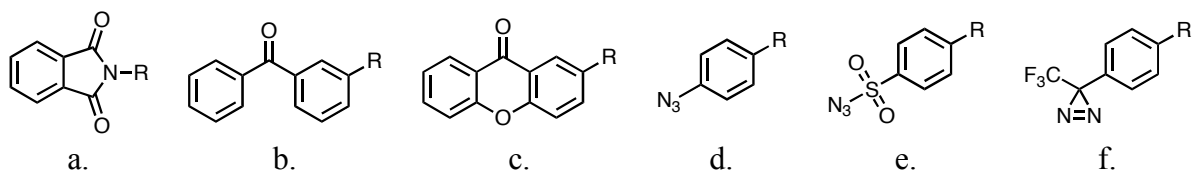
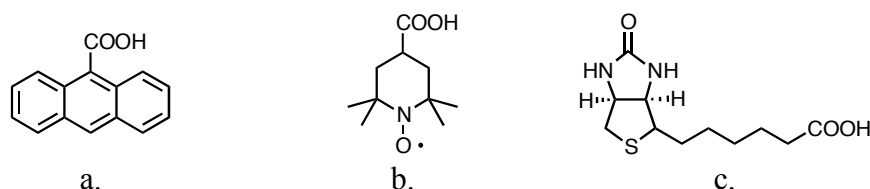
**Figure 5.6.** Synthesis of 6-azidohexanol, **22**.



**Figure 5.7.** Synthesis of 6-azidohexyl 3-benzoylbenzoate, **23**.

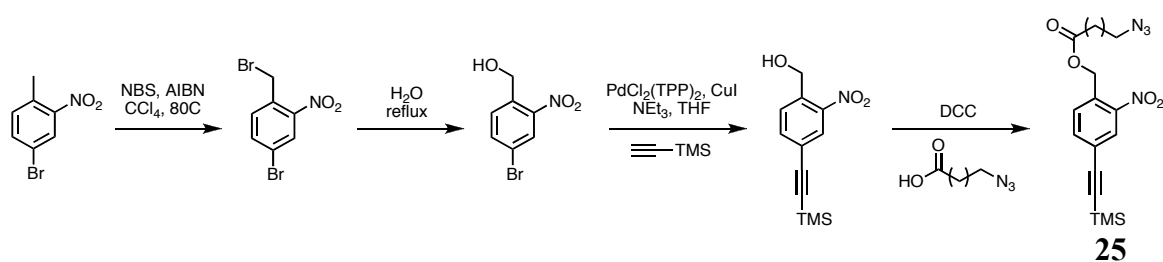


22

**Figure 5.8.** Synthesis of 6-azidohexyl pyrene-1-carboxylate, **24**.**Figure 5.9.** Photoactive moieties: (a) phthalimide; (b) benzophenone; (c) xanthone; (d) phenyl azide; (e) sulfonyl azide; and (f) trifluoromethyl phenyl diazirine.**Figure 5.10.** Other carboxylic acid precursors to ‘reporter’ molecules: (a) anthracene-9-carboxylic acid; (b) TEMPO-carboxylic acid; and (c) biotin-carboxylic acid.

The  $\alpha$ -(TMS-alkyne), $\omega$ -azido heterobifunctional photodegradable CuAAC monomer, **25**, was synthesized according to Figure 5.11.<sup>70</sup> Free radical bromination of 4-bromo-2-nitrotoluene in carbon tetrachloride yielded 4-bromo-1-(bromomethyl)-2-nitrobenzene which was then refluxed in water to yield 4-bromo-1-(hydroxymethyl)-2-nitrobenzene. Sonogashira coupling of 4-bromo-1-(hydroxymethyl)-2-nitrobenzene with 1-trimethylsilylacetylene in triethylamine and tetrahydrofuran yielded 4-(2-(trimethylsilyl)ethynyl)-1-(hydroxymethyl)-2-nitrobenzene. DCC coupling with an  $\alpha$ -azido, $\omega$ -carboxylic acid generated the photodegradable CuAAC monomer, **25**, which bears an ortho-nitrobenzyl (ONB) moiety between the azide and the TMS-protected alkyne. A photodegradable CuAAC-functional monomer such as **25** forms an integral part of the ‘toolkit’ by facilitating the release of surface-bound dendrons, the destruction of a hyperbranched network, or the selective decomposition of complex dendrimers upon irradiation with light.<sup>71-76</sup> Additional uses of the ONB group in polymer architectures are discussed above in Section 1.4.2.





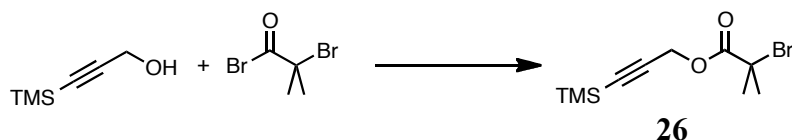
**Figure 5.11.** Synthesis of  $\alpha$ -(TMS-alkyne), $\omega$ -azido heterobifunctional photodegradable CuAAC monomer, **25**.

### 5.2.2. $\alpha$ -(TMS-alkyne), $\omega$ -azide Heterobifunctional Polymers

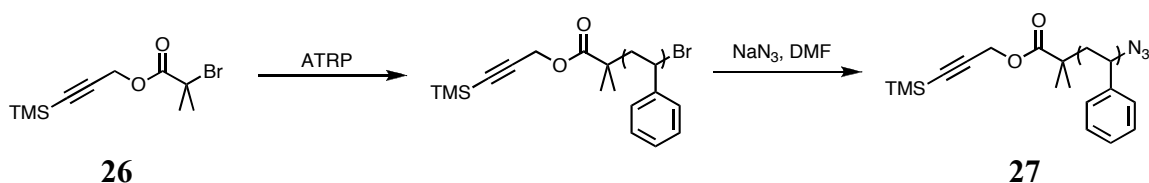
The synthesis of  $\alpha$ -(TMS-alkyne), $\omega$ -azide polymers has been reported elsewhere, and begins with a TMS-alkyne functional ATRP initiator, **26**.<sup>74,77-82</sup> The ATRP initiator is the condensation product of 3-(trimethylsilyl)-2-propyn-1-ol with  $\alpha$ -bromoisobutyryl bromide (Figure 5.12).<sup>74,83</sup> Polymerization proceeds when **26** is subjected to standard ATRP conditions in the presence of a vinyl monomer (e.g. styrene) to form an  $\alpha$ -(TMS-alkyne), $\omega$ -bromide polymer (Figure 5.13).<sup>84</sup> Reaction with sodium azide replaces the terminal bromide to make the desired  $\alpha$ -(TMS-alkyne), $\omega$ -azide polymer, **27**.

$\alpha$ -(TMS-alkyne), $\omega$ -azide polymers have been used for the synthesis of ABC block copolymers via a successive addition-deprotection strategy in solution<sup>77,78</sup> and for polymer brushes grown from a surface<sup>79</sup>. They have also been used to make macrocycles in dilute solution<sup>80</sup>, to generate periodic arrays<sup>81</sup> and to form networks bearing degradable functionalities<sup>82</sup>. In an approach similar to the ‘toolkit’ strategy described below for macromolecules, Urbani, et al, have end-functionalized  $\alpha$ -(TMS-alkyne), $\omega$ -azide polymers with diols for a built-in branching unit to synthesize dendrimeric macromolecules.<sup>74</sup> Although it does not allow for the sequential flexibility of our

approach, the  $\alpha$ -(TMS-alkyne), $\omega$ -diol polymers were shown to degrade at the ester linkages via reaction with sodium methoxide.



**Figure 5.12.** Synthesis of 3-(trimethylsilyl)prop-2-yn-1-yl 2-bromo-2-methylpropanoate, **26**.



**Figure 5.13.** Atom transfer radical polymerization (ATRP) of styrene and subsequent reaction with sodium azide to yield  $\alpha,\omega$ -heterobifunctional polystyrene, **27**.

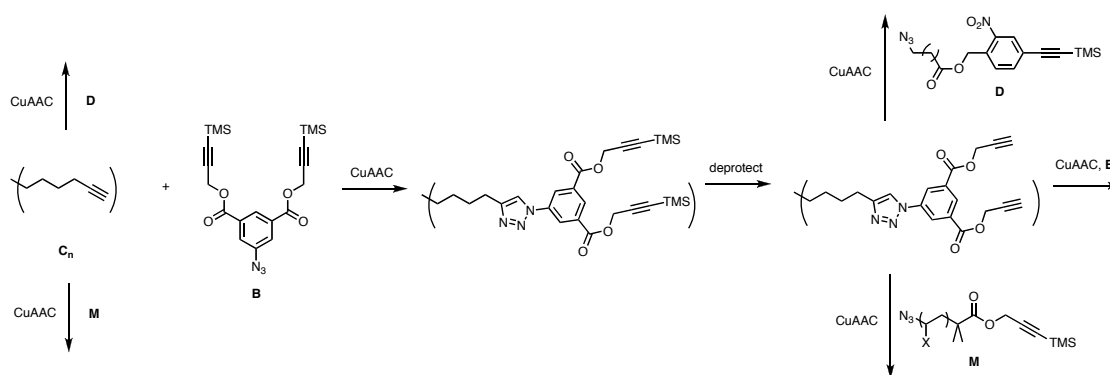
### 5.3. Construction of Dendrimacromers

The possibilities for the construction of the complex architectures become clear with the preliminary set of ‘toolkit’ molecules in hand. Typically, a dendrimeric macromolecule can be assembled in either a divergent or convergent approach, and selection of an appropriate scheme depends largely on the chemical functionalities used to build the structure. All of the heterofunctional molecules that will be used to construct the interior portions of the macromolecules bear azides and protected alkynes, so growth must proceed by linking together an azide to a free alkyne, then deprotecting the alkyne before it can react with another azide.<sup>85</sup> Classifying the approach used here as convergent or divergent is not straightforward, however, because it is simultaneously both depending on the focus of interest. If the focus is on the growing macromolecule, then additional components are added divergently to the periphery, but if focus is placed on the addition of macromonomers such as **27** to the multifunctional core, then the

synthesis could be considered convergent. Regardless of its particular classification, the approach brings together for the first time small molecules, e.g. **21**, and macromonomers, e.g. **27**, to generate macromolecules with high molecular weights determined largely by the molecular weights of the macromonomers used for construction.

To distinguish dendrimers built from small molecules *and* macromonomers from conventionally assembled dendrimers built only from small molecules (e.g. < 600 Da), we have termed this class of molecule dendrimacromers: a branched structure (*dendri-*) build from large (*-macro-*) subunits (*-mers*). In addition to the new possibilities for architectures discussed below, there is a need to redefine the notion of ‘generation’ in dendrimer synthesis. Traditionally a generation has been defined by an increase in the number of functional ends dependent upon the functionality of the branch points used to build the dendrimer. Here, instead, we will loosely define generations by the addition of a ‘toolkit’ component via a triazole linkage. Simplifying the notion of ‘generation’, however, discards some information about the dendrimacromer structure because each generation could be comprised of one or more ‘toolkit’ components.



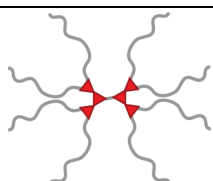
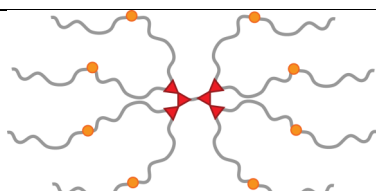
In order to further generalize the discussion below, **B** will refer to branching molecules such as **21**, **M** will refer to macromonomers such as **27**, and **D** will refer to degradable components such as **25**. Terminal ‘toolkit’ components, **T**, such as **23** and **24** are not considered since they would be used only at the periphery of the complex architectures.



**Figure 5.14.** Possibilities for dendrimer synthesis from toolkit.

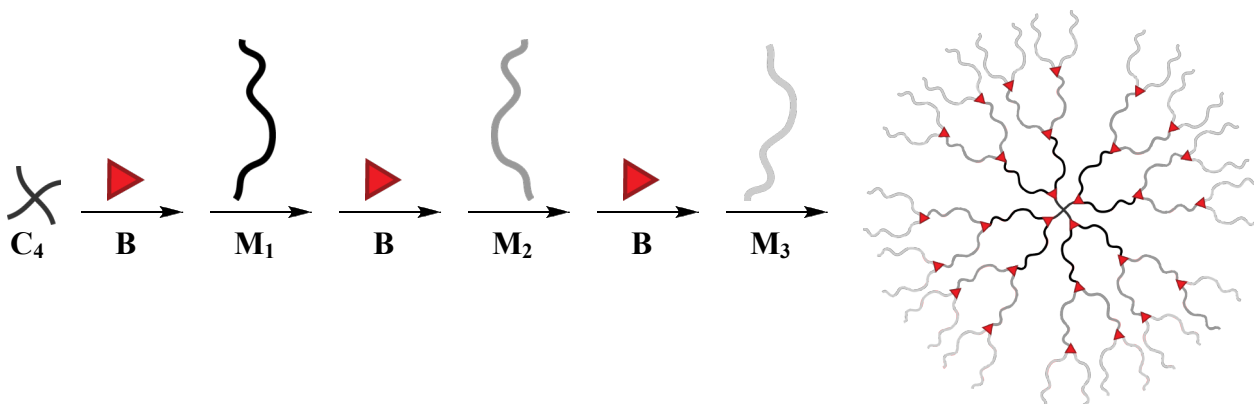
Construction of the dendrimacromer will begin with a multifunctional core,  $C_n$ , where  $n$  is the number of terminal alkynes available for CuAAC.  $n$  can range from 1 for a heterofunctional molecule bearing a single alkyne (e.g. **8**, Section 3.3), to many hundred for a nanoparticle functionalized with alkyne terminal ligands<sup>86</sup> (Section 3.1.1), to many thousand for a high molecular weight polymer bearing pendant alkyne functionalities (Section 1.3.2). As shown in Figure 5.14,  $C_n$  will first react via CuAAC with the branching unit, **B**, a macromonomer, **M**, or a degradable unit, **D**. If  $C_n$  reacts with **B**, the number of TMS-protected alkyne ends will double to  $2n$ , but if  $C_n$  reacts with **M** or **D** the number of TMS-protected alkyne ends will remain the same. The TMS protection limits uncontrolled growth of the dendrimacromer at each step in order to generate a well-defined overall architecture. Deprotection of the TMS groups using potassium carbonate in methylene chloride and methanol regenerates terminal alkynes that are once again available to react with **B**, **M**, or **D** for the addition of a second ‘toolkit’ component.<sup>87</sup> Table 5.1 summarizes the possible architectures made from a bifunctional core ( $C_2$ ), a branch point (**B**) and a macromonomer (**M**) through the fourth cycle of component addition. Each branch point is represented as a red triangle while triazole linkages between linear components are represented as orange circles. If the

**Table 5.1.** First, second, third and fourth ‘generation’ dendrimers from a bifunctional ( $C_2$ ) core with branches ( $B$ ) and macromonomers ( $M$ ).

Generation	Combinations	Examples
First ‘generation’ dendrimers	$C_2B$	 $C_2B$ $C_2M$
	$C_2M$	
Second ‘generation’ dendrimers	$C_2BB$	 $C_2BB$ $C_2BM$ $C_2MB$ $C_2MM$
	$C_2MM$	
	$C_2BBB$	
	$C_2BBM$	
Third ‘generation’ dendrimers	$C_2BMB$	 $C_2BBM$ $C_2BMM$ $C_2MBB$ $C_2MBM$ $C_2MMB$ $C_2MMM$
	$C_2MMB$	
	$C_2MMM$	
	$C_2BBBB$	
	$C_2BBBM$	
	$C_2BBMB$	
	$C_2BBMM$	
	$C_2BMBB$	
$C_2BMBM$		
Fourth ‘generation’ dendrimers	$C_2BMMB$	 $C_2BBMM$ $C_2BMBM$ $C_2MBMM$ $C_2MBBB$ $C_2MBBM$ $C_2MBMB$ $C_2MBMM$ $C_2MMBB$ $C_2MMBM$ $C_2MMMB$ $C_2MMMM$
	$C_2BMMM$	
	$C_2MBBB$	
	$C_2MBBM$	
	$C_2MBMB$	
	$C_2MBMM$	
	$C_2MMBB$	
	$C_2MMBM$	
	$C_2MMMB$	
	$C_2MMMM$	

degradable unit ( $D$ ) were also considered, the number of possible architectures would increase exponentially. In addition to varying the sequence of component addition, diverse libraries of complex dendrimacromers could be generated by varying the functionality of the core, the molecular weight of the macromonomer, or the identity of the macromonomer,  $M_1$ ,  $M_2$ ,  $M_3$ , etc. Figure 5.15 represents a sixth ‘generation’

$C_4BM_1BM_2BM_3$  dendrimacromer composed of different macromonomers at the second, fourth, and sixth component additions.



**Figure 5.15.**  $C_4BM_1BM_2BM_3$  dendrimacromer constructed from multiple macromonomers and a branch unit.

Purification will be challenging at each stage of component addition.

Conventional polymer purification techniques such as precipitation will likely no longer be effective to separate the growing dendrimacromer from unreacted macromonomer, **M**. Instead, nanoparticles or microparticles functionalized with alkynes will be used as scavengers to bind excess ‘toolkit’ components. Centrifugation, filtration, or magnetic separation will remove the particles from solution and leave only the growing dendrimacromer in solution for subsequent cycles of functionalization.

#### 5.4. Outlook and Other Possible Architectures

Detailed below are a few of the possible ways in which the ‘toolkit’ methodology can be used and modified to produce novel architectures. Chief among all of these strategies is that the ‘toolkit’ presents a straightforward way to synthesize materials with very high molecular weights while maintaining a well-defined architecture. High

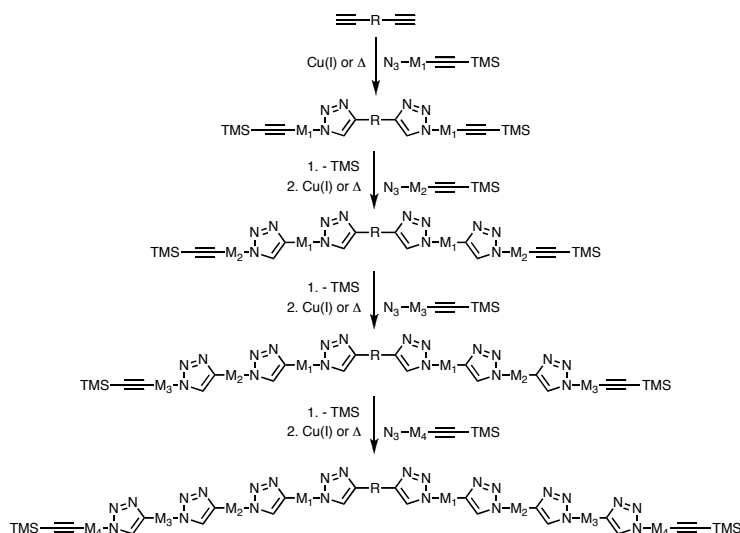
molecular weight macromolecules should generate materials with high fracture energies while their well-defined architectures may imbue the materials with novel properties.<sup>88</sup>

#### 5.4.1. Sequence-Specific Brush and Bottle-Brush Polymers

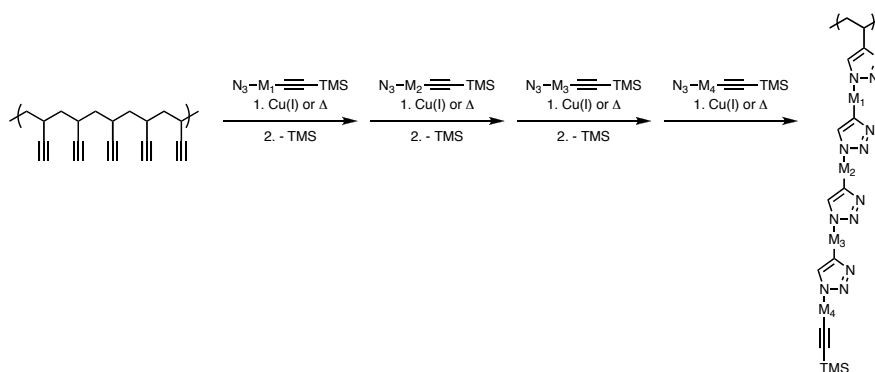
The ‘toolkit’ approach is especially well suited to the creation of polymers with monomers and blocks of monomers aligned in complex arrangements. Sequence-specific polymers are synthetic analogues of biopolymers such as polypeptides, polynucleotides, and polysaccharides in which the sequence of the monomers encodes a material particular properties. Cycles of addition and deprotection can yield polymers with high degrees of complexity, which should be accompanied by the low polydispersities commonly seen in materials made by Merrifield-like solid-phase synthesis.<sup>9,89,90</sup> Regardless of the complexity of an alkyne-functional ‘core’, growth proceeds via cycles of addition of a  $\alpha,\omega$ -heterobifunctional TMS-alkyne-azide monomer followed by deprotection of the TMS group to regenerate a terminal alkyne. The versatility of the method is derived from the variability of the monomer; it can either be a small molecule monomer such as protected variations of those in Figure 5.2, a macromonomer such as **M**, a branched molecule such as **B**, etc.

Versatility is also provided by the diverse selection of possible alkyne ‘cores’ which can be incorporated by this method. A small bifunctional molecule or homobifunctional polymer with terminal alkynes (Figure 5.16), a polymer with pendant alkynes (Figure 5.17), or an alkynated surface (Figure 5.18) can all equally serve as the platform upon which to generate sequence-specific polymers. Furthermore, the number of alkynes on the ‘core’ could range from one on a mono- or heterobifunctional molecule

such as the phthalimide-alkyne, **8**, to many hundreds on an alkyne-functional nanoparticle such as the ones described in Section 1.3.2.

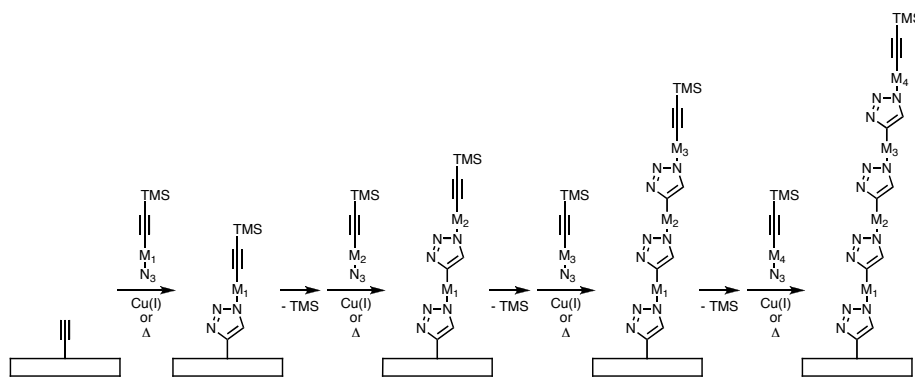


**Figure 5.16.** Monomer-by-monomer growth from a homobifunctional bisalkyne core via sequential addition of  $\alpha,\omega$ -heterobifunctional TMS-alkyne-azide monomer followed by deprotection of the TMS group to regenerate a terminal alkyne.



**Figure 5.17.** Monomer-by-monomer growth from a polymer with pendant alkynes via sequential addition of  $\alpha,\omega$ -heterobifunctional TMS-alkyne-azide monomer followed by deprotection of the TMS group to regenerate a terminal alkyne.



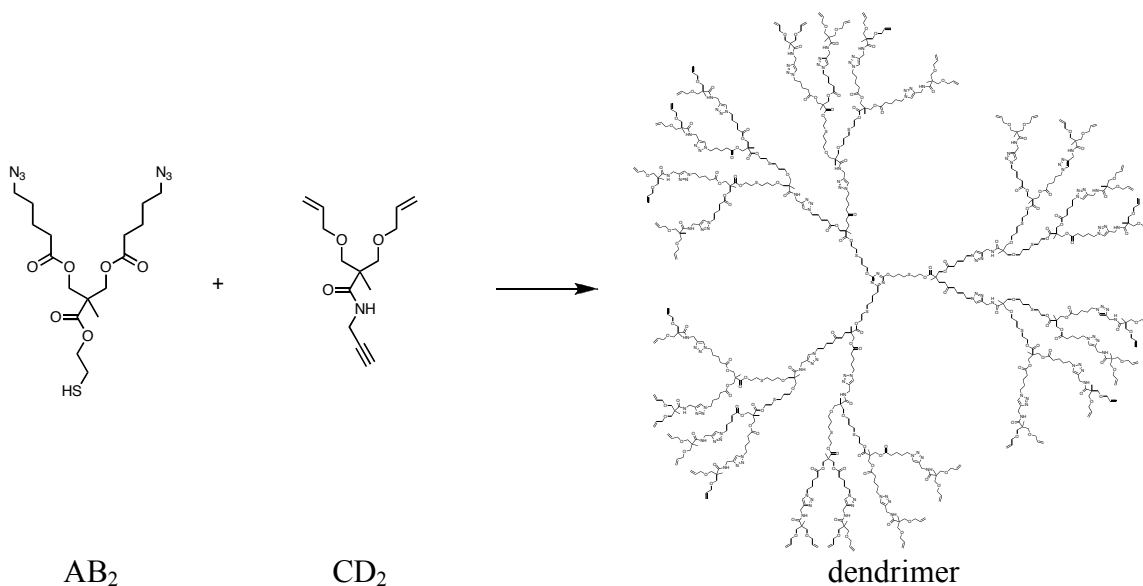


**Figure 5.18.** Monomer-by-monomer growth from an alkyne-functional surface via sequential addition of  $\alpha,\omega$ -heterobifunctional TMS-alkyne-azide monomer followed by deprotection of the TMS group to regenerate a terminal alkyne.

#### 5.4.2. AB-CD<sub>2</sub> and AB-CD Dendrimers

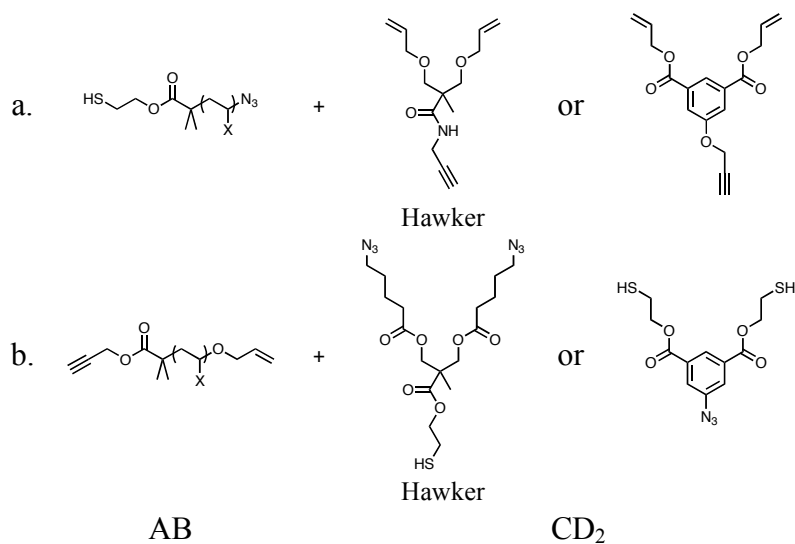
The branch molecule, **B**, and macromonomer, **M**, described above rely upon a protection/deprotection scheme in order to add additional components to a growing architecture. Instead, the orthogonality of different click chemistries can be leveraged to avoid protection/deprotection steps. The Hawker group has employed complementary click functionalities on small molecules to synthesize a six-generation dendrimer in the span of a single day by an AB<sub>2</sub>-CD<sub>2</sub> approach (Figure 5.19).<sup>31</sup> Two low molecular weight branched molecules were prepared, one bearing a thiol for thiol-ene chemistry and two azides for CuAAC, AB<sub>2</sub>, and one bearing an alkyne for CuAAC and two alkenes for thiol-ene, CD<sub>2</sub>. As discussed in Section 1.2, a thiol (A) does not react with an azide (B) and an alkyne (C) does not react with an alkene (D). Thus, the AB<sub>2</sub> and CD<sub>2</sub> molecules do not react with themselves like an alkyne-diazide, AB<sub>2</sub> (Section 5.1.2), but only with the intended complementary moiety on the opposite molecule: A with D, and B with C. Beginning with a poly-ene core, growth proceeds by the alternate addition of the thiol-diazide, AB<sub>2</sub>, by thiol-ene chemistry followed by the addition of the alkyn-diene, CD<sub>2</sub>, by CuAAC. Dendrimers have also been grown by other orthogonal AB<sub>2</sub>-CD<sub>2</sub> systems such

as CuAAC and Diels-Alder where a maleimide connected to two alkynes ( $AB_2$ ) is sequentially coupled to an azide connected to two furans ( $CD_2$ ).<sup>38</sup>

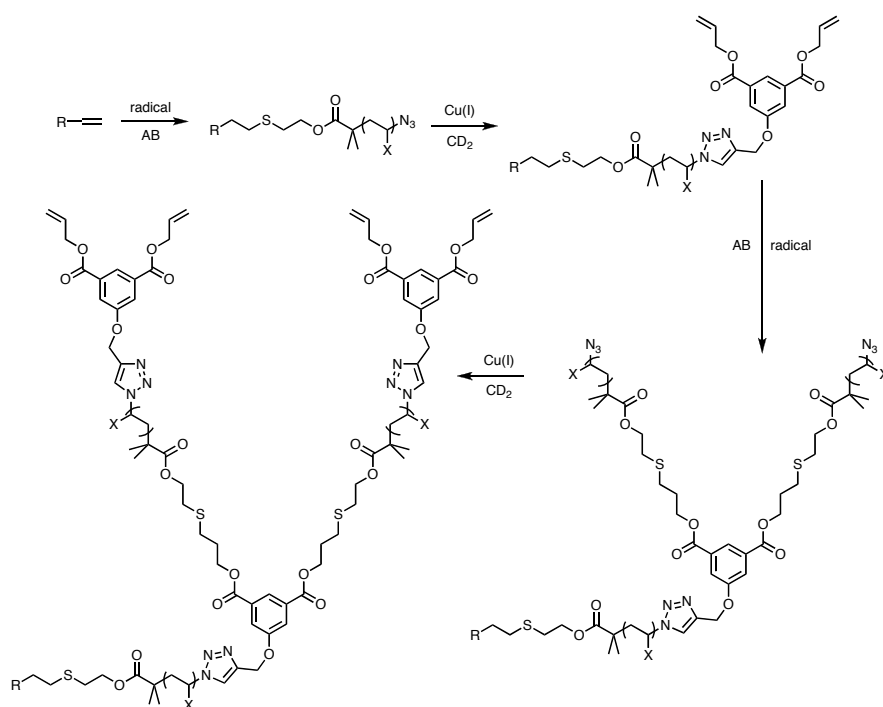


**Figure 5.19.** The  $AB_2$ - $CD_2$  synthesis of a dendrimer (4<sup>th</sup> generation is shown) using complementary heterotrifunctional branched small molecules.

Using complementary click systems to quickly assemble complex architectures in the absence of protecting groups could also be used to assemble branch points such as those used by Hawker, et al, with  $\alpha,\omega$ -heterobifunctional macromonomers such as those in Figure 5.20. Beginning with a poly-ene core, alternate addition of the thiol-azide macromonomer,  $AB$ , and alkyne-diene branch point,  $CD_2$ , would generate an  $AB$ - $CD_2$  dendrimacromer (Figure 5.20a, Figure 5.21). With this approach, small heterobifunctional thiol-azides (e.g. 11-azido-1-undecanethiol) and alken-yne (e.g. 1-penten-4-yne) can be added to the periphery in order to control the radial density of the growing dendrimacromer. Addition of a small molecule thiol-azide would facilitate the rapid increase of the number of peripheral functionalities by keeping many branching units close together, while the addition of a small molecule alken-yne would facilitate the



**Figure 5.20.** Potential building blocks for an AB-CD<sub>2</sub> dendrimer using complementary heterobifunctional and heterotrifunctional molecules.



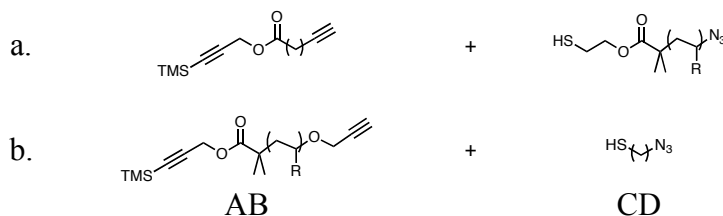
**Figure 5.21.** Building blocks for an AB-CD<sub>2</sub> dendrimer using the complementary heterobifunctional and heterotrifunctional molecules in Figure 5.20a.

rapid coupling of macromonomers for long, unbranched portions of the dendrimacromer.

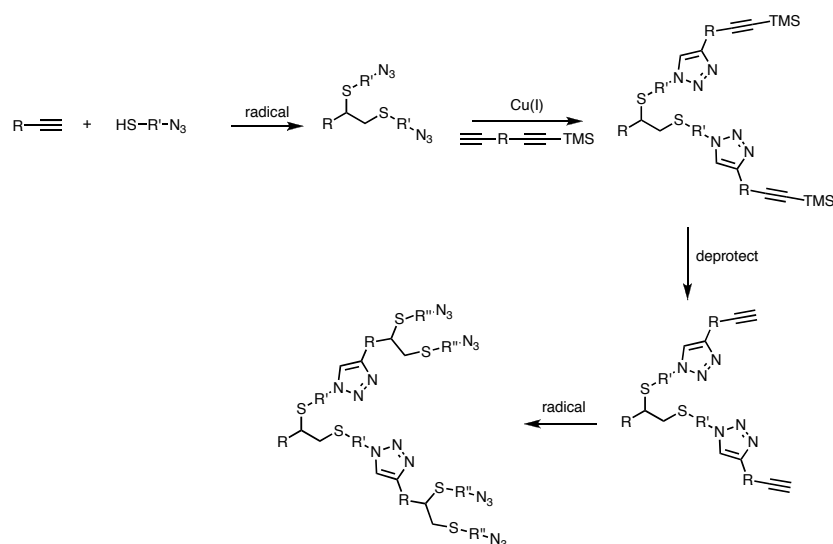
Similar components could also be synthesized where the alkyne and alkenes are instead

on the macromonomer while the azide and thiol are on the branching component (Figure 5.20b).

In addition to the AB-CD<sub>2</sub> approach described above, the twofold addition of thiols across an alkene can be adopted for use in an AB-CD approach. Instead of requiring a heterotrifunctional molecule for branching, the addition of two thiols to an alkyne (Section 1.2.3) provides branching naturally via a dithioacetal.<sup>91-93</sup> Figure 5.22 details the two heterobifunctional molecules that would be used for the AB-CD approach: a bis-alkyne with one protected and one terminal alkyne, AB, and a thiol-azide, CD, similar to Figure 5.20a. In this case, uncaging of the TMS-protected alkyne is still necessary for reaction at the periphery. Following a similar pathway as the AB-CD<sub>2</sub> approach, a poly-yne core can be reacted with the thiol-azide, CD, via thiol-yne chemistry to generate a branched structure with twice as many TMS-protected alkynes at the periphery as were on the core (Figure 5.23). CuAAC reaction with the TMS-alkyne followed by deprotection of the TMS group would regenerate a terminal alkyne.



**Figure 5.22.** Two sets of building blocks for an AB-CD dendrimer using complementary heterobifunctional molecules.



**Figure 5.23.** Synthesis of an AB-CD dendrimer using complementary heterobifunctional molecules.

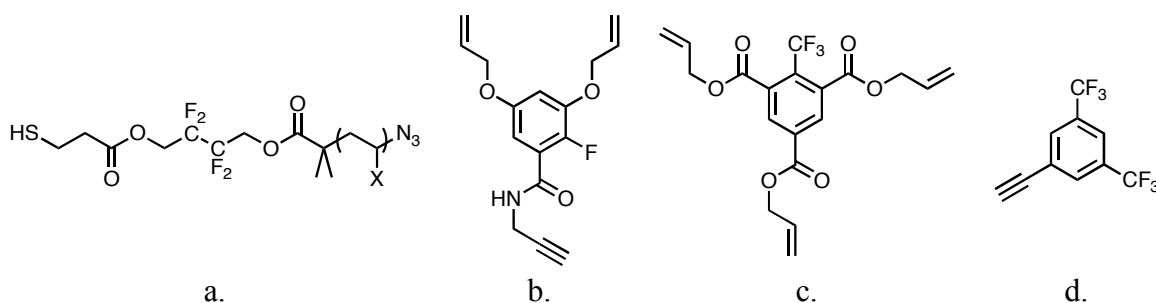
As described above for Figure 5.15, an advantage of both the AB-CD<sub>2</sub> and AB-CD approaches is that each macromonomer component can have vastly different properties because each has been synthesized separately. In contrast, standard ATRP synthesis of linear block copolymers is limited by the need for blocks to be added in order of decreasing activity of monomers. As a result, a block copolymer where the activity of a subsequent block is higher than the previous block is not directly possible. Using the ‘toolkit’ approach, however, block copolymers and block copolymer dendrimers are possible regardless of the activity of the monomers because each block has been synthesized and functionalized separately. Judicious selection of the order in which the macromonomeric polymers are added to the dendrimer should generate materials with novel, unique properties.

### 5.4.3. Fluorinated Dendrimers

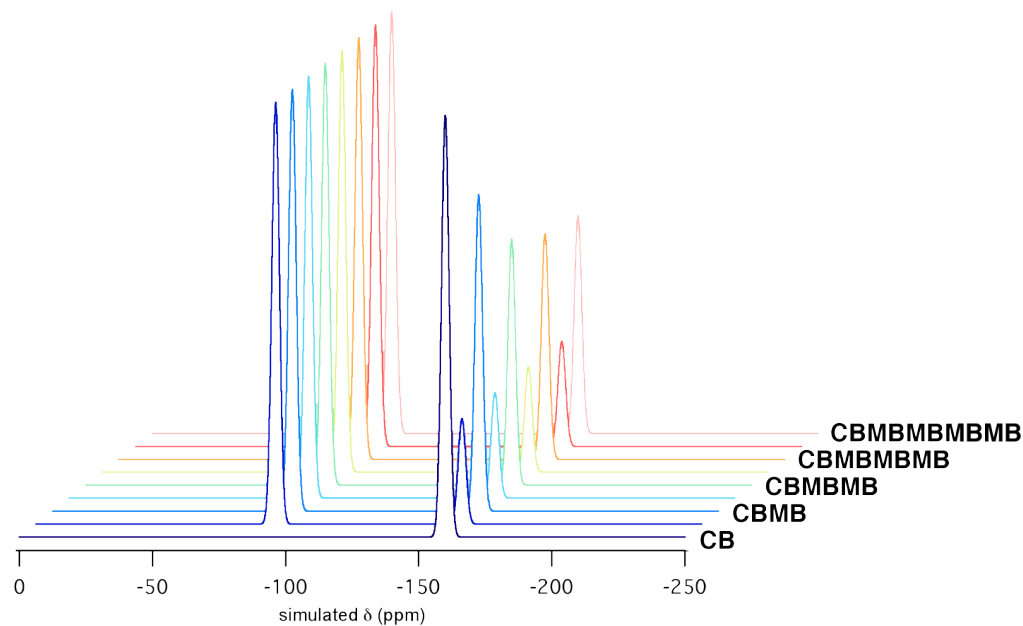
Extending the AB-CD<sub>2</sub> approach for CuAAC and thiol-ene chemistry, molecules have been designed that take advantage of <sup>19</sup>F NMR to better characterize dendrimacromers (Figure 5.24). Small molecules and macromonomers with fluorines in unique chemical environments will allow for the quantitative monitoring of dendrimacromer growth via integration of fluorine resonances in the NMR.<sup>94</sup> The macromonomer and branching unit below (Figure 5.24a,b) are analogous to the small molecules in Figure 5.20a and include alkyl and aromatic fluorines, respectively. The fluorines in these molecules ought to have significantly different chemical shifts –  $\delta$  -90 ppm for the alkyl fluorines of the macromonomer and -160 ppm for the aromatic fluorine of the branch unit – and together provide a way to monitor the relative incorporation of units on the dendrimacromer. A simulated <sup>19</sup>F NMR spectrum of a growing dendrimacromer (**CBMBMBMBMB**) made from alternating addition of branches containing one fluorine and macromonomers with two fluorines is shown in Figure 5.25 where all spectra have been normalized to the contribution from the macromonomer. Comparison of experimental data to this simulated data would determine the efficiency of incorporation at each generation.

The simulated spectrum in Figure 5.25 lacks an internal standard, however. By including a fluorinated core (e.g. Figure 5.24c) in this approach, the <sup>19</sup>F NMR spectra can be normalized to a resonance that does not change over the course of dendrimacromer growth (Figure 5.26). The aromatic trifluoromethyl fluorines ought to be separate from the alkyl and aromatic fluorines with a resonance at approximately  $\delta = -70$  ppm. Additionally, a terminator molecule with fluorines in yet a different chemical

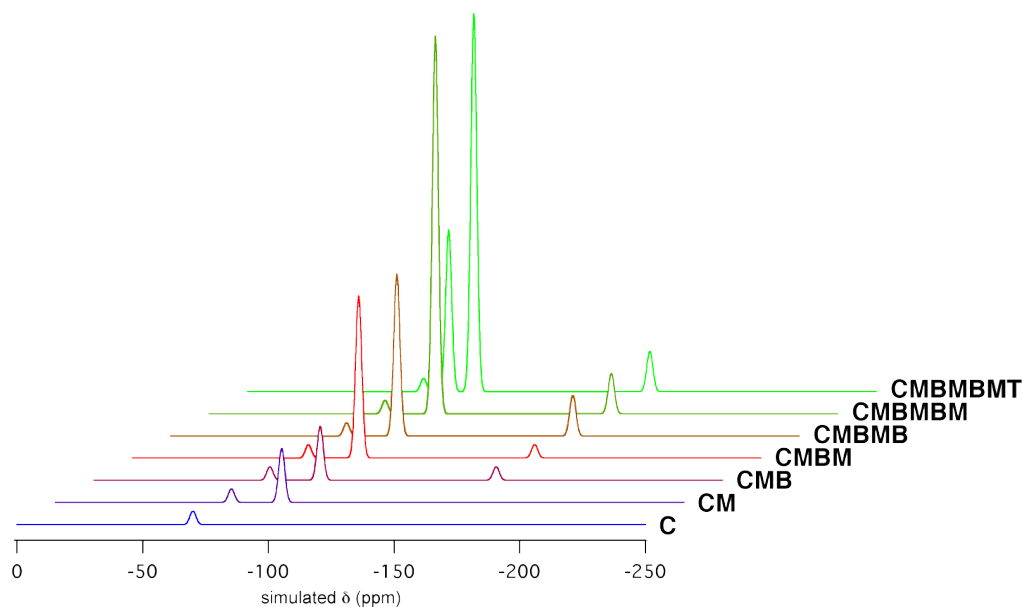
environment (e.g. Figure 5.24d,  $\delta = -80$  ppm) will act to quantitatively count the number of endgroups of the grown dendrimacromer in order to determine the overall efficiency of dendrimacromer growth. The dendrimacromer in Figure 5.26 is a **CMBMBMT** architecture.



**Figure 5.24.** Proposed fluorinated components for the synthesis of dendrimacromers by AB-CD<sub>2</sub> approach and their characterization using <sup>19</sup>F NMR: (a) macromonomer; (b) branch; (c) core; and (d) chain terminator.



**Figure 5.25.** Simulated <sup>19</sup>F NMR spectra of dendrimers grown using fluorinated branch and macromonomer, normalized to macromonomer intensity.



**Figure 5.26.** Simulated  $^{19}\text{F}$  NMR spectra of dendrimers grown using fluorinated branch, macromonomer, core, and terminator.

## 5.5. Summary

- Small molecules were synthesized that contain complementary end groups – azide and trimethylsilyl-protected alkyne – for the creation of a molecular ‘toolkit’.
- A branching unit facilitates the growth of dendritic architectures within the ‘toolkit’.
- The ‘toolkit’ also contains several heterobifunctional monomeric components, including an  $\alpha,\omega$ -heterobifunctional macromonomer and a photodegradable monomer containing the orthonitrobenzyl functionality, and several heterobifunctional terminating units.
- Dendrimacromer construction is sketched schematically and systematically to show the variety of architectures it is possible to create using a simple set of components.
- Construction systems other than CuAAC are discussed and detailed, including an AB- $\text{CD}_2$  approach, an AB-CD approach, and a fluorinated ‘toolkit’, each of which takes advantage of the chemical orthogonality of different ‘click’ systems.



## 5.6. References

---

1. Tang, Y.; Jim, C. K. W.; Liu, Y.; Ye, L.; Qin, A.; Lam, J. W. Y.; Zhao, C.; Tang, B. Z. Synthesis and curing of hyperbranched poly(triazole)s with click polymerization for improved adhesion strength. *Applied Materials & Interfaces* **2010**, *2*, 566-574.
2. Scheel, A.; Komber, H.; Voit, B. Hyperbranched thermolabile polycarbonates derived from a A2+B3 monomer system. *Macromolecular Symposia* **2004**, *210*, 101-110.
3. Qin, A.; Lam, J. W. Y.; Tang, B. Z. Click Polymerization: Progresses, Challenges, and Opportunities. *Macromolecules* **2010**, *43*, 8693-8702.
4. Binder, W. H.; Sachsenhofer, R.; Straif, C. J.; Zirbs, R. Surface-modified nanoparticles via thermal and Cu(I)-mediated “click” chemistry: Generation of luminescent CdSe nanoparticles with polar ligands guiding supramolecular recognition. *Journal of Materials Chemistry* **2007**, *17*, 2125-2132.
5. Kolb, H. C.; Finn, M. G.; Sharpless, K. B. Click Chemistry: Diverse Chemical Function from a Few Good Reactions. *Angewandte Chemie International Edition* **2001**, *40*, 2004-2021.
6. Sumerlin, B. S.; Vogt, A. P. Macromolecular Engineering through Click Chemistry and Other Efficient Transformations. *Macromolecules* **2010**, *43*, 1-13.
7. Binauld, S.; Dameron, D.; Hamaide, T.; Pascault, J.-P.; Fleury, E.; Drockenmuller, E. Click chemistry step growth polymerization of novel alpha-azide-omega-alkyne monomers. *Chemical Communications* **2008**, 4138-4140.
8. Qin, A.; Lam, J. W. Y.; Tang, B. Z. Click polymerization. *Chemical Society Reviews* **2010**, *39*, 2522-2544.
9. Binauld, S.; Hawker, C. J.; Fleury, E.; Drockenmuller, E. A modular approach to functionalized and expanded crown ether based macrocycles using click chemistry. *Angewandte Chemie International Edition* **2009**, *48*, 6654-6658.
10. Montagnat, O. D.; Lessene, G.; Hughes, A. B. Synthesis of azide-alkyne fragments for “click” chemical applications; formation of oligomers from orthogonally protected trialkylsilyl-propargyl azides and propargyl alcohols. *Tetrahedron Letters* **2006**, *47*, 6971-6974.
11. Xue, X.; Zhu, J.; Zhang, Z.; Zhou, N.; Tu, Y.; Zhu, X. Soluble Main-Chain Azobenzene Polymers via Thermal 1,3-Dipolar Cycloaddition: Preparation and Photoresponsive Behavior. *Macromolecules* **2010**, *43*, 2704-2712.
12. Johnson, J. A.; Finn, M. G.; Koberstein, J. T.; Turro, N. J. Construction of Linear Polymers, Dendrimers, Networks, and Other Polymeric Architectures by Copper-Catalyzed Azide-Alkyne Cycloaddition “Click” Chemistry. *Macromolecular Rapid Communications* **2008**, *29*, 1052-1072.
13. Nicholson, J. W. In *Chemistry of Polymers*; Royal Society of Chemistry: Cambridge, 2006; pp. 130-145.
14. Kim, Y. H. Hyperbranched polymers 10 years after. *Journal of Polymer Science Part A: Polymer Chemistry* **1998**, *36*, 1685-1698.
15. Tomalia, D. A.; Fréchet, J. M. J. Discovery of dendrimers and dendritic polymers: A brief historical perspective. *Journal of Polymer Science Part A: Polymer Chemistry* **2002**, *40*, 2719-2728.
16. Klajnert, B.; Bryszewska, M. Dendrimers: properties and applications. *Acta Biochimica Polonica* **2001**, *48*, 199-208.
17. Röglin, L.; Lempens, E. H. M.; Meijer, E. W. A synthetic “tour de force”: well-defined multivalent and multimodal dendritic structures for biomedical applications. *Angewandte Chemie International Edition* **2011**, *50*, 102-112.
18. Zhou, Y.; Huang, W.; Liu, J.; Zhu, X.; Yan, D. Self-assembly of hyperbranched polymers and its biomedical applications. *Advanced Materials* **2010**, *22*, 4567-4590.

- 
19. Lubick, N. Promising Green Nanomaterials. *Environmental Science & Technology* **2009**, *43*, 1247-1249.
  20. Boas, U.; Christensen, J. B.; Heegaard, P. M. H. In *Dendrimers in Medicine and Biotechnology*; The Royal Society of Chemistry: Cambridge, UK, 2006; Vol. 32, pp. 1-27.
  21. Wooley, K. L.; Hawker, C. J.; Fréchet, J. M. J. A "Branched-Monomer Approach" for the Rapid Synthesis of Dendrimers. *Angewandte Chemie International Edition* **1994**, *33*, 82-85.
  22. Chen, C.; Geng, J.; Pu, F.; Yang, X.; Ren, J.; Qu, X. Polyvalent Nucleic Acid/Mesoporous Silica Nanoparticle Conjugates: Dual Stimuli-Responsive Vehicles for Intracellular Drug Delivery. *Angewandte Chemie International Edition* **2010**, 882 -886.
  23. Carlmark, A.; Hawker, C.; Hult, A.; Malkoch, M. New methodologies in the construction of dendritic materials. *Chemical Society Reviews* **2009**, *38*, 352-362.
  24. Franc, G.; Kakkar, A. K. "Click" methodologies: efficient, simple and greener routes to design dendrimers. *Chemical Society Reviews* **2010**, *39*, 1536-1544.
  25. Kohman, R. E.; Zimmerman, S. C. Degradable dendrimers divergently synthesized via click chemistry. *Chemical Communications* **2009**, 794-796.
  26. Franc, G.; Kakkar, A. Dendrimer design using Cu(I)-catalyzed alkyne-azide "click-chemistry". *Chemical Communications* **2008**, 5267-5276.
  27. Wu, P.; Feldman, A. K.; Nugent, A. K.; Hawker, C. J.; Scheel, A.; Voit, B.; Pyun, J.; Fréchet, J. M. J.; Sharpless, K. B.; Fokin, V. V. Efficiency and fidelity in a click-chemistry route to triazole dendrimers by the copper(I)-catalyzed ligation of azides and alkynes. *Angewandte Chemie International Edition* **2004**, *43*, 3928-3932.
  28. Wu, P.; Fokin, V.; Sharpless, K. B. Method of Using Click Chemistry to Functionalize Dendrimers **2009**, 31. US Application 20090306310.
  29. Joralemon, M. J.; O'Reilly, R. K.; Matson, J. B.; Nugent, A. K.; Hawker, C. J.; Wooley, K. L. Dendrimers Clicked Together Divergently. *Macromolecules* **2005**, *38*, 5436-5443.
  30. Killops, K. L.; Campos, L. M.; Hawker, C. J. Robust, efficient, and orthogonal synthesis of dendrimers via thiol-ene "click" chemistry. *Journal of the American Chemical Society* **2008**, *130*, 5062-5064.
  31. Antoni, P.; Robb, M. J.; Campos, L.; Montanez, M.; Hult, A.; Malmström, E.; Malkoch, M.; Hawker, C. J. Supporting information to Pushing the Limits for Thiol-Ene and CuAAC Reactions: Synthesis of a 6th Generation Dendrimer in a Single Day. *Macromolecules* **2010**, *43*, 6625-6631.
  32. Rissing, C.; Son, D. Y. Application of Thiol-Ene Chemistry to the Preparation of Carbosilane-Thioether Dendrimers. *Organometallics* **2009**, *28*, 3167-3172.
  33. Kang, T.; Amir, R. J.; Khan, A.; Ohshimizu, K.; Hunt, J. N.; Sivanandan, K.; Montañez, M. I.; Malkoch, M.; Ueda, M.; Hawker, C. J. Facile access to internally functionalized dendrimers through efficient and orthogonal click reactions. *Chemical Communications* **2010**, *46*, 1556-1558.
  34. Pfeifer, S.; Zarafshani, Z.; Badi, N.; Lutz, J.-F. Liquid-phase synthesis of block copolymers containing sequence-ordered segments. *Journal of the American Chemical Society* **2009**, *131*, 9195-9197.
  35. Kub, C.; Tolosa, J.; Zuccherro, A. J.; McGrier, P. L.; Subramani, C.; Khorasani, A.; Rotello, V. M.; Bunz, U. H. F. Hyperbranched Conjugated Polymers: Postfunctionalization. *Macromolecules* **2010**, *43*, 2124-2129.
  36. Montañez, M. I.; Campos, L. M.; Antoni, P.; Hed, Y.; Walter, M. V.; Krull, B. T.; Khan, A.; Hult, A.; Hawker, C. J.; Malkoch, M. Accelerated Growth of Dendrimers via Thiol-Ene and Esterification Reactions. *Macromolecules* **2010**, *43*, 6004-6013.

- 
37. Antoni, P.; Hed, Y.; Nordberg, A.; Nyström, D.; von Holst, H.; Hult, A.; Malkoch, M. Bifunctional dendrimers: from robust synthesis and accelerated one-pot postfunctionalization strategy to potential applications. *Angewandte Chemie International Edition* **2009**, *48*, 2126-2130.
38. Vieyres, A.; Lam, T.; Gillet, R.; Franc, G.; Castonguay, A.; Kakkar, A. Combined Cu(I)-catalysed alkyne-azide cycloaddition and furan-maleimide Diels-Alder "click" chemistry approach to thermoresponsive dendrimers. *Chemical Communications* **2010**, *46*, 1875-1877.
39. Polaske, N. W.; McGrath, D. V.; McElhanon, J. R. Thermally Reversible Dendronized Step-Polymers Based on Sequential Huisgen 1,3-Dipolar Cycloaddition and Diels-Alder "Click" Reactions. *Macromolecules* **2010**, *43*, 1270-1276.
40. Heyl, D.; Rikowski, E.; Hoffmann, R. C.; Schneider, J. J.; Fessner, W.-D. A "clickable" hybrid nanocluster of cubic symmetry. *Chemistry - A European Journal* **2010**, *16*, 5544-5548.
41. Juríček, M.; Kouwer, P. H. J.; Reháč, J.; Sly, J.; Rowan, A. E. A novel modular approach to triazole-functionalized phthalocyanines using click chemistry. *The Journal of Organic Chemistry* **2009**, *74*, 21-25.
42. Beltrán, E.; Serrano, J. L.; Sierra, T.; Giménez, R. Tris(triazolyl)triazine via click-chemistry: a C3 electron-deficient core with liquid crystalline and luminescent properties. *Organic Letters* **2010**, *12*, 1404-1407.
43. Ornelas, C.; Broichhagen, J.; Weck, M. Strain-Promoted Alkyne Azide Cycloaddition for the Functionalization of Poly(amide)-Based Dendrons and Dendrimers. *Journal of the American Chemical Society* **2010**, *132*, 3923-3931.
44. Djeda, R.; Rapakousiou, A.; Liang, L.; Guidolin, N.; Ruiz, J.; Astruc, D. Click Syntheses of 1,2,3-Triazolylbiferrocenyl Dendrimers and the Selective Roles of the Inner and Outer Ferrocenyl Groups in the Redox Recognition of ATP(2-) and Pd(2+). *Angewandte Chemie International Edition* **2010**, *49*, 8152-8156.
45. Fernandez-Megia, E.; Correa, J.; Rodríguez-Meizoso, I.; Riguera, R. A Click Approach to Unprotected Glycodendrimers. *Macromolecules* **2006**, *39*, 2113-2120.
46. Vestberg, R.; Malkoch, M.; Kade, M.; Wu, P.; Fokin, V. V.; Barry Sharpless, K.; Drockenmuller, E.; Hawker, C. J. Role of architecture and molecular weight in the formation of tailor-made ultrathin multilayers using dendritic macromolecules and click chemistry. *Journal of Polymer Science Part A: Polymer Chemistry* **2007**, *45*, 2835-2846.
47. Matyjaszewski, K. In *Modification and Blending of Synthetic and Natural Macromolecules*; Ciardelli, F.; Penczek, S., Eds.; Kluwer Academic Publishers., 2004; pp. 123-134.
48. Wijmans, C. M.; Zhulina, E. B. Polymer brushes at curved surfaces. *Macromolecules* **1993**, *26*, 7214-7224.
49. Hill, H. D.; Millstone, J. E.; Banholzer, M. J.; Mirkin, C. A. The role radius of curvature plays in thiolated oligonucleotide loading on gold nanoparticles. *ACS Nano* **2009**, *3*, 418-424.
50. Zhulina, E. B.; Birshtein, T. M.; Borisov, O. V. Curved polymer and polyelectrolyte brushes beyond the Daoud-Cotton model. *The European physical journal. E, Soft Matter* **2006**, *20*, 243-256.
51. Panyukov, S.; Zhulina, E. B.; Sheiko, S. S.; Randall, G. C.; Brock, J.; Rubinstein, M. Tension amplification in molecular brushes in solutions and on substrates. *The Journal of Physical Chemistry B* **2009**, *113*, 3750-3768.
52. Harton, S. E.; Kumar, S. K.; Yang, H.; Koga, T.; Hicks, K.; Lee, H.; Mijovic, J.; Liu, M.; Vallery, R. S.; Gidley, D. W. Immobilized Polymer Layers on Spherical Nanoparticles. *Macromolecules* **2010**, *43*, 3415-3421.

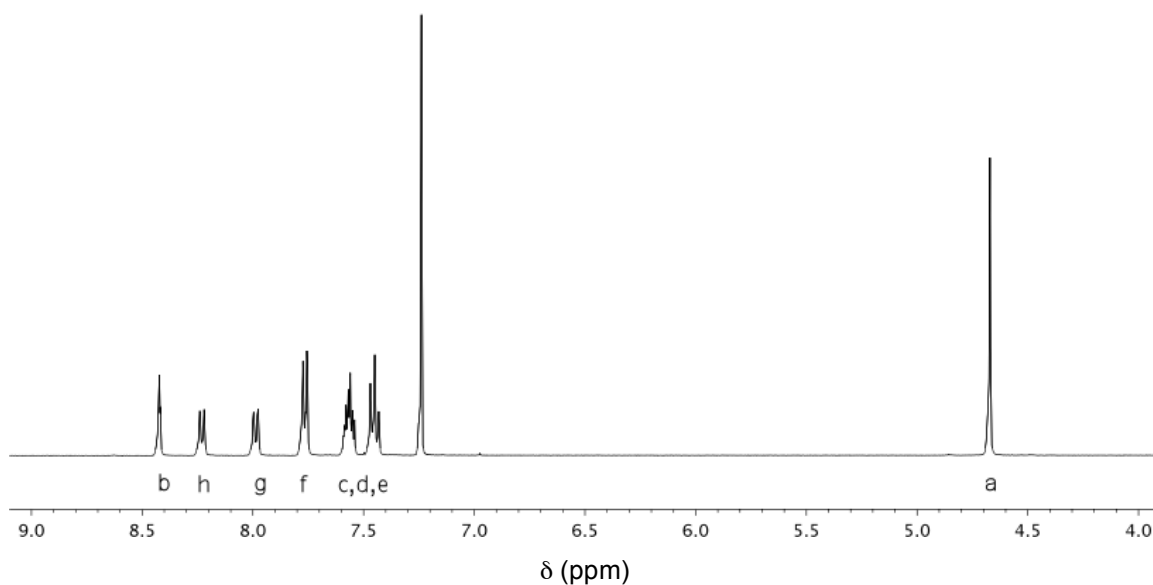
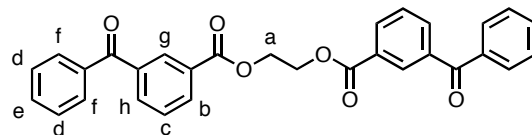
- 
53. Polotsky, A. A.; Gillich, T.; Borisov, O. V.; Leermakers, F. A. M.; Textor, M.; Birshtein, T. M. Dendritic versus Linear Polymer Brushes: Self-Consistent Field Modeling, Scaling Theory, and Experiments. *Macromolecules* **2010**, *43*, 9555-9566.
54. Förster, S.; Wenz, E.; Lindner, P. Density Profile of Spherical Polymer Brushes. *Physical Review Letters* **1996**, *77*, 95-98.
55. Dach, B. I.; Rengifo, H. R.; Turro, N. J.; Koberstein, J. T. Cross-Linked "Matrix-Free" Nanocomposites from Reactive Polymer-Silica Hybrid Nanoparticles. *Macromolecules* **2010**, *43*, 6549-6552.
56. Caminade, A.-M.; Laurent, R.; Majoral, J.-P. Characterization of dendrimers. *Advanced Drug Delivery Reviews* **2005**, *57*, 2130-2146.
57. Tomalia, D. A.; Fréchet, J. M. J. In *Dendrimers and Other Dendritic Polymers*; Tomalia, D. A.; Fréchet, J. M. J., Eds.; John Wiley & Sons Ltd, 2001; pp. 3-44.
58. Knežević, N. Ž.; Trewyn, B. G.; Lin, V. S.-Y. Light- and pH-Responsive Release of Doxorubicin from a Mesoporous Silica-Based Nanocarrier. *Chemistry - A European Journal* **2011**, *17*, 3338-3342.
59. Pierrat, P.; Vanderheiden, S.; Muller, T.; Bräse, S. Functionalization of hexakis methanofullerene malonate crown-ethers: promising octahedral building blocks for molecular networks. *Chemical Communications* **2009**, 1748-1750.
60. Synthesis of **20**: JRL2p59, JRL2p147. <sup>1</sup>H NMR of **20**: JRL\_10\_0418\_5-azidoisophthalic\_acid, JRL\_10\_0526\_5-azidoisophthalic\_acid. <sup>1</sup>H NMR of 5-aminoisophthalic acid: JRL\_10\_0403\_5-aminoisophthalic\_acid.
61. Synthesis of **21**: JRL2p65, JRL2p67, JRL2p151. <sup>1</sup>H NMR of **21**: JRL\_10\_0604\_5-azidoisophthalic\_alkyne\_TMS, JRL\_11\_0228\_bis-TMS-alkyne-phenyl\_azide-branch.
62. Budyka, M. F. Photodissociation of aromatic azides. *Chemical Reviews* **2008**, *77*, 709-723.
63. Rentsch, D.; Görlach, J.; Vogt, E.; Amrhein, N.; Martinoia, E. The tonoplast-associated citrate binding protein (CBP) of *Hevea brasiliensis*. Photoaffinity labeling, purification, and cloning of the corresponding gene. *The Journal of Biological Chemistry* **1995**, *270*, 30525-30531.
64. Voskresenska, V.; Wilson, R. M.; Panov, M.; Tarnovsky, A. N.; Krause, J. A.; Vyas, S.; Winter, A. H.; Hadad, C. M. Photoaffinity labeling via nitrenium ion chemistry: protonation of the nitrene derived from 4-amino-3-nitrophenyl azide to afford reactive nitrenium ion pairs. *Journal of the American Chemical Society* **2009**, *131*, 11535-11547.
65. Szewczyk, A.; Nałecz, M. J.; Wojtczak, L. Azido derivatives of dicarboxylic acids for photoaffinity labeling of mitochondrial carriers. *Journal of Biochemical and Biophysical Methods* **1989**, *18*, 125-134.
66. Van Wuytswinkel, G.; Verheyde, B.; Compennolle, F.; Toppet, S.; Dehaen, W. A convergent synthesis of heterocyclic dendrimers using the 1,3-dipolar cycloaddition reaction of organic azides and acetylenedicarboxylate esters. *Journal of the Chemical Society, Perkin Transactions 1* **2000**, 1337-1340.
67. Synthesis of **22**: JRL2p73. <sup>1</sup>H NMR of **22**: DM\_10\_0611\_6azidohexanol. Synthesis of 11-azidoundecanol: JRL2p113. <sup>1</sup>H NMR of 11-azidoundecanol: JRL\_10\_1117\_azidoundecanol.
68. Synthesis of **23**: DMp25. <sup>1</sup>H NMR of **23**: DM\_10\_0621\_BPazidohexylester\_column1.
69. Synthesis of **24**: DMp27. <sup>1</sup>H NMR of **24**: DM\_10\_0625\_1pyreneazidohexylester\_column1\_2.
70. Synthesis of **25**: JRL2p121, JRL2p123, JRL2p127, JRL2p133. <sup>1</sup>H NMR of **25**: JRL\_11\_0217\_TMS-alkyne-ONBP-N3.
71. Ramos, R.; Manning, B.; Aviñó, A.; Gargallo, R.; Eritja, R. Photocleavage of Peptides and Oligodeoxynucleotides Carrying 2-Nitrobenzyl Groups. *Helvetica Chimica Acta* **2009**, *92*, 613-622.

- 
72. Wong, D. Y.; Griffin, D. R.; Reed, J.; Kasko, A. M. Photodegradable Hydrogels to Generate Positive and Negative Features over Multiple Length Scales. *Macromolecules* 2010, *43*, 2824-2831.
  73. Urbani, C. N.; Lonsdale, D. E.; Bell, C. A.; Whittaker, M. R.; Monteiro, M. J. Divergent synthesis and self-assembly of amphiphilic polymeric dendrons with selective degradable linkages. *Journal of Polymer Science Part A: Polymer Chemistry* 2008, *46*, 1533-1547.
  74. Urbani, C. N.; Bell, C. A.; Lonsdale, D.; Whittaker, M. R.; Monteiro, M. J. Self-Assembly of Amphiphilic Polymeric Dendrimers Synthesized with Selective Degradable Linkages. *Macromolecules* 2008, *41*, 76-86.
  75. Yesilyurt, V.; Ramireddy, R.; Thayumanavan, S. Photoregulated release of noncovalent guests from dendritic amphiphilic nanocontainers. *Angewandte Chemie International Edition* 2011, *50*, 3038-3042.
  76. Kostianen, M. A.; Kotimaa, J.; Laukkanen, M.-L.; Pavan, G. M. Optically degradable dendrons for temporary adhesion of proteins to DNA. *Chemistry - A European Journal* 2010, *16*, 6912-6918.
  77. Opsteen, J. A.; van Hest, J. C. M. Modular synthesis of ABC type block copolymers by "click" chemistry. *Journal of Polymer Science Part A: Polymer Chemistry* 2007, *45*, 2913-2924.
  78. Aucagne, V.; Leigh, D. A. Chemoselective formation of successive triazole linkages in one pot: "click-click" chemistry. *Organic Letters* 2006, *8*, 4505-4507.
  79. Koberstein, J. T.; Grigoras, C.; Rengifo, H. R. Heterobifunctional Polymers and Methods for Layer-by-Layer Construction of Multilayer Films 2010, *70*, Patent WO 2010/053993 A1.
  80. Eugene, D. M.; Grayson, S. M. Efficient Preparation of Cyclic Poly(methyl acrylate)-block-poly(styrene) by Combination of Atom Transfer Radical Polymerization and Click Cyclization. *Macromolecules* 2008, *41*, 5082-5084.
  81. Berthet, M.-A.; Zarafshani, Z.; Pfeifer, S.; Lutz, J.-F. Facile Synthesis of Functional Periodic Copolymers: A Step toward Polymer-Based Molecular Arrays. *Macromolecules* 2010, *43*, 44-50.
  82. Johnson, J. A.; Finn, M. G.; Koberstein, J. T.; Turro, N. J. Synthesis of Photocleavable Linear Macromonomers by ATRP and Star Macromonomers by a Tandem ATRP-Click Reaction: Precursors to Photodegradable Model Networks. *Macromolecules* 2007, *40*, 3589-3598.
  83. Synthesis of **26**: JRL2p135. <sup>1</sup>H NMR of **26**: JRL\_11\_0204\_TMS-alkyne-ATRP-init.
  84. Synthesis of **27**: JRL2p139, JRL2p141. <sup>1</sup>H NMR of **27**: JRL\_11\_0214\_TMS-alkyne-PS-N3. <sup>1</sup>H NMR of  $\alpha$ -(TMS-alkyne) $\omega$ -bromo-polystyrene: JRL\_11\_0214\_TMS-alkyne-PS-Br.
  85. Lim, J.; Mintzer, M. A.; Perez, L. M.; Simanek, E. E. Synthesis of odd generation triazine dendrimers using a divergent, macromonomer approach. *Organic Letters* 2010, *12*, 1148-1151.
  86. White, M. A. Design, synthesis, and application of functional nanomaterials, Columbia University, 2007, pp. 1-135.
  87. Rengifo, H. R.; Chen, L.; Grigoras, C.; Ju, J.; Koberstein, J. T. "Click-functional" block copolymers provide precise surface functionality via spin coating. *Langmuir* 2008, *24*, 7450-7456.
  88. Lake, G. J.; Thomas, A. G. The Strength of Highly Elastic Materials. *Proceedings of the Royal Society A: Mathematical, Physical and Engineering Sciences* 1967, *300*, 108-119.
  89. Merrifield, R. B. Solid Phase Peptide Synthesis. I. The Synthesis of a Tetrapeptide. *Journal of the American Chemical Society* 1963, *85*, 2149-2154.
  90. Takizawa, K.; Tang, C.; Hawker, C. J. Molecularly defined caprolactone oligomers and polymers: synthesis and characterization. *Journal of the American Chemical Society* 2008, *130*, 1718-1726.
  91. Chan, J. W.; Hoyle, C. E.; Lowe, A. B. Sequential phosphine-catalyzed, nucleophilic thiol-ene/radical-mediated thiol-yne reactions and the facile orthogonal synthesis of polyfunctional materials. *Journal of the American Chemical Society* 2009, *131*, 5751-5753.

- 
92. Hensarling, R. M.; Doughty, V. A.; Chan, J. W.; Patton, D. L. "Clicking" polymer brushes with thiol-yne chemistry: indoors and out. *Journal of the American Chemical Society* **2009**, *131*, 14673-14675.
  93. Konkolewicz, D.; Gray-Weale, A.; Perrier, S. Hyperbranched polymers by thiol-yne chemistry: from small molecules to functional polymers. *Journal of the American Chemical Society* **2009**, *131*, 18075-18077.
  94. Thurecht, K. J.; Blakey, I.; Peng, H.; Squires, O.; Hsu, S.; Alexander, C.; Whittaker, A. K. Functional hyperbranched polymers: toward targeted in vivo  $^{19}\text{F}$  magnetic resonance imaging using designed macromolecules. *Journal of the American Chemical Society* **2010**, *132*, 5336-5337.

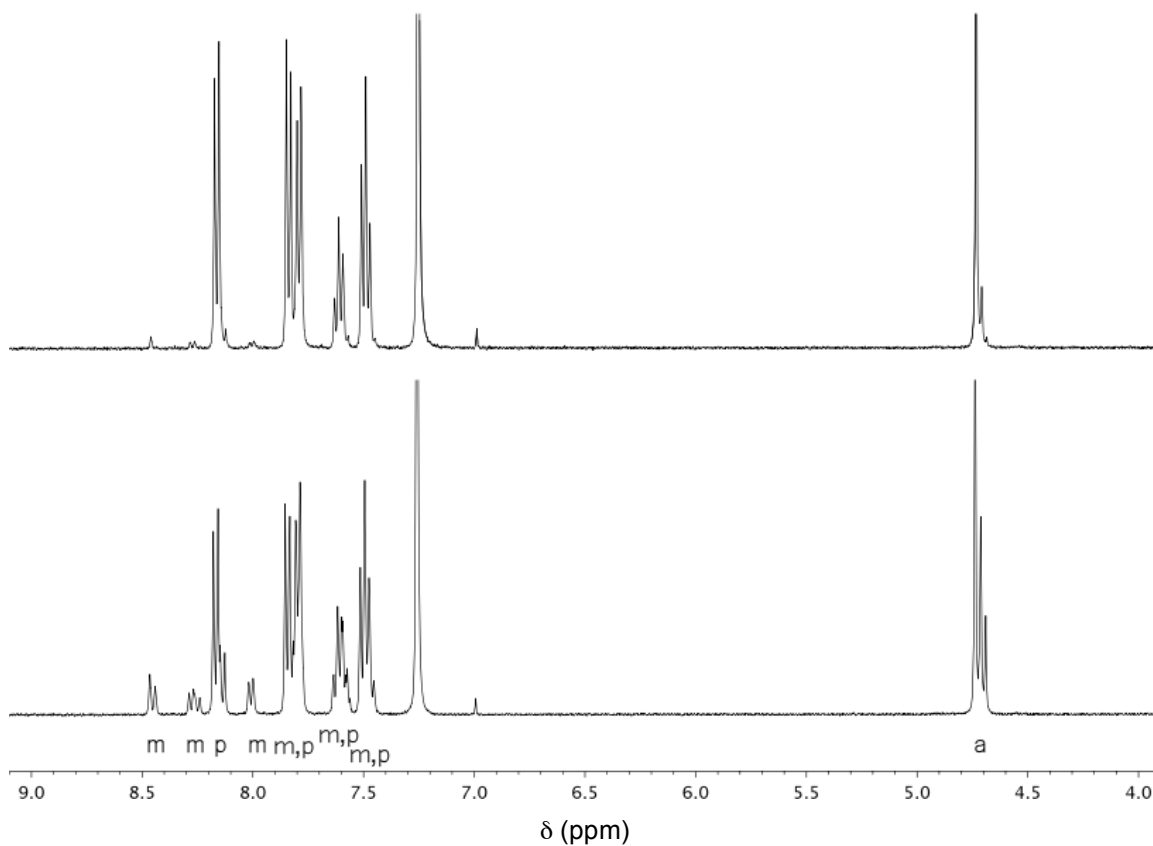
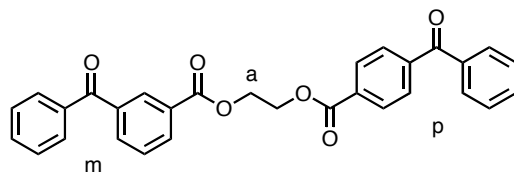
## 6. Appendix

Bis-benzophenone, **1**



<sup>1</sup>H NMR (400 MHz, CDCl<sub>3</sub>) δ 8.42 (dd,  $J = 1.7, 1.2$  Hz, 2H), 8.27 – 8.19 (m, 2H), 8.03 – 7.94 (m, 2H), 7.80 – 7.72 (m, 4H), 7.62 – 7.52 (m, 4H), 7.50 – 7.41 (m, 4H), 4.67 (s, 4H).

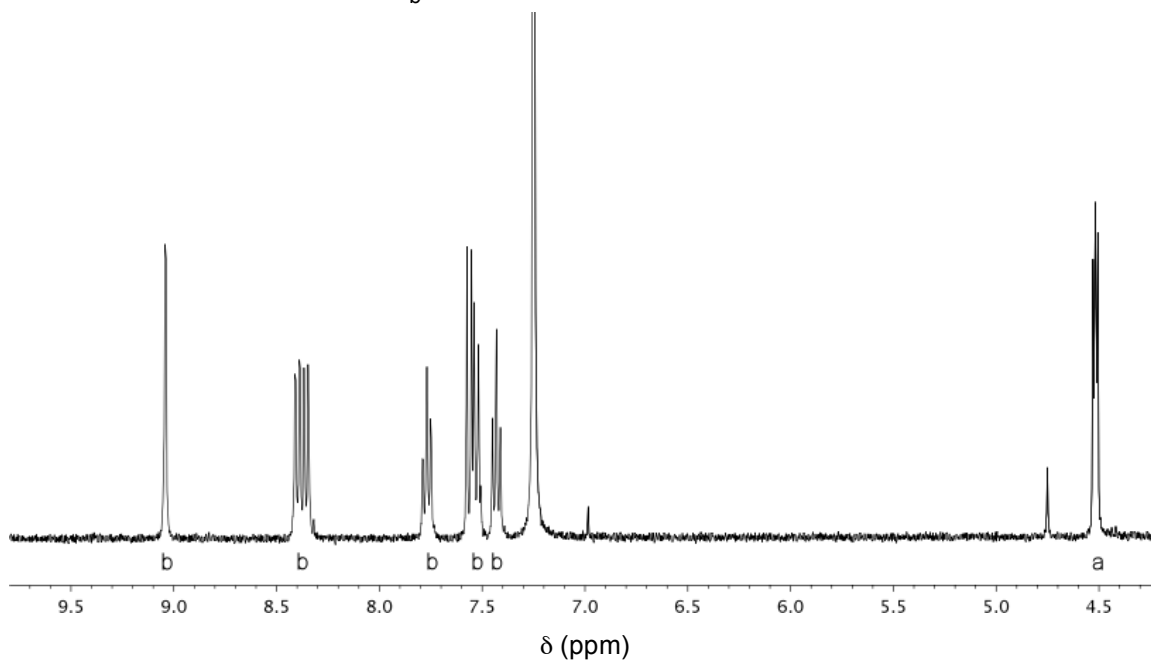
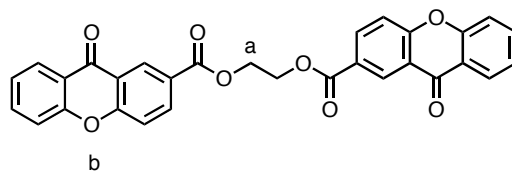
This compound was prepared according to the procedure in Carroll, G. T.; Sojka, M. E.; Lei, X.; Turro, N. J.; Koberstein, J. T. *Langmuir* **2006**, *22*, 7748-7754.

m,p-Bis-benzophenone, **2**

$^1\text{H}$  NMR (400 MHz,  $\text{CDCl}_3$ )  $\delta$  8.45 (d,  $J = 9.5$  Hz), 8.31 – 8.22 (m), 8.17 (d,  $J = 8.5$  Hz), 8.01 (d,  $J = 7.9$  Hz), 7.89 – 7.74 (m), 7.60 (m), 7.48 (m), 4.79 – 4.65 (m).

These compounds were prepared according to the procedure in Carroll, G. T.; Sojka, M. E.; Lei, X.; Turro, N. J.; Koberstein, J. T. *Langmuir* **2006**, *22*, 7748-7754, using a 1:1 mixture of 3-benzoylbenzoic acid and 4-benzoylbenzoic acid in place of the 3-benzoylbenzoic acid of the reference. The resultant white sticky hard gum was recrystallized from hot ethanol to afford two fractions. The first fraction (A, bottom) was isolated from the filtrand, and the second fraction (B, top) was solid which precipitated from the filtrate. Both A and B were dried overnight in a vacuum oven and used without further purification. NMR analysis of fractions A and B in comparison to **1** yielded approximate ratios of meta:para incorporation of 1:3 (A) and 1:15 (B).

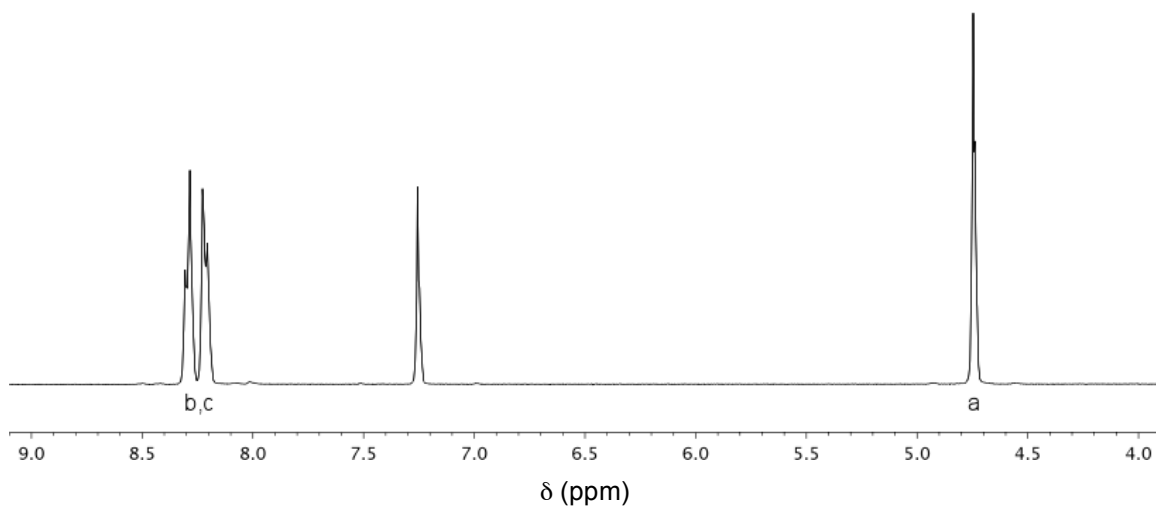
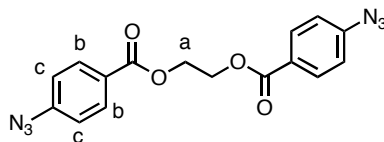


Bis-xanthone, **3**

$^1\text{H}$  NMR (400 MHz,  $\text{CDCl}_3$ )  $\delta$  9.04 (d,  $J = 2.1$  Hz, 2H), 8.47 – 8.30 (m, 4H), 7.77 (t,  $J = 7.8$  Hz, 2H), 7.55 (dd,  $J = 13.7, 8.7$  Hz, 4H), 7.43 (t,  $J = 7.7$  Hz, 2H), 4.56 – 4.47 (m, 4H).

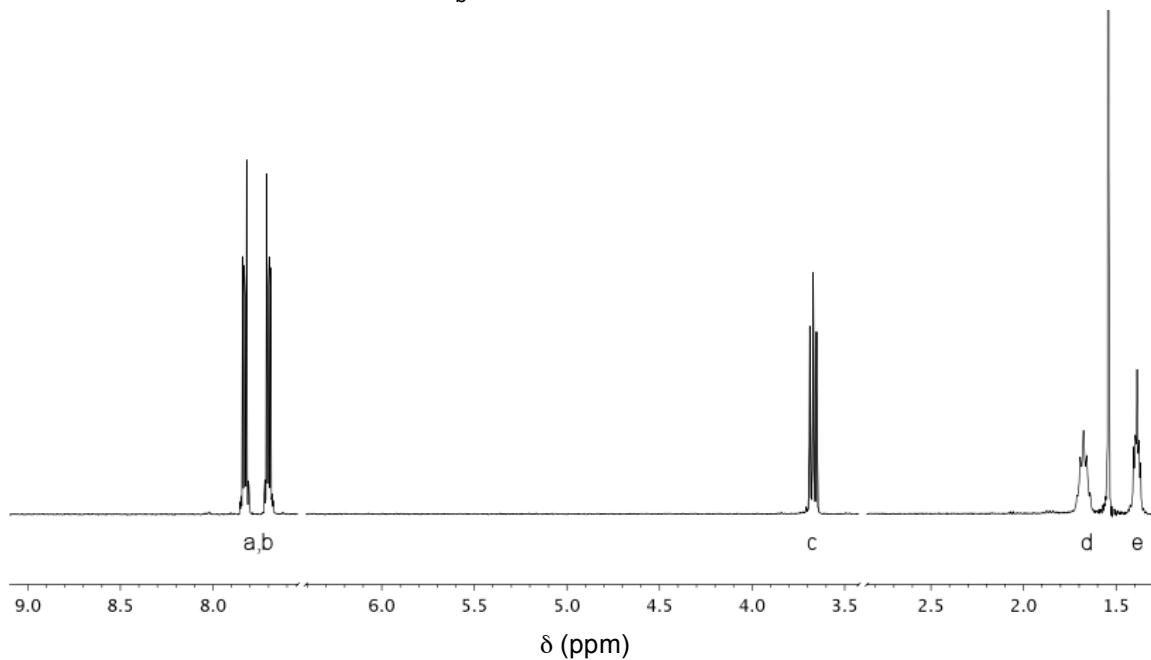
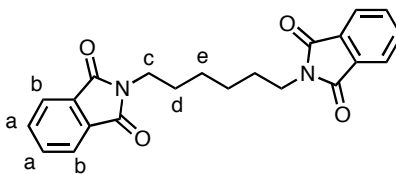
This compound was prepared according to the procedure in Carroll, G. T.; Sojka, M. E.; Lei, X.; Turro, N. J.; Koberstein, J. T. *Langmuir* **2006**, *22*, 7748-7754, using 2-carboxyxanthone in place of 3-benzoylbenzoic acid.

## Bis-phenyl azide, 4



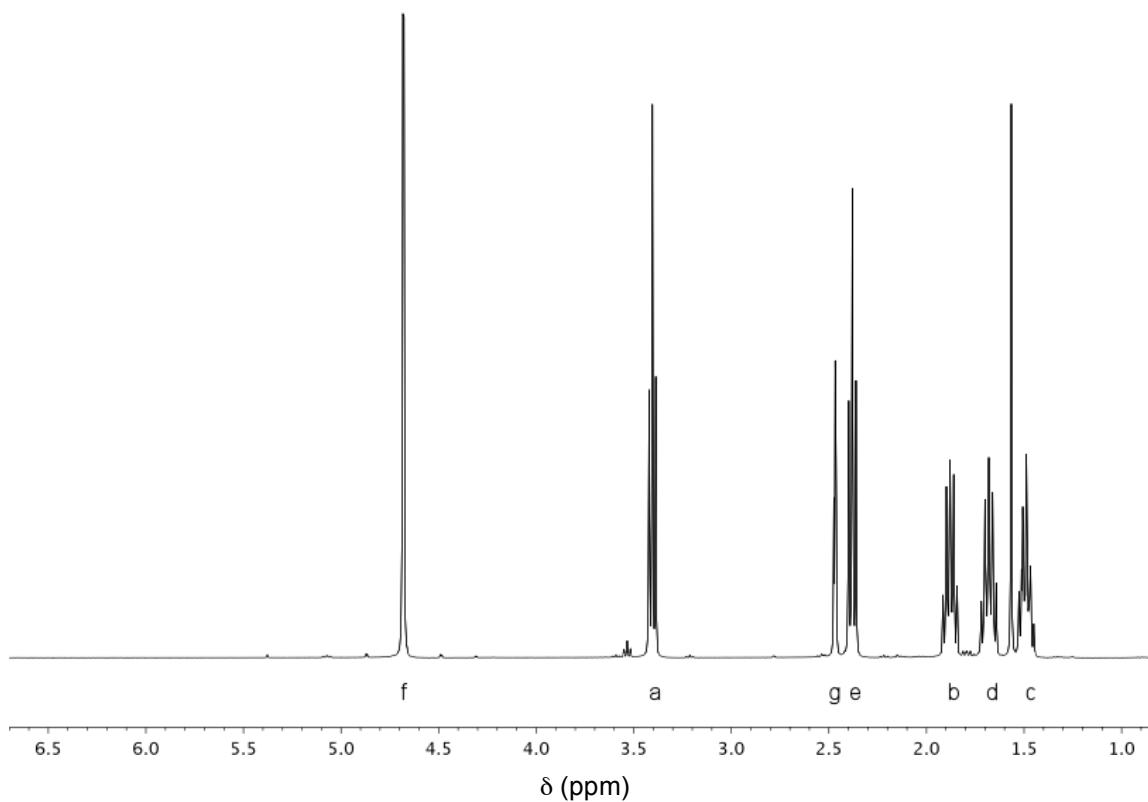
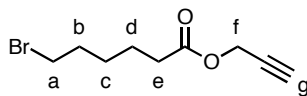
<sup>1</sup>H NMR (400 MHz, CDCl<sub>3</sub>) δ 8.36 – 8.25 (m, 4H), 8.25 – 8.16 (m, 4H), 4.74 (d, *J* = 2.9 Hz, 4H).

This compound was prepared according to the procedure in Carroll, G. T.; Sojka, M. E.; Lei, X.; Turro, N. J.; Koberstein, J. T. *Langmuir* **2006**, *22*, 7748-7754, using 4-azidobenzoic acid in place of 3-benzoylbenzoic acid.

Bis-phthalimide (C6), **5**

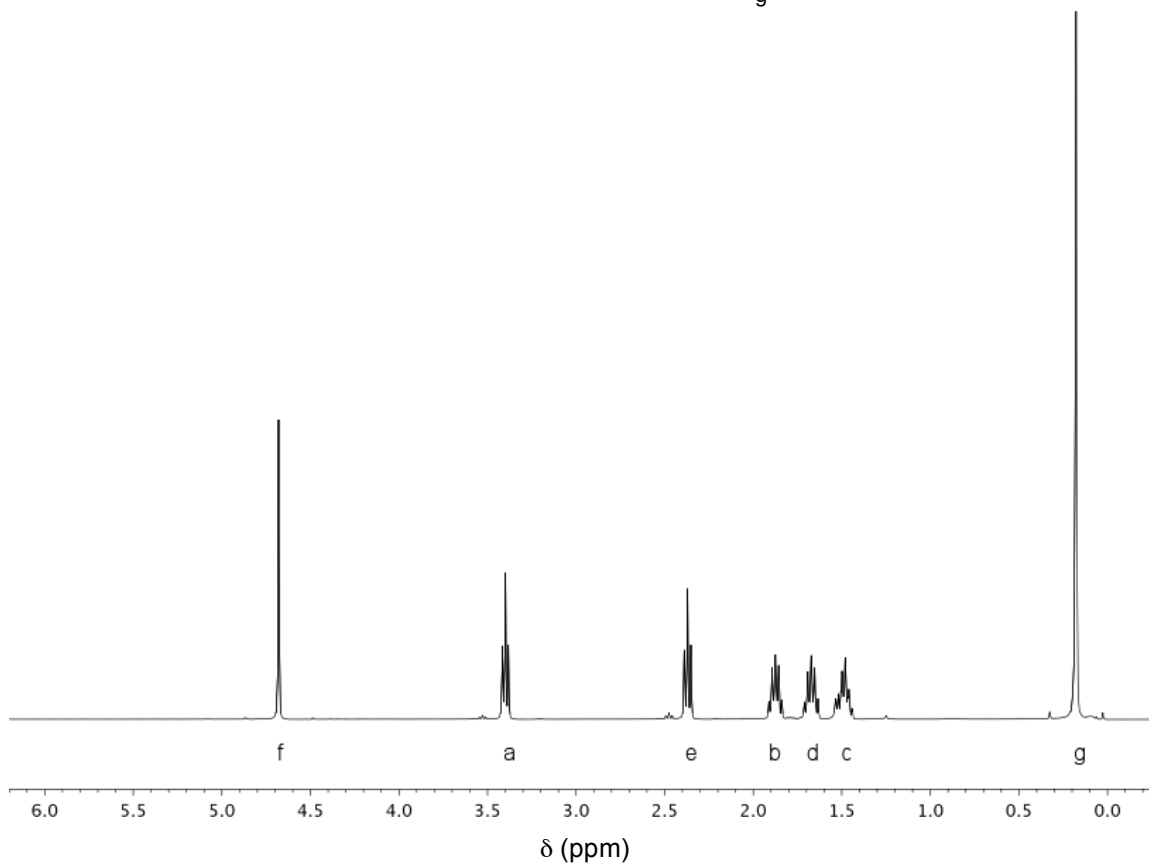
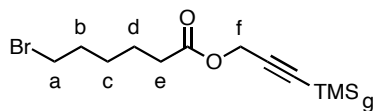
$^1\text{H}$  NMR (400 MHz,  $\text{CDCl}_3$ )  $\delta$  7.83 (dd,  $J = 5.5, 3.0$  Hz, 4H), 7.74 – 7.66 (m, 4H), 3.71 – 3.63 (m, 4H), 1.67 (dd,  $J = 14.0, 7.0$  Hz, 4H), 1.47 – 1.31 (m, 4H).

Compound **5** is prepared by stirring 1,6-dibromohexane with excess potassium phthalimide salt in *N,N*-dimethylformamide under nitrogen according to Carroll, G.; Wang, D.; Turro, N. J.; Koberstein, J. T. *Langmuir* **2006**, *22*, 2899. Addition of chloroform and aqueous workup yielded **5**.

Prop-2-yn-1-yl 6-bromohexanoate, **6**

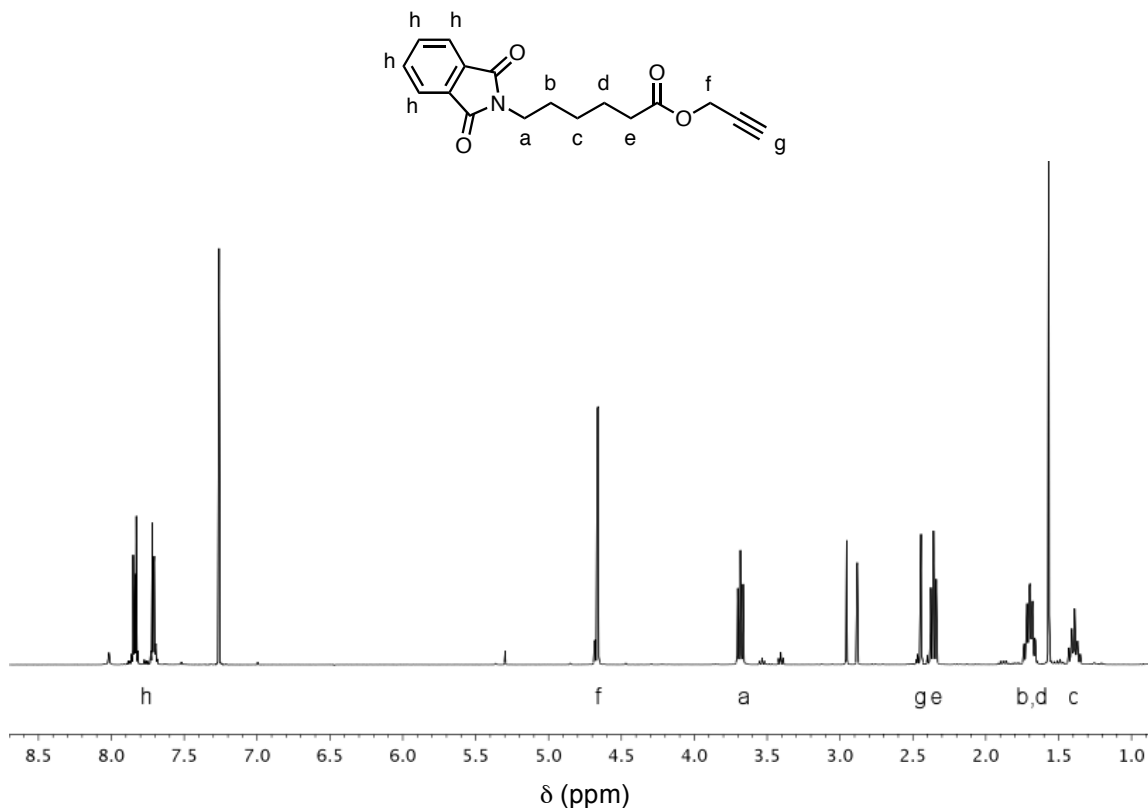
$^1\text{H}$  NMR (400 MHz,  $\text{CDCl}_3$ )  $\delta$  4.68 (d,  $J = 2.5$  Hz, 2H), 3.40 (t,  $J = 6.7$  Hz, 2H), 2.47 (t,  $J = 2.5$  Hz, 1H), 2.38 (t,  $J = 7.4$  Hz, 2H), 1.95 – 1.81 (m, 2H), 1.68 (dt,  $J = 20.6, 7.5$  Hz, 2H), 1.55 – 1.43 (m, 2H).

The synthesis of **6** involved dissolving propargyl alcohol (0.5 mL, 3.41 mmol, 1 eq.) in 10 mL of dry pyridine and 10 mL of dry benzene under argon and cooling this solution in an ice bath. 6-bromohexanoyl chloride (0.612 mL, 4.1 mmol, 1.2 eq.) was dissolved in 10 mL of dry benzene under argon was then added dropwise to the propargyl alcohol solution and stirred overnight. The solution was acidified with 1M HCl, then extracted twice with  $\text{CH}_2\text{Cl}_2$ . The organic layers were twice washed with 1M NaOH, once washed with brine, and dried over  $\text{Na}_2\text{SO}_4$ . The solvent was removed on a rotary evaporator to yield a light brown oil.

3-(Trimethylsilyl)-prop-2-yn-1-yl 6-bromohexanoate, **7**

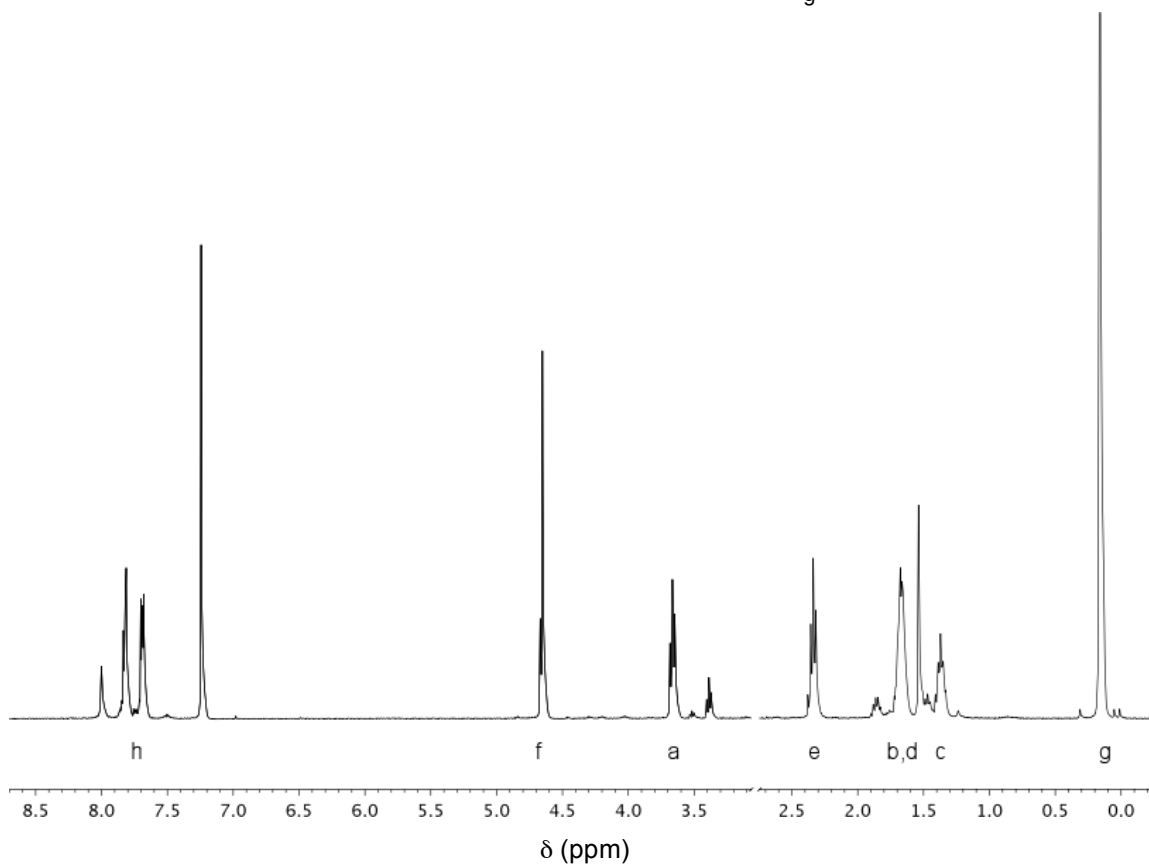
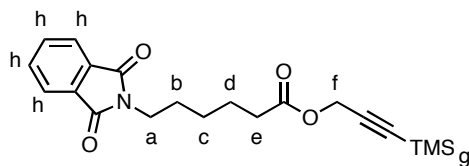
$^1\text{H}$  NMR (400 MHz,  $\text{CDCl}_3$ )  $\delta$  4.68 (s, 2H), 3.40 (t,  $J = 6.8$  Hz, 2H), 2.37 (t,  $J = 7.4$  Hz, 2H), 1.95 – 1.81 (m, 2H), 1.67 (dt,  $J = 15.2, 7.4$  Hz, 2H), 1.62 – 1.41 (m, 2H), 0.18 (s, 9H).

Compound **7** was prepared in the same way as **6** using 3-(trimethylsilyl)-prop-2-yn-1-ol in place of propargyl alcohol.

Prop-2-yn-1-yl 6-phthalimidohexanoate, **8**

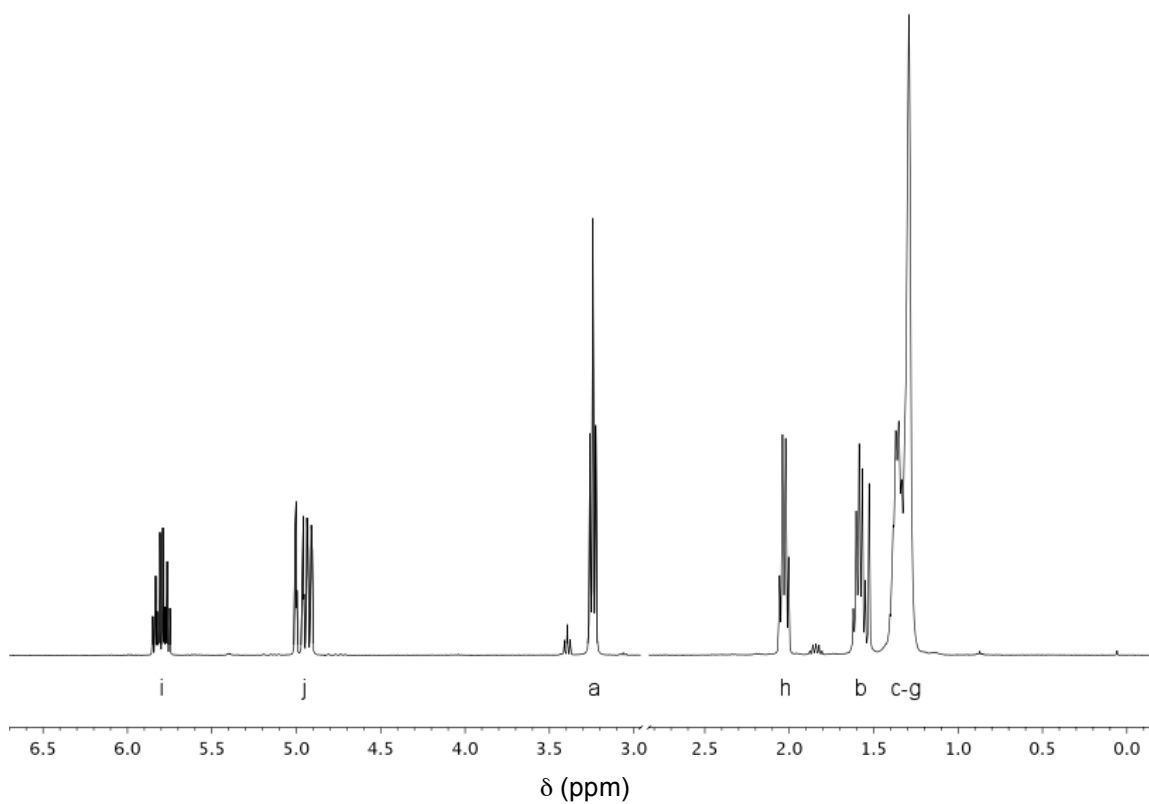
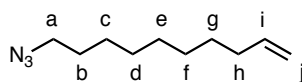
$^1\text{H}$  NMR (400 MHz,  $\text{CDCl}_3$ )  $\delta$  7.84 (dd,  $J = 5.5, 3.0$  Hz, 2H), 7.71 (dd,  $J = 5.4, 3.0$  Hz, 2H), 4.66 (s,  $J = 2.5$  Hz, 2H), 3.73 – 3.64 (m, 2H), 2.44 (t,  $J = 2.5$  Hz, 1H), 2.36 (dd,  $J = 12.1, 4.6$  Hz, 2H), 1.76 – 1.63 (m, 4H), 1.39 (ddt,  $J = 13.1, 10.1, 6.4$  Hz, 2H).

To substitute the terminal bromide with phthalimide, **6** (0.606 g, 2 mmol, 1 eq.) was added to a solution of phthalimide potassium salt (0.441 g, 2.4 mmol, 1.2 eq.) in 50 mL of DMF and stirred overnight under argon.  $\text{CHCl}_3$  was added to the solution flask and the contents were transferred to a separatory funnel containing water. The aqueous layer was separated and twice extracted with  $\text{CHCl}_3$ . The combined organic layers were twice extracted with water and the solvent was removed on a rotary evaporator. Remaining solvent was removed under high vacuum overnight to yield a brown oil, **8**.

3-(Trimethylsilyl)-prop-2-yn-1-yl 6-phthalimidohexanoate, **9**

$^1\text{H}$  NMR (400 MHz,  $\text{CDCl}_3$ )  $\delta$  7.87 – 7.72 (m, 2H), 7.69 (dd,  $J = 5.4, 3.1$  Hz, 2H), 4.65 (s, 2H), 3.67 (t,  $J = 7.3$  Hz, 2H), 2.34 (t,  $J = 7.5$  Hz, 2H), 1.67 (dd,  $J = 10.2, 5.0$  Hz, 4H), 1.43 – 1.15 (m, 2H), 0.16 (t,  $J = 2.4$  Hz, 9H).

Compound **9** was prepared in the same way as **8** using **7** in place of **6**.

10-Azidodecene, **10**

$^1\text{H}$  NMR (400 MHz,  $\text{CDCl}_3$ )  $\delta$  5.80 (ddt,  $J = 16.9, 10.2, 6.7$  Hz, 1H), 5.03 – 4.88 (m, 2H), 3.24 (t,  $J = 7.0$  Hz, 2H), 2.03 (dd,  $J = 14.3, 6.9$  Hz, 2H), 1.67 – 1.51 (m, 2H), 1.50 – 1.19 (m, 10H).

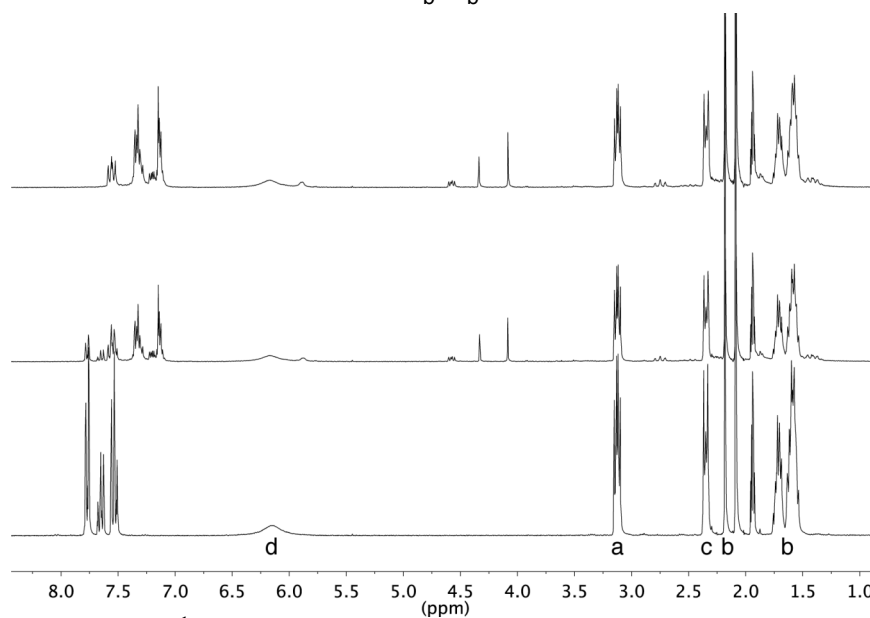
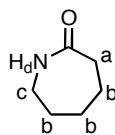
The simple heterobifunctional ‘click transfer’ agent 10-azidodec-1-ene, **10**, was synthesized by stirring 10-bromodec-1-ene with excess sodium azide in DMF followed by aqueous workup according to Tsai, S.-C.; Fu, Y.-S.; Liao, J.-H.; Yu, S. J. *Helvetica Chimica Acta* **2006**, *89*, 3007.



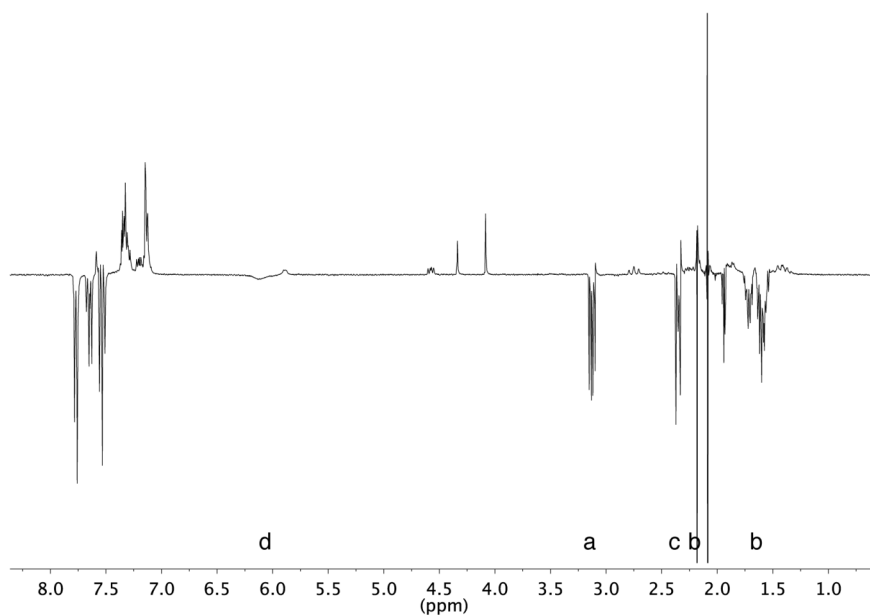
Note: In the  $^1\text{H}$  NMR spectra for compounds **11** - **19** peaks for  $\text{CH}_3\text{CN}$  ( $\delta$ 1.94),  $\text{H}_2\text{O}$  ( $\delta$ 2.13), and benzophenone ( $\delta$ 7.0-7.6) have not been labeled for the sake of clarity.

Methods for determination of bond dissociation energies from Luo, Y.-R. *Handbook of bond dissociation energies in organic compounds*; CRC Press LLC, 2003.

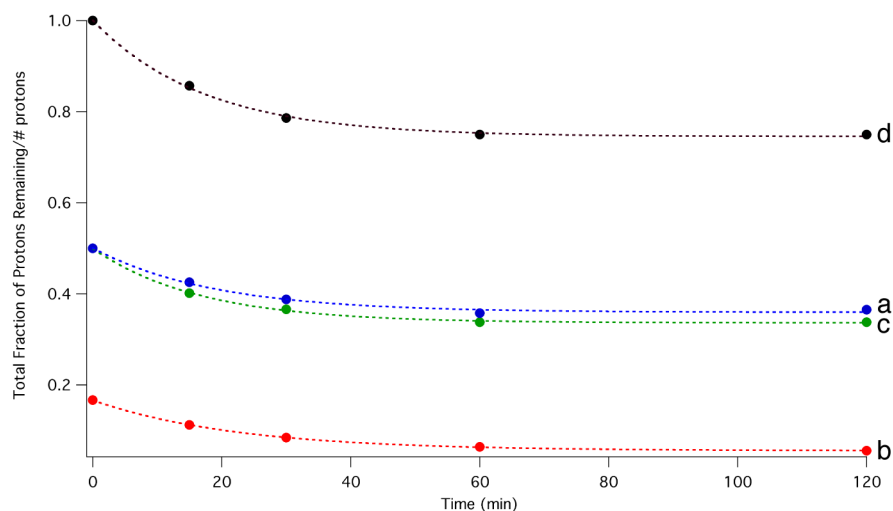
- a. Correlation
- b. Polanyi correlation
- c. Kinetics
- d. Photobromination
- e. Intersecting parabolas
- f. Acidity-oxidation potential measurement
- g. Very low pressure pyrolysis technique
- h. Single-pulse shock tube technique
- i. Electron impact
- j. Reanalysis of pyrolysis data
- k. Fourier transform ion cyclotron resonance spectrometry
- l. Proton affinity
- m. Review
- n. Photoionization mass spectrometry
- o. Resonance fluorescence detection
- p. Appearance energy measurements
- q. Laser flash photolysis
- r. Derived from  $\Delta H_f$
- s. Recommended

Caprolactam, **11**

**Figure S11a.** 300 MHz  $^1\text{H}$  NMR spectra of a 96.9 mM solution of **11** ( $\text{CD}_3\text{CN}$ ) after 0 min (bottom), 30 min (middle), and 120 min (top).

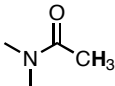
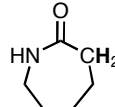
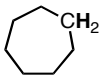
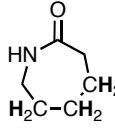
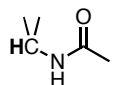
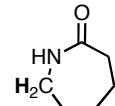
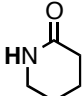
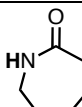


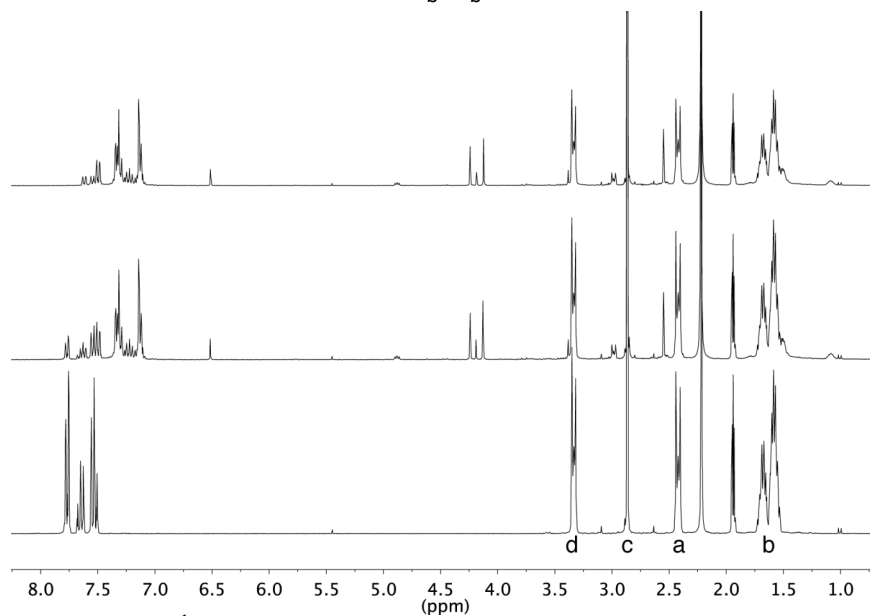
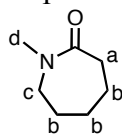
**Figure S11b.** Difference between 300 MHz  $^1\text{H}$  NMR spectra of **11** ( $\text{CD}_3\text{CN}$ ) before and after 120 min irradiation at 350 nm.



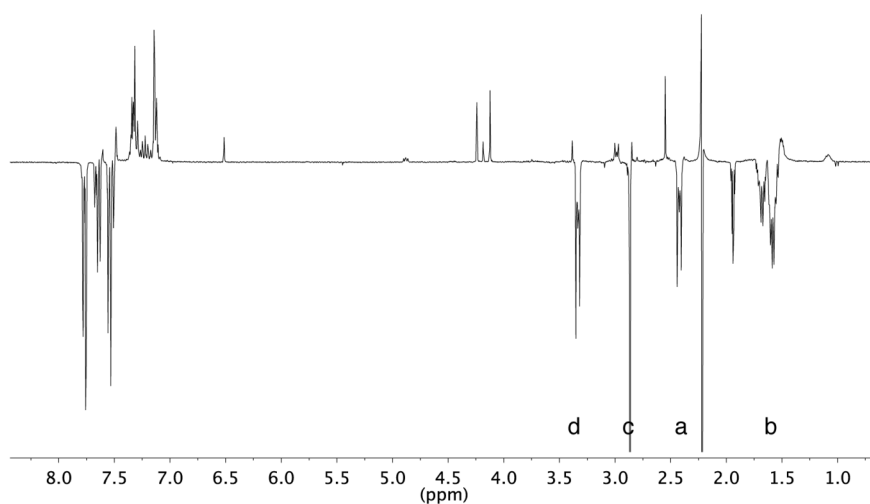
**Figure S11c.** Plot of decreasing  $^1\text{H}$  NMR integrals scaled by initial integral and number of protons with increasing irradiation time of **11**. Each set of data is fit by  $y = Ae^{-kt} + C$ .

**Table S11.** Compounds with representative bond dissociation energies for the protons of **11**, the relation of each representative bond to **11**, and the competitive rate value of  $k/k_a$  scaled for the number of protons.

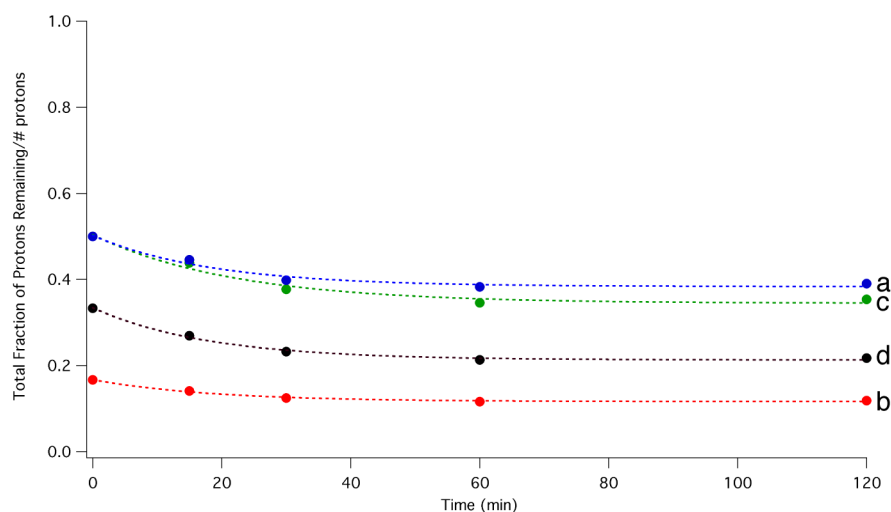
Representative compound	X-H BDE (kcal/mol)	Relation to <b>11</b>	$k/k_a$
N,N-dimethylacetamide 	91.0 <sup>a</sup>	 H <sub>a</sub>	1
cycloheptane 	93.3 <sup>b</sup> 94.0 <sup>c</sup> 92.5±1 <sup>d</sup> 96.5 <sup>e</sup>	 H <sub>b</sub>	0.28
N-isopropylacetamide 	93.1 <sup>a</sup>	 H <sub>c</sub>	1.13
2-piperidone 	109.5 <sup>f</sup>	 H <sub>d</sub>	2.19

Methyl-caprolactam, **12**

**Figure S12a.** 300 MHz <sup>1</sup>H NMR spectra of a 92.3 mM solution of **12** (CD<sub>3</sub>CN) after 0 min (bottom), 30 min (middle), and 120 min (top).

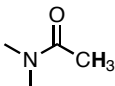
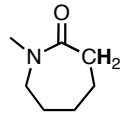
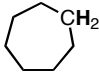
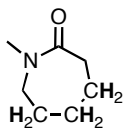
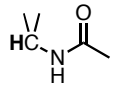
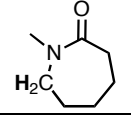
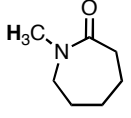


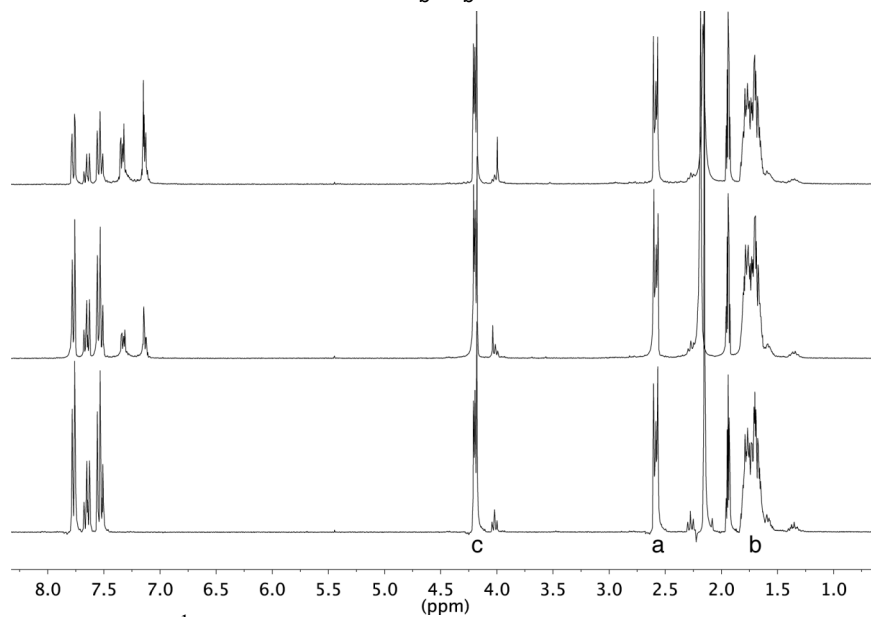
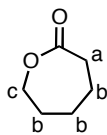
**Figure S12b.** Difference between 300 MHz <sup>1</sup>H NMR spectra of **12** (CD<sub>3</sub>CN) before and after 120 min irradiation at 350 nm.



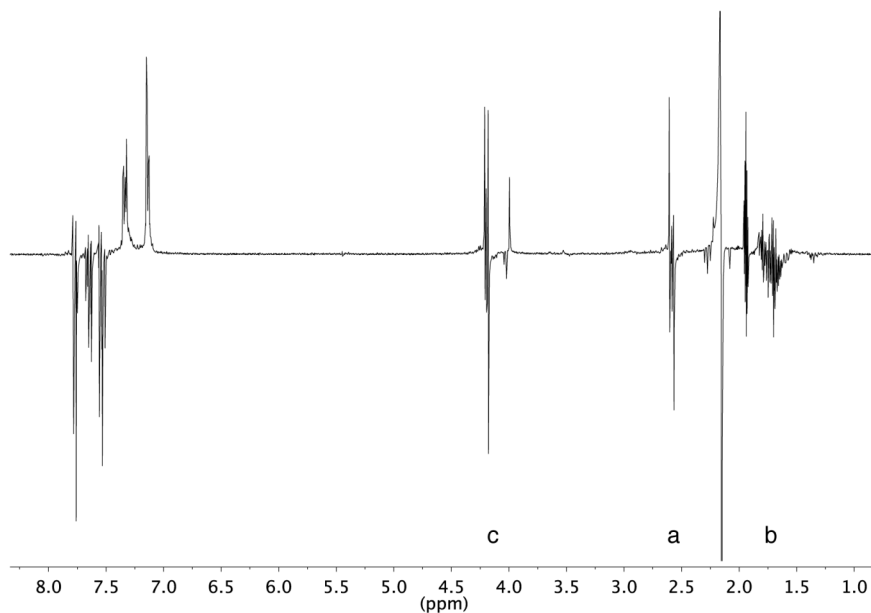
**Figure S12c.** Plot of decreasing  $^1\text{H}$  NMR integrals scaled by initial integral and number of protons with increasing irradiation time of **12**. Each set of data is fit by  $y = Ae^{-kt} + C$ .

**Table S12.** Compounds with representative bond dissociation energies for the protons of **12**, the relation of each representative bond to **12**, and the competitive rate value of  $k/k_a$  scaled for the number of protons.

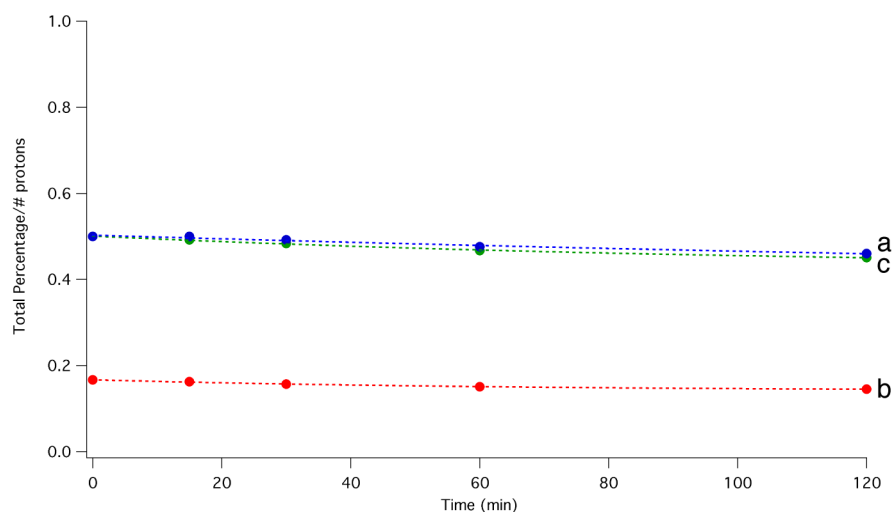
Representative compound	X-H BDE (kcal/mol)	Relation to <b>12</b>	$k/k_a$
N,N-dimethylacetamide 	91.0 <sup>a</sup>	 H <sub>a</sub>	1
cycloheptane 	93.3 <sup>b</sup> 94.0 <sup>c</sup> 92.5±1 <sup>d</sup> 96.5 <sup>e</sup>	 H <sub>b</sub>	0.36
N-isopropylacetamide 	93.1 <sup>a</sup>	 H <sub>c</sub>	0.90
methylamine H <sub>3</sub> C-NH <sub>2</sub>	93±2.5 <sup>g</sup> 96.6 <sup>h</sup> 93.9±2 <sup>i</sup> 88.7 <sup>g</sup>	 H <sub>d</sub>	0.75

$\epsilon$ -Caprolactone, **13**

**Figure S13a.** 300 MHz  $^1\text{H}$  NMR spectra of a 95.7 mM solution of **13** ( $\text{CD}_3\text{CN}$ ) after 0 min (bottom), 30 min (middle), and 120 min (top).

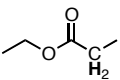
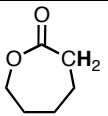
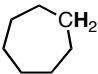
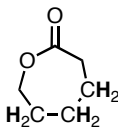
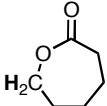
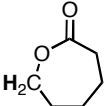


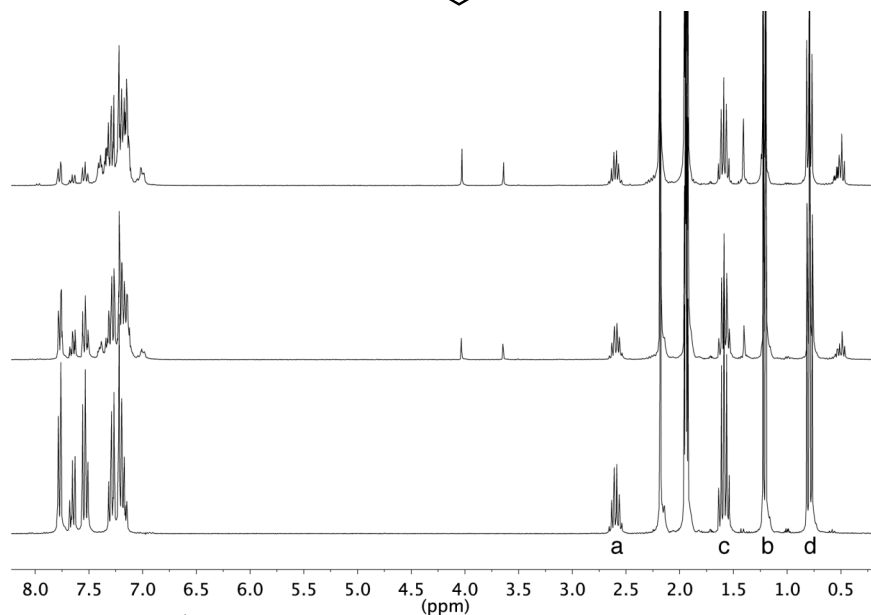
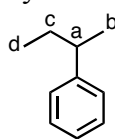
**Figure S13b.** Difference between 300 MHz  $^1\text{H}$  NMR spectra of **13** ( $\text{CD}_3\text{CN}$ ) before and after 120 min irradiation at 350 nm.



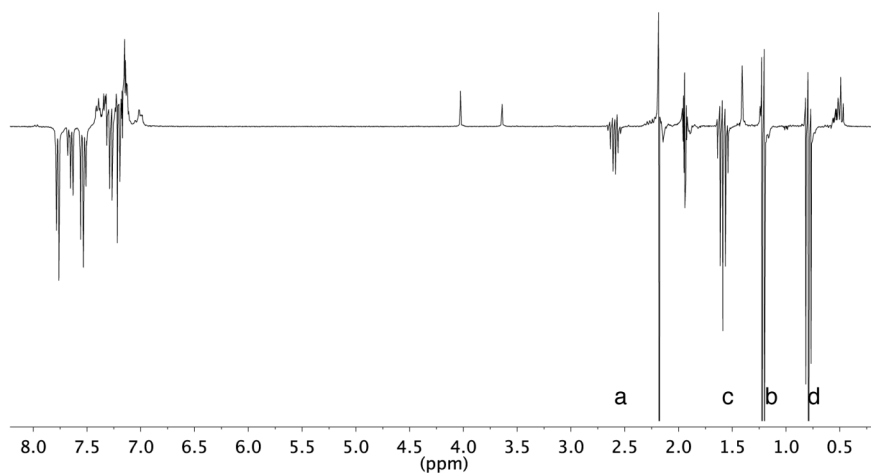
**Figure S13c.** Plot of decreasing  $^1\text{H}$  NMR integrals scaled by initial integral and number of protons with increasing irradiation time of **13**. Each set of data is fit by  $y = Ae^{-kt} + C$ .

**Table S13.** Compounds with representative bond dissociation energies for the protons of **13**, the relation of each representative bond to **13**, and the competitive rate value of  $k/k_a$  scaled for the number of protons.

Representative compound	X-H BDE (kcal/mol)	Relation to <b>13</b>	$k/k_a$
ethyl propanoate 	95.6 <sup>j</sup>	 H <sub>a</sub>	1
cycloheptane 	93.3 <sup>b</sup> 94.0 <sup>c</sup> 92.5±1 <sup>d</sup> 96.5 <sup>e</sup>	 H <sub>b</sub>	1.33
$\epsilon$ -caprolactone 	92.8±2.4 <sup>k</sup>	 H <sub>c</sub>	5

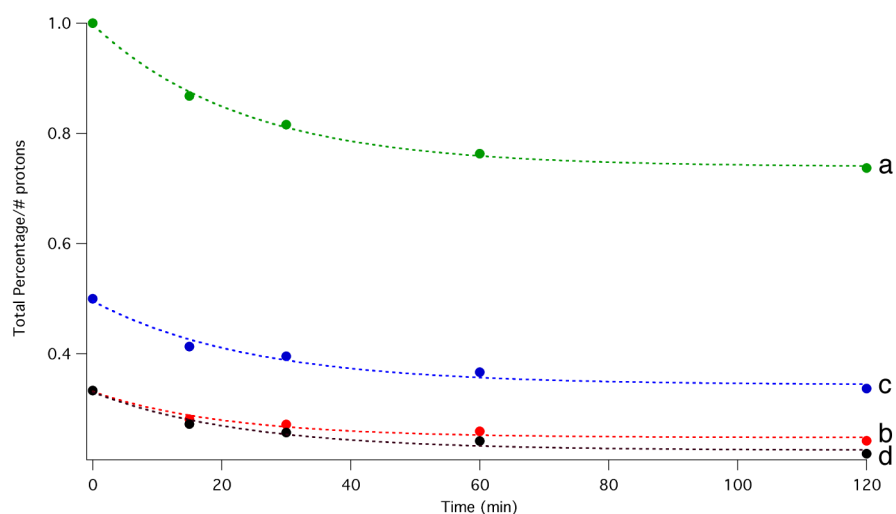
*Sec*-butylbenzene, **14**

**Figure S14a.** 300 MHz <sup>1</sup>H NMR spectra of a 88.6 mM solution of **14** (CD<sub>3</sub>CN) after 0 min (bottom), 30 min (middle), and 120 min (top). Signals from the aromatic protons of **14** overlap adduct proton signals in the region δ7.0-7.4.



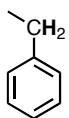
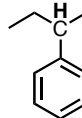
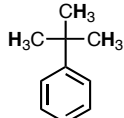
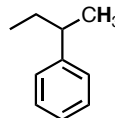
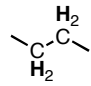
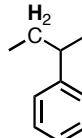
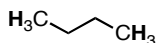
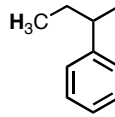
**Figure S14b.** Difference between 300 MHz <sup>1</sup>H NMR spectra of **14** (CD<sub>3</sub>CN) before and after 120 min irradiation at 350nm. Signals from the aromatic protons of **14** overlap adduct proton signals in the region δ7.0-7.4.

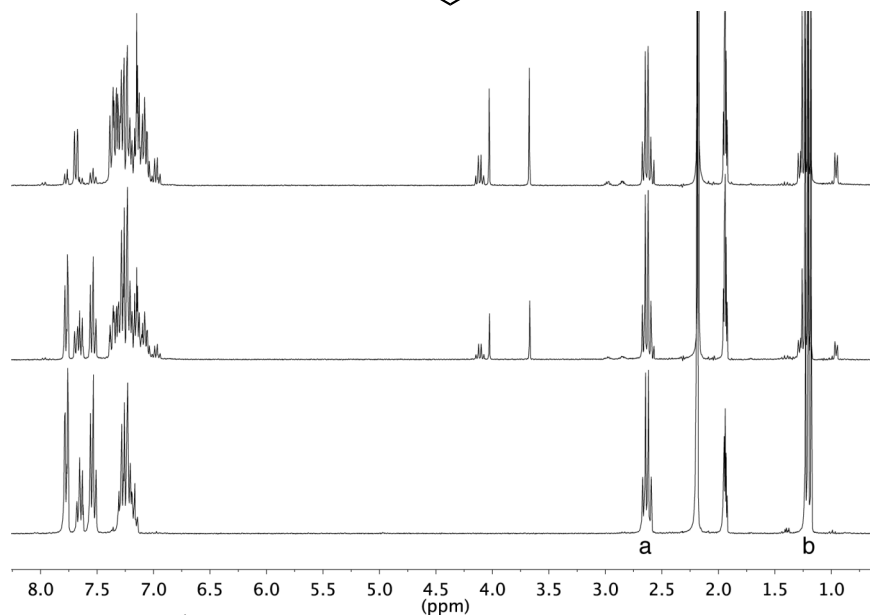
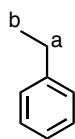




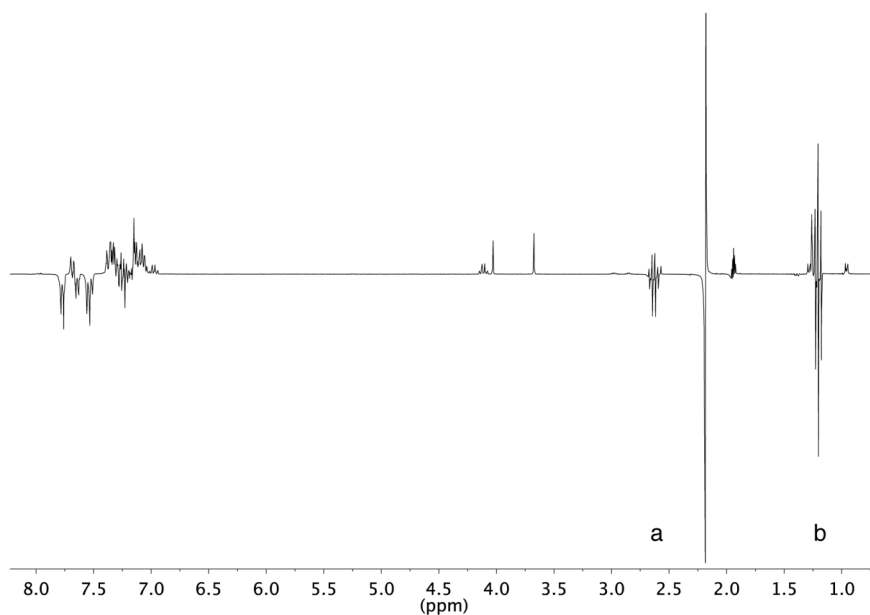
**Figure S14c.** Plot of decreasing  $^1\text{H}$  NMR integrals scaled by initial integral and number of protons with increasing irradiation time of **14**. Each set of data is fit by  $y = Ae^{-kt} + C$ .

**Table S14.** Compounds with representative bond dissociation energies for the protons of **14**, the relation of each representative bond to **14**, and the competitive rate value of  $k/k_a$  scaled for the number of protons.

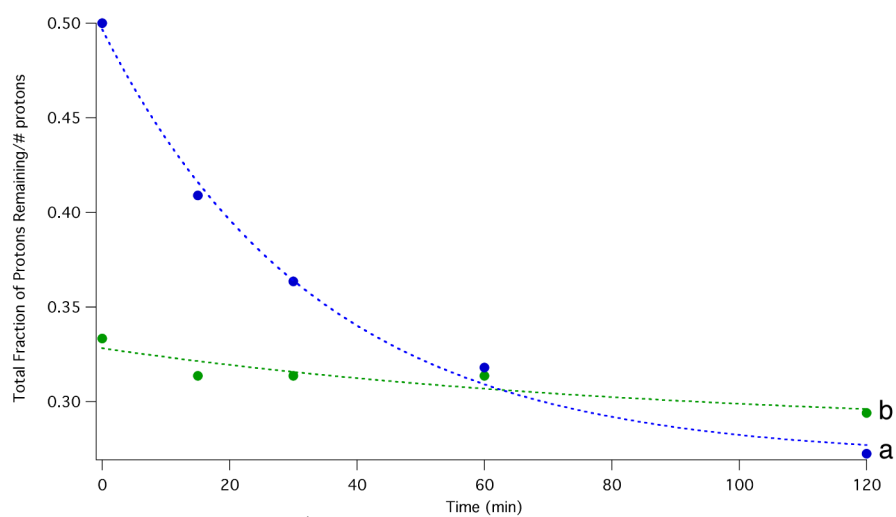
Representative compound	X-H BDE (kcal/mol)	Relation to <b>14</b>	$k/k_a$
ethylbenzene 	84.6 <sup>g</sup> 86.2 <sup>l</sup> 85.4±1.5 <sup>m</sup> 90.3 <sup>j</sup> 87.0 <sup>e</sup>	 $\text{H}_a$	1
<i>tert</i> -butylbenzene 	98.7 <sup>a</sup>	 $\text{H}_b$	0.39
butane 	99.1±0.4 <sup>n</sup> 98.3±0.5 <sup>o</sup> 98.6±0.5 <sup>m</sup> 98.3±0.5 <sup>n</sup> 97.4±1.0 <sup>h</sup>	 $\text{H}_c$	0.52
butane 	101±2 <sup>l</sup> 100.2 <sup>p</sup> 100.7 <sup>h</sup> 101.7±0.5 <sup>n</sup>	 $\text{H}_d$	0.35

Ethylbenzene, **15**

**Figure S15a.** 300 MHz <sup>1</sup>H NMR spectra of a 81.7 mM solution of **15** (CD<sub>3</sub>CN) after 0 min (bottom), 30 min (middle), and 120 min (top). Signals from the aromatic protons of **15** overlap adduct proton signals in the region  $\delta$ 7.0-7.4.

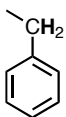
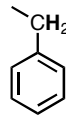
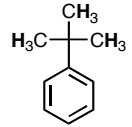
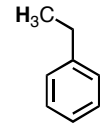


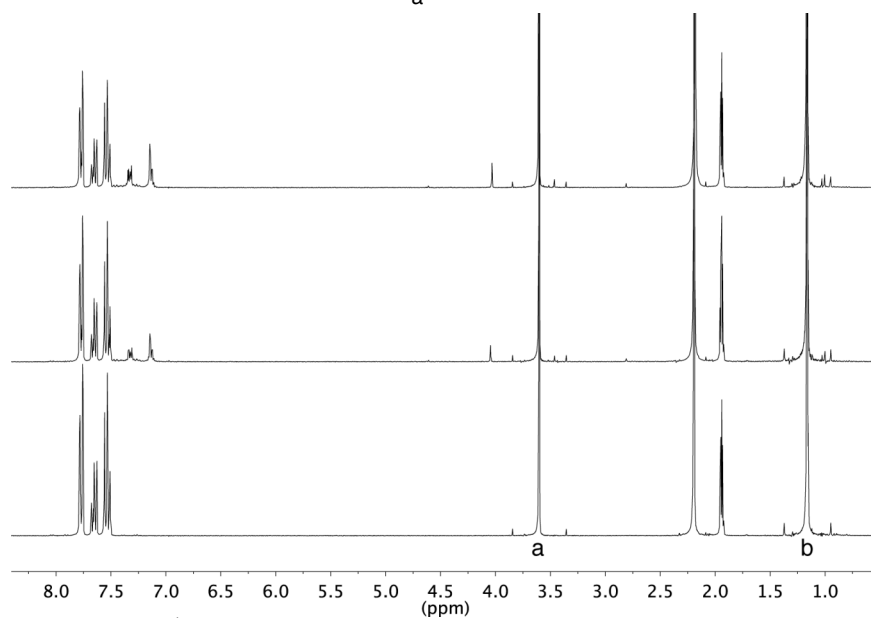
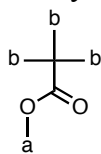
**Figure S15b.** Difference between 300 MHz <sup>1</sup>H NMR spectra of **15** (CD<sub>3</sub>CN) before and after 120 min irradiation at 350nm. Signals from the aromatic protons of **15** overlap adduct proton signals in the region  $\delta$ 7.0-7.4.



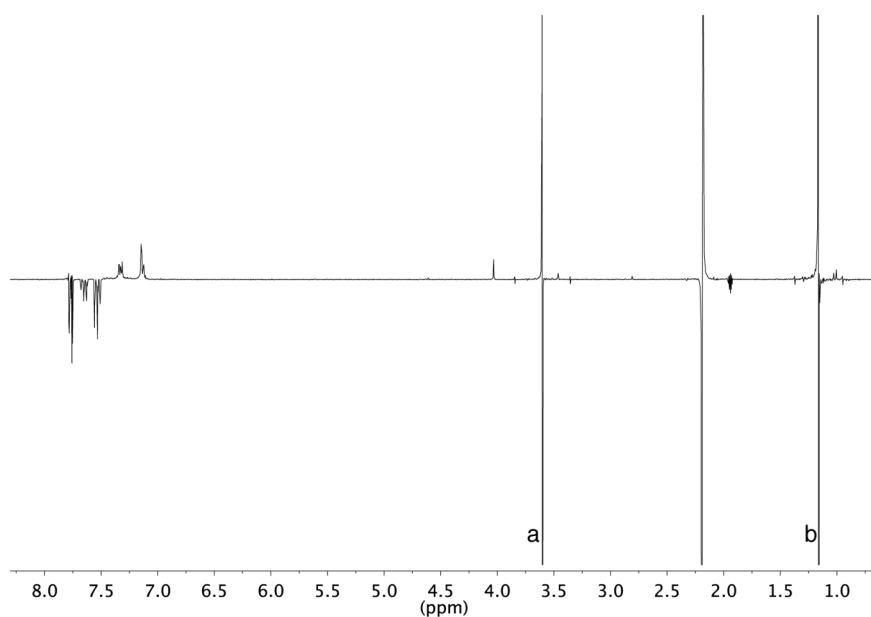
**Figure S15c.** Plot of decreasing  $^1\text{H}$  NMR integrals scaled by initial integral and number of protons with increasing irradiation time of **15**. Each set of data is fit by  $y = Ae^{-kt} + C$ .

**Table S15.** Compounds with representative bond dissociation energies for the protons of **15**, the relation of each representative bond to **15**, and the competitive rate value of  $k/k_a$  scaled for the number of protons.

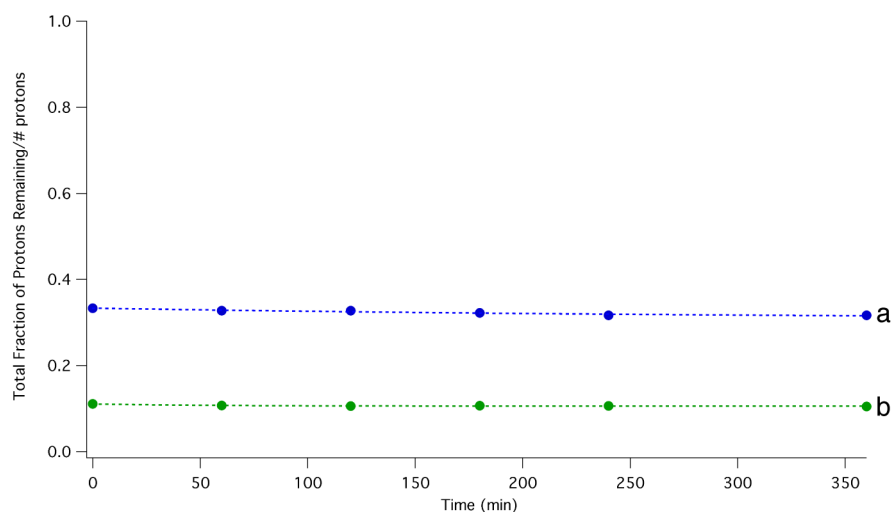
Representative compound	X-H BDE (kcal/mol)	Relation to <b>15</b>	$k/k_a$
ethylbenzene 	84.6 <sup>g</sup> 86.2 <sup>l</sup> 85.4±1.5 <sup>m</sup> 90.3 <sup>j</sup> 87.0 <sup>e</sup>	 $\text{H}_a$	1
<i>tert</i> -butylbenzene 	98.7 <sup>a</sup>	 $\text{H}_b$	0.25

Methyl trimethylacetate, **16**

**Figure S16a.** 300 MHz  $^1\text{H}$  NMR spectra of a 81.4 mM solution of **16** ( $\text{CD}_3\text{CN}$ ) after 0 min (bottom), 120 min (middle), and 360 min (top).

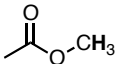
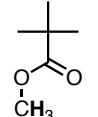
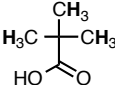
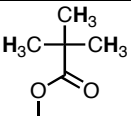


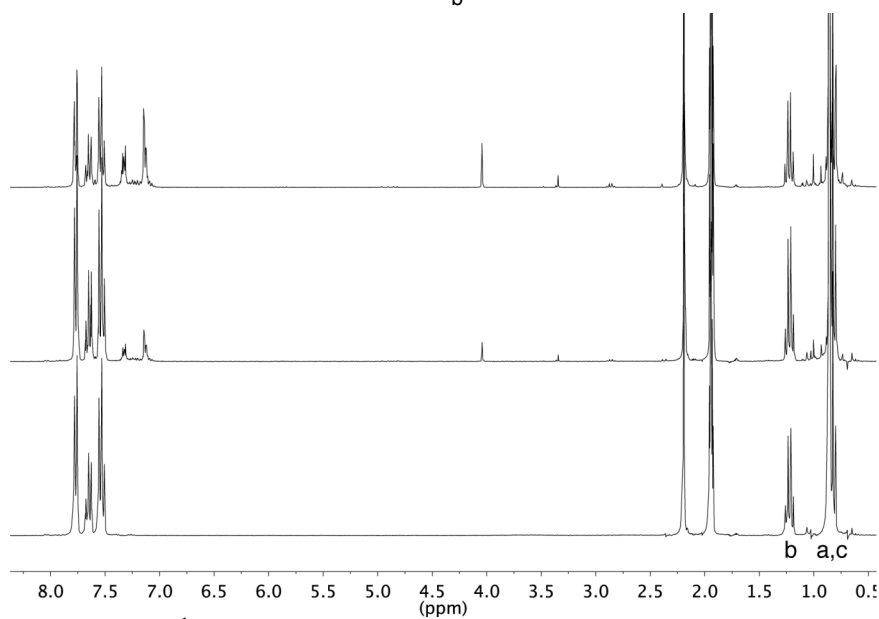
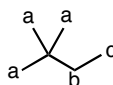
**Figure S16b.** Difference between 300 MHz  $^1\text{H}$  NMR spectra of **16** ( $\text{CD}_3\text{CN}$ ) before and after 360 min irradiation at 350nm.



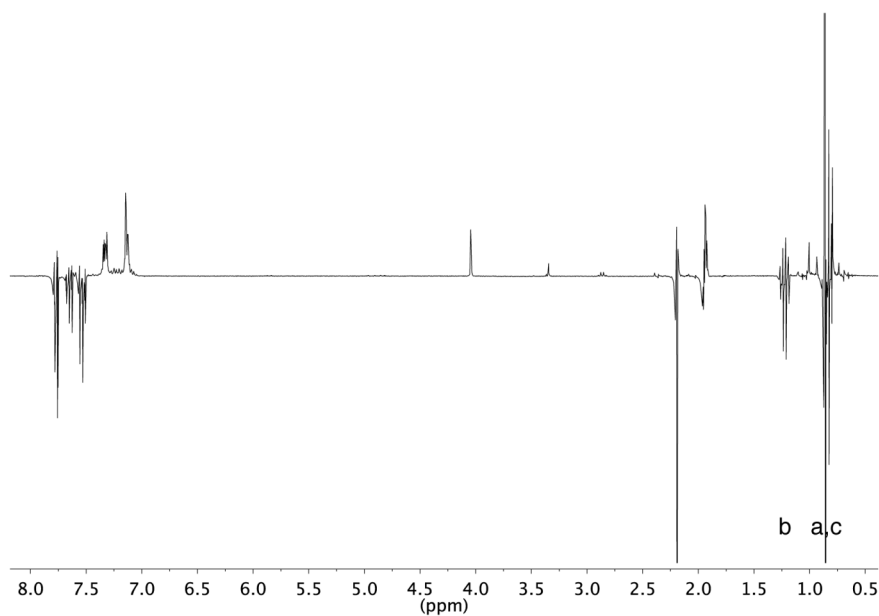
**Figure S16c.** Plot of decreasing  $^1\text{H}$  NMR integrals scaled by initial integral and number of protons with increasing irradiation time of **16**. Each set of data is fit by  $y = Ae^{-kt} + C$ .

**Table S16.** Compounds with representative bond dissociation energies for the protons of **16**, the relation of each representative bond to **16**, and the competitive rate value of  $k/k_a$  scaled for the number of protons.

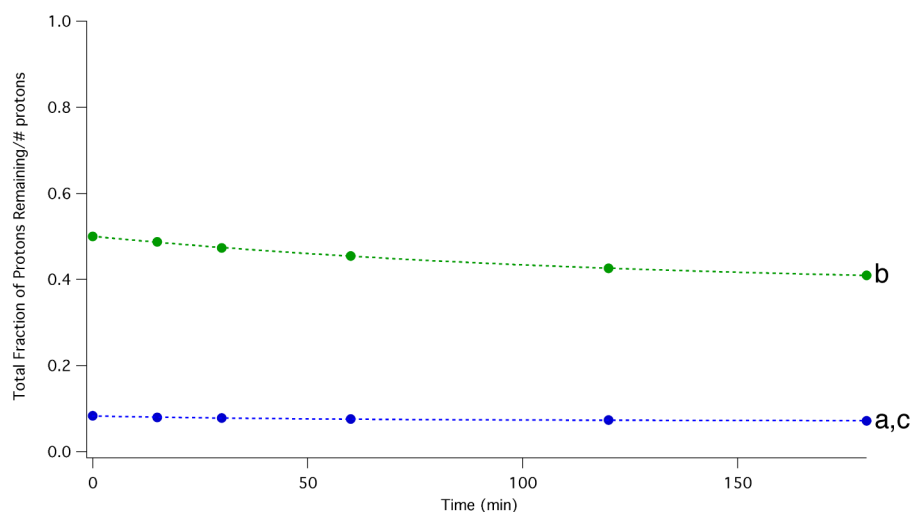
Representative compound	X-H BDE (kcal/mol)	Relation to <b>16</b>	$k/k_a$
acetic acid methyl ester 	96.7 <sup>a</sup>	 $\text{H}_a$	1
2,2-dimethylpropanoic acid 	99.2 <sup>a</sup>	 $\text{H}_b$	2.22

2,2-Dimethylbutane, **17**

**Figure S17a.** 300 MHz  $^1\text{H}$  NMR spectra of a 98.6 mM solution of **17** ( $\text{CD}_3\text{CN}$ ) after 0 min (bottom), 30 min (middle), and 120 min (top).

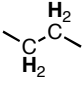
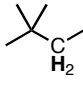
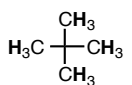
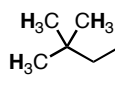
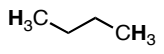
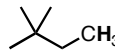


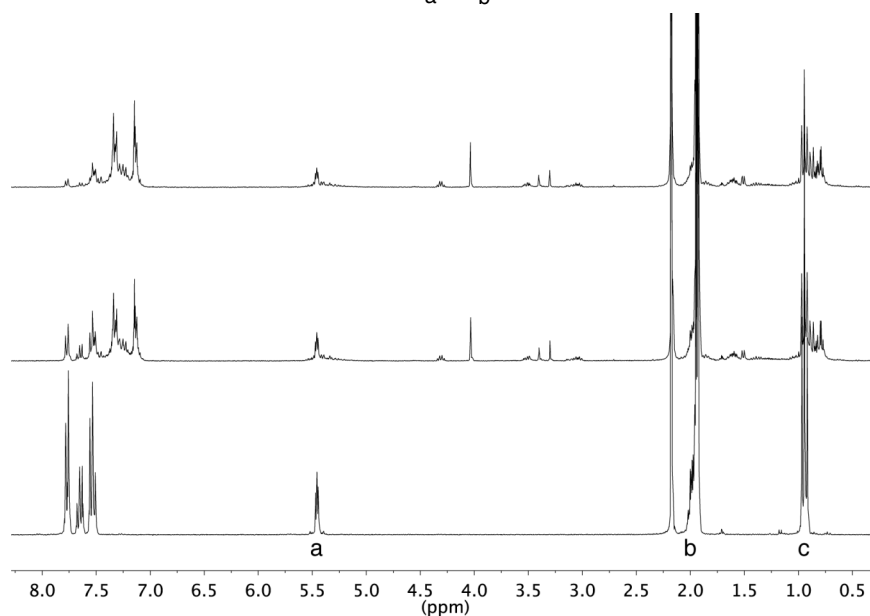
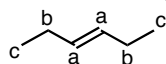
**Figure S17b.** Difference between 300 MHz  $^1\text{H}$  NMR spectra of **17** ( $\text{CD}_3\text{CN}$ ) before and after 120 min irradiation at 350 nm.



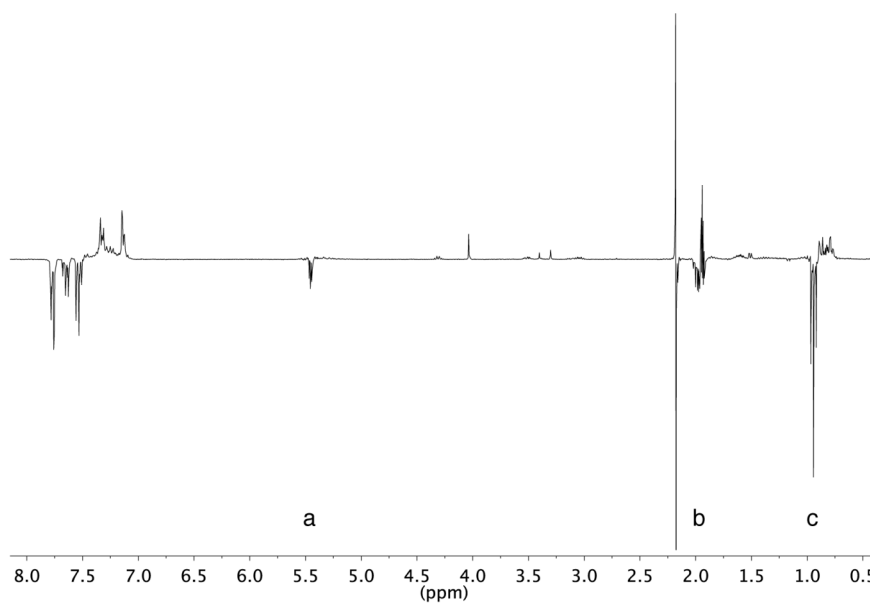
**Figure S17c.** Plot of decreasing  $^1\text{H}$  NMR integrals scaled by initial integral and number of protons with increasing irradiation time of **17**. Each set of data is fit by  $y = Ae^{-kt} + C$ .

**Table S17.** Compounds with representative bond dissociation energies for the protons of **17**, the relation of each representative bond to **17**, and the competitive rate value of  $k/k_a$  scaled for the number of protons.

Representative compound	X-H BDE (kcal/mol)	Relation to <b>17</b>	$k/k_a$
butane 	99.1±0.4 <sup>n</sup> 98.3±0.5 <sup>o</sup> 98.6±0.5 <sup>m</sup> 98.3±0.5 <sup>n</sup> 97.4±1.0 <sup>h</sup>	 H <sub>b</sub>	1
neopentane 	99.4±1 <sup>b</sup> 100.3±1 <sup>c</sup> 99.4±1 <sup>h</sup> 101.0±2 <sup>m</sup> 101.1 <sup>q</sup>	 H <sub>a</sub>	0.38
butane 	101±2 <sup>i</sup> 100.2 <sup>p</sup> 100.7 <sup>h</sup> 101.7±0.5 <sup>n</sup>	 H <sub>c</sub>	

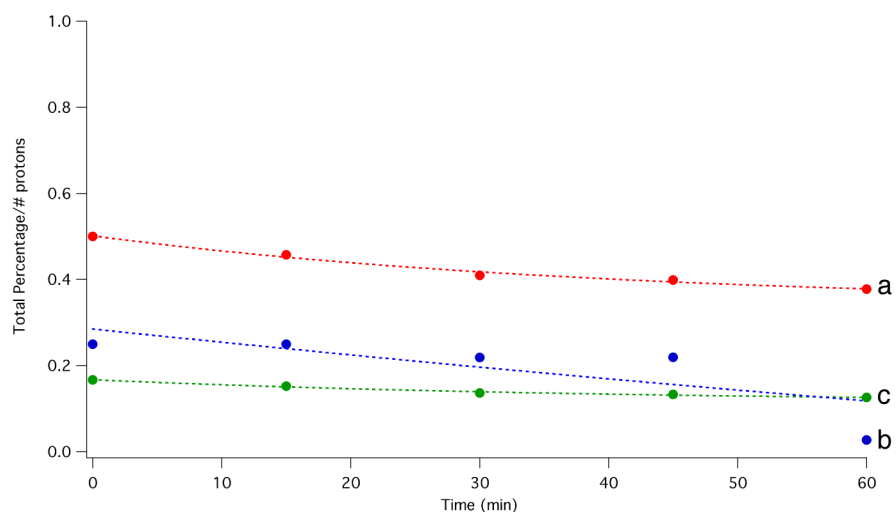
Trans-3-hexene, **18**

**Figure S18a.** 300 MHz <sup>1</sup>H NMR spectra of a 85.2 mM solution of **18** (CD<sub>3</sub>CN) after 0 min (bottom), 30 min (middle), and 60 min (top).



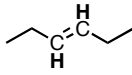
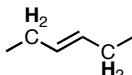
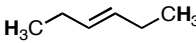
**Figure S18b.** Difference between 300 MHz <sup>1</sup>H NMR spectra of **18** (CD<sub>3</sub>CN) before and after 60 min irradiation at 350nm.

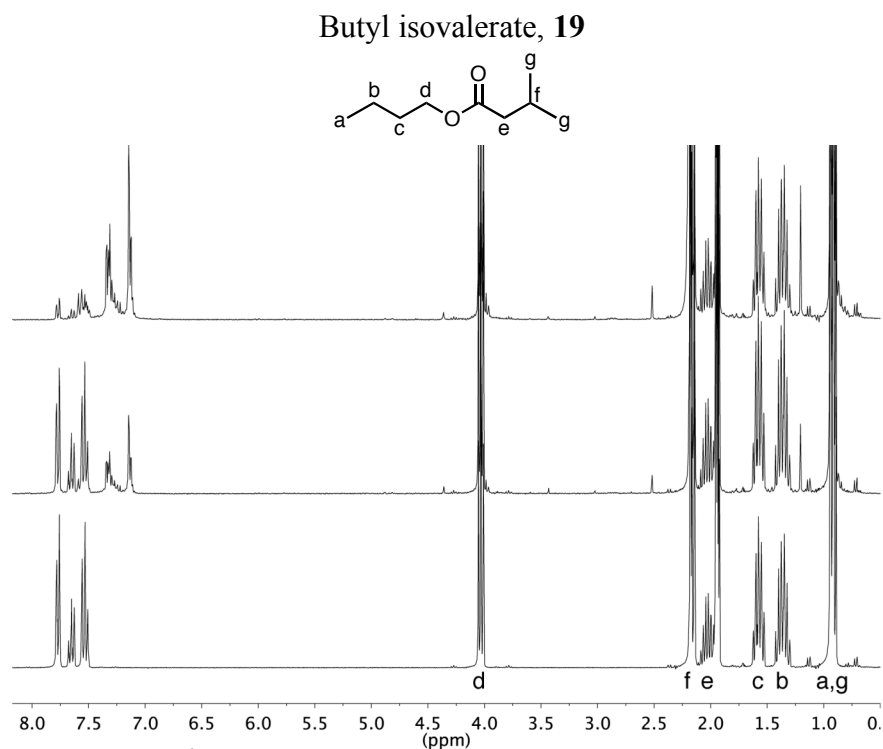




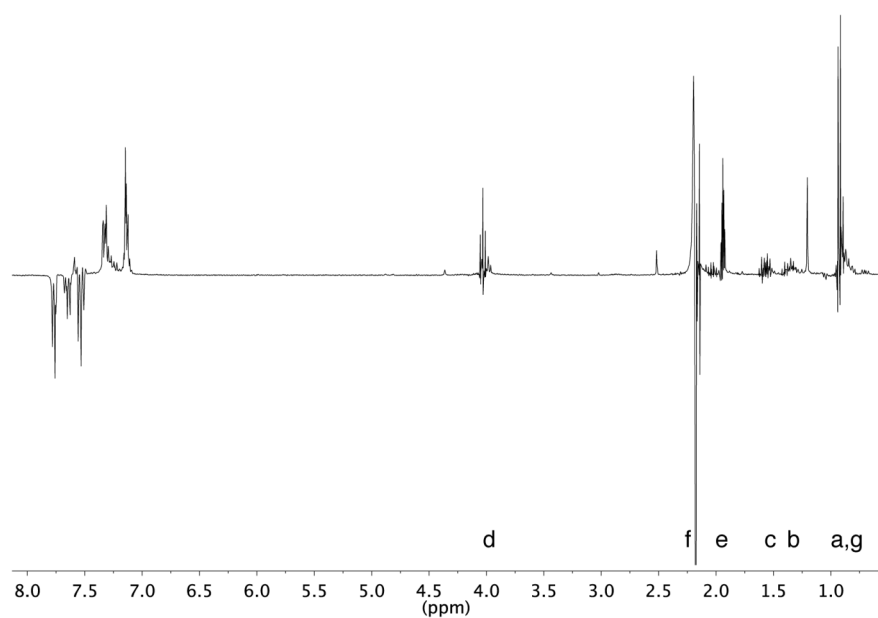
**Figure S18c.** Plot of decreasing  $^1\text{H}$  NMR integrals scaled by initial integral and number of protons with increasing irradiation time of **18**. Each set of data is fit by  $y = Ae^{-kt} + C$ .

**Table S18.** Compounds with representative bond dissociation energies for the protons of **18**, the relation of each representative bond to **18**, and the competitive rate value of  $k/k_a$  scaled for the number of protons.

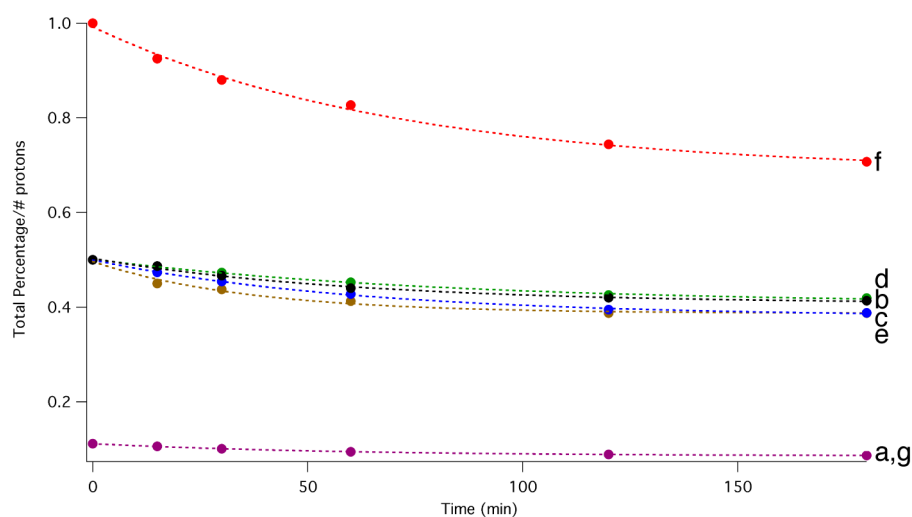
Representative compound	X-H BDE (kcal/mol)	Relation to <b>18</b>	$k/k_a$
propene <chem>H2C=CH2</chem>	$109 \pm 2.4^h$ $111.1^h$	 $\text{H}_a$	1
( <i>E</i> )-2-pentene <chem>CH3CH=CHCH2CH3</chem>	$81.7 \pm 1.5^r$ $82.5^a$	 $\text{H}_b$	3.13
butane <chem>H3CCH2CH2CH3</chem>	$101 \pm 2^i$ $100.2^p$ $100.7^h$ $101.7 \pm 0.5^n$	 $\text{H}_c$	2.08



**Figure S19a.** 300 MHz  $^1\text{H}$  NMR spectra of a 89.2 mM solution of **19** ( $\text{CD}_3\text{CN}$ ) after 0 min (bottom), 30 min (middle), and 180 min (top).

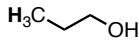
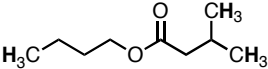
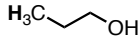
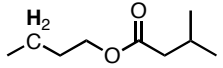
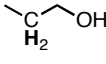
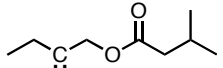
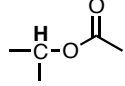
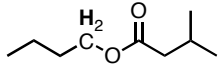
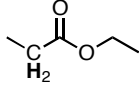
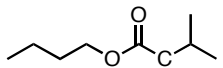
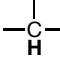
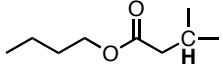


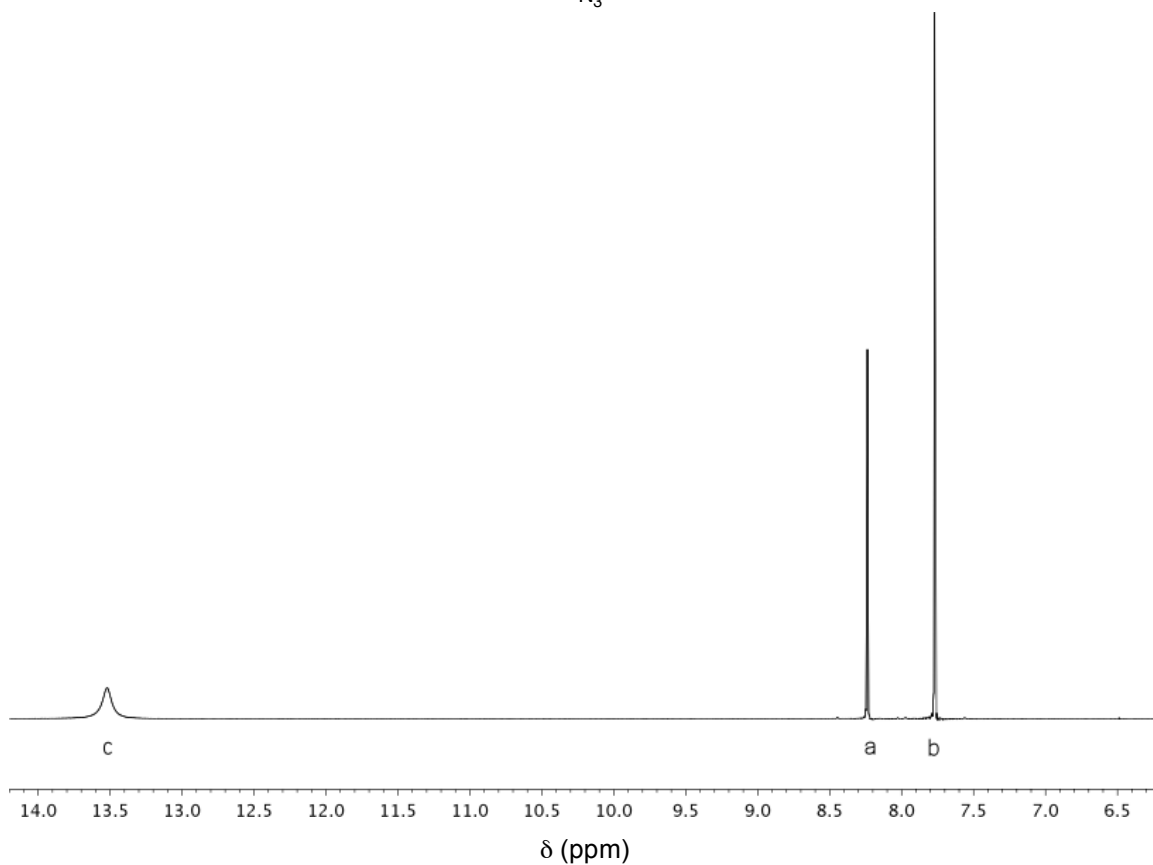
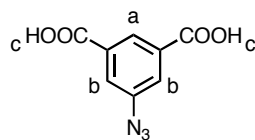
**Figure S19b.** Difference between 300 MHz  $^1\text{H}$  NMR spectra of **19** ( $\text{CD}_3\text{CN}$ ) before and after 180 min irradiation at 350nm.



**Figure S19c.** Plot of decreasing  $^1\text{H}$  NMR integrals scaled by initial integral and number of protons with increasing irradiation time of **19**. Each set of data is fit by  $y = Ae^{-kt} + C$ .

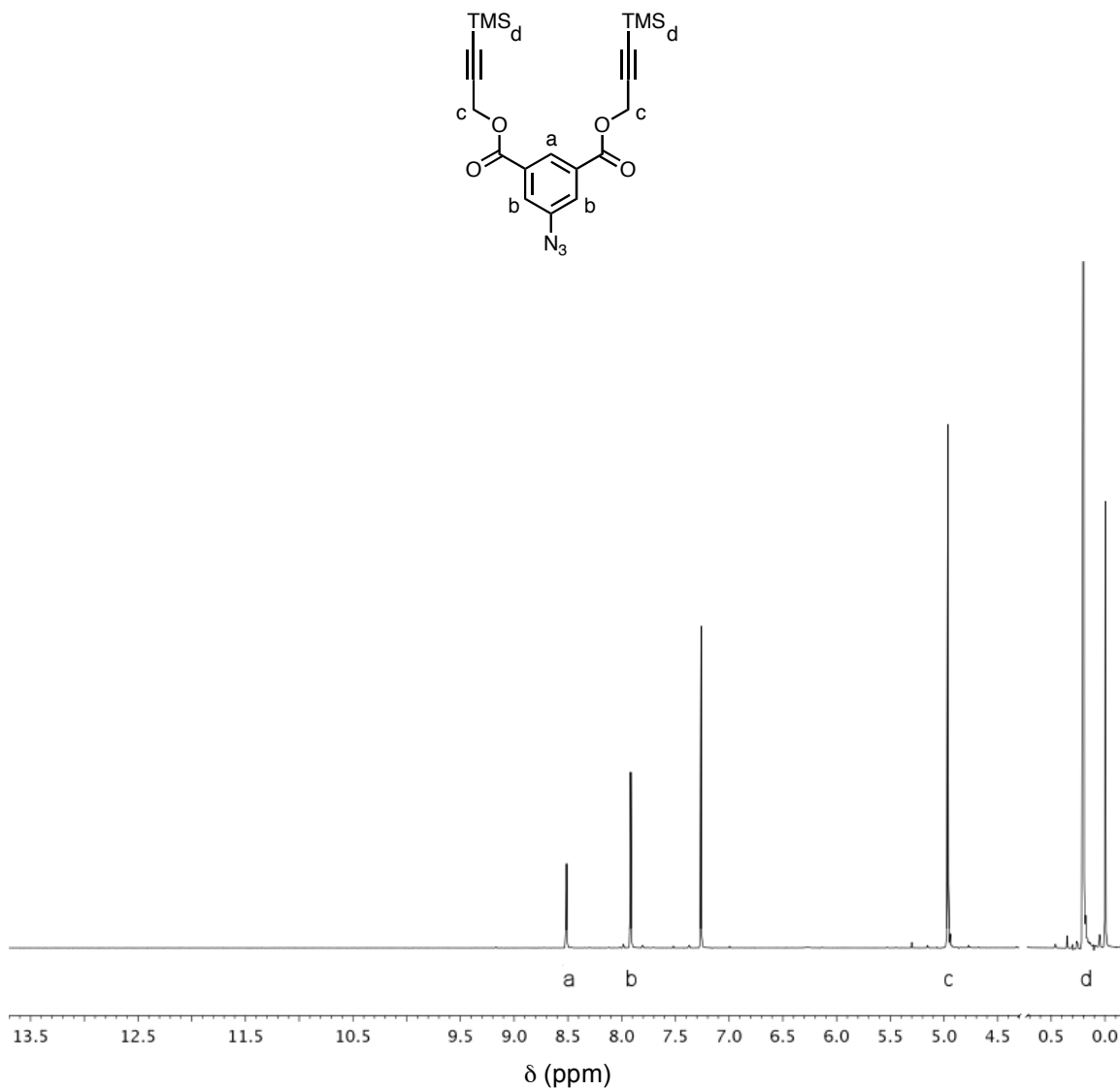
**Table S19.** Compounds with representative bond dissociation energies for the protons of **19**, the relation of each representative bond to **19**, and the competitive rate value of  $k/k_a$  scaled for the number of protons.

Representative compound	X-H BDE (kcal/mol)	Relation to <b>19</b>	$k/k_a$
propanol 	97.1±2 <sup>p</sup>	 H <sub>a</sub> H <sub>g</sub>	1
propanol 	97.1±2 <sup>p</sup>	 H <sub>b</sub>	4.26
propanol  H <sub>2</sub>	94.3±2 <sup>p</sup>	 H <sub>c</sub>	4.26
acetic acid isopropyl ester 	93.8 <sup>a</sup>	 H <sub>d</sub>	3.19
ethyl propanoate  H <sub>2</sub>	95.6 <sup>j</sup>	 H <sub>e</sub>	7.45
isobutane 	95.6±0.7 <sup>h</sup> 95.0 <sup>g</sup> 95.5±0.7 <sup>o</sup> 95.5±0.3 <sup>o</sup> 95.7±0.7 <sup>s</sup>	 H <sub>f</sub>	7.45

5-Azidoisophthalic acid, **20**

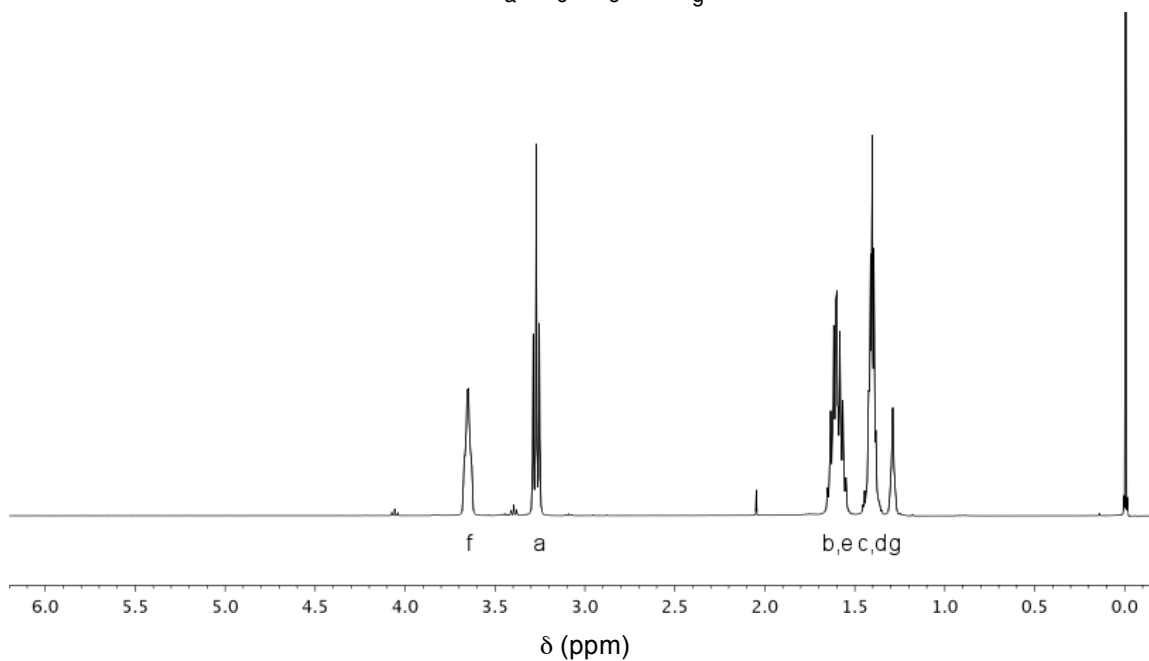
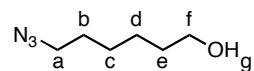
$^1H$  NMR (400 MHz, DMSO)  $\delta$  13.52 (s, 2H), 8.24 (s, 1H), 7.77 (s, 2H).

The heterotrifunctional branching unit, **21**, begins with the diazotization of 5-aminoisophthalic acid in hydrochloric acid by sodium nitrite according to Pierrat, P.; Vanderheiden, S.; Muller, T.; Bräse, S. *Chemical Communications* **2009**, 1748-1750. Addition of sodium azide yielded 5-azidoisophthalic acid, **20**, as a white powder.

CuAAC functional branch unit, **21**

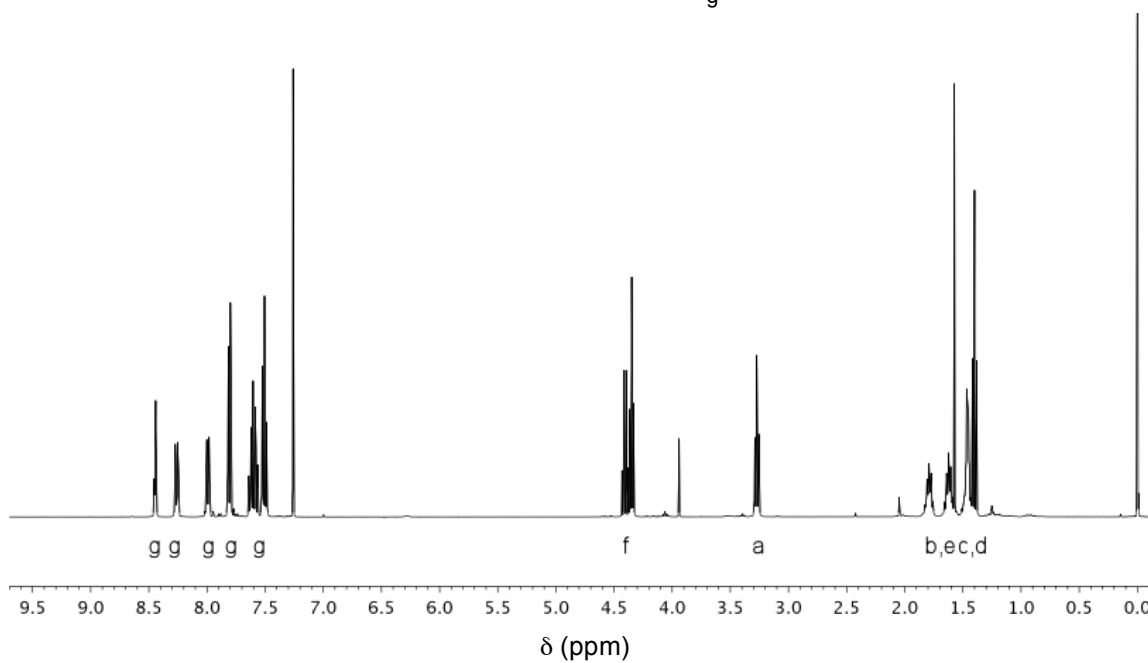
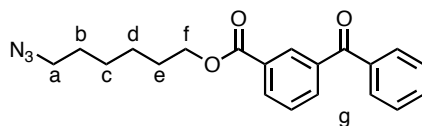
<sup>1</sup>H NMR (400 MHz, CDCl<sub>3</sub>) δ 8.51 (s, 1H), 7.91 (s, 2H), 4.96 (s, 8H), 0.20 (s, 18H).

DCC coupling of **20** according to Carroll, G. T.; Sojka, M. E.; Lei, X.; Turro, N. J.; Koberstein, J. T. *Langmuir* **2006**, *22*, 7748-7754 with two equivalents of 3-(trimethylsilyl)-2-propyn-1-ol followed by column chromatography yielded **21** as a brown oil.

6-Azidohexanol, **22**

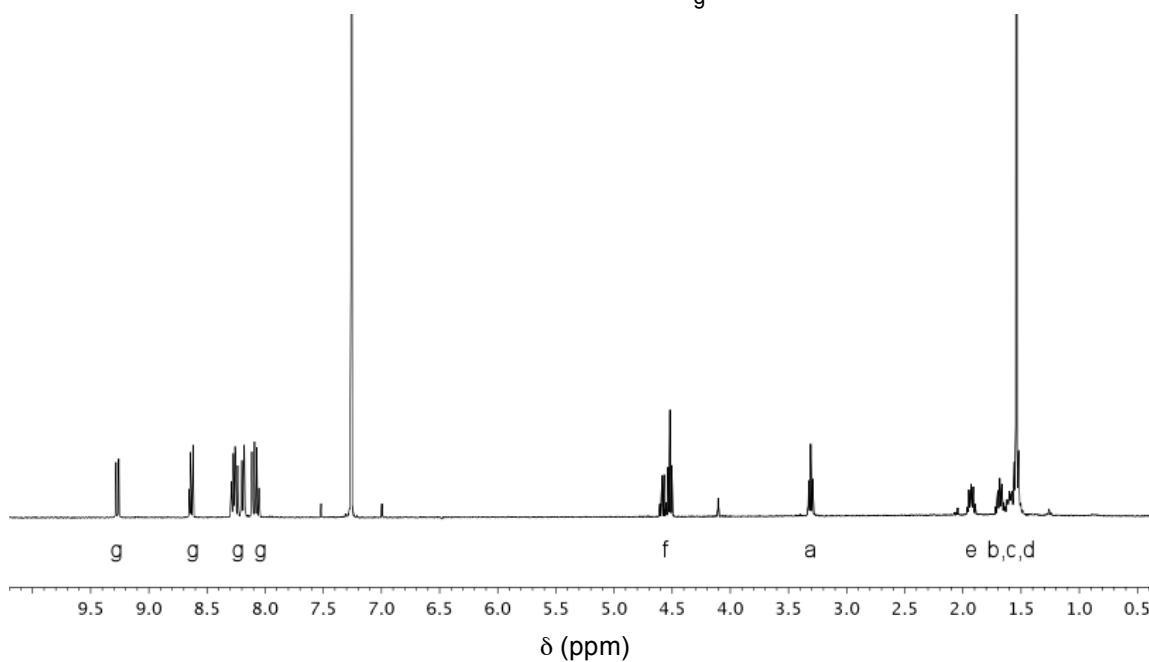
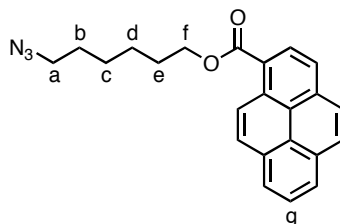
<sup>1</sup>H NMR (400 MHz, CDCl<sub>3</sub>) δ 3.65 (dd, *J* = 9.6, 6.3 Hz, 2H), 3.27 (t, *J* = 6.9 Hz, 2H), 1.72 – 1.51 (m, 4H), 1.49 – 1.33 (m, 4H), 1.29 (s, 1H).

Compound **22** was prepared by stirring 6-bromohexanol with excess sodium azide in *N,N*-dimethylformamide overnight under nitrogen. Aqueous workup removed remaining sodium azide to yield **22**.

Benzophenone azide, **23**

$^1\text{H}$  NMR (400 MHz,  $\text{CDCl}_3$ )  $\delta$  8.48 – 8.41 (m, 1H), 8.31 – 8.22 (m, 1H), 7.99 (m, 1H), 7.81 (dt,  $J = 8.5, 1.7$  Hz, 2H), 7.67 – 7.46 (m, 4H), 4.46 – 4.31 (m, 2H), 3.27 (t,  $J = 6.9$  Hz, 2H), 1.89 – 1.70 (m, 2H), 1.62 (dd,  $J = 9.1, 4.8$  Hz, 2H), 1.46 (dt,  $J = 6.7, 2.7$  Hz, 2H), 1.40 (t,  $J = 7.1$  Hz, 2H).

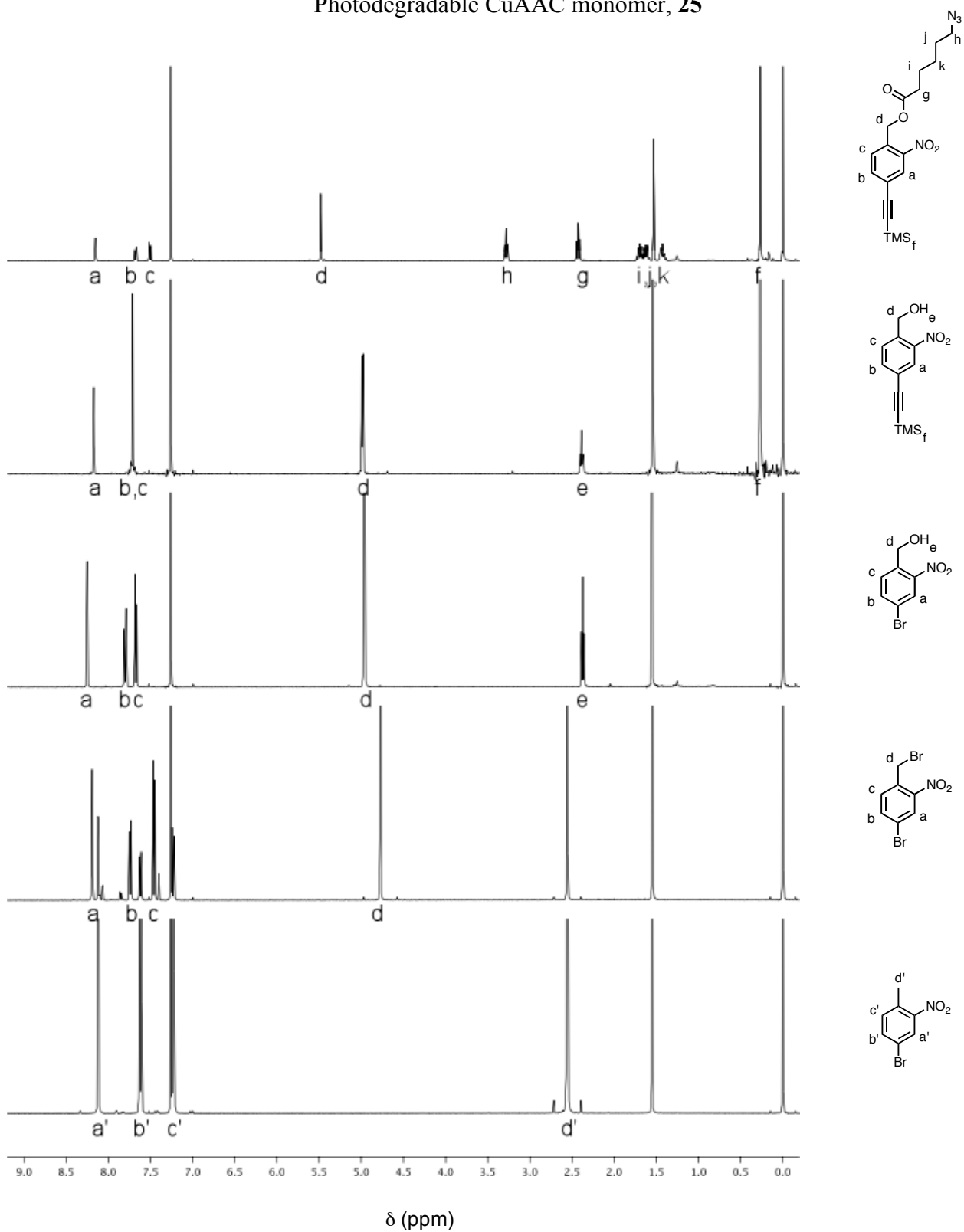
DCC coupling of **22** with 3-benzoylbenzoic acid according to Carroll, G. T.; Sojka, M. E.; Lei, X.; Turro, N. J.; Koberstein, J. T. *Langmuir* **2006**, *22*, 7748-7754 yielded azide-functional benzophenone, **23**.

Pyrene azide, **24**

$^1\text{H}$  NMR (400 MHz,  $\text{CDCl}_3$ )  $\delta$  9.27 (d,  $J = 9.4$  Hz, 1H), 8.64 (dd,  $J = 8.1, 5.0$  Hz, 1H), 8.23 (ddd,  $J = 11.0, 10.2, 4.4$  Hz, 4H), 8.14 – 8.03 (m, 3H), 4.77 – 4.44 (m, 2H), 3.31 (t,  $J = 6.9$  Hz, 2H), 1.92 (dd,  $J = 14.7, 6.7$  Hz, 2H), 1.78 – 1.63 (m, 2H), 1.62 (d,  $J = 2.9$  Hz, 4H).

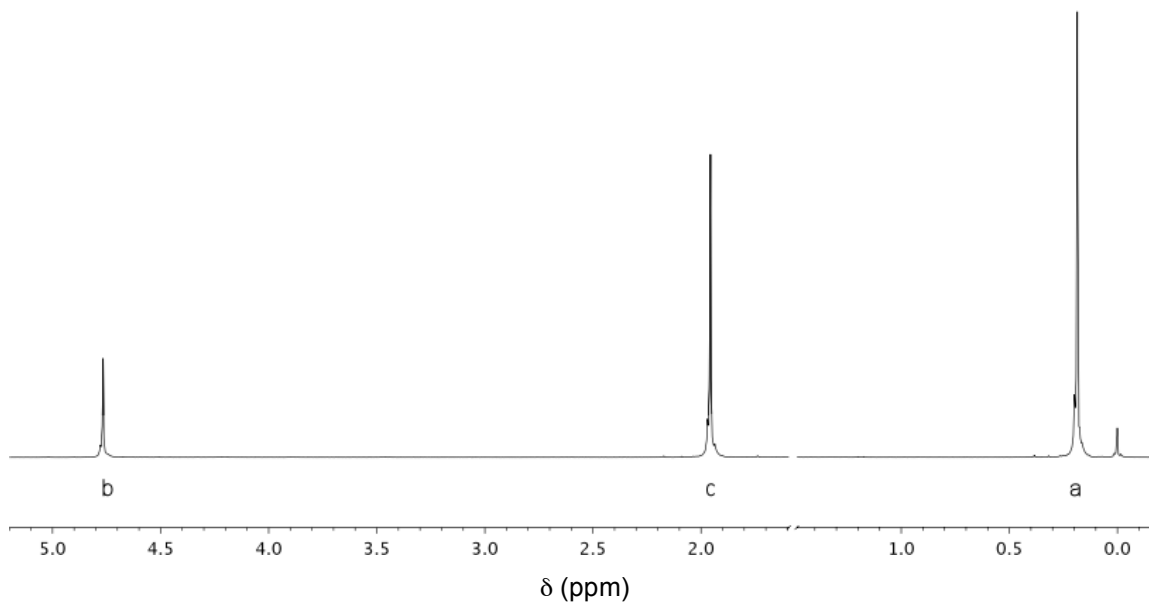
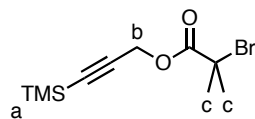
DCC coupling of **22** with pyrene-1-carboxylic acid according to Carroll, G. T.; Sojka, M. E.; Lei, X.; Turro, N. J.; Koberstein, J. T. *Langmuir* **2006**, *22*, 7748-7754 yielded azide-functional pyrene, **24**.



Photodegradable CuAAC monomer, **25**

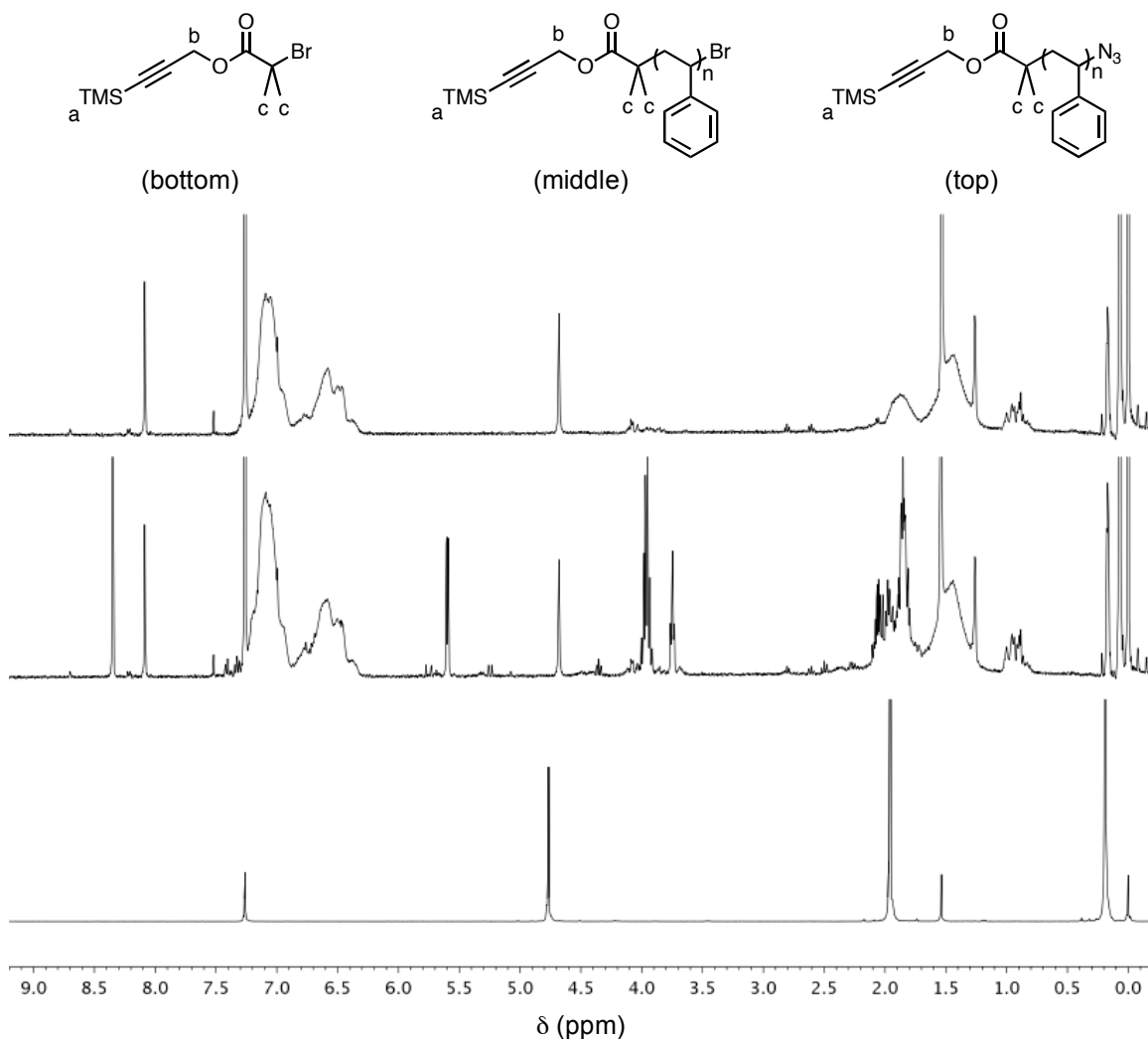
(top)  $^1\text{H}$  NMR (400 MHz,  $\text{CDCl}_3$ )  $\delta$  8.16 (d,  $J = 1.5$  Hz, 1H), 7.68 (dd,  $J = 8.0, 1.5$  Hz, 1H), 7.50 (d,  $J = 8.1$  Hz, 1H), 5.48 (s, 2H), 3.28 (t,  $J = 6.8$  Hz, 2H), 2.43 (t,  $J = 7.4$  Hz, 2H), 1.77 – 1.55 (m, 4H), 1.46 – 1.36 (m, 2H), 0.27 (s, 9H).

Free radical bromination of 4-bromo-2-nitrotoluene in carbon tetrachloride yielded 4-bromo-1-(bromomethyl)-2-nitrobenzene (Rzasa, R. M. et al. *Bioorganic & Medicinal Chemistry* **2007**, *15*, 6574) which was then refluxed in water to yield 4-bromo-1-(hydroxymethyl)-2-nitrobenzene. Sonogashira coupling of 4-bromo-1-(hydroxymethyl)-2-nitrobenzene with 1-trimethylsilylacetylene in triethylamine and tetrahydrofuran yielded 4-(2-(trimethylsilyl)ethynyl)-1-(hydroxymethyl)-2-nitrobenzene (Hiraoka, S.; Hirata, K.; Shionoya, M. *Angewandte Chemie International Edition* **2004**, *43*, 3814). DCC coupling with an  $\alpha$ -azido, $\omega$ -carboxylic acid generated the photodegradable CuAAC monomer, **25**.

TMS-alkyne-functional ATRP initiator, **26**

$^1\text{H}$  NMR (300 MHz,  $\text{CDCl}_3$ )  $\delta$  4.77 (s, 2H), 1.96 (s, 6H), 0.19 (s, 9H).

Compound **26** is the condensation product of 3-(trimethylsilyl)-2-propyn-1-ol with  $\alpha$ -bromoisobutyryl bromide promoted by triethylamine according to Urbani, C. N.; Bell, C. A.; Lonsdale, D.; Whittaker, M. R.; Monteiro, M. J. *Macromolecules* 2008, *41*, 76-86.

TMS-alkyne-PS-Br and TMS-alkyne-PS-N<sub>3</sub>, **27**

(top) <sup>1</sup>H NMR (400 MHz, CDCl<sub>3</sub>) δ 8.09 (s), 7.09 (s), 6.54 (d), 4.68 (s), 1.88 (s), 1.43 (s), 1.26 (s), 1.09 – 0.74 (m), 0.48 – 0.05 (m).

(middle) <sup>1</sup>H NMR (400 MHz, CDCl<sub>3</sub>) δ 8.35 (s), 8.09 (s), 7.09 (s), 6.54 (d), 5.60 (dd), 4.68 (s), 4.08 – 3.88 (m), 3.75 (s), 1.85 (s), 1.44 (s), 1.26 (s), 1.10 – 0.79 (m), 0.17 (s), 0.07 (d).

(bottom) <sup>1</sup>H NMR (300 MHz, CDCl<sub>3</sub>) δ 4.77 (s, 2H), 1.96 (s, 6H), 0.19 (s, 9H).

Compound **27** is prepared by polymerization of styrene under standard ATRP conditions using **26** as the ATRP initiator. Stirring the resulting polymer with sodium azide in *N,N*-dimethylformamide replaces the terminal bromide to make the desired α-(TMS-alkyne),ω-azide polymer, **27**.

## Colophon

This document was laid out in Times New Roman, Arial, and Symbol using Microsoft Word. Images were prepared in Adobe Illustrator and Adobe Photoshop, graphs were plotted using Igor Pro, NMR spectra were processed using MestreNova, and chemical structures were drawn using ChemDraw. Section endnotes were organized and inserted using Mendeley.

The document will be deposited in portable document format (PDF) in the Academic Commons digital repository at Columbia University.